Characterisation of EphA1 and its potential role in Alzheimer's Disease

by

Helen Anne Owens, MSc.

September 2019

Division of Psychological Medicine and Clinical Neurosciences School of Medicine, Cardiff University

A thesis submitted to Cardiff University for the Degree of Doctor of Philosophy

Declaration

This work has not been submitted in substance for any other degree or award at this or any other university or place of learning, nor is being submitted concurrently in candidature for any degree or other award.

Signed …… (candidate) Date…….……..……

STATEMENT 1

This thesis is being submitted in partial fulfillment of the requirements for the degree of …… (insert MCh, MD, MPhil, PhD etc, as appropriate)

Signed …… (candidate) Date …….……..……

STATEMENT 2

This thesis is the result of my own independent work/investigation, except where otherwise stated, and the thesis has not been edited by a third party beyond what is permitted by Cardiff University's Policy on the Use of Third Party Editors by Research Degree Students. Other sources are acknowledged by explicit references. The views expressed are my own.

Signed …… (candidate) Date …….……..……

STATEMENT 3

I hereby give consent for my thesis, if accepted, to be available online in the University's Open Access repository and for inter-library loan, and for the title and summary to be made available to outside organisations.

Signed …… (candidate) Date …….……..……

STATEMENT 4: PREVIOUSLY APPROVED BAR ON ACCESS

I hereby give consent for my thesis, if accepted, to be available online in the University's Open Access repository and for inter-library loans **after expiry of a bar on access previously approved by the Academic Standards & Quality Committee.**

Signed …… (candidate) Date …….……..……

Acknowledgments

I would like to begin by thanking my supervisors, Professor Ann Ager, Dr. Vera Knäuper and Professor Julie Williams. Your advice and support, both professionally and personally have been pivotal for the completion of my lab work and thesis. My PhD journey would have been impossibly difficult without the constant emotional support from my office girls, Dr. Rhiannon Griffiths and (soon to be, Dr.) Shannon Turberville.

I cannot express enough how thankful I am for my friends and family. I thank all those friends in non-science fields who sit there and listen when I talk about things they have no idea about and still take an interest! To my amazing family, my brother Steven, my mother, Susan and my "Step-Dad" Ian. You have all been instrumental in getting me to this point, and I love you all more than I could ever put into words. Mam – you are and always will be my best friend, how could I have done this without you? To Lewis – thanks for always putting a smile on my face and for providing that stability that was so greatly needed! You're the best.

Lastly, a special mention to my late friend, Dr. Javier Uceda Fernández. I will never forget you, my friend. I hope you've found your Neverland.

Thesis Summary

Recent genetic evidence has identified the *EphA1* gene as a susceptibility locus in Alzheimer's disease with targeted sequencing identifying a nonsynonymous variant ($P^{460}L$) within intron 1 (Vardarajan et al., 2015). *EphA1* encodes the type-I transmembrane protein EphA1, a member of the Eph family of receptor tyrosine kinases. Eph receptors and their surface associated ligands, ephrins, play a role in immunity and inflammation, with inflammatory mechanisms a central component of AD neuropathology. This study aimed to characterise the WT EphA1 molecule as a means to understand the pathological potential of $P^{460}L$ EphA1.

WT EphA1 was shown to be proteolytically processed at the ectodomain following ligand engagement, resulting in C-terminal internalisation and degradation, which is not mediated by MMPs or γ-secretase activity. However, a degree of constitutive proteolysis was apparent which may be partially mediated by MMPs. WT EphA1 C-terminal fragments may be trans-endocytosed within endosomes. Comparatively, N-terminal expression of EphA1 $P^{460}L$ is reduced in comparison to WT in the absence of ligand, which is increased with the addition of ephrinA1-Fc. MMP inhibition was shown to partially prevent the degradation of potentially trans-endocytosed N-terminal fragments. EphA1 $P^{460}L$ ligand-induced degradation of C-terminal terminal fragments is not γ-secretase dependant.

Expedited proteolysis of $P^{460}L$ EphA1 could result in an increase in the amount of circulating ECD in the bloodstream as EphA1 is expressed on leucocytes. Using a microfluidic assay, it was determined that soluble EphA1 is capable of priming a brain endothelial cell line (hCMEC/D3s) for Molt 3 T cell recruitment, potentially offering an AD pathomechanism. This thesis provides an insight to the regulatory mechanisms of WT EphA1, which was previously not elucidated. Moreover, for the first time, it offers a potential pathomechanism of the *EphA1* AD SNP, $P^{460}L$.

Table of Contents

List of Abbreviations

aa	Amino acid
Aβ	Amyloid β
ACH	Amyloid cascade hypothesis
α-CTF	α-C-terminal fragment
AD	Alzheimer's disease
ADGC	Alzheimer's Disease Genetics Consortium
AdJ	Adherens junction
ADRDA	Alzheimer's Disease and Related Disorders Association
ApoE	Apolipoprotein E
APP	Amyloid precursor protein
BACE1	β-secretase
BBB	Blood-brain barrier
β-CTF	β-C-terminal fragment
BM	Basement membrane
Ca^{2+}	Calcium
CCL2/5	CC-chemokine ligand 2/5
CCR2/5	Chemokine receptor 2/5
CD2AP	CD2-associated protein
CFSE	Carboxyfluorescein diacetate succinimidyl ester
CIE	Clathrin-independent endocytosis
CLR	C-type lectin receptor
CME	Clathrin-mediated endocytosis
CNS	Central nervous system
CSF	Cerebrospinal fluid
CTF	C-terminal fragment
CXCL4/5	CXC-chemokine ligand 4/5
CXCR2	C-X-C chemokine receptor type 2
DAMP	Damage-associated molecular pattern molecules
DAPT	N-[N-(3, 5-difluorophenacetyl-L-alanyl)]-S-phenylglycine t-butyl ester

EADII	The European Alzheimer Disease Initiative Investigators
ECD	Ectodomain
EC	Endothelial cell
EDTA	Ethylenediaminetetraacetic acid
EOAD	Early-onset Alzheimer's disease
EphA1	Erythropoietin producing hepatocellular carcinoma receptor 1
fAD	Familial Alzheimer's disease
FBS	Fetal bovine serum
FNIII	Fibronectin type III domain
GERAD1	Genetic and Environmental Risk for Alzheimer's Disease
GJ	Gap junction
GPCR	G-protein coupled receptor
GPI	Glycosylphosphatidylinositol
GSK-3β	Glycogen synthase kinase-3β
GWAS	Genome wide association study
hEGF	Human epidermal growth factor
HEPES-BSS	4-(2-hydroxyethyl)-1-piperazineethanesulfonic acid buffered saline solution
hFGF-β	Human fibroblast growth factor-β
ICAM-1	Intercellular adhesion molecule-1
iCLiPs	Intramembrane cleaving proteases
IFN-γ	Interferon-γ
I-GAP	International Genomics of Alzheimer's Project
Il-1	Interleukin-1
Il-6	Interleukin-6
Il-1β	Interleukin-1β
ISF	Interstitial fluid
JAM-A/B/C	Junctional adhesion molecules-A/B/C
LFA-4	Lymphocyte function-associated antigen-4
LD	Linkage disequilibrium
LOAD	Late-onset Alzheimer's disease

LRP	Lipoprotein receptor related protein
MAC1	Macrophage receptor 1
MAdCAM1	Mucosal vascular addressin cell adhesion molecule 1
MAF	Minor allele frequency
MCI	Mild cognitive impairment
MCP-1	Monocyte chemoattractant protein-1
MMP-2	Matrix metalloproteinase-2
MMP-9	Matrix metalloproteinase-9
MS	Multiple sclerosis
NET	Neutrophil extracellular trap
NFTs	Neurofibrillary tangles
NIA-AA	National Institute on Aging–Alzheimer's Association
NINCDS	National Institute of Neurological and Communicative Disorders and Stroke
NLR	NOD-like receptor
NLRP3	NLR family pyrin domain containing 3
NVU	Neurovascular unit
O/N	Overnight
P	Passage
PAMP	Pathogen-associated molecular pattern molecule
PBS	Phosphate buffered saline
PBS-T	Phosphate buffered saline-Tween 20
PECAM-1	Platelet and endothelial cell adhesion molecule-1
PET	Positron emission tomography
PHF	Paired helical filaments
PI-3K	Phosphoinositide 3-kinase
PiB	Pittsburgh Compound B
PICALM	Phosphatidylinositol clathrin assembly protein
PKC	Protein kinase C
PMA	Phorbol-12-myristate-13-acetate

PP2A	Protein phosphatase 2A
PRR	Pattern recognition receptor
PSEN1	Presenilin 1
PSEN2	Presenilin 2
PSGL-1	P-selectin glycoprotein-1
pTau	Phosphorylated tau
PUFA	Polyunsaturated fatty acids
R3-IGF-1	R3-insulin-like growth factor-1
RAGE	Receptor for advanced glycation end products
RIP	Regulated intramembrane proteolysis
RLR	RIG-I-like receptor
ROS	Reactive oxygen species
RT	Room temperature
RTK	Receptor tyrosine kinase
sAD	Sporadic Alzheimer's disease
SAM	Sterile α-motif
sAPPα	Soluble amyloid precursor protein α
sAPPβ	Soluble amyloid precursor protein β
SF	Straight filaments
SNP	Single nucleotide polymorphisms
T2D	Type 2 diabetes
TEER	Transendothelial electrical resistance
TEM	Transendothelial migration
TIM-1	T-cell immunoglobulin and mucin domain 1
TJ	Tight junction
TLR	Toll-like receptor
TNFα	Tumour necrosis factor α
TNS	Trypsin neutralising solution
TREM2	Triggering receptors expressed on myeloid cells
VCAM-1	Vascular cell adhesion protein 1

VEGF	Vascular endothelial growth factor
VLA-3	Very late antigen-3
VLA-4	Very late antigen-4
vSMCs	Vascular smooth muscle cells
WES	Whole exome sequencing
WGS	Whole genome sequencing
WHO	World Health Organization
ZO-1/2/3	Zona occludens-1/2/3

List of Tables

List of Figures

Chapter One
Introduction

1.1 Alzheimer's disease

1.1.2 Overview

Alzheimer's disease (AD) is a neurodegenerative disorder characterised by inexorable cognitive decline and neuropathological hallmarks including aggregation of cytotoxic β-amyloid (Aβ) oligomers and intracellular accumulation of neurofibrillary tangles (NFTs) comprised of hyperphosphorylated tau protein. Macroscopically, AD manifests as cortical atrophy resulting from myelin reduction, degeneration of axons and dendrites and subsequent neuronal death (Sjöbeck et al., 2005). The aetiological basis of AD has not been fully ascertained with several putative pathomechanisms. Early-onset AD (EOAD), which accounts for approximately 5-6% of all AD cases (Zhu et al., 2015a), presents clinically before the age of 65, has a direct autosomal dominant transmission, high polygenic risk, with the patients' clinical course often deteriorating rapidly (Wattmo and Wallin, 2017). Late-onset AD (LOAD) is the most common cause of dementia with age considered the biggest risk factor (Sloane et al., 2002). There is a plethora of LOAD associated risk factors, including epidemiological, genetic and environmental.

1.1.3 Prevalence

Due to an increase in both population growth and life expectancy, the number of people living globally with dementia has increased by 117% since 1990, estimated at approximately 43.8 million in 2016 (GBD 2016 Dementia Collaborators et al., 2019). Approximately 70% of these dementia cases can be attributed to dementia due to AD. The number of individuals living with AD in the UK stands at ~816,000 costing the government approximately £26.3 billion per annum (Prince et al., 2014). Prevalence rates of AD increases exponentially with age, with approximately 7% of people suffering from dementia at 65, rising to ~17% at the age of 80 (Qiu et al., 2009). Sex is another sociodemographic contributing factor, with females more likely to develop AD when compared to their male counterparts (Prince et al., 2014). Although, whether this is related to a longer life expectancy in females is unclear.

1.1.4 Clinical presentation and diagnoses

The World Health Organization (WHO) has defined dementia as a "loss of intellectual capability of such severity as to interfere with the social or occupational functioning. "Symptomatic impairments are evident in various cognitive domains such as communication, language and learning, attention, memory, comprehension, motor functioning and the ability to orient both spatially and temporally (Guarino et al., 2018). Emotional and social functioning is also impaired (Kipps et al., 2009) causing much distress to both patients and their families. Initial manifestations of the disease (the pre-dementia phase of AD) begins with episodic memory loss with the ability for patients to recall their most recent memories and experiences impaired first (Förstl and Kurz, 1999; McKhann et al., 2011). Executive functioning, such as problem solving, multitasking and planning are also considered to be impaired in the pre-dementia phase (e.g. Bondi et al., 2002), fundamentally due to degeneration of the prefrontal cortex (Salat et al., 2001). Development to the dementia phase involves deteriorating memory, with patients losing the ability to recall their earliest memories, with communication and orienting impairments also becoming evident (Hodges et al., 2006).

Definitive diagnosis of AD is confirmed at post mortem analyses of brain tissue, nevertheless, revised clinical criteria building upon the National Institute of Neurological and Communicative Disorders and Stroke and the Alzheimer's Disease and Related Disorders Association (NINCDS-ADRDA; McKhann et al., 1984) supports diagnoses in living patients. These revised guidelines, devised by the National Institute on Aging–Alzheimer's Association (NIA–AA) altered the criteria for both mild cognitive impairment (MCI) and the various stages of dementia due to AD (Albert et al., 2011; McKhann et al., 2011b; Sperling et al., 2011). The NIA-AA guidelines include tiers of probability, described as "proven AD", "probable AD" and "possible AD" and their diagnostic guidelines are outlined in Table 1.1**.** Recent advancements in non-invasive techniques, such as Aβ and tau positron emission tomography (PET), genotyping and an increasing understanding of potential AD biomarkers (e.g. through cerebrospinal fluid (CSF) testing) can support current clinical diagnostic tools, allowing a more precise diagnosis. However, these are infrequently

used (Sabbagh et al., 2017). Future work must focus on including clinical criteria with identified pathophysiology so that diagnoses can be made earlier and more precisely.

Table 1.1 Diagnostic guidelines for Alzheimer's disease from the National Institute on Aging–Alzheimer's Association . Adapted from (McKhann et al., 2011b) and (Sabbagh et al., 2017)

Disease state	**Definition**
Dementia core criteria	Cognitive or behavioural symptoms interfering with ability to function at work or at usual activities, represent a decline from previous levels of functioning, and not explained by delirium or major psychiatric disorder. The cognitive or behavioural impairment involves a minimum of two of the following domains: impaired ability to acquire and remember new information, impaired reasoning and handling of complex tasks, impaired visuospatial abilities, impaired language functions, and changes in personality or behaviour or comportment.
Probable Alzheimer's dementia	Meets criteria for dementia, in addition to insidious gradual onset, history of worsening cognition by report or observation, or initial and most prominent cognitive deficits in either amnestic (impaired learning or recent recall) or non-amnestic (language, visuospatial, or executive dysfunction).
Possible Alzheimer's dementia	Above criteria with: Atypical course (sudden onset, insufficient historical detail, or objective progressive decline) or etiologically mixed presentation (meets all core clinical criteria, but has evidence of cerebrovascular disease, features of dementia with Lewy bodies, or evidence of another neurologic or non-neurologic disease or medication that could affect cognition).
Proven Alzheimer's dementia	Patient meets the clinical and cognitive criteria for AD dementia, and the neuropathologic examination demonstrates the presence of the AD pathology.

1.1.5 Non genetic risk and protective factors

As alluded to, there are a number of non-genetic risk and protective factors for AD. These non-genetic risk factors include cerebrovascular changes such as haemorrhagic infarction, ischemic stroke and vasculopathies. An association has also been discovered between mid-life incidence of hypertension and subsequent impaired cognitive functioning (Whitmer et al., 2005), potentially due to the effect hypertension has on the integrity of the blood-brain barrier (BBB) (Kalaria, 2010) which is an additional hallmark of AD. Type 2 diabetes (T2D) is

a well-documented non-genetic risk factor for AD, believed to almost double the risk of AD (Leibson et al., 1997). Lifestyle choice such as alcohol intake, body weight (both low and high) and smoking are both considered risk factors for AD. Protective non-genetic risk factors on the other hand show that a diet high in antioxidants and polyunsaturated fatty acids (PUFAs) reduce risk of AD. Moreover, high physical activity and intellectual activity are also associated with reduced AD risk.

1.1.6 Diagnostic neuropathology of AD

Whilst identification of clinical features associated with AD can aid in the diagnosis of AD, definitive diagnosis can only be confirmed after the death of a patient with clinical manifestations of the disease. These confirmatory diagnostic lesions consist of the cardinal pathologic features of AD, i.e. neuritic plaques and NFTs, as described in section 1.1 (see Fig 1.1 for post-mortem analyses of the temporal cortex of a patient with confirmed AD diagnosis, highlighting both neuritic plaques and NFTs). Diagnosis is also based on the density and morphology of the lesions, as well as their topographic distribution (DeTure and Dickson, 2019). Unfortunately, brain regions which are prone to AD pathological changes are also vulnerable to other diseases of the central nervous system (CNS) with mixed pathology, along with co-morbidities, a common problem. This may highlight the need to expand the diagnostic hallmarks in AD, with the help from clinical observations.

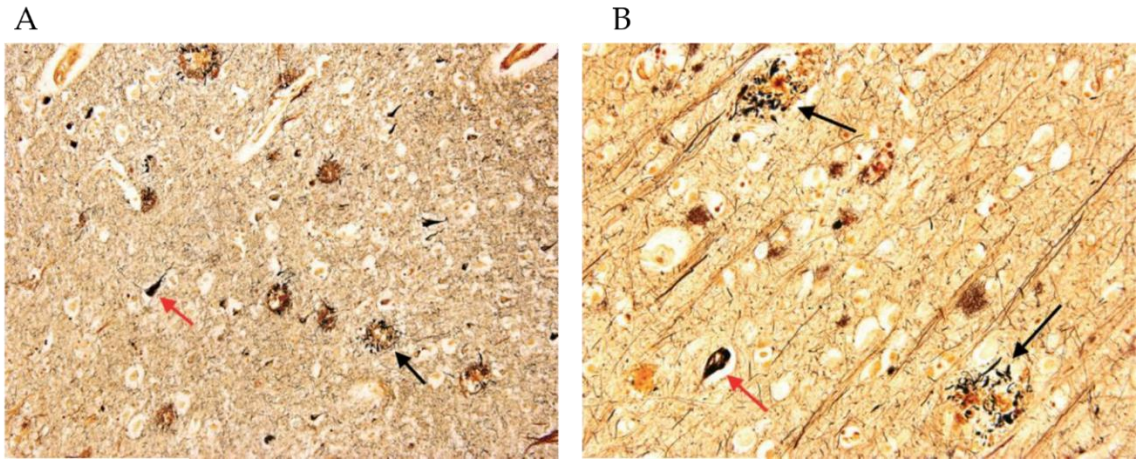

Figure 1.1 Neuropathological hallmarks in AD patients. Photomicrographs from the temporal cortex of an AD patient (using a modified Bielschowski stain; a silver staining method used to demonstrate neuritic plaques (black arrows) and NFTs (red arrows)). **A)** 40x magnification **B)** 100x magnification. From; Fig 1 & 2 (Perl, 2010).

1.1.6.1 Neuritic Plaques

The molecular composition of neuritic plaques consists primarily of Aβ, apolipoprotein E (ApoE; Yamaguchi et al., 1994), α1-antichymotrypsin, sulphated glycosaminoglycans, and complement factors (Verga et al., 1989). The Aβ peptide and its amyloid fibrillar form has been recognised as the pathological instigator of AD since the inception of the amyloid cascade hypothesis (ACH) almost 30 years ago (Hardy and Higgins, 1992b), driving all other pathological changes in AD. This hypothesis remains pervasive in the area of AD research, whilst undergoing numerous refinements as the understanding of AD pathogenesis grows. The Aβ peptide is formed through the sequential cleavage of the amyloid precursor protein (APP), a glycosylated integral type I transmembrane protein, expressed highly in the synapses of neurons. The precise biological function of APP is unclear, which has provided one of the most vexing problems in the AD field (O'Brien and Wong, 2011). APP is processed via two alternative pathways, namely the nonamyloidgenic and amyloidgenic pathways. Processing via the nonamyloidgenic pathway begins with α-secretase cleavage resulting in the release of sAPPα from the cell surface and a membrane tethered 83 amino acid α-C terminal fragment (C83/α-CTF). α-CTF is subsequently cleaved by γ-secretase, liberating the P3 peptide (Kahle and De Strooper, 2003). These cleaved proteins are largely considered benign in the pathology of AD and this signalling pathway has been identified as a potential therapeutic target in AD.

APP amyloidogenic processing begins with β-secretase (BACE1) cleavage at the N-terminus, resulting in a 99 amino acid CTF (C99/β-CTF) and the release of sAPPβ. β-CTF is subsequently internalised, undergoing additional processing by γ-secretase at various sites through endopeptidase/carboxypeptidase cleavage resulting in products of 43-51 amino acids. These fragments undergo final processing to become the main Aβ isoforms, namely Aβ40 and Aβ42 (Olsson et al., 2014; Takami et al., 2009), localized to endocytic compartments. Whilst Aβ40 is the most abundant isoform, Aβ42 has been identified as aggregation prone and is thus, the main constituent of neuritic plaques. Studies suggest that a high Aβ42/40 ratio is the key determining factor in amyloidogenesis rather than total Aβ load (Duering et al., 2005; Kim et al., 2007; Kumar-Singh et al., 2006). Unfortunately, in trials where Aβ burden has been successfully reduced, there has been little or no recovery of

cognitive decline (Cummings et al., 2019). γ-secretase cleavage of C99 also results in the release of an APP intracellular domain (AICD) where, upon translocation to the nucleus, is capable of inducing differential gene expression of targets that result in a cell death signal, such as glycogen synthase kinase-3β (GSK-3β), p53, and caspases 3 and 6 (Müller et al., 2008). A neurotoxic peptide, known as C31, is also produced following caspase cleavage of C99 (Lu et al., 2000). Due to the disappointing outcome of human trials targeting Aβ or γ-secretase, many in the field now consider AD to be more than simply an Aβ initiated disease.

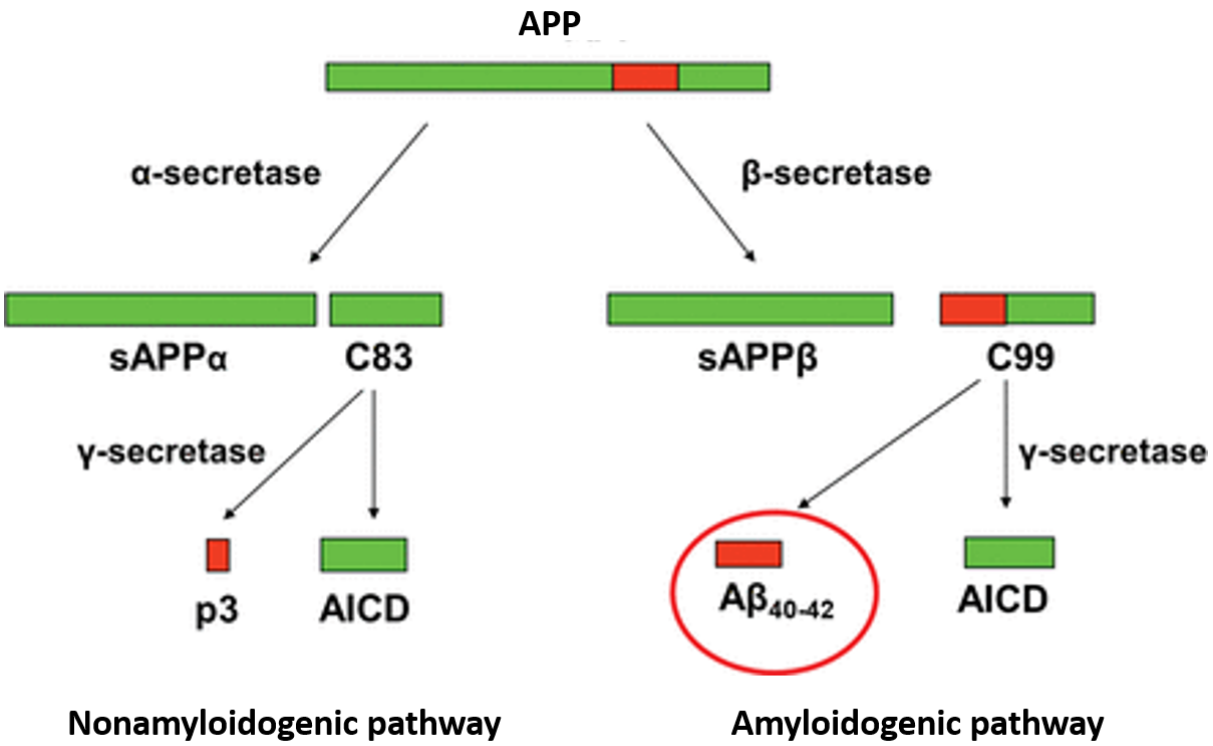

Figure 1.2 Schematic detailing Aβ generation through the sequential cleavage of APP. APP is processed via 2 alternative pathways, the nonamyloidogenic pathway (left) and the amyloidogenic pathway (right). The Aβ region of APP is indicated in red. Nonamyloidogenic processing begins with α-secretase cleavage within the Aβ region, resulting in sAPPα and C83/αCTF. C83/αCTF is subsequently cleaved by γ-secretase to form P3, and a membrane bound AICD. In amyloidogenic processing, APP is cleaved by β-secretase, resulting in sAPPβ and C99/β-CTF. C99/β-CTF is then further processed by γ-secretase to form Aβ40-42. Adapted from Figure 1. (Teich and Arancio, 2012)

1.1.6.2 Neurofibrillary Tangles

It was Alois Alzheimer himself whom identified the presence of degenerating neurons with the inclusion of bundles of intracellular fibrils (or NFTs). With the aid of electron microscopy, these NFTs were found to consist of abnormal filaments (Kidd, 1963; Terry, 1963) appearing to be wound helically around one another and thus became known as paired helical filaments (PHF). NFTs were also shown to include straight filament (SF), but these were present at much lower levels. The structural and molecular composition of these NFTs was not elucidated for several years due to their insolubility in denaturing agents. In 1985, tau (tubulin-associated unit) protein was found to be the main constituent of NFTs, both in crude extracts and histologically (Brion et al., 1985) and these aggregates were eventually found to be due to the hyperphosphorylation of the tau protein (pTau). Tau, as a major microtubule-associated protein, plays a crucial role in stabilising microtubules and promoting their assembly (Ma et al., 2017). Increased tau phosphorylation results from imbalanced regulation of various kinases and phosphatases. GSK-3β and protein phosphatase 2A (PP2A) are amongst those most implicated in the hyperphosphorylation of tau (Ma et al., 2017). Tau exists in six isoforms, of which all are found hyperphosphorylated and aggregated into NFTs in AD patients (Iqbal et al., 2010). In healthy patients, almost all tau is in a soluble state, however in AD brains it also recovered in a oligomeric and fibrillized form (Bancher et al., 1989). The precise molecular basis of pTau mediated toxicity is not completely understood, and whether oligomeric or highly polymerized PHFs cause more toxicity is also highly debated. The ACH holds that the hyperphosphorylation of tau is a secondary consequence of Aβ deposition.

1.2.1 Additional neuropathological hallmarks of AD

1.2.1.1 Neuroinflammation

As alluded to, the ACH supposes that Aβ is the main causative agent in the pathology of AD and the disease is viewed as primarily neural-centric. However, that basic tenet that AD is initiated by one pathological agent alone is being progressively challenged as the disease is becoming increasingly understood. For instance, other well-documented insults in AD include altered BBB integrity and neuroinflammation (Heneka et al., 2015). Indeed, some hold the view that neuroinflammation may be capable of instigating the onset of AD (Zhang et al., 2013), initiated by brain resident macrophages, or via the infiltration of peripheral immune cells, either through a jeopardized BBB or via alterations in the interactions between peripheral immune cells and the endothelial cells which line the BBB. This is further supported by the recent findings that immune receptor genes, such as triggering receptors expressed on myeloid cells (*TREM2*) (Guerreiro et al., 2013a) and *CD33* (Bradshaw et al., 2013; Griciuc et al., 2013) have been identified as AD risk loci. By definition, inflammation is a vital response to a range of harmful factors, including infection, disease and trauma. Non-pathogenic immune responses are initiated via pro-inflammatory pathways to the area where the insult occurred. Recruitment of these immune cells results in the initiation of a range of mechanisms, aimed at removing injurious stimuli and promote healing, such as phagocytosis of pathogens and debris and increased vascularization (Newcombe et al., 2018). Whilst the exact inflammatory response depends on the nature of the injurious stimuli and its precise location within the body, they in fact share common mechanisms

1.2.1.2 Brain resident contributors to neuroinflammation

1.2.1.3 Microglia

Microglia are the resident innate immune cells within the CNS and are maintained independently of peripheral immune cells. Alios Alzheimer noted that microglial cells had "developed numberous fibers" in the first described case of AD. However, it was not known whether this alteration was helpful, deleterious or inconsequential in the progression of AD. Now, it is generally accepted that unbridled microglial activation can be detrimental by directly mediating synaptic loss through phagocytosis (Spangenberg and Green, 2017) thus

disrupting normal cognitive function. Moreover, microglia are capable of releasing inflammatory mediators in response to synaptic injury and aggregating proteins such as neuritic plaques and NFTs. For instance, studies have shown that the NLR family pyrin domain containing 3 (NLRP3) inflammasome in microglia can be activated by Aβ peptides, *in vivo,* (Heneka et al., 2013) causing the release of the inflammatory cytokine interleukin-1β (IL-1β). Furthermore, NLRP3(-/-) mice carrying familial AD (fAD) mutations were protected from AD-associated sequelae (Heneka et al., 2013) (fAD mutations are described in section 1.3). There is also evidence that somatic mutations in erythromyeloid progenitor cells, from which microglia are derived, are capable of driving neurodegenerative processes in mouse models, with microglia activation preceding deposition of Aβ and synaptic loss (Mass et al., 2017).

1.2.1.4 Astrocytes

The most abundant glial cells within the CNS are astrocytes and they play a pivotal role in the regulation of neuroinflammation (Colombo and Farina, 2016). Early work showed that astrocytes associate with neuritic plaques in AD patients and more recently that astrogliosis is a pertinent feature of AD-like pathology in mice (Matsuoka et al., 2001) and AD pathology in patients (Nagele et al., 2003). These reactive astrocytes will phagocytose degenerated dendrites and synapses as a consequence of cytotoxic Aβ deposition and are subsequently co-localised with neuritic plaques. Exacerbation of the neurodegenerative process will also occur via the release of inflammatory cytokines such as interleukin-1 (IL-1), interleukin-6 (IL-6) and tumour necrosis factor (TNF)-α via astrocyte activation (occurring through either Aβ or damage signals) (Sajja et al., 2016). The precise mechanisms behind Aβ-induced astrogliosis remains incompletely understood, but astrocytes are known to express a range of receptors which bind Aβ, such as the receptor for advanced glycation end products (RAGE) and lipoprotein receptor related proteins (LRPs) (Ries and Sastre, 2016; Wyss-Coray and Rogers, 2012). Aggregation of Aβ has also been shown to promote the release of chemotactic molecules such as monocyte chemoattractant protein-1 (MCP-1), initiating the trafficking of astrocytes towards the deleterious Aβ aggregate (Smits et al., 2002; Wyss-Coray et al., 2003). However, whether this Aβ mediated astrogliosis is beneficial or detrimental remains an active area of debate. There are some which suggest that activated

astrocytes partake in Aβ clearance in mice (Koistinaho et al., 2004) with the clearance thought to be promoted by astrocytic release of the metzincin group of proteases such as matrix metalloproteinase (MMP)-2 and MMP-9 (Yin et al., 2006). However, others have suggested that astrocytes can promote the production of Aβ under some conditions of inflammation; for instance interferon-γ (IFN-γ) in concert with TNFα has been shown to promote Aβ production by enhancing astrocytic levels of BACE-1, APP, and secreted Aβ40 (Zhao et al., 2011). Ultimately, whether astrogliosis is detrimental or beneficial is entirely context dependant and future work must focus on this duality in order to develop effective therapeutic options.

1.2.2 Infiltration of peripheral immune cells in AD

1.2.2.1 Overview

As suggested, neuroinflammation can also occur via the infiltration of peripheral immune cells into the parenchyma of the CNS. To understand this process, it is important to understand the inflammatory response in other organs and tissue. Ultimately, the resolution of infection, disease or any injurious stimuli, requires peripheral immune cells to migrate to the site of damage. Initiation of inducible leucocyte migration can be triggered in a number of ways, for instance, in innate immunity, pattern recognition receptor (PRR)-bearing cells recognise pathogen-associated molecular pattern molecules (PAMPs) derived from invading microorganisms. Damage-associated molecular patterns (DAMPs), cell-derived signals, induce and perpetuate an inflammatory response to non-infections stimuli, such as tissue injury and cellular stress (Medzhitov, 2008). Antigen experienced T cells, or memory T cells, activated by cognate antigens can initiate the recruitment of immune cells through the secretion of a number of primary inflammatory cytokines (Nourshargh and Alon, 2014). Leucocyte migration is subsequently promoted by the detection of these cytokines by mast cells, macrophages and dendritic cells through the release of proinflammatory mediators.

The prerequisite of leucocyte transmigration into inflamed tissue is a sequential but overlapping series of events which involve margination, capture or tethering, rolling, slow rolling, arrest, adhesion strengthening and spreading, intravascular crawling and eventual transmigration, which can be achieved both paracellularly and/or transcellularly (Ley et al.,

2007). This phenomenon, termed the leucocyte adhesion cascade, is accomplished through the combined effort of chemoattractants and various leucocyte and endothelium expressed adhesion receptor families and their respective ligands (Ley et al., 2007). Broadly speaking, the lectin-like adhesion molecules, known as selectins, mediate the rolling of leucocytes along the endothelium, whereas the subsequent steps of adhesion and transmigration is mediated by leucocyte expressed integrins (the lymphocyte function-associated antigen-4 (LFA-4), and very late antigen-4 (VLA-4) and their interaction with EC expressed immunoglobulin-like adhesion molecules (e.g., intercellular adhesion molecule-1 (ICAM-1), vascular cell adhesion protein 1 (VCAM-1)) (Medzhitov, 2008). See Fig 1.3 for an overview of the leucocyte adhesion cascade.

1.2.2.2 The leucocyte adhesion cascade

1.2.2.2.1 Initiation of the inflammatory response

Initiation of the inflammatory cascade begins with recognition of PAMP/DAMP signals by cells of the innate immune system. These signals are recognised by both surface expressed and cytoplasmic PRRs, such as toll-like receptors (TLRs), C-type lectin receptors (CLRs), NOD-like receptors (NLRs) and RIG-I-like receptors (RLRS) (Iwasaki and Medzhitov, 2010; Takeuchi and Akira, 2010). PRR activation results in the transcriptional expression of pro-inflammatory genes, (via the translocation of transcription factors, such as NF-κb) (Medzhitov, 2008). Translational regulation of pro-inflammatory genes results in the release of various chemokines and cytokines (e.g. TNFα), acting as chemoattractants for circulating leucocytes.

Circulating immune cells are swept passively along in the bloodstream, through the centre of the vessel under laminar flow. The initial capture of circulating leucocytes signifies the first contact between immune cells with the activated endothelial wall following the radial migration of randomly distributed immune cells towards the venular walls in a process known as margination. The physical process of leucocyte margination is determined by simple flow dynamics, augmented by the interactions with erythrocytes in post capillary venules (where the low shear rates promote the axial aggregation of erythrocytes and thus the radial migration of leucocytes towards the EC layer). The activation of ECs in post-

capillary venules is a crucial step in the leucocyte adhesion cascade. Endothelial cell activation at the site of inflammation can occur rapidly (i.e. within minutes) and is induced by inflammatory stimuli such as histamine, resulting in the cell-surface expression of specialised adhesion molecules (e.g. P-selectin). EC activation can also be initiated more slowly (within hours) by a range of cytokines such as stromal derived TNFα and IFN-γ and induces the transcriptional activity of leucocyte-trafficking molecules. The rapid and slow modes of EC activation are termed type I and type II activation, respectively (Pober and Sessa, 2007). Ultimately, EC activation results in the expression of adhesion molecules and chemokines where marginalised leucocytes sampling the EC layer are subsequently co-ordinated from these positional cues. These induced adhesion molecules form transient bonds with their leucocyte expressed counter ligands and are responsible for the tethering of leucocytes from flowing blood and include a member of the immunoglobulin super-family (IgSF), VCAM-1 and E- and P-selectin.

1.2.2.2.2 Rolling and Selectins

As described above, the type-I transmembrane Ca^{2+}-dependant lectins of the selectin family of cell adhesion molecules mediate the first adhesive step in the leucocyte adhesion cascade. Under flow conditions, the rapid association and dissociation of interactions between selectins and their ligands supports a dynamic and characteristic type of adhesion, termed rolling (Alon et al., 1995) which is not dependant on leucocyte activation. These transient interactions allow sufficient reduction in the velocity at which leucocytes roll on endothelial cells for the subsequent step of the cascade. P-selectin is expressed by both, ECs; in preformed pools in Weibel-Palade bodies and in the membranes of α-granules of platelets (McEver, 2015). Rapid mobilisation of P-selectin to the plasma membranes of ECs requires stimulation by the mediators histamine or thrombin (Geng et al., 1990; Hattori et al., 1989) and can also be initiated by reactive oxygen species (ROS) (Cucullo et al., 2011). Transcription dependant increase in P-selectin mRNA can be achieved in most mammals by TNFα or Il-1β, but is not seen in humans (Liu et al., 2010b; Yao et al., 1999). Synthesis of E-selectin, another EC expressed molecule, usually requires TNFα or IL-1β stimulation in humans (Vestweber and Blanks, 1999), although it has been shown to be constitutively expressed on venular EC cells of bone marrow and skin. Another member of the selectin

family, L-selectin, is a leucocyte expressed adhesion molecule and is constitutively present on the tips of microvillus cell surface protrusions (Smith et al., 1991), facilitating the presentation of L-selectin on circulating leucocytes to their counter ligands expressed on ECs. L-selectin binds a range of distinct EC expressed mucins, including glycosylation-dependent cell adhesion molecule-1 (GlyCAM-1) and mucosal addressin cell adhesion molecule 1 (MAdCAM-1) which contain the typically O-linked Sialyl Lewis X (sLe^X): the minimal structural determinant for L-selectin ligands (Ivetic et al., 2019). Leucocyte activation through L-selectin binding results in the proteolytic cleavage of the molecule. The transmembrane homodimeric mucin, P-selectin glycoprotein-1 (PSGL-1) is primarily a leucocyte expressed counter receptor for the EC selectins E- and P-selectin and the co-expressed L-selectin during secondary capture by adhered leucocytes. However, it has also been shown to be present on certain ECs (da Costa Martins et al., 2007; Rivera-Nieves et al., 2006). As well as PSGL-1, E-selectin has been shown to bind E-selectin ligand 1 (ESL-1) and CD44 (Hidalgo et al., 2007). The subsequent slowing of leucocytes as a result of these interactions is eventually sufficient for the cells to receive additional signals from mediators, such as platelet-activating factor (PAF) and leukotriene-B4 (LTB4) (Bélanger et al., 2008) or immobilized chemokines expressed on the apical surface of the ECs (Luu et al., 2000; Rainger et al., 1997). Upon receipt of these activating stimuli, the integrin adhesion molecules become activated, resulting in slower rolling and eventual arrest (Ley et al., 2007).

1.2.2.2.3 Integrins

Integrins are a family of heterodimeric adhesion molecules consisting of one α- and one β-unit (Hogg et al., 2011) which upon activation (e.g. via chemokines or PSGL-1 ligation) mediates the cell adhesion event in the leucocyte adhesion cascade. Classically, integrins were considered to participate in this event alone, but growing evidence indicates that they also participate in rolling events at the endothelium. For instance, $\alpha_4\beta_7$-intergin expressing cell lines will roll, under laminar flow conditions, on immobilized recombinant mucosal vascular addressin cell adhesion molecule 1 (MAdCAM-1) and the leucocyte expressed VLA-4 can engage immobilized VCAM-1 to support rolling in the absence of selectin contribution (Berlin et al., 1995). Within the venules of the CNS, VLA-4 can also support leucocyte rolling in concert with P-selectin (Kerfoot and Kubes, 2002) or firm adhesion in

absence of P-selectin (Vajkoczy et al., 2001). Specifically, it appears integrins mediate slow rolling events in the cascade: *in vivo*, slow rolling requires both E-selectin (Kunkel and Ley, 1996) and the β2 integrins, LFA-1 or macrophage receptor 1 (MAC-1) (Dunne et al., 2002).

Leucocyte firm adhesion has been shown, both *in vivo* and *in vitro*, to require integrin activation. Initiation of this event begins with the expression of adhesion molecules and the release and synthesis of various chemoattractants and chemokines by inflammatory cytokine-activated ECs. Chemoattractants can also be deposited on ECs by some activated immune cells through proteolytic cleavage. For instance, platelets have been shown to release both CC-chemokine ligand 5 (CCL5) and CXC-chemokine ligand 4 and 5 (CXCL4 and CXCL5) onto activated ECs, leading to the monocyte arrest (von Hundelshausen et al., 2001; Huo et al., 2003). Arrest is mediated by the activation of G protein coupled receptors (GPCRs) in response to chemokine deposition Integrins dynamically regulate their adhesiveness via a mechanism called "inside-out signalling". Integrin activation, mediated by GPCR activation shifts its conformation from a bent-closed (inactive) state to an extended-open state (Nishida et al., 2006), exposing their ligand binding site and subsequent interaction with their respective ligands, such as ICAM-1 or VCAM-1 (Mitroulis et al., 2015). The conformational state of the integrin subunits regulates the strength of the bond between an individual integrin and its corresponding ligand, described as integrin affinity. Integrin valency is governed by receptor-ligand clustering or density. Affinity and valency, taken together, describes overall integrin avidity, thus determining the overall strength of cellular adhesiveness (Carman and Springer, 2003).

1.2.2.2.4 Transendothelial cell migration

The final event in the leucocyte adhesion cascade is termed transendothelial migration (TEM) and defines the method by which immune cells emigrate into inflamed tissues. This can occur both paracellularly (i.e. between the junctions of ECs) or transcellularly (i.e. through the body of an individual EC). The precise route taken by immune cells may be determined by the tightness of the EC junction, with the cells taking the route that will provide the least resistance. In both cases, rolling immune cells will firstly identify regions within the EC where they can preferentially extravasate and is termed intraluminal crawling or "locomotion". The directionality of this process is guaranteed by the presentation of a

chemotactic gradient formed at the EC surface and also relies on interactions between MAC-1 and ICAM-1. This chemotactic gradient is created by localised chemokine release and attracts crawling immune cells to preferred regions for TEM. These cells then overcome the ECs themselves, the basement membrane, and eventually the pericytes. However, it is worth noting that not all leucocytes that roll will eventually adhere and not all firmly adhered cells will eventually emigrate (Muller, 2015), adding an extra layer of complexity to the TEM process. Immune cells will traverse in an amoeboid fashion (Marchesi, 1961; Marchesi and Florey, 1960), to maintain the integrity of the EC barrier (Winger et al., 2014).

The TEM of leucocytes will occur predominantly between endothelial cells (i.e. paracellularly) and is largely irreversible (Muller, 2013). Whilst the alternative path (i.e. transcellular migration) is less understood, the two routes share some common mechanisms. In contrast to the heterophilic interactions of the preceding steps of the adhesion cascade, TEM interactions are largely homophilic (Muller, 2013). Several molecules, such as VCAM-1, ICAM-1 and JAMs are involved in the preceding steps of TEM (i.e. firm adhesion) which is a fundamental prerequisite for migration. Thus, during both paracellular and transcellular transmigration, VCAM-1 and ICAM-1 binding to their respective integrins is the leading event (Williams et al., 2011) for effective TEM, with VCAM-1 and ICAM-1 becoming enriched on microvilli-like projections which surround emigrating leucocytes on the apical side of the endothelium, causing leucocyte expressed integrins to redistribute in a linear fashion, parallel to the direction of TEM (Carman and Springer, 2004). Both JAM-A and JAM-C molecules are concentrated at EC borders and are ordinarily involved homophilic interactions. During inflammation, however, JAM-A can bind the leucocyte expressed LFA-1 (Ostermann et al., 2002) and JAM-C can adhere to both JAM-B and CD11b/CD18 (Muller, 2013). The aforementioned interaction is thought to be involved in paracellular TEM *in vivo* (Chavakis et al., 2004), and *in vitro* (Johnson-Léger et al., 2002).

The first molecule shown to exclusively mediate paracellular TEM both *in vivo* (Bogen et al., 1994; Vaporciyan et al., 1993), and *in vitro* (Muller et al., 1993), was PECAM-1. PECAM-1 is condensed at the EC borders and diffusely expressed on the surface of leucocytes. CD99 shares a similar expression pattern and has also been shown to support the TEM of immune cells both *in vivo,* (Bixel et al., 2010) and *in vitro* (Schenkel et al., 2002). Vascular permeability

is maintained by leucocyte encapsulation in endothelial domes (Phillipson et al., 2008). Engagement of ICAM-1 can also lead to the disassembly of VE-Cadherin in mice (Schnoor et al., 2011) with VE-Cadherin an important molecule in the maintenance of tight junction between ECs. Once immune cells have overcome the EC layer, studies have shown that they will continue to crawl between the abluminal layer of the EC and pericytes in a MAC-1 and LFA-1 dependant fashion (Proebstl et al., 2012). The final stage, emigrating past the basement membrane (BM) requires immune cells to detach their tails from the basolateral side of the BM; how this is achieved is unclear, but recently, a role for very late antigen-3 (VLA-3) has been suggested (Hyun et al., 2012).

As discussed, direct, *in vivo* observations support the notion that immune cells will preferentially transmigrate via a paracellular route; however, increasing evidence indicates that leucocytes can also pass directly through an individual EC (transcellularly). Moreover, leucocytes may prefer this route in regions of tight EC junctions, such as those found at the BBB. Whilst transcellular TEM is less understood, it requires, at a minimum, displacement of cytoplasmic organelles within the EC and merging of both the apical and basal plasma membranes. Moreover, transcellular TEM could be instigated by immune cells, the ECs, or through a combinatory effort of both. The displacement of EC organelles by the leucocytes themselves may be achieved through actin-dependant protrusive structures such as lamellipodia, filopodia, podosomes ("foot protrusions") or invadopodia (Buccione et al., 2004; Linder and Aepfelbacher, 2003; Ridley et al., 2003; Yamaguchi et al., 2005). Evidence for this supposition has been demonstrated by Carman and colleagues (2007) both *in vivo* and *in vitro*, where immune cells inserted podosomes, whilst extending invasive podosomes, similar to invadopodia, into the EC surface. Moreover, *in vitro*, studies have shown that ICAM-1 redistributes and becomes concentrated at the site of transmigration and enriched in the channel surrounding the extravasating immune cell (Carman et al., 2007; Mamdouh et al., 2009). Similarly to paracellular TEM, molecules previously considered to be restricted to EC borders, such as PECAM-1, JAM-A and CD99, surround immune cells extravasating transcellularly (Muller, 2013) and appear functional. Blocking of PECAM-1 and CD99 inhibits the transcellular TEM of immune cells (Mamdouh et al., 2009).

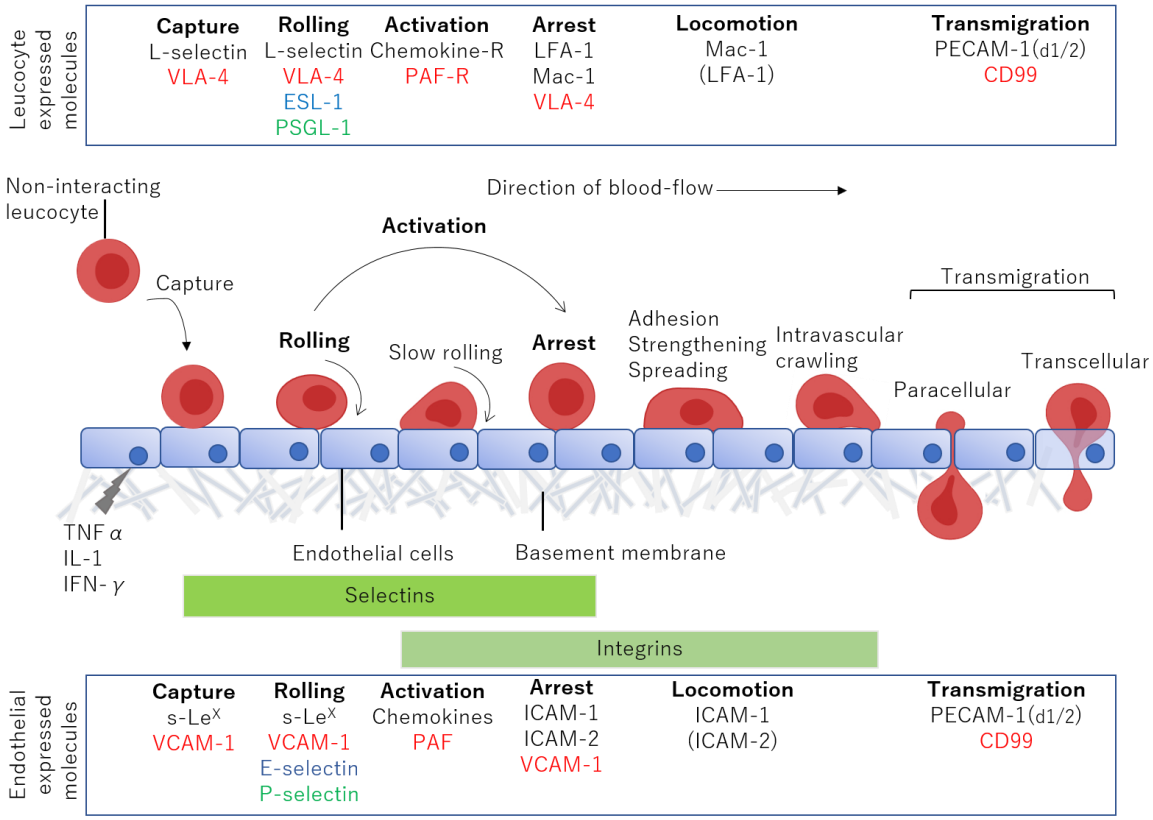

Figure 1.3 Schematic delineating the multistep adhesion cascade and molecular contributors of leucocyte recruitment. Following chemokine mediated endothelial cell activation, expression of molecules such as E- and P-selectin increase, resulting in low affinity adhesive interactions (capture and rolling). This in turn leads to the activation of leucocytes, firm adhesion and transendothelial migration. Each step in the inflammatory cascade is mediated by specific leucocyte expressed molecules interacting with their counter-receptors on ECs. Interacting molecules at each step are depicted in the same colour. Parentheses indicate that these molecules have not been verified *in vivo*. Please note, the full range of molecules mediating the leucocyte adhesion cascade is not depicted here, but is reviewed elsewhere (Ley et al., 2007).

1.2.2.3 The BBB and the leucocyte adhesion cascade

1.2.2.3.1 Overview

The BBB is a highly selective, semi-permeable membrane which grants the brain immune privilege by separating the circulatory system from the brain. The integrity of the BBB barrier can be jeopardized as a result of extrinsic pathological agents such as bacterial meningitis or in diseases such as amyotrophic lateral sclerosis (Rosenberg, 2011) and can result in infiltration of neurotoxic plasma derived proteins, pathogens and leucocytes. This invasion can cause neuroinflammation and further damage to the brain parenchyma.

Increased BBB permeability and immune activation, as described, are well-documented, deleterious insults within the CNS of AD patients. Both CD2-associated protein (*CD2AP*) and phosphatidylinositol clathrin assembly protein (*PICALM*) genes are leading susceptibility loci for the development of LOAD and both *CD2AP* (Cochran et al., 2015) and *PICALM* (Zhao et al., 2015) have been suggested to assert their risk through influencing the integrity of the BBB - potentially providing a *de facto* route for therapeutic intervention.

1.2.2.3.2 The blood brain barrier

The non-fenestrated vessels of the CNS contain unique properties which allow them to regulate the transport of various ions, molecules and cells between the periphery and the CNS, thus supporting CNS homeostasis. Two main cell types comprise blood vessels, namely ECs which comprise the blood vessel walls, and pericytes which cover capillaries on the abluminal surface of the endothelial layer. Additionally, immune cells and astrocyte foot projections provide additional cellular support to the BBB. The BM, a non-cellular component of the BBB, is involved in cell anchoring, structural support and signal transduction, although recent evidence may point to a role in maintaining BBB integrity (Xu et al., 2019). Between the BM and neuronal cells is an area referred to as the Virchow-Robin space where microglia reside. Together, these structures are referred to as the neurovascular unit (NVU, Fig 1.4) (Serlin et al., 2015)

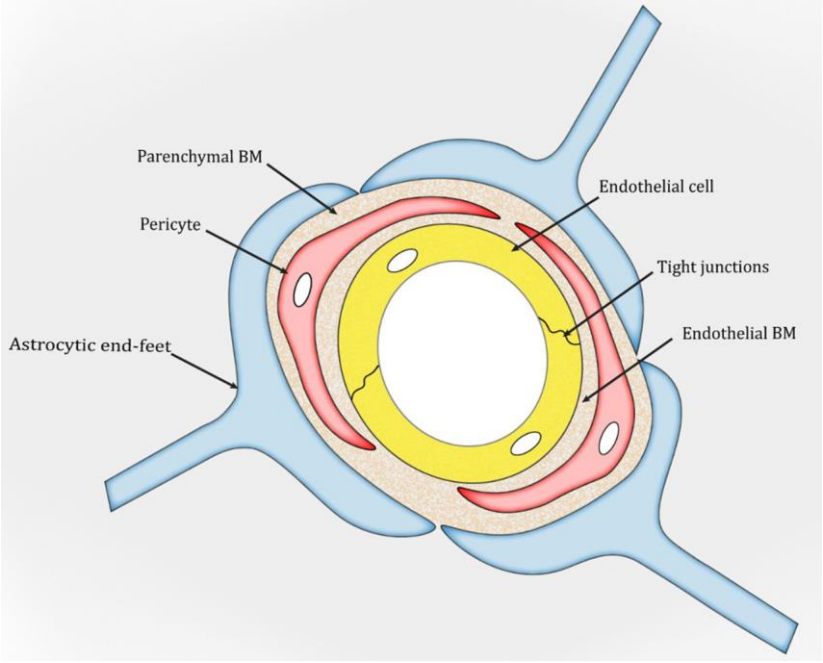

Figure 1.4 Schematic depicting the cellular and non-cellular constituents of the BBB. BM, basement membrane. From Fig. 1 (Xu et al., 2019).

1.2.2.4 Junctional complexes

1.2.2.4.1 Tight Junctions

BBB capillaries are comprised of a single layer of mesoderm derived squamous ECs. To selectively restrict paracellular diffusion of material from the CNS, ECs are sealed by tight junctions (TJs), forming continuous intercellular contact (Van Itallie and Anderson, 2006). The TJ represent the most apical intercellular junctional complex in endothelia and are dynamic structures containing both transmembrane and membrane-associated cytoplasmic proteins. The primary biological roles of TJs consist of: maintaining cell polarisation by occluding the lateral diffusion of integral membrane proteins and lipids (Cereijido et al., 1998), restricting the paracellular diffusion of unwanted polarised bloodborne substances (Tsukita et al., 2001) and provide a means for intercellular signalling (Luissint et al., 2012).

The transmembrane proteins which comprise the TJ include claudins, occludin and junctional adhesion molecules (JAM)-A, B and C (Redzic, 2011). Occludin, a 65kDa integral membrane protein, is considered essential for correct barrier functioning of TJs. Structurally, it contains two extracellular loops, with the second loop purported to determine the transendothelial electrical resistance (TEER) of the BBB (Feldman et al., 2005). The TEER at

the BBB is approximately 1500 Ω cm^2 (plial vessels), almost 50-fold higher than other tissues (Crone and Christensen, 1981), providing the vital high electrical resistance essential for the correct barrier functioning of the BBB. The 150 aa C-terminal region of occludin, binds the scaffold proteins zona occludens (ZO) 1, ZO-2 and ZO-3 (which provide cytoskeletal anchorage for TJ proteins), with the 27 aa coiled stretch of the C-terminus shown to interact with regulatory proteins such as the p85 subunit of phosphoinositide 3-kinase (PI-3K), protein kinase C (PKC), and connexin 26, a gap junction component (Feldman et al., 2005). Claudins, tetraspan transmembrane proteins, provide structural barrier formation. This is carried out by neighbouring claudins from opposing ECs providing TJ strand formation via homophilic interactions (Piontek et al., 2008). The most enriched claudin at the BBB is claudin-5, more highly expressed at hundreds of times the order of other BBB expressed claudins (namely claudin-1, 3 and -12) (Krause et al., 2008). JAM-A, B and C are present at the intracellular junctions of brain ECs (BECs) and studies have shown that they are able to control cell permeability and increase the BBBs resistance to macromolecules; for instance, monoclonal antibodies to the ECD of JAM-A increases vascular endothelial permeability in the T84 epithelial cell line (Liu et al., 2000). It has been shown that the loss of BBB integrity through tight junction alterations is a risk factor in AD.

1.2.2.4.2 Adherens Junctions

Adherens junctions (AdJs) contain Ca^{2+} dependant transmembrane proteins known as cadherins. Cadherins mediate homophilic adhesion and can organize multimeric complexes at cellular borders (Bazzoni and Dejana, 2004) with VE-cadherin the most abundantly expressed cadherin in brain endothelial cells, followed by low expression of the N- and E cadherins (Abbruscato and Davis, 1999; Luo and Radice, 2005). Part of the AdJ also comprises cytoplasmic proteins which are formed by a complex of p120, β-catenin and γ-catenin/plakoglobin. Both β- and γ- catenin link α-catenin, anchoring the complex to actin (Ben-Ze'ev and Geiger, 1998; Vleminckx and Kemler, 1999). The src substrate, p120, binds the membrane proximal tail of VE-Cadherin and supports the stabilization of AdJs.

1.2.2.4.3 Gap Junctions

Cx37, Cx40 and Cx43 are brain endothelial expressed members of the connexin (Cx) family of proteins that form the gap junctions (GJs) in the BBB (Stamatovic et al., 2016). These connexins are oligomerized in the endoplasmic reticulum (ER)/Golgi and before their eventual plasma membrane localisation to form GJs. Opposing hexamers on neighbouring cells come together to form proper GJ function, functions which include intercellular communication (Stamatovic et al., 2016). cX43 in particular has also been shown to be important in migration by interfering with cytoskeletal remodelling, tubulin dynamics and receptor signalling, (Kameritsch et al., 2012) and cellular proliferation (Ionta et al., 2009)

1.2.2.5 Leucocyte adhesion cascade at the BBB

Historically, leucocyte migration into the CNS has been investigated in the context of stroke and multiple sclerosis (MS). The transmigration of peripheral immune cells into the brain parenchyma can occur through several routes from peripheral blood: via the choroid plexus; to the subarachnoid space via meningeal vessels and lastly via the parenchymal perivascular spaces (Ransohoff et al., 2003). Immune cells trafficking through the BBB follows the paradigm of the leucocyte adhesion cascade as described in section 1.2.2.2. However, as described, the endothelial layer and the astrocytic end feet, which form the glia limitans represent barriers to cellular entry into the CNS allowing strictly controlled inflammatory responses. Thus, the mechanisms by which emigration is achieved will alter slightly from the classical view of the adhesion cascade. The specialized structure means that eventual migration into the brain parenchyma requires migration across the BBB and then overcoming the glia limitans, requiring the expression of glycosidases and proteases to allow degradation of BM molecules.

Immune responses in the CNS can be driven by endogenous (i.e. glial activation), as described, and/or via exogenous (i.e. peripheral immune cells) factors. In AD, neuroinflammation has generally focussed on explaining brain resident macrophage instigation of the disease. However recent work has described the potential AD initiation in terms of a break down in the integrity of the BBB; with accelerated degeneration seen in patients with MCI (Montagne et al., 2015) and vasculature deposition of Aβ can also cause

changes in BBB integrity through pro-inflammatory and cytotoxic events (Erickson and Banks, 2013). Vascular dysfunction can also result from peripheral immune infiltration into the brain parenchyma. It has been shown that inhibition of neutrophil trafficking through blockade of the leucocyte expressed integrin LFA-1 can reduce AD-like pathology and cognitive dysfunction in mice (Zenaro et al., 2015a) with adhered leucocytes releasing inflammatory mediators and neutrophil extracellular traps (NETs). NETs are believed to damaging the integrity of the BBB and neuronal cells (Pietronigro et al., 2017), exacerbating neuroinflammatory processes.

Upon initiation of the inflammatory events, ECs of the leptomeningeal brain microvessels upregulate a range of signals to initiate leucocyte rolling along the endothelium. The initial tethering and rolling is mediated by leucocyte expressed PSGL-1 and T-cell immunoglobulin and mucin domain 1 (TIM-1) and its EC expressed ligand P-selectin and E-selectin respectively (Engelhardt and Ransohoff, 2012). Integrins associated with CNS TEM include VLA-4, LFA-1 and MAC1, which bind VCAM-1, ICAM-1 and ICAM-2 respectively (Zenaro et al., 2017). Unfortunately, the role of peripheral immune cells in AD pathogenesis is poorly understood and predominantly investigates this phenomenon as a secondary consequence of Aβ deposition, showing that the ACH is still the driving force behind much of the recent literature on AD neuropathology. For instance, Aβ has been shown as a chemotactic agent for monocytes, allowing their extravasation through the chemokine-ligand 2 (CCL2)-chemokine receptor 2 (CCR2) axis (Mildner et al., 2007). Aβ results in the secretion of proinflammatory mediators in a BBB model involving RAGE, the Aβ receptor, and endothelial expressed platelet and endothelial cell adhesion molecule-1 (PECAM-1) (Fiala et al., 1998; Giri et al., 2000). In addition, both neutrophils and T cells accumulate in the brains of AD patients; although the mechanisms behind this infiltration is still unclear. AD patients have been shown to overexpress macrophage inflammatory protein (MIP)-1α, promoting T cell extravasation through EC TJs, by binding CCR5 (Man et al., 2007) on ECs; and also overexpress C-X-C chemokine receptor type 2 (CXCR2) potentially promoting TEM (Liu et al., 2010a). Ultimately, research must focus on whether the infiltration of immune cells into the CNS is an epiphenomenon in the pathogenesis of AD. Whatever the mechanism, the infiltration of these immune cells can be cytotoxic to neurons and either initiate or exacerbate the neuropathological manifestation of AD. In fact, recent genetic findings have

suggested a direct role in some variants associated with AD which might directly instigate the onset of AD neuroinflammation, for instance, *TREM2* and *CD11*

1.3 The genetics of AD

This chapter has so far described the traditional manner in which AD has been characterised, namely delineating EOAD and LOAD primarily by the age-of-onset. From a genetic perspective, AD is categorised by their mode of inheritance, falling into either Mendlian/familial AD (fAD) or sporadic AD (sAD). EOAD accounts for approximately 5.5% of all AD cases (Zhu et al., 2015a) of which only around 5-10% of these follow the autosomal dominant inheritance or fAD (Jarmolowicz et al., 2015), which represents just 1% of all AD cases. Early-onset fAD has been linked to highly penetrant variants in *APP*, Presenilin 1 (*PSEN1*) and Presenilin 2 (*PSEN2*, Dai et al., 2018). However, the genetic background of the majority of Mendelian EOAD and sporadic EOAD (accounting for ~5% of all early onset cases) remains unexplained (Janssen et al., 2003; Jarmolowicz et al., 2015; Wallon et al., 2012). Accounting for the vast majority of AD cases (~95%), sporadic AD is predominantly associated with late-onest AD, although familial forms have been identified (Abbate et al., 2016). With the advent of powerful genome wide-association studies (GWAS), knowledge of the genetic risk factors of sporadic LOAD has advanced greatly.

1.3.1 Familial Alzheimer's disease

1.3.1.1 Amyloid Precursor Protein

The *APP* gene encodes the Aβ precursor protein, which following BACE1 and γ-secretase processing gives rise to the Aβ peptide. It was this finding that first implicated *APP* in the aetiology of AD, with recent knowledge suggesting that APP mutations account for 13-16% of all fAD cases (Janssen et al., 2003; Raux et al., 2005). *APP* is located on chromosome 21q21.3, consisting of 19 exons. The precise biological function of APP is not fully understood, however studies have pointed to a role in synaptic development (Priller et al., 2006), neuronal migration (Young-Pearse et al., 2007) and controversially, acting as a cell surface receptor (Thinakaran and Koo, 2008). To date, there have been over 30 identified risk variants, with mutations identified predominantly within or adjacent to the Aβ domain. APP duplications are sufficient to cause fAD, due to increased production and aggregation of Aβ42 (as well as Down's syndrome, where patients develop AD-type pathology) (Hooli et al., 2012; Sleegers et al., 2006). See section 1.1.6.1 for an overview of the potential impact of

amyloidogenic processing that can occur from aberrant processing of APP due to *APP* mutations.

1.3.1.2 The presenilins

The presenilin genes, *PSEN1* and *PSEN2* are highly homologous genes which, importantly, encode vital catalytic components of the APP cleavage complex, γ-secretase. The structural homology is estimated at 67%, both containing 12 exons and ~450 aa (Rademakers et al., 2003). The greatest percentage of fAD cases can be attributed to mutations in the *PSEN1* gene (Kelleher et al., 2017), with estimates in the range of ~20-50% (Ridge et al., 2013a). *PSEN1* mutations are known to cause the most severe manifestations of AD, with disease occurring as early as 25 years of age, in some cases (Cruts et al., 2012) but have a wide age-of-onset variability (25-65 years). This is most likely due to the vast number of *PSEN1* mutations which have been identified, approximately 220 in total. *PSEN1* is located on chromosome 14 (14q14.3) and has at least 2 isoforms. The precise mechanisms by which *PSEN1* results in fAD is not completely understood. However, some early studies reported a potential gain-of-function mechanism resulting in increased levels of the aggregate prone Aβ42 in the plasma of fAD patients, as well as transgenic mice and *PSEN1* transfected cells, presumably the result of enhanced proteolysis of APP. Revision of the ACH which proposed that it was in fact the relative levels of Aβ42/Aβ40 altered this hypothesis slightly (Selkoe and Hardy, 2016), with the supposition being that mutations in *PSEN1* increased the Aβ42/Aβ40 ratio either through impeding γ-secretase sequential cleavage of longer Aβ peptides an thus increasing overall levels of Aβ42 (Wolfe, 2007), or by decreasing levels of the Aβ40 peptide (Sun et al., 2017; Xia et al., 2015), depending on the mutation present. *PSEN2*, located on chromosome 1 (1q42.13) and similarly to *PSEN1* is alternatively spliced into 2 isoforms, Mutations in *PSEN2* are thought to assert their AD risk via a similar mechanism as that of *PSEN1* variants, due to their roles in complex formation of γ-secretase (Cai et al., 2015)

1.3.2 Sporadic Alzheimer's disease

Accounting for over 95% of all AD cases, sAD cases are known to predominantly result in a late-onset form of AD (Zhu et al., 2015b). Until 2009, only one susceptibility locus was

identified for sAD, namely apolipoprotein E (*ApoE*) with the remaining genetic risk factors undetermined. However, the genetic epidiomiology of sAD has advanced rapidly over the last decade with the help of high-powered GWAS. To date, >20 susceptibility loci have now been identified (Lambert et al., 2013), cementing the view that Alzheimer's disease is a truly polygenic disorder. It is with this discovery that gene-based therapeutics may become a possibility in the future and also begs the question of whether all these genetic variants can have one detrimental outcome, i.e. the deposition of Aβ plaques.

1.3.2.1 Apolipoprotein E

Human ApoE, a ~34kDa, 299 aa protein encoded by the ApoE gene, binds and transports cholesterol and other lipids through the lymphatic and circulatory systems and is predominantly expressed in the liver, brain as well as in macrophages and monocytes. There are three major allelic variants of *ApoE* at a single gene locus in humans, ε2, ε3 and ε4 (Das et al., 1985), with differential expression related to two nonsynonymous single nucleotide polymorphisms (SNPs), rs429358 and rs7412 within exon 4 of the *ApoE* gene, corresponding to the N-terminal domain of the encoded protein. This differential expression results in three heterozygous (ε2/ε3, ε2/ε4 and ε3/ε4) and three homozygous ε2/ε2, ε3/ε3, ε4/ε4) phenotypes causing three possible protein isoforms (E2, E3 and E4). The rs429358 SNP, associated with the *ApoE* ε4 allele, has shown to be strongly associated with the risk of developing sAD in dose dependant manner (Corder et al., 1993). Heterozygous ε4 carriers increases AD risk by up to 3-times, whereas homozygotes (ε4/ε4) have a risk almost 8-12 times compared to that of ε2 carriers (Verghese et al., 2011), with the ε2 allele considered protective (West et al., 1994). Whilst *ApoE* allelic frequencies can vary by demographics, the most frequent allele is the ε3 with estimates in the range of 30-90%, and ε4 and ε2 frequencies in the range of 5-35% to 1-5%, respectively (Mahley and Rall, 2000). Associated risk of ApoE alleles is ε4>ε3>ε2, with ε4 homozygosity present in 50% of all AD patients (Farrer et al., 1995).

Post mortem analysis of AD brain tissue found a positive correlation between *ApoE* ε4 allele dose and Aβ plaque burden (Rebeck et al., 1993). Moreover, Aβ plaque burden in healthy patients increases in an ε4 dose dependant manner using the amyloid imaging tracer, Pittsburgh Compound B (PiB) (Reiman et al., 2009). ApoE has also been implicated in clearance of monomeric Aβ; *in vivo*, ApoE ε4 mouse models exhibit higher levels and slower

clearance of Aβ in their interstitial fluid (ISF) when compared to ApoE ε3 mice (Castellano et al., 2011). Even with evidence of association between ApoE and Aβ, the precise mechanism by which it exerts AD risk is unclear but will likely remain a complex area of investigation. Beyond the relationship between ApoE ε4 and Aβ deposition and clearance, recent studies have highlighted roles in tau phosphorylation (El Haj et al., 2016), neuronal maintenance and repair (Kim et al., 2014) and neuroinflammation and ε4 mediated impairment in lymphatic drainage of the brain (Weller et al., 2015) and thus it is likely that *ApoE* ε4 contributes to all AD-associated neuropathology (Tzioras et al., 2019). It is clear that *ApoE* has a complex role in AD pathogenesis and developing effective therapies may require a shift in focus to additional neuropathological hallmarks.

1.3.3 Common variants associated with Alzheimer's disease

The genetic underpinnings of sAD have been significantly advanced through the work of large-scale collaborative GWAS and the landmark International Genomics of Alzheimer's Project (I-GAP) meta-analysis. 11 new susceptibility loci for sAD were identified through GWAS meta-analysis and genotyping; stage 1 consisted of 17,008 sAD cases and 37,154 controls. This was later replicated in an independent sample of 8,572 sAD cases and 11,312 controls (Lambert et al., 2013). This landmark paper paved the way for functional studies on newly identified AD risk loci.

Until 2009, ApoE was the only confirmed risk gene associated with sAD. Through the work of 2 large GWAS studies, 3 additional susceptibility loci were identified. Variants were found in or near the *CLU*, *CR1* and *PICALM* genes (Harold et al., 2009; Lambert et al., 2009). In the intervening 5 years, additional susceptibility loci were identified: *BIN1* (Seshadri et al., 2010), *EphA1*, *CD2AP*, *ABCA7*, *MS4A/MS4A6E* (Hollingworth et al., 2011; Naj et al., 2011), *PTK2B*, *HLA-DRB5/HLA-DRB1*, *CELF1*, *SORL1*, *ZCWPW1*, *RIN3*, *FERMT2*, *CASS4*, *INPP5D*, *NME8 and SLC24A4* (Lambert et al., 2013). More recently, genome wide gene wide analyses using the I-GAP dataset, have identified an additional genome-wide significant loci in AD, *TP53INP1*, *IGHV1-67* (Escott-Price et al., 2014), *PPARGC1A*, *RORA* and *ZNF423* (Baker et al., 2019). Building further on the IGAP dataset, further genome wide susceptibility loci have been identified, *TRIP4* (Ruiz et al., 2014), *ECHDC3* (Jun et al., 2017; Kunkle et al., 2019) , *IQCK*, *ACE*, *ADAM10* and *ADAMTS1* (Kunkle et al., 2019). Despite GWAS studies

advancing our understanding of the genetic underpinnings of AD; much of it remains unexplained, with estimates in the range of 60% not accounted for by *ApoE* or common susceptibility loci (Ridge et al., 2013b). The remaining "missing heritability" is likely due to the difficulty in the detection of rare variants with larger effect sizes than common variants.

1.3.4 Rare variants associated with AD

Rare variant identification is usually achieved through whole genome sequencing (WGS); which will identify all variants, whether they be pathogenic, structural or non-coding (Grozeva et al., 2019). However, given the inherent rarity of these variants, achieving sufficient statistical power will require enormous data sets, making WGS economically infeasible in some instances. An alternative method is whole exome sequencing (WES) which allows identification of variants within the protein coding regions, meaning these identified variants will likely have a functional impact.

Through a combination of WES, WGS and Sanger sequencing, a SNP ($R^{47}H$) in *TREM2* has been independently identified as a sAD risk variant (Guerreiro et al., 2013b; Jonsson et al., 2013). *TREM2* encodes a 230 aa transmembrane glycoprotein, TREM2, expressed in the myeloid lineage of cells that mediates the inflammatory response, particularly macrophages, monocytes, dendritic cells and microglia (Gratuze et al., 2018). The protein expression of the TREM2 receptor is low in resting microglia, but found to be greatly upregulated in microglia adjacent to plaques of Aβ (Fahrenhold et al., 2018). Signalling through TREM2 results in complexing to the adaptor protein DNAX-activation protein 12 (DAP12), with the TREM2-DAP12 complex recruiting the tyrosine-protein kinase Syk and the ultimate phosphorylation of downstream mediators such as PI-3K and VAV2/3 (Gussago et al., 2019). Activation regulates proliferation, phagocytosis and migration/chemotaxis (Kober and Brett, 2017; Takahashi et al., 2005) and thus TREM2 can work to facilitate the removal of neurotoxic Aβ. Indeed, defects in cytokine production, phagocytosis and cell survival have been detailed in situations of impaired TREM2 signalling (Gussago et al., 2019) with the $R^{47}H$ variant associated with a loss of receptor expression and a loss of its function (Guerreiro et al., 2013c). This will impair the ability of microglia to function as Aβ phagocytes and thus cause exacerbation of AD related pathogenesis. Whilst TREM2 is exclusively expressed by microglia in the brain, it is unclear whether TREM2 is expressed by a subset or is present on

all microglia (Schmid et al., 2002). TREM2 expression varies between regions of the CNS (Chertoff et al., 2013; Sessa et al., 2004) with higher expression evident in the spinal cord, white matter and more importantly, the hippocampus (Forabosco et al., 2013). To date, 66 variants have been identified in *TREM2* (https://www.alzforum.org/mutations/trem2) with only one additional SNP ($R^{62}H$) achieving significant genome wide association with AD, independently of $R^{47}H$ (Sims et al., 2017). This study also identified two new susceptibility loci, *PLCG2* and *AB13,* which encode proteins expressed in microglia; further implicating immunity in the pathogenesis of AD (Sims et al., 2017).

Interestingly, a coding variant in *APP* ($A^{673}T$) was also identified as a sAD association gene, offering a protective effect in an Icelandic cohort (Jonsson et al., 2012). The mutation is adjacent to the β-secretase/BACE1 cleavage site in APP and resulted in a 40% reduction in amyloid peptide formation, *in vitro.* This protective effect provides proof of principle for the suggestion that a reduction in β-secretase/BACE1 cleavage of APP may provide a therapeutic approach in AD.

1.4 The LOAD risk gene, *EphA1*

EphA1 was first identified as a potential susceptibility locus for sAD in a three-stage GWAS. Combining data from The European Alzheimer Disease Initiative Investigators (EADI1), 38 variants in ten loci were identified at $p < 10^{-5}$, including the *EphA1* SNP, rs11771145. This SNP was located on chromosome 7 in the 5' upstream promoter/regulatory region of *EphA1*. With the addition of data from Genetic and Environmental Risk for Alzheimer's Disease (GERAD1) consortium, rs11771145 failed to reach genome wide association during this phase (i.e. $p \leq 5.0 \times 10^{-8}$; rs11771145 reached $p = 1.7 \times 10^{-6}$). Strengthened evidence for *EphA1*-AD association came from a GWAS performed by the Alzheimer's Disease Genetics Consortium (ADGC) where the rs11767557 SNP, again located in the promoter region of *EphA1*, reached genome wide significance ($p = 6.0 \times 10^{-10}$) with the minor allele of this variant protective (minor allele frequency, MAF, = 0.19; Naj et al., 2011). rs11771145 and rs11767557 were found to be in low linkage disequilibrium (LD) with conditional analysis confirming independent association signals (r^2=0.28, D'=0.75) That same year, the GERAD+ consortium independently confirmed AD risk association for rs11767557 (Hollingworth et al., 2011). In the largest power AD GWAS to date, the IGAP consortium found evidence for *EphA1* rs11771145 association with sAD, obtaining an overall meta-*p* value of 1.1×10^{-13}, a new SNP corresponding to the top conditional analysis hit was also identified rs10808026 ($p = 1.4 \times 10^{-11}$).

Recently, a nonsynonymous variant (rs202178565; MAF 0.001) has been identified in a Caribbean Hispanic sample ($p = 2.6 \times 10^{-3}$); reaching only nominal significance in a Caucasian sample ($p = 3.07 \times 10^{-2}$) (Vardarajan et al., 2015), potentially due to a lack of statistical power. This nonsynonymous variant is proline to leucine substitution at position 460 with P^{460} being highly conserved across species, thus uncovering the impact of this protein-coding mutation is vital and may reveal a novel mode of action in sAD. As this $P^{460}L$ mutation is in a protein coding region of EphA1, it makes it an attractive target for functional characterisation. The $P^{460}L$ mutation is located within the second FNIII repeat within the ECD of EphA1.

Table 1.2 Key GWAS identifying EphA1 as a sAD susceptibility gene

ID	Type	Minor allele frequency	Major allele frequency	Risk allele	Genetic evidence
rs11771145 (A/G)	ncRNA, intron of EphA1-antisense RNA 1	A (0.35)	G (0.65)	G	Top IGAP meta-analysis hit $p = 1.1x10^{-13}$
rs11767557 (C/T)	ncRNA, intron of EphA1-antisense RNA 1	C (0.21)	T (0.79)	T	$p = 6.0 X 10^{-10}$
rs10808026 (A/C)	ncRNA, intron of EphA1-antisense RNA 1	A (0.21)	C (0.79)	A	IGAP meta-analysis $p = 2.11x10^{-11}$ Top conditional analysis hit $p = 2.09x10^{-5}$
rs202178565 (A/G)	Missense, exon 1 of *EphA1*	A (0.001)	G (0.999)	A	**N/A**

1.4.1 EphA1 Overview

EphA1, the 108kDa encoded protein of the *EphA1* gene, was the first of the transmembrane erythropoietin-producing hepatocellular (Eph) family of receptor tyrosine kinases (RTKs) to be discovered and isolated in an erythropoietin-producing human hepatocellular carcinoma cell line (ETL-1) following a screen for gene sequences with homology to the viral oncogene, v-*fps* (Hirai et al., 1987). Despite this, EphA1 remains the most incompletely characterised Eph family member and most of what is known about EphA1 has been inferred from its closest homolog, EphA2. The Eph receptors are considered the largest of the RTK families in the mammalian genome (Kullander and Klein, 2002) and are vital for normal cellular processes during development and mediate tissue homeostasis in adults (Darling and Lamb, 2019). Cell signalling is initiated through activation of their kinase domain following interaction with membrane-anchored proteins, known as ephrins (Eph receptor—interacting). Both Eph receptors and their surface-associated ligands belong to one of two major subclasses based on their binding affinities for their cognate proteins and on the homology of their extracellular domain sequence; the human genome contains 14 Eph RTK receptors, 9 belonging to the A-subclass and five to the B-subclass. Similarly, there are six glycosylphosphatidylinositol (GPI) linked ephrin-A ligands and three transmembrane ephrin-B ligands. Eph/ephrin interactions are characterised by promiscuity and - uniquely to the RTK family – contact-dependant bi-directional signalling which affects both the Eph-bearing ('forward signalling') and ephrin-bearing ('reverse signalling') cells.

1.4.2 Eph receptors and ligands

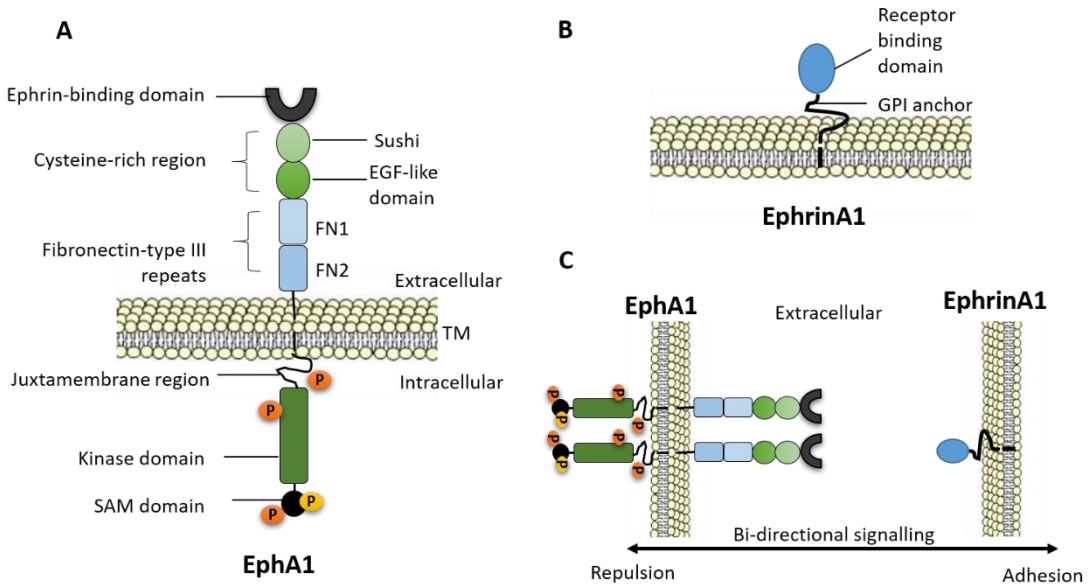

Figure 1.5 Schematic delineating the structural composition of the EphA1 receptor. EphA1 comprises an ephrin-binding extracellular N-terminal domain, with an adjacent cysteine rich region and a pair of fibronectin type-III repeats (FNIII; FN1 and FN2), a lone α-helix spanning the membrane domain and an intracellular C-terminal region which includes a regulatory juxtamembrane region, an uninterrupted dual lobe kinase domain and an Eph-specific SAM domain. B) Structural composition of EphrinA1 ligand. EphrinA1 comprises a receptor binding domain and a GPI anchor which tethers it to the membrane C) Signalling dynamics of the Eph/Ephrin system. The prototypical forward-signalling of the Eph/Ephrin system typically results in cellular disengagement, repulsion and the withdrawal of processes (Flanagan and Vanderhaeghen, 1998). Conversely, the distinctive reverse-signalling of the Eph/ephrin system is thought to largely promote adhesion (Pasquale, 2010). Receptor activation requires the formation of multimeric Eph/ephrin clusters.

The overall structure of members of both the A and B – class of Eph receptors is highly conserved, with EphA and EphB receptors sharing the same domains and structural features. The main sequence differences reside within the ligand binding domain (LBD) and thus likely to determine binding specificity to ephrin subclasses (Himanen et al., 1998). This sequence similarity necessitates different spatial and temporal patterns of expression by activated Eph receptors in order to determine the correct functional outcome. A distinguishing aspect of Eph activation is that dimerization is inadequate in eliciting phosphorylation and a subsequent biological response with the formation of multimeric Eph/ephrin signalling clusters also required (Vearing and Lackmann, 2005). Interestingly, it is purported that the magnitude of the multimerization is indicative of the strength of the response and also on the type of response elicited (Stein et al., 1998). Activation of Eph receptors can also occur *in cis*, and or *in trans*.

Similarly to other RTKs, the structural composition of the Eph receptors comprises an ephrin-binding extracellular N-terminal domain with an adjacent cysteine rich region and a pair of fibronectin type-III repeats, an α-helix spanning the membrane domain and an intracellular C-terminal region which includes a regulatory juxta membrane region, an uninterrupted dual lobe kinase domain, a sterile α-motif (SAM) and a PDZ binding motif (Pasquale, 2005). Heterocomplex formation required for signalling is mediated by receptor dimerization and are assembled through the PDZ-binding motifs which also functions as scaffold proteins (Ye and Zhang, 2013). EphA1 lacks a PDZ-binding domain (Coulthard et al., 2001a), suggesting that EphA1 interacts with divergent effector molecules and that receptor aggregation is elicited by alternative means. The SAM domain, a unique characteristic of Eph RTKs, are increasingly being recognised as an important modulator of receptor oligomerisation, either supporting unliganded dimerization for EphA3 (Singh et al., 2015) or reducing the propensity for aggregation and thus inhibiting the kinase activity of EphA2 (Shi et al., 2017) . Consequently, the SAM domain of EphA1 may represent the mechanism by which EphA1 molecules aggregate. EphA1 also includes a non-conserved membrane-embedded ionogenic residue within its TMD Glu^{547}. The ionization state of Glu^{547} has been shown to alter the structural-dynamic properties of the EphA1 TMD suggesting that the dimerization and formation of lateral clusters of EphA1 can be regulated by external

and local factors such as pH and plasma membrane lipid composition (Bocharov et al., 2008).

As mentioned, the ephrinA subclass of ligands consist of six GPI-tethered members; whilst these ligands lack a cytoplasmic tail, they are able to elicit phosphorylation of certain kinases in downstream pathways (such as the phosphoinositide 3-kinase or PI3K pathway; Holen et al., 2008), possibly via a coreceptor such as a neurotrophin receptor (Lim et al., 2008) or through microdomain clustering (Pitulescu and Adams, 2010). The GPI-anchored ephrinA1 represents the cognate ligand of EphA1. There is a growing body of evidence which also suggests that some ephrinA ligands can be liberated from the cell surface whilst remaining functionally active (Wykosky et al., 2008) and thus may represent a mechanism of signalling which does not necessitate cell contact. The B-ephrins, conversely, contain a cytoplasmic domain and signalling is considered receptor-like in its nature (Pitulescu and Adams, 2010). Given the promiscuity of Eph-ephrin interactions, their temporal and spatial patterns of expression dictating outcome and their ability for bi-directional signalling makes the Eph-ephrin system a unique and challenging prospect.

Delineation of the functional role of the Eph/ephrin system has unveiled its biological significance. The prototypical forward-signalling of the Eph/ephrin system typically results in cellular disengagement, repulsion and the withdrawal of processes (Flanagan and Vanderhaeghen, 1998). Conversely, the distinctive reverse signalling of the Eph/ephrin system is thought to largely promote adhesion. The largely contact-dependent system is also responsible for de-adhesion and migration and thus considered to be particularly important during developmental morphogenesis, organogenesis, pattern formation and cell fate determination (Klein, 2012). Throughout maturation, Eph/ephrin interactions are thought to regulate synaptic remodelling, differentiation of epithelial cells, angiogenesis/vascular network remodelling and have been shown to harbour immunoregulatory properties.

1.4.3 Eph/Ephrin family in disease

Given the range of indispensable roles performed by Eph receptors and their ligands, it is unsurprising that the dysregulation of this system has been implicated in a number of disorders. (Pasquale, 2008). Perhaps most notable is their association with oncogenesis and metastatic disease (Pasquale, 2010) as well as atherosclerosis (Sakamoto et al., 2008), a

chronic inflammatory disease of the vessel wall and the leading cause of cardiovascular disease in the developed world.

Atherosclerosis causes the deposition of fibrous material within the arteries and gene expression profiling of these atherosclerotic plaques has uncovered altered expression in ephrinB1, EphB2, EphA2, ephrinA3, ephrinA4, ephrinA5 and ephrinB2 (Sakamoto et al., 2008). During atherogenesis, EC activation can be initiated in response to pro-inflammatory factors, such as circulating TNFα, and cause phenotypic changes within these cells. Notably, this activation can alter the permeability of the endothelium and drive the activation of cell adhesion molecules such as VCAM-1 and ICAM-1. As described, increased expression of ICAM-1 and VCAM-1 leads to the recruitment of leucocytes and thus is capable of mediating their subsequent extravasation through endothelial monolayers and proliferation of the inflammatory response. Importantly, the expression patterns of Ephs and ephrins are significantly altered during endothelial cell activation and it has been purported that EphA2 transduction initiated through endothelial cell activation can exacerbate the expression of pro-inflammatory genes (Funk et al., 2012a) and contribute to the permeability of the endothelial layer (Funk and Orr, 2013). These findings have alluded to the fact that Eph receptors and their ligands may play an important role in immunity and the inflammatory response.

1.4.4 Eph-ephrin roles in immunity

The expression of both Eph receptors and ephrins play a role in the cell fate of hematopoietic progenitors. EphB receptors have been shown to be the important determinants in the hematopoiesis of both erythrocytes and leucocytes. Erythropoiesis is mediated by EphB2 positive hematopoietic progenitors and ephrinB2 expressing bone marrow stromal cells, where upon co-culture, the hematopoietic progenitors detached and differentiated into mature erythroid cells (Suenobu et al., 2002). *In vitro*, the early introduction of EphB4 into hematopoietic cells using a retroviral vector promotes the differentiation into the erythroid/megakaryocyte lineage (Wang et al., 2002).

One of the preliminary processes in initiation of an immune response, as previously described, is leucocyte activation. Whilst the data is in its infancy, there is some evidence that Eph receptors and their ligands are capable of mediating the activation of leucocytes.

For instance, the response of dendritic cells to TLR-PAMP ligation has been shown to be mediated by EphB2 (Mimche et al., 2015). Human B-cells are also known to express various Eph receptors and their ligands (Aasheim et al., 2000; Alonso-C et al., 2009; Nakanishi et al., 2007). Differential expression of Ephs and ephrins has also been identified in naïve and activated B cells suggesting facilitation of B cell activation (Alonso-C et al., 2009). EphB6 is also expressed by 10-12% of $CD4^+$ and $CD8^+$ human peripheral T cells (Luo et al., 2002). Additional studies have identified the three ephrinB ligands to be expressed by T cells (Yu et al., 2003a, 2003b, 2004). The expression of Eph receptors and ligands on antigen presenting cells indicates that their expression on T cells may play a part in their activation and differentiation (Darling and Lamb, 2019). Taken together, this highlights the role of the Eph-ephrin system in cell stem fate and leucocyte activation. Growing evidence has also pointed to a role in controlling immune cells trafficking which could highlight potential pathologically relevant processes in AD and *EphA1* SNPs.

1.4.5 Eph-ephrin role in immune cell trafficking

Systemic migration of leucocytes is controlled by the interaction of various chemokines, cytokines, selectins and integrins. Interestingly, however, the Eph-ephrin system is also believed to be important in controlling steps in the leucocyte adhesion cascade. For instance, stimulation of human umbilical vein ECs (HUVECs) with soluble ephrinA1 increases the adhesion of both primary human monocytes and the monocyte-like THP-1 cell line through activation of EphA4 on HUVECs (Jellinghaus et al., 2013). The mRNA expression of both VCAM-1 and ICAM-1 remain unaltered after short term exposure (30 min) to ephrinA1 treatment and adhesion was suggested to occur through RhoA dependant cytoskeletal remodelling downstream of the EphA4 receptor. Moreover, interactions between endothelial expressed ephrinB2 and EphB4 expressing monocytes has been shown to support both adhesion and TEM of the monocytes (Pfaff et al., 2008). It is possible that signalling events which occur downstream of Eph-ephrin activation interact with the molecular pathways supporting integrin mediated cellular adhesion (Darling and Lamb, 2019).

The A-class of Eph receptors and ephrins have been implicated in the trafficking of B and T cells. EphA2 is expressed on the high endothelial venules (HEVs) of human lymph nodes (Trinidad et al., 2010). *In vivo*, activation of ephrinA ligands on T cells initiates reverse

signalling causing T cell to enter the lymph nodes (Sharfe et al., 2008a). T lymphocytes also express EphA1 and EphA4 receptors with their ephrinA1 ligand expressed on HEV ECs. EphrinA1 binding to EphA1 and EphA4 expressed on $CD4^+$ T cells stimulates stromal cell-derived factor 1 (SDF-1) and macrophage inflammatory protein 3β (MIP3β) mediated chemotaxis of the CD4+ T cells (Aasheim et al., 2005). This chemotactic effect was thought to be controlled by the effect EphA-ephrinA1 interactions on actin polymerization. The exact relationship between Eph-ephrin communication and chemokines is not clear but both SDF-1 and MIP3β is mediated not only by ephrinA ligands, but also ephrinBs (Sharfe et al., 2002) pointing to a role of both subsets of ligands in T cell migration into chemokine concentration gradients (Darling and Lamb, 2019). A range of signalling molecules have been implicated in T cell EphA-ephrinA mediated migration including Lck, a member of the Src kinase family, the focal adhesion like kinase, proline-rich tyrosine kinase 2 (Pyk2) and the guanidine exchange factor (Vav1) as well as Rho GTPases (Hjorthaug and Aasheim, 2007).

The precise expression patterns of EphA1 on leucocytes and ECs and its exact role in immune cell trafficking is unclear. However, upregulation of EphA1 in hepatocellular carcinoma (HCC) cells promoted the chemotaxis of endothelial progenitor cells (EPCs) to tumour cells (Wang et al., 2016). EPC migration to tumour tissue is detrimental as EPCs promotes angiogenesis of HCC. Moreover, this increased expression led to increase in SDF-1 concentrations in the tumour microenvironment, enhancing EPC recruitment to HCC which was shown to be partly mediated by the PI3K and mTOR pathways. This highlights not only the role of EphA1 in cellular migration but also on the pathological potential of EphA1 mediated migration of cells. How this relates to AD-associated *EphA1* SNPs is unclear but considering the clear role of Eph-ephrins in immunity and inflammation and the AD related neuropathology of BBB dysfunction and neuroinflammation, one might suppose that *EphA1* AD SNPs might alter the interactions of peripheral immune cells and the BBB. In order to appreciate the potential pathological processes of the EphA1 molecule, it is first vital to understand the regulatory mechanisms associated with the molecule.

1.5 Eph-ephrin regulation

Typically, activation of RTKs by ligand binding at the cell surface results in the internalisation of the receptor through clathrin-mediated (CME) and/or clathrin-independent endocytosis (CIE) (Goh and Sorkin, 2013a). Signalling from endocytosed RTKs persists from intracellular compartments prior to targeting for dephosphorylation, degradation by endosomes and lysosomes or recycling to the cell surface by retroendocytosis. The surface association of ephrins means activation of the Eph receptor through ligand binding has unique endocytic features. The prototypical RTK signalling modality (i.e. 'forward signalling) of Ephs and ephrins on juxtaposed cells results in macromolecular complexes (Vearing and Lackmann, 2005). The mechanism of intact receptor-ligand complex internalisation – known as *trans*-endocytosis - is not completely understood. However, the termination of these adhesive contact sites is thought to require actin polymerisation and activity of Ras related C3 botulinum toxin substrate 1 (Rac1), which is part of the Rho family of GTPases (Marston et al., 2003). Cbl, an E3 ubiquitin-protein ligase, can also promote Eph receptor internalisation and degradation (Fasen et al., 2008; Walker-Daniels et al., 2002a). Complex internalisation can occur in either the Eph or ephrin-bearing cell, mediated by the direction of signal transduction (Marston et al., 2003; Zimmer et al., 2003).

Trans-endocytosis is not the only mechanism by which Eph/ephrin complexes are disrupted and internalised. There is an emerging role of proteases in the regulation of both Eph and ephrin shedding, internalisation and signalling (Atapattu et al., 2014a). Proteases are enzymes which primarily hydrolyse peptide bonds within both proteins and polypeptides. Mammalian proteases belong to one of 5 major groups, cysteine, serine, metallo, aspartic and threonine, classified based on their mechanism of catalysis (López-Otín and Bond, 2008). Many transmembrane proteins are cleaved at the ectodomain, with the extracellular region then released into the extracellular space. Autocrine and paracrine signalling is generally facilitated by proteolysis of receptor ligands at a distance, this is true for many receptor families, including RTKs. Juxtacrine signalling, which defines Eph/ephrin interactions, does not intuitively appear to necessitate proteolytic regulation. However, as mentioned, the tethering of Eph- and ephrin-bearing cells regulated by large receptor-ligand complexes

results in either cellular spreading and adhesion or withdrawal of processes and repulsion. Consequently, dynamic interference of these complexes, via a range of mechanisms, is required to convert the high-affinity interaction into a repulsive outcome. It is now widely reported that Eph-ephrin functions are mediated by a range of proteases, including A Disintegrin And Metalloproteases (ADAMs), matrix metalloproteases (MMPs), γ-secretase and a number of serine proteases, such as Neurospin (Atapattu et al., 2014a)

1.5.2 A disintegrin matrix metalloproteinases (ADAMs)

ADAMs are transmembrane and cleaved proteins which belong to the Metzincins superfamily of metalloproteases. 17 of the 23 known mammalian ADAM genes encode a functional protease. The primary purpose of these functional ADAMs is to shed the ectodomain of growth factors, cytokines, receptors and adhesion molecules. ADAM-10/Kuzbanian is considered pivotal in the regulation of Eph/ephrin signalling. Seminal work concluded that Eph-induced cellular retraction between EphA3-ephrinA2 complexes necessitated the cleavage of ephrinA2, by ADAM-10 (Hattori et al., 2000). The ephrinA2 recognition motif by ADAM10 is not found in ephrinA1 suggesting an alternative protease may be responsible for cleavage of ephrinA1. Cleavage of Eph-bound ephrin has also been shown in *trans;* formation of EphA3-ephrinA5 complexes presents a new recognition motif for ADAM10, allowing binding via the substrate recognition pocket in the cys-rich domain causes ADAM10 to position the adjacent N-terminal metalloproteinase domain for effective non cell autonomous cleavage of its target, ephrinA5 (Janes et al., 2005). Following disruption of the complex, EphA3 complexed to cleaved ephrinA5 is internalised into the Eph bearing cell.

There are a number of other ADAMs which regulate Eph/ephrin signalling. ADAM12 is thought to contribute to EphA1-ephrinA1 complex interference (Ieguchi et al., 2014). Interestingly, this study concluded that EphA1-ephrinA1 complexes do not become internalised within the cell and rather remain bound at the cell membranes (after 12h) where ephrinA1 is expressed in its natural GPI anchored form. ADAM12 cleaved ephrinA1 can become deleterious by disrupting these cellular contacts and increasing endothelial lung permeability. Moreover, adherence was not reliant on the activity of the EphA1 kinase domain, suggesting the primary purpose of EphA1-ephrinA1 complexes is to mediate cell

adherence and that these proteins are both necessary and sufficient to control this event as it occurred even in the absence of E-cadherin (Ieguchi et al., 2014).

1.5.3 Matrix metalloproteases

The 25 members of MMPs, similarly to ADAMs belong to the superfamily, metzincin and exist in either a membrane bound or secreted form. Consequently, MMPs are capable of cleaving membrane bound proteins, proteins in the secretory pathway or those within the extracellular space (Page-McCaw et al., 2007). They have also been identified in the regulation of both Ephs and ephrins. EphrinA1 proteolysis has been shown to be blocked by MMP inhibitors ; particularly MMP1, 2, 9 and 13 in cancer studies (Beauchamp et al., 2012).

EphA2, the closest homolog to EphA1 is known to recruit MT1-MMP when ephrinA1 is bound, promoting *in cis* cleavage of EphA2 at the fibronectin type III domain 1 (see supplement I for the cleavage site). Constitutive shedding was present without added ligand but was enhanced by the addition of ephrinA1-Fc. This subsequently caused Src/Rho mediated invasion and internalisation of C-terminal EphA2 and the release of N-terminal fragments in the media (Sugiyama et al., 2013). The EphA1 $P^{460}L$ mutation, as described in section 1.4 and Table 1.2. resides within the second fibronectin type-III repeat and subsequently may interfere with or promote proteolytic processes mediated by MT1-MPP. Secondly, it may provide the closest insight to the mechanism by which EphA1 may be processed in the presence of clustered ephrinA1-Fc due to the described similarity between EphA1 and EphA2.

1.5.4 Regulated intramembrane proteolysis (RIP)

Ectodomain shedding mediated by ADAMs or MMPs is a pre-requisite for regulated intramembrane proteolysis (RIP) and is conducted by proteases known as intramembrane cleaving proteases (iCLiPs). RIP represents the second cleavage of ectodomain proteins and generally results in the secretion of a small peptide into the vesicle lumen or extracellular region and internalisation of the intracellular region of the protein into the cytosol (Brown et al., 2000). iCLiPs are represented by 3 protease families, S2P-metalloproteases, rhomboid serine proteases and the GxGD-type aspartyl proteases. 2 types of RIP control sequential cleavage of integral membrane proteins; type II processes proteins whose N-terminus is

within the cytosol and is carried out by S2P-metalloproteases. Relevantly, type I RIP regulates proteins whose C-terminus is within the cytoplasm, as with Ephs, and employs the aspartyl proteases (e.g γ-secretase).

1.5.5 Y-secretase

γ-secretase is a well-studied proteolytic complex in the field of Alzheimer's research, given its role in APP processing. The complex is membrane bound and topologically consists of a number of subunits, namely: Pen-1, Pen-2 Nicastrin and Aph1. Eph-ephrin RIP, where the membrane-bound C-terminal fragments (CTFs) are processed by γ-secretase has been reported for a number of Ephs and ephrins. It has been shown that endogenous EphA4 intermediate CTF accumulates in rat hippocampal neurons treated with compound E, a γ-secretase inhibitor, following primary processing by MMPs (Inoue et al., 2009). EphB2 has also been shown to undergo initial ADAM10 processing and subsequent γ-secretase regulation producing C-terminal peptides EphB2/CFT1 and EphB2/CTF2 (Xu et al., 2009a).

1.6 Summary

It is clear from the literature that EphA1 remains the least characterised of the Eph receptors, making hypotheses of the potential pathomechanisms of AD-related *EphA1* SNPs difficult. This is further compounded by the inherent complexity of the Eph-ephrin system. However, building on the literature of Eph family members, their identified regulatory processes and roles in vascular biology and immune cell trafficking allows an insight into how *EphA1* SNPs might contribute to the neuropathology of AD.

From analysis of post-mortem brains, it is clear that infiltration of peripheral immune cells into the brain parenchyma is a characteristic of AD neuropathology (Hultman et al., 2013; Zenaro et al., 2015b). Most evidence points to this infiltration as a by-product of jeopardised BBB integrity. This loss of BBB integrity is primarily considered to occur through age-related processes or as a secondary consequence of Aβ deposition. However, Eph receptors, including EphA1, can directly regulate immune cell trafficking. As a result, it is plausible that *EphA1* mutations could alter peripheral immune cell trafficking to the BBB eventually supporting their eventual extravasation into the CNS causing cytotoxicity to neuronal cells. How the mutations could promote this effect is unclear.

It is known that Eph-receptors and their ligands are proteolytically processed, but there is little data on EphA1 cleavage mechanisms. As the $P^{460}L$ mutation occurs in the second fibronectin tyepe III repeat, it could be hypothesized that this induces an MT1-MMP cleavage site, as this enzyme is known to cleave the homologue EphA2 in this region (Sugiyama et al., 2013). EphA1 is expressed by a range of leucocytes, so if the $P^{460}L$ mutation introduces an additional cleavage site, this could cause aberrant proteolysis of the molecule resulting in an increase in the amount of circulating soluble $P^{460}L$ EphA1 ECD. It is hypothesised that this increase in circulating soluble EphA1 is capable of priming ECs for leucocyte recruitment, as the Eph-ephrin system is important in immune cell trafficking. Indeed, preliminary work has shown that activation of the human brain microvessel endothelial (hCMEC/D3) cell line using soluble EphA1, corresponding to the ECD, stimulates leucocyte adhesion independently of changes in ICAM1-1 or VCAM-1, suggesting a novel EphA1-dependant pathway may control leucocyte extravasation across the BBB (Ager, unpublished).

1.7 Hypothesis

With this in mind, it is hypothesized that that the EphA1 $P^{460}L$ AD SNP alters membrane turnover of EphA1, resulting in an increase in circulating soluble EphA1 within the vasculature which ultimately primes brain ECs for leucocyte recruitment and their eventual extravasation. Elucidation of this hypothesis would provide a potential pathomechanism for AD initiated by EphA1 and provide a potential therapeutic target.

1.8 Aims

The overall aim of this thesis is to characterise the WT EphA1 molecule, including regulatory processes with a goal to decipher the potential role of $P^{460}L$ EphA1 in AD pathogenesis. To assess the hypothesis, the following aims will need to be achieved:

- Generation of cell lines stably expressing WT EphA1 and $P^{460}L$ EphA1 using the human embryonic kidney (HEK)-293 Flp-In expression system.
- Characterisation and comparison of WT EphA1 and $P^{460}L$ EphA1 membrane expression using western blotting (WB) and immunocytochemistry (ICC) in the absence of ligand.
- Characterisation and comparison of WT EphA1 and $P^{460}L$ EphA1 membrane expression using WB and ICC in the presence of ligand,
- If WT EphA1 and $P^{460}L$ EphA1 appear to be proteolytically processed, determine which proteases are responsible for this effect.
- Generation and purification of soluble ectodomains WT EphA1 and $P^{460}L$ EphA1 using the HEK-293 Flp in system.
- Assessing the effect of soluble WT EphA1 and $P^{460}L$ EphA1 on recruitment of leucocytes to both HUVECs and the human brain microvessel endothelial (hCMEC/D3) cell line under shear flow.

Chapter Two

General Materials and Methods

2.1 Materials and methods

ddH_20 or PBS was used to prepare stock solutions/buffers as described in Appendix I. All experiments used analytical grade chemicals from either Sigma (St. Louis, Missouri, USA) or ThermoFisher Scientific (Waltham, Massachusetts, USA) unless otherwise stated.

2.1.1 Cell culture materials

Reconstituted complete media for all cell lines used in this thesis is detailed in Table 2.1. Dulbecco's Modified Eagle Media (DMEM) and RPMI 1640 culture mediums were obtained from Gibco, Endothelial Cell Growth Basal Media (EBM-2) and EBM-2 reconstruction reagents were all obtained from Lonza (Basel, Switxerland). Trypsin/EDTA and Hygromycin B were obtained from Sigma-Aldrich. All culturing plastic ware were obtained from Sarstedt Ltd.

The Flp-In expression system (Invitrogen) was used to create stably expressing EphA1 cell lines using HEK-293 cells delivered with the target site vector integrated and is discussed in more detail in chapter 3.

Table 2.1 Culture conditions for all cell lines

Cell line	**Origin**	**Culture Medium**	**Freezing Medium**
HEK-293 Flp-In	Human embryonic kidney	90% DMEM, 10% fetal bovine serum (FBS)	Complete DMEM with 10% dimethyl sulfoxide (DMSO)
HEK-293 WT EphA1-V5	Human embryonic kidney	90% DMEM, 10% FBS 100μg/ml hygromycin B	Complete DMEM with 10% DMSO
HEK-293 $P^{460}L$ EphA1-V5	Human embryonic kidney	90% DMEM, 10% FBS 100μg/ml hygromycin B	Complete DMEM with 10% DMSO
HEK-293 X2 EphA1-V5	Human embryonic kidney	90% DMEM, 10% FBS 100μg/ml hygromycin B	Complete DMEM with 10% DMSO
hCMEC/D3	Temporal lobe of the human brain	EBM-2, 5 % FBS, 0.1 % GA-1000, 0.01 % hydrocortisone, 0.1 % Human fibroblast growth factor-β (hFGF-β), 0.025 % Vascular endothelial growth factor (VEGF), 0.025 % R3-insulin-like growth factor-1 (R3-IGF-1), 0.025 % Human epidermal growth factor (hEGF)	Complete EBM-2 with 10% DMSO
HUVECs (immortalized with a lentiviral hTERT construct)	Vein of the human umbilical cord	M199, 20% FBS and P/S	Complete M199 with 10% DMSO
Molt 3 T cells	T lymphoblast from peripheral blood	RPMI 1640, 10 % FBS, 2mM L-Glutamine, 100 IU penicillin, 100 μg/mL streptomycin and 1 mM sodium pyruvate	Complete RPMI 1640 with 10% DMSO

2.1.2 Cell passaging of adherent cells

Cells were maintained at 37°C in a humidified incubator with 5% CO_2. Cells were passaged during the log phase of growth at approximately 70-80 % confluency. Spent media was removed from the culturing vessels and the cells washed in 10 ml of sterile 1 x PBS. Cells were subsequently trypsinized in 3-5 mls of pre-warmed trypsin/EDTA (depending on vessel size) and incubated at 37^{0}C for 2 mins. The efficacy of trypsinization was assessed using phase contrast microscopy with adherent cells encouraged to disassociate using mechanical agitation of the flask and/or further incubation at 37^{0}C. Trypsin/EDTA activity was quenched using 5 ml of media and harvested cells were collected in sterile tubes prior to centrifugation at 250x g for 5 minutes. The supernatant was removed, and the cell pellet was re-suspended in an appropriate volume of fresh media and dispensed into culturing vessels at a ratio or 1:5 or 1:10. Cells were maintained at 37^{0}C and fed on alternate days with fresh media.

2.1.3 Cell passaging of suspension cells

Molt 3 T cells were brought into a single cell suspension before centrifugation at 250x g, and re-suspension in 10 ml of fresh media. Molt 3 T cells were then counted (as described in section 2.1.4), maintaining a density of 1.5 x 10^6 cells/ml. Molt 3 T cells were passaged every 2-3 days.

2.1.4 Cell counting and plating

An accurate live cell count of the re-suspended cell pellets was achieved using the Trypan Blue exclusion test (Strober, 2001). A haemocytometer was moistened with exhaled breath and a coverslip affixed to create a cavity within which cells would be counted. The presence of Newton's refraction rings confirms that the coverslip has adhered via suction to the haemocytometer. The cell suspension was mixed and combined with an equal volume of 0.4 % trypan blue. 10 μl of the cell:trypan blue solution was dispensed at the chamber, near the edge of the coverslip, allowing the solution to flow into the cavity through capillary action. The haemocytometer was then visualised under a phase contrast microscope and live, refractile cells were counted in each large corner square (1 mm^2) with a tally counter (trypan blue stains dead, non-refractile cells and were excluded from the subsequent calculation).

Calculation of the cell concentration of the suspension, per ml, was achieved as follows: Average number of cells in the corner squares × dilution factor (1:1) × 10^4. Cells were then seeded at the required density after diluting the cell suspension with an appropriate volume of media.

2.1.5 Thawing and freezing of cell lines

Cells were cryopreserved in liquid nitrogen for long-term storage. In order to resuscitate cells for culturing, they were rapidly thawed in a 37^0C waterbath, resuspended in fresh media in a dropwise fashion and centrifuged at 250x g for 5 mins. They were then cultured according to their culturing conditions. A complete media change was conducted the following day to remove all residual traces of cryoprotectant.

In order to prepare cells for long-term storage, they were cultured in a T-75 flask until reaching confluency. The cells were washed once in pre-warmed PBS, trypsinized and re-suspended in 2 ml their respective freezing media (as indicated in Table 2.1). Cells were then distributed between 2 cryovials and retained at -80^0C in a freezing container for 24 hours before being moved to liquid nitrogen.

2.2 SDS-PAGE

2.2.1 Cell lysis

Media was removed and retained and cells were washed in 1x ice-cold PBS and lysed for 30 mins in 35-50µl of lysis buffer containing 25 mM HEPES, 150 mM NaCl, 10 mM $MgCl_2$, 1 mM EDTA, 2% glycerol, 1% Triton-X and supplemented with proteinase inhibitor and orthophenanthroline prior to use. Lysates were then centrifuged 250x g for 5 mins to pellet cellular debris and the supernatant retained.

2.2.2 Determining protein concentration of lysates (BCA assay)

Protein concentrations were determined using the BCA protein assay (Pierce™) according to manufacturer's instructions. Briefly, BCA standards with concentrations ranging from 0-2 mg/ml (diluent – 1:25 lysis buffer) were used to create a standard curve. 5 µl of each BCA standard and sample were plated in duplicates in a 96-well plate. The BCA working reagent was prepared with a 50:1 ratio reagent A:reagent B with 200 µl added to each well. Following a 30 min incubation at 37^{0}C, the absorbance was read on a microplate reader (Omega Plate Reader, BMG Labtech) at 570 nm. Protein concentrations were determined from the gradient of the standard curve.

Briefly, this assay relies upon the protein induced Biuret reaction, whereby cupric ions (Cu^{2+}) are reduced to cuprous cations (Cu^{1+}) under alkaline condition with the reduction proportional to the protein composition of a solution. This reaction results in the formation of a light blue coloured chelate complex which displays a strong linear absorbance at 550 nm.

2.2.3 Immunoblotting

Proteins concentrations were equalised prior to SDS-PAGE by mixing with an appropriate volume of 3 x Laemmli sample buffer (660 mM Tris-HCl (pH 6.8), 26 % glycerol (v/v), 4 % SDS (w/v), 0.01 % bromophenol blue (w/v), 5 % β2-mercaptoethanol (v/v) and denatured at 95^{0}C for 5 minutes on a heat block. 10-30 µg of protein was loaded into pre-cast 4-10% gradient gels (Bio-Rad) with 4 µl of Geneflow protein ladder and electrophoresed at 120V for 1 h or until the dye reached the bottom of the gel.

Polyvinylidene difluoride (PVDF) membranes (Immobion-P^{SQ}) were activated for 30s in methanol followed by equilibration in transfer buffer. Wet transfer of proteins was conducted at 75V for 1h at room temperature (RT) or 20V overnight (O/N) at 4^{0}C in a Bio-Rad transfer cell containing transfer buffer and a cooling block. To prevent non-specific antibody binding, the blots were blocked in 5% milk (in PBS-T) for 1h at RT prior to O/N incubation with primary antibodies at 4^{0}C. Membranes were washed 3 x for 5 mins prior to incubation in species-specific horseradish peroxidase (HRP)-conjugated secondary antibodies diluted in 5% milk (in PBS-T). Secondary antibodies were detected using ECL reagent (Pierce) for 1 minute with an X-ray film and developer. GAPDH was used as a loading control to adjust for sample-to-sample variability. Primary and secondary antibodies used for Western blotting are listed in Table 2.2.

Table 2.2 Primary and Secondary antibodies used for Western blotting, *denotes loading control

Primary antibodies					
Antibody/ Reactivity	**Antigen/ Epitope**	**Species/ Clonality**	**Dilution**	**Source**	**Catalogue number**
V5	V5 synthetic peptide GKPIPNPLLGLDST	Mouse monoclonal	1:2000	Invitrogen	R960-25
EphA1	EphA1 R24-Q547	Mouse monoclonal	1:500	R&D systems	MAB368
GAPDH	GAPDH	Mouse Monoclonal	1:2000	ThermoFisher	MA5-15738
Secondary Antibodies					
Mouse IgG HRP-conjugated		Mouse polyclonal	1:7000	Stratech	715-035-150-JIR

2.2.4 Densitometry

Semiquantitative densitometry analysis was performed using ImageJ or Gel EZ Doc Imager software (Bio-Rad). Briefly, scanned blots were converted to gray-scale images and individual bands were demarcated using the *Rectangular Selections* tool. Profile plots representing the relative density of each band is then created using the *Plot Lanes* tool. The *Straight Line* selection tool is then used to enclose the area of individual bands and subsequently quantified using the *Wand* tool. The band intensities of the protein of interest were compared to internal loading controls to obtain normalised density ratios. For analyses, three individual experiments were conducted (n=3).

Statistical analyses were conducted using GraphPad Prism 6 (GraphPad Software, CA, USA).

2.2.5 Medium concentration

For analysis of cleaved products in the media, the supernatant was removed and centrifuged at 250x g for 5 mins at 4 ^{0}C to pellet cellular debris. The supernatant was the concentrated using the Amicon centrifugal filter unit with a nominated MW cut-off of 3kDa, according to the manufacturer's instructions and immunoblotted as described above.

2.3 Immunodetection of EphA1-V5/EphA1-P^{460}L-V5 expressing HEK-293 cells

Cells were seeded in a 24-well plate at a density of 1x10^5 on poly-L-lysine coated glass coverslips. They were cultured overnight at 37◦C in DMEM/10% FBS and stimulated with ephrinA1-Fc or inhibitors, as described in subsequent chapters. The cells were washed in pre-warmed PBS (37◦C) and fixed in 3% paraformaldehyde. Cells were washed following all subsequent steps for 3 x 5 mins in PBS. Free aldehydes were quenched with 50 mM NH_4Cl, cells were permeabilised in 0.4% saponin for 10 mins and blocked in 1% BSA for 30 mins. The antibody diluent contained 0.4% saponin, 2% FBS and 2% BSA. Antibodies (Abs) were diluted to a final concentration (as described in Table 2.3) and incubated for 1h at RT. The cells were then incubated with species-specific fluorophore conjugated secondary Ab in blocking buffer for 1h at RT. DAPI Vectashield mounting media was used as a nuclear counter stain and slides were imaged using the ZEISS Apotome fluorescent microscope (running ZEN software) with a 63x oil immersion objective scanning at 488 and 543 nm or the ZEISS confocal microscope,

as detailed. Statistical analyses were conducted using GraphPad Prism 6 (GraphPad Software, CA, USA). Primary and secondary antibodies used for immunocytochemistry are outlined in Table 2.3.

Table 2.3 Primary and secondary antibodies used for immunocytochemistry. Antibody name, specificity, species/clonality, dilution and source of primary antibodies used for western immunocytochemistry.

Primary antibodies					
Antibody/ Reactivity	**Antigen/ Epitope**	**Species/ Clonality**	**Dilution**	**Source**	**Catalogue number**
V5	V5 synthetic peptide GKPIPNPLLGLDST	Mouse monoclonal	1:500	Invitrogen	R960-25
V5	V5 synthetic peptide GKPIPNPLLGLDST	Rabbit polyclonal	1:500	Abcam	Ab9166
EphA1	EphA1 R24-Q547	Mouse monoclonal	1:250	R&D systems	MAB368
Secondary antibodies					
AlexaFluor 594 goat anti-mouse IgG	Heavy and light gamma immunoglobulin chains (mouse)	Mouse polyclonal	1:500	Molecular Probes by Life Technologies	A-11005
AlexaFluor 488 goat anti-rabbit IgG	Heavy and light gamma immunoglobulin chains (rabbit)	Rabbit polyclonal	1:500	Molecular Probes by Life Technologies	A-11008

2.4 Microfluidic assay – Bioflux 200, Fluxion Biosciences

The Bioflux 200 system (Fluxion Biosciences) uses Well Plate Microfluidic technology, embedding fluidic channels (350 µm x 70 µm) along the underside of a standard well plate. A control unit connects to interface unit mounted upon the well plate which controls shear flow, temperature and direction of flow. As is standard for studies exploiting the Bioflux system, shear flow is expressed as dynes/cm^2 and as such shear flow will be expressed as dynes/cm^2 (Tremblay et al., 2015). As a reference point, 1 dyne/cm^2 is equal to the SI unit 0.1 pascals (Pa). Molt 3 T cells were flowed over HUVECs and hCMEC/D3 cells at 0.5 and 0.25 dynes/cm^2, equating to a flow rate of 38 µl/h and 19 µl/h, respectively. See Figure 2.1 for an overview of the Bioflux 200 system.

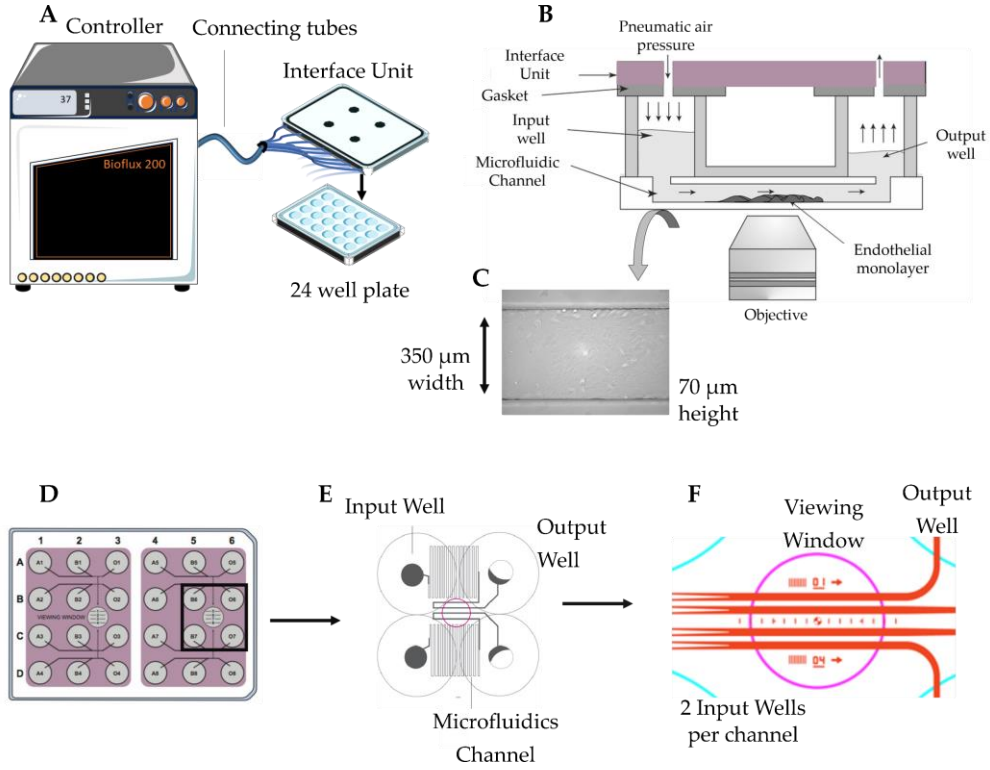

Figure 2.1 Overview of the Bioflux 200 system. **A)** The Bioflux controller connects to the interface unit and controls all aspects of the experiment, including pneumatic pressure and temperature. The interface unit is mounted securely onto the 24-well Bioflux plate which both sit upon an inverted fluorescent microscope. **B)** Schematic showing a vertical cross-section of a Bioflux chamber. Pneumatic pressure delivered from the control unit to the interface is pushed into the input well, and through the microfluidic channel, over the endothelial cells and subsequently into the output well. **C)** Each microfluidic channel is micron-scale at 350 µm x 70 µm. **D)** A 24 well plate, with 2 input wells, 2 output wells, and the viewing channel highlighted, **E)** and **D)** show this magnified.

Chapter Three

Generation of EphA1 expression constructs and cell lines for investigation of EphA1 function

3.1 Introduction

The aim of this chapter was to establish cell lines stably expressing functional, V5-tagged, full-length WT EphA1 and $P^{460}L$ EphA1 for subsequent investigation on the function and stability of membrane EphA1. Characterisation of EphA1 and its regulatory mechanisms is critical if the pathological consequences of AD SNPs are to be understood. Generation of a cell line stably expressing $P^{460}L$ EphA1 will allow us to determine whether the mutation alters these regulatory mechanisms and thus offer a potential disease mechanism. It is known that Eph family members are proteolytically processed (Atapattu et al., 2014) and as the mutation is located in the second FNIII repeat, we have hypothesised that this induces an MT1-MPP cleavage site, since this enzyme is known to cleave its closest homolog, EphA2 in this region (Sugiyama, 2013). As the $P^{460}L$ mutation is protein coding, it makes it an attractive target for functional characterisation as it may inform the mechanisms associated with the non-coding *EphA1* AD SNPs. Importantly, the Flp-In™ expression system (ThermoFisher) will be used to integrate our gene-of-interest (GOI) into our chosen cell line using pOG44-mediated homologous recombination (see Fig 3.1 for an overview of the Flp-In™ expression system). This will allow the generation of isogenic cell lines, permitting direct comparisons between wild-type and $P^{460}L$ mutant and thus, changes in EphA1 cell surface expression levels would not be due to variations in gene expression.

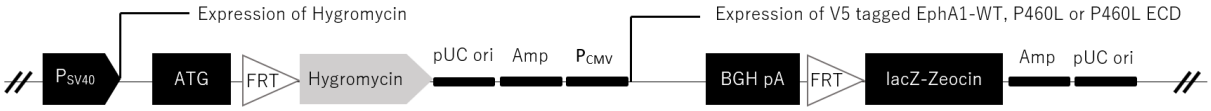

Figure 3.1 Schematic representation of the integrated V5-tagged EphA1 WT amd $P^{460}L$ expression constructs. The model cell line is transfected with the target site vector, Prft/LacZeo, with stable transfectants subsequently selected for zeocin resistance. The introduction of an integrated FRT site allows the POG44 flp recombinase to bind and cleave. Co-transfection of the POG44 flp recombinase and a pcDNA5/FRT vector (holding EphA1 or EphA1 $P^{460}L$) into the model cell line mediates a homologous recombination event at the FRT site. pcDNA integration brings the SV40 promotor and ATG start codon into frame, inactivating LacZ-Zeocin, allowing future selection for stable transfectants using Hygromycin B.

Since unpublished data from the Ager lab has shown that the ECD of EphA1 is capable of priming endothelial cells for leucocyte binding in a static adhesion assay and we

hypothesise that the $P^{460}L$ mutation causes an increase of EphA1 proteolysis; EphA1 and $P^{460}L$ EphA1 will also be expressed as soluble recombinant proteins for future analyses of the effect of EphA1 on leucocyte recruitment using a microfluidic system, which mimics blood flow through the vasculature,. Ultimately, generation of these cell lines will allow determination of whether the EphA1 AD mutation, firstly, causes aberrant proteolysis of the molecule as hypothesised, and additionally, whether any ensuing alterations in peripheral EphA1-ECD levels is capable of modifying leucocyte-endothelium interactions. Should this prove to be the case, this would provide an EphA1-initiated pathomechanism for AD.

3.1.2 HEK-293 as a model cell line

Human embryonic kidney (HEK)-293 cells will be used as a model cell line in this study as they are robust, amenable to transfection and the biochemical machinery of this cell line allows it to efficiently carry out most post-translational modifications and processing necessary to produce functional, mature proteins. Since HEK-293 cells lack endogenous expression of EphA1, future analyses of EphA1 can be conducted without endogenous interference.

This chapter introduces two modified recipient pcDNA5 vectors (Vera Knäuper, unpublished) containing multiple cloning sites (MCS) and C-terminal V5-His tags which will allow the cloning of our EphA1 DNA fragments following PCR amplification from EphA1 cDNA. The first of these vectors will carry our full-length EphA1 and EphA1 $P^{460}L$. The V5 tag will allow us detection of EphA1 in lysates using a previously validated V5 Ab (Invitrogen). We will use a monoclonal EphA1 Ab (R&D systems), to detect the N-terminal region of EphA1 (aa 27-547). This allows us to track the N-terminal and C-terminal regions of EphA1 and consequently allows the investigation of proteolytic events. The second of these vectors, carrying human Fc-coding sequences, allows expression of EphA1 and EphA1- $P^{460}L$ as soluble recombinant proteins for subsequent purification using protein G magnetic beads.

3.1.3 Aims

1. Establish cell lines stably expressing full-length WT EphA1 and $P^{460}L$ EphA1, containing a V5 tag.
2. Confirm that EphA1 WT and $P^{460}L$ is expressed by immunoblotting and immunocytochemistry.
3. Establish cell lines expressing soluble EphA1-ECD and $P^{460}L$-ECD.
4. Purify soluble EphA1-ECD and EphA1 $P^{460}L$-ECD from cell-free supernatant.

3.2 Methods

3.2.1 Generating full-length EphA1 and EphA1 P^{460}L expression constructs and stably expressing HEK-293 cells

3.2.1.1 Cloning of EphA1 and P^{460}L EphA1

Primers were designed as shown in Table 3.1 using the Eurofins Genomics PCR primer design tool. Lyophilised primers (Eurofins Genomics) were reconstituted in PBS to a final concentration of 100 μM.

Table 3.1 Primer sequences for EphA1 and EphA1 P^{460}L. Nucleotides differing from the wild-type sequence are given in red. The introduction of N*heI* (5′-GCTAG-3′) and N*otI* (5′-GCGGCCGC-3′) restriction sites by the primers given underlined in **bold.**

Products	**Forward Primer**	**Reverse Primer**
EphA1	5′AAA**GCTAGC**ATGGAGCGGCG CTGGCCCCTGGGGCTA-3′	5′AAA**GCGGCCG**CCAGTCCTTGA ATCCCTGAATACTGCAAAG-3′
EphA1 P^{460}L N-term	As EphA1 For	5′CCAG**GTCAGC**TCTAGTTGCCTC AGTTCTTTCTTCACCAGTCTCAG-3′
EphA1 P^{460}L C-term	5′CTGAGACTGGTGAAGAAAGA ACTGAGGCAACTAGAGCTGAC CTGG-3′	As EphA1 Rev

3.2.1.2 Full-length WT EphA1 PCR

Full-length EphA1 was amplified using Herculase II Fusion DNA polymerase (Agilent) with 2 μM each of EphA1 For and EphA1 Rev primers (Table 3.1), 10 μL 5 x Herculase reaction buffer supplemented with 1 or 2 μL DMSO, 25 mM dNTP's (all Agilent), 0.2 μg EphA1 template DNA (pDNOR223-EphA1; Addgene) and ddH_2O up to a final volume of 50 μL. PCR cycles are shown in table 3.2

Table 3.2 PCR cycles for full-length WT EphA1 construct

Stage	**Temperature (°C)**	**Time**	**Cycles**
	95	5 mins	
Denaturing	95	15 secs	
Annealing	65	15 secs	X 20
Extension	70	1 min 30 secs	
	70	10 mins	

3.2.1.3 Full-length EphA1 $P^{460}L$ PCR

Full-length EphA1-$P^{460}L$ (herein described as EphA1-$P^{460}L$) was amplified using overlap extension PCR (OE-PCR; see Figure 3.2 for an overview of OE-PCR). Two separate PCR reactions were performed to amplify the cDNA coding sequences for the N-terminal and C-terminal regions of EphA1 $P^{460}L$ using EphA1 For and EphA1 $P^{460}L$ Rev and EphA1 $P^{460}L$ For and EphA1 Rev, respectively (see Table 3.1 for primer sequences). The PCR products were subsequently gel purified from 1% agarose gels using the qiaQuick gel extraction kit. A subsequent PCR reaction in the presence of both products from the first round of PCR amplification and the EphA1 For and EphA1 Rev primers created a full-length EphA1 $P^{460}L$ cDNA fragment containing *NheI* and *NotI* restriction enzyme sites for subsequent cloning. PCR cycles are shown in table 3.3.

Table 3.3 Overlap extension PCR cycles for full-length $P^{460}L$ EphA1 construct. *PCR conditions were identical for the amplification of EphA1-$P^{460}L$ N-terminus and C-terminus in stage 1.

Stage 1*	**PCR Stage**	**Temperature (°C)**	**Time**	**Cycles**
		95	5 mins	
	Denaturing	95	15 secs	
	Annealing	65	15 secs	X 20
	Extension	72	1 min 30 secs	
		72	10 mins	
Stage 2 Overlap Extension	**PCR Stage**	**Temperature (°C)**	**Time**	**Repeats**
		95	5 mins	
	Denaturing	95	15 secs	
	Annealing	65	15 secs	X 25
	Extension	72	2 mins	
		72		

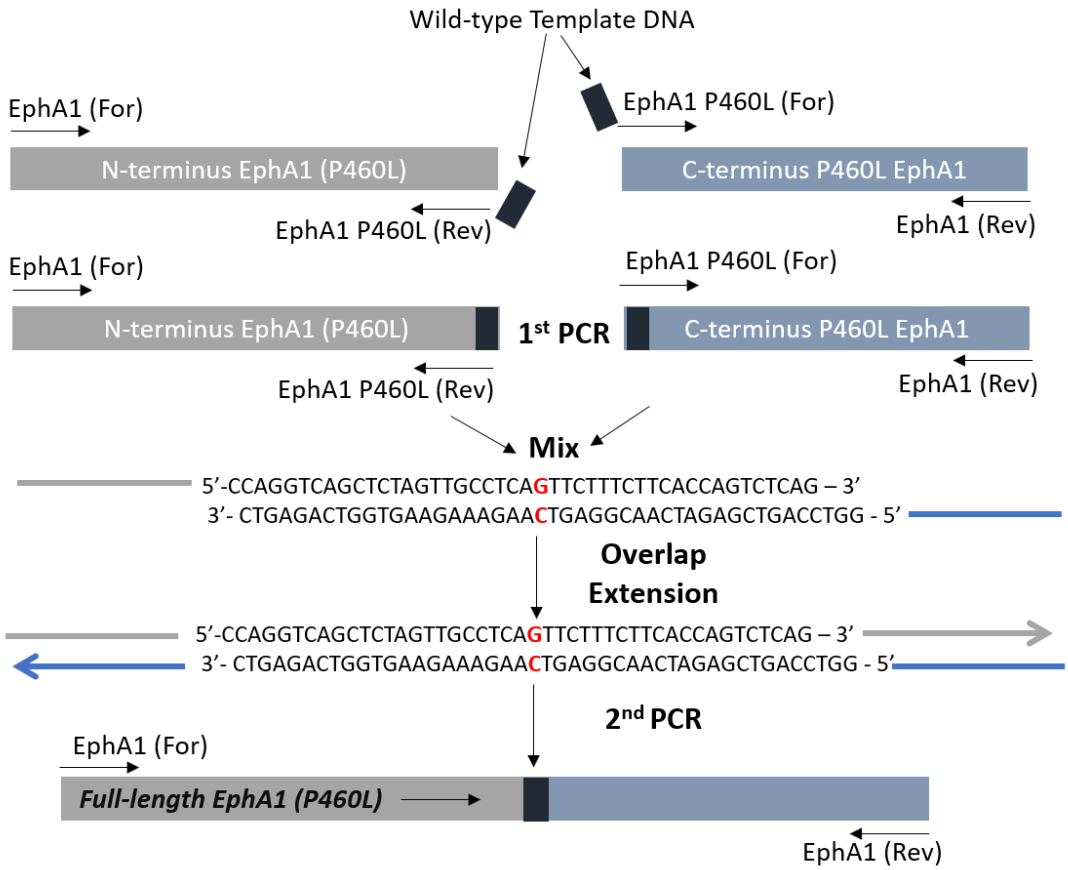

Figure 3.2 Overview of overlap extension PCR During the first round of PCR; the N-terminus and C-terminus are created; both carrying the $P^{460}L$ mutation. During the second round of PCR the complementary ends of the N-terminus and C-terminus are hybridised using the outside primers (EphA1 For and EphA1 Rev).

3.2.1.4 Cloning of EphA1 and EphA1 $P^{460}L$ into pcDNA5-V5-His vector

PCR fragments were purified using the QIAquick PCR purification kit (QIAgen, Manchester, UK) according to the manufacturers' instructions. The purified products were eluted in 40 µL of elution buffer and cleaved with N*heI* and N*otI*. In parallel, the pcDNA5-V5-His vector (Invitrogen) was cleaved with the same restriction enzymes. The cleaved fragments were run on a 1% agarose gel and bands extracted using the QIAquick gel extraction kit (QIAgen). A subsequent ligation reaction was carried out using T4 DNA ligase (Promega) for 1h at RT. 200 µL of XL1-Blue competent *E .coli* (made in house) were transformed with 5 µL ligation mixture by heath shock at 42°C for 90 seconds, cooled on ice for 5 minutes and subsequently grown for 1 h at 37 °C in 200 µL of LB media in an orbital shaker. The cells were then spread over LB agar plates containing 100 µg/mL carbenicillin

(Sigma) in order to select for bacteria that have taken up the plasmid. Plates were incubated overnight at 37 °C, single colonies picked and transferred into 3 ml of LB media containing 100μg/mL carbenicillin and grown overnight at 37 °C in a shaker. Bacterial pellets were then collected by centrifugation at 300x g for 5 mins and plasmid DNA purified using the QIAquick miniprep kit (QIAgen) according to the manufacturers' instructions.

3.2.1.5 Analysis of miniprep DNA for positive clones and DNA sequencing

Miniprep DNA from various clones were cleaved with N*heI* and N*otI* to identify EphA1 and EphA1 $P^{460}L$ containing clones. Positive clones, identified as those containing a 2.6Kb insert, were selected for maxiprep DNA production and sequenced using MWG Eurofins DNA sequencing service and they were confirmed to contain the relevant sequences.

3.2.1.5 Generating stable cell lines containing EphA1 WT and EphA1 $P^{460}L$

Following sequencing of clones, the Invitrogen Flp-In expression system and Fugene® 6 Transfection Reagent (Promega) were used to establish stable HEK-293 cell lines expressing EphA1 WT and EphA1 $P^{460}L$. Briefly, 6 well plates (Startedt) were coated in 100 μg/ml poly-L-lysine for 1h at 37 °C, washed once with serum-free media and allowed to air-dry in a class-I safety cabinet. 1 x 10^6 HEK-293 Flp-In cells were seeded per well and grown overnight. The medium was then replaced with antibiotic-free DMEM containing 10% FBS. 0.2 μg of the plasmids containing EphA1 WT or EphA1 $P^{460}L$ was mixed with 6 μL of Fugene® 6 Transfection Reagent (Promega) and 1.8 μg of the pOG44 recombinase expression vector. Following a 30 min incubation at RT, the mixture was added to the cells in a drop-wise fashion. Control cells were transfected with pOG44 only. Media was replaced after 48 h with DMEM containing 10% FBS and 100 μg/ml of hygromycin-B to select for stable transfectants. Cells were grown to confluency in the presence of hygromycin-B, prior to testing for EphA1 expression by immunoblotting and immunocytochemistry.

3.3 Generating soluble EphA1 and EphA1-P^{460}L-ECD IgG expression constructs and stably expressing HEK-293 cells

3.3.1 Cloning of EphA1-ECD and EphA1-P^{460}L-ECD

Primers were designed as shown in Table 3.4 using the PCR primer design tool by Eurofins Genomics. Lyophilised primers (Eurofins Genomics) were reconstituted in EB to a final concentration of 100 μM.

Table 3.4 Primer sequences for EphA1-ECD and EphA1 P460L-ECD. Nucleotides differing from the wild-type sequence are given in red. The introduction of N*heI* (5′-GCTAG-3′) and *XhoI* (5′-CTCGAG3′) restriction sites by the primers are given underlined in **bold**.

	Forward Primer	**Reverse Primer**
EphA1 ECD	5′-AAA**GCTAG**CATGGAGCGGCGCTGGCCCCTGGGGCTA-3′	5′-TAT**CTCGAG**CTCTCCTCCAGTCAGGCCCCT GGACAC -3′
EphA1 P^{460}L ECD N-term	As EphA1 ECD For	5′-CCAGGTCAGCTCTAGTTGCCTCAGTTCTTTCTTCACCAGTCTCAG-3′
EphA1 P^{460}L ECD C-term	5′-CTGAGACTGGTGAAGAAAGAACTGAGGCAACTAGAGCTGACCTGG-3′	As EphA1 ECD Rev
EphA1 P^{460}L N-terminus and C-terminus fragments were hybridised in the final stage using EphA1 ECD For and Rev primers		

3.3.2 EphA1-ECD PCR

EphA1-ECD was amplified using Herculase II Fusion DNA polymerase (Agilent) with 2 μM each of EphA1 ECD For and EphA1 Rev primers (Table 3.4), 10 μL 5 x Herculase reaction buffer supplemented with 1 or 2 μL DMSO, 25 mM dNTP's (all Agilent), 0.2 μg EphA1

template DNA (pDNOR223-EphA1; Addgene) and ddH_2O up to a final volume of 50 μL. PCR cycles are shown in table 3.5

Table 3.5 PCR cycles for EphA1-ECD

Stage	**Temperature (°C)**	**Time**	**Cycles**
Initialization	95	5 mins	
Denaturing	95	15 secs	
Annealing	70	15 secs	X 20
Extension	72	1 min 15 secs	
Final Elongation	72	10 mins	

3.3.3 EphA1- P^{460}L-ECD PCR

EphA1- P^{460}L -ECD was amplified using Herculase II Fusion DNA polymerase (Agilent) with 2 μM each of the primers, 10 μL 5 x Herculase reaction buffer supplemented with 1 or 2 μL DMSO, 25 mM dNTP's (all Agilent), 0.2 μg EphA1 template DNA (as specified) and ddH_2O up to a final volume of 50 μL. The wild-type EphA1-ECD was used as a DNA template for the P^{460}L mutant. PCR cycles are shown in table 3.6.

Table 3.6 Overlap extension PCR cycles for EphA1- P460L-ECD construct. *PCR conditions were identical for the amplification of EphA1-P^{460}L N-terminus and C-terminus and the subsequent hybridisation using the outside primers

Stage	**Temperature (°C)**	**Time**	**Cycles**
Initialization	95	5 mins	
Denaturing	95	15 secs	
Annealing	65	15 secs	X 20
Extension	72	1 min 15 secs	
Final Elongation	72	10 mins	

3.3.4 Cloning of EphA1 ECD and EphA1 P^{460}L-ECD into pcDNA5-V5-His-Fc vector

The EphA1-P^{460}L-ECD PCR fragment was purified using the QIAquick PCR purification kit (QIAgen, Manchester, UK) according to the manufacturers' instructions. The purified products were eluted in 40 μL of elution buffer and cleaved with N*heI* and X*hoI*. A modified pcDNA5 plasmid carrying human Fc-coding sequences (Vera Knäuper, unpublished) was cleaved with the same restriction enzymes. Following gel extraction, subsequent ligation of the 1.6 kb EphA1-P^{460}L-ECD and cleaved pcDNA5-Fc was performed using T4 DNA polymerase and transformed into XL1 blue competent *E.coli* as described for full length EphA1 and EphA1 P^{460}L. Bacterial colonies were screened for EphA1-ECD and EphA1-P^{460}L-ECD using N*heI* and X*hoI* prior to analysis using 1% agarose gels.

3.3.5 Generating stable cell lines expressing EphA1-ECD EphA1-P^{460}L-ECD

The Invitrogen Flp-In expression system and Fugene® 6 Transfection Reagent (Promega) were used to establish stable cell lines (HEK-293), according to the manufacturer's instructions. Cells were maintained as detailed in Table 2.1**.** The transfection methodology was as described in section 3.2.1.5.

3.3.6 Optimisation of EphA1-P^{460}L-ECD expression and purification

We first aimed to determine the optimal growth medium and incubation period for collection of EphA1-P^{460}L-ECD media to determine which gave us the highest yield of EphA1-P^{460}L-ECD in the media (expected MW of EphA1-P^{460}L-ECD, 75kDa).

Following optimisation, 3x10^{6} of EphA1-P^{460}L-ECD stably transfected HEK-293 cells were seeded in TripleFlasks 500cm^{2} (ThermoScientific Nunc) in 250 ml Serum Free Media II (SFMII) (ThermoFisher) until confluent. Conditioned media containing EphA1-P^{460}L-ECD-Fc was collected and centrifuged a 250x g to pellet cellular debris and the cell free supernatant was retained, supplemented with protease inhibitor and stored at -80°C until use.

3.3.7 Purification of EphA1-P^{460}L-ECD-Fc

3.3.7.1 Preparation of Pierce™ protein G magnetic beads

500 µL (5mg) of protein G magnetic beads were washed with repeated inversion in 10ml of TST buffer (50 mM Tris-HCl pH 7.6, 150 mM NaCl, 0.05% Tween 20). The beads were collected using a magnetic bead stand and the supernatant discarded. This wash step was repeated once prior to sample incubation.

3.3.7.2 Binding and elution of EphA1-P^{460}L-ECD-Fc

400 ml of conditioned media containing EphA1-P^{460}L-ECD-Fc was thawed overnight at 4°C and the pH adjusted to 7.0 with 100 mM HCl prior to filtration using 0.22 µM nitrocellulose filter membranes (Millipore). The pre-washed protein G magnetic beads were added to the filtered media, mixed thoroughly by repeated inversion and incubated overnight at 4°C on a tube roller (Stuart). Bound EphA1-P^{460}L-ECD-Fc was collected using the magnetic stands and washed twice in TS buffer (50 mM Tris-HCl pH 7.6, 150 mM NaCl). Unbound solution/supernatant was retained, and bound EphA1-P^{460}L-ECD-Fc eluted with 0.1 M glycine-HCl pH 2.7 with 6x5 min elutions performed to determine elution efficiency. 80µL of 1M Tris-HCl Ph 9.0 was added to 500 µL of eluted fractions to neutralise the pH. A PBS buffer exchange was subsequently performed on the elution with highest EphA1-P^{460}L-ECD-Fc concentration using PD SpinTrap G-25 columns (as per manufacturer's instructions) and protein concentrations determined using the Pierce BCA assay and Nanodrop. 5 elutions

were performed to ensure all EphA1 P^{460}L-ECD protein was captured during the buffer exchange procedure.

3.4 Results

3.4.1 Optimising PCR conditions for cloning of full length wild-type EphA1

To amplify EphA1 for cloning, PCR reactions were performed using Herculase and Phusion DNA polymerases (either Phusion High Fidelity buffer (HF) or Phusion GC-Rich buffer). Analysis of the PCR products using 1% agarose gel indicated that Herculase amplified a product of ~2.6kb, the expected weight of full-length EphA1 (Fig. 3.3A) whilst both Phusion HF and GC polymerase reactions failed to produce the expected amplicons. Subsequently, Herculase amplified EphA1 and pcDNA5-V5-His cleaved with N*heI* and *NotI* were isolated (Fig 3.3 B) and ligated.

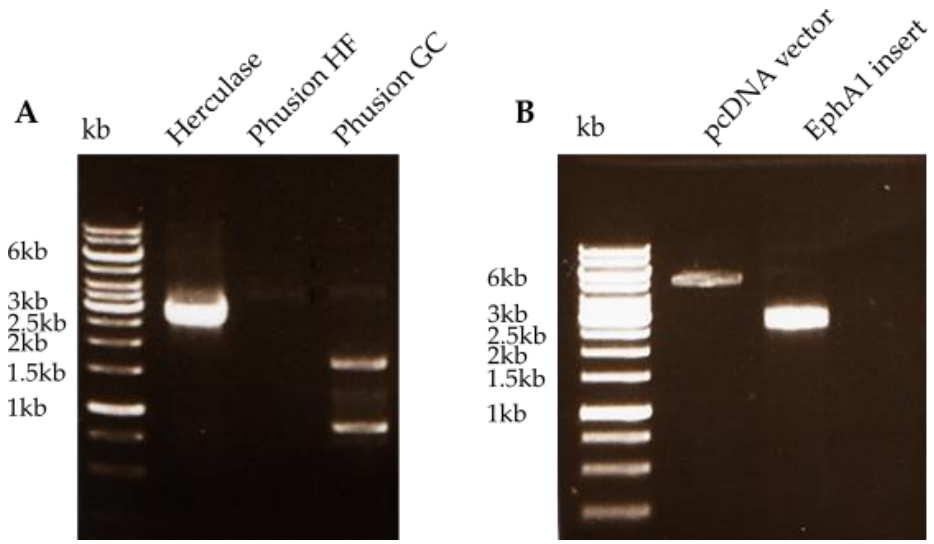

Figure 3.3 Cloning of full-length EphA1 **A)** Optimisation of PCR conditions; H (Herculase buffer) Phusion HF (Phusion High-Fidelity buffer) Phusion GC (Phusion GC-Rich buffer). Expected insert size of EphA1 ~2.6kb **B)** Yield analysis for the ligation reaction of pcDNA vector and EphA1 insert.

3.4.2 Initial EphA1 clone inserts encoding EphA1 transcript variant X2

Initial screening of 4 clones by restriction analysis showed the presence of 2 potentially EphA1 positive clones, here denominated as clone 1 and 3 (Fig. 3.4 A) Sequencing of the clones indicated that both isolated clones corresponded to the EphA1 variant X2, a splice variant lacking the first fibronectin type III repeat (Fig 3.4 B & C) here depicted as FN1. Since

the pDNOR223-EphA1 template plasmid encoded full-length EphA1, it was surprising the initial EphA1 clones encoded the X2 splice variant.

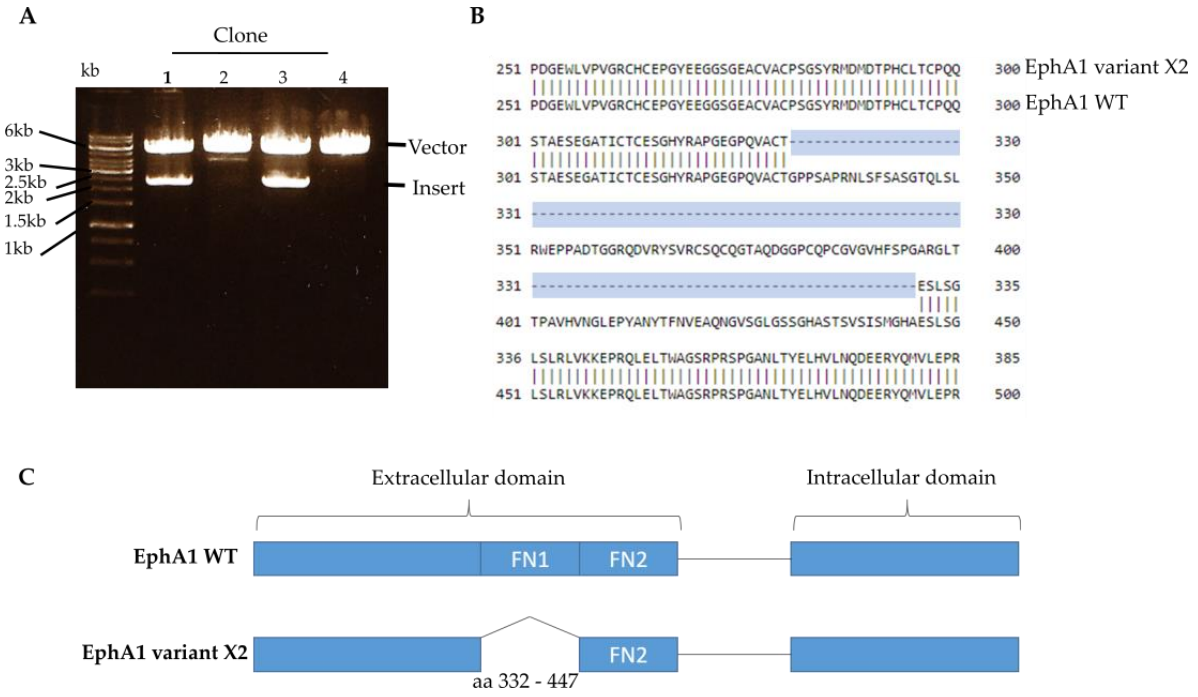

Figure 3.4 Initial EphA1 clone inserts encoding EphA1 transcript variant X2 **A)** Restriction analysis of clones, identifying clones 1 and 3 as potentially EphA1 positive. Expected insert size following BamHI cleavage ~2.6kb **B)** Sequence analysis indicated these clones represented a truncated variant of EphA1, variant X2 which is lacking the first fibronectin type III repeat, highlighted here in blue**. C)** Schematic delineating the topological difference between the EphA1 FL WT sequence and EphA1 variant X2. EphA1 variant X2 lacks aa332-447, corresponding to the first fibronectin type III repeat (FN1).

3.4.3 Further screening of EphA1 ligations identify full-length EphA1 clone

The cloning was repeated, and additional clones were screened for EphA1 inserts using B*amHI* restriction analysis which would generate a 2.6kb fragment for WT EphA1 and ~2.4kb fragment for the X2 splice variant. The analysis of 11 clones is shown in Fig 3.5 and demonstrates that both WT and X2 variant clones were present in our ligation mixture. Two full-length EphA1 clones were selected for sequencing and showed the presence of full-length EphA1 coding sequences.

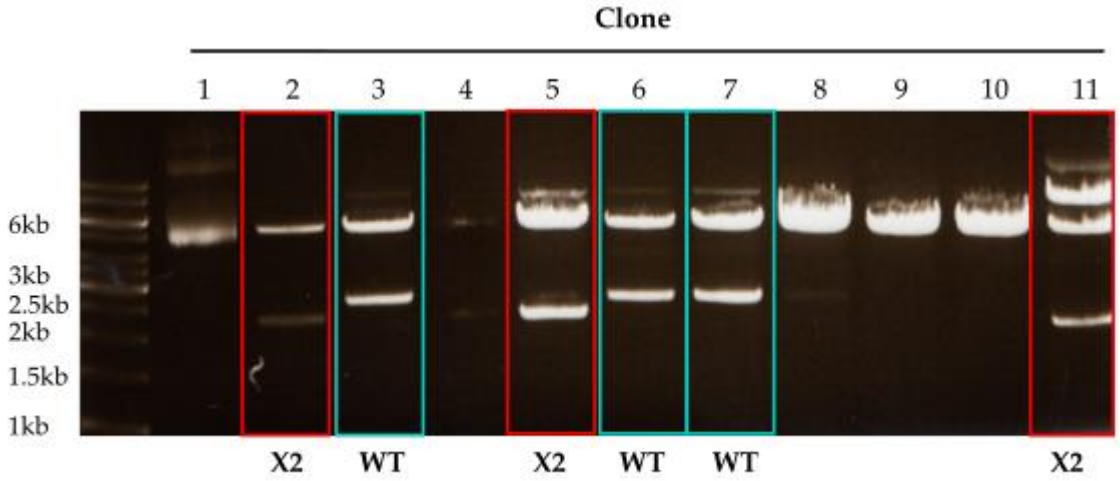

Figure 3.5 Further screening of EphA1 ligations identify full-length EphA1 clone Restriction analysis of additional clones; cleaved with BamHI. Weights are shown in kb. Expected insert size 2.6 kb with BamHI cleavage. Clones 3, 6 and 7 identified as potential full-length EphA1 positive; whilst clones 2, 5 and 11 are likely to represent transcript variant X2 previously isolated (clones 1 and 3, see Figure 3.4a**)**

3.5 Cloning full-length $P^{460}L$

To generate a full-length $P^{460}L$ clone we used OE mutagenesis using mutant PCR primers to introduce the codon changes converting proline to leucine at aa position 460. Two separate PCR reactions lead to the amplification of the coding sequences for N-terminal EphA1 $P^{460}L$ and C-terminal EphA1 $P^{460}L$ respectively (Fig. 3.6 A). The purified fragments were overlap extended in a third round of PCR reactions (Fig. 3.6 B) and cloned into pcDNA5-V5-His. Two positive clones were isolated and sequenced by MWG confirming the introduction of a proline to leucine substitution at position 460.

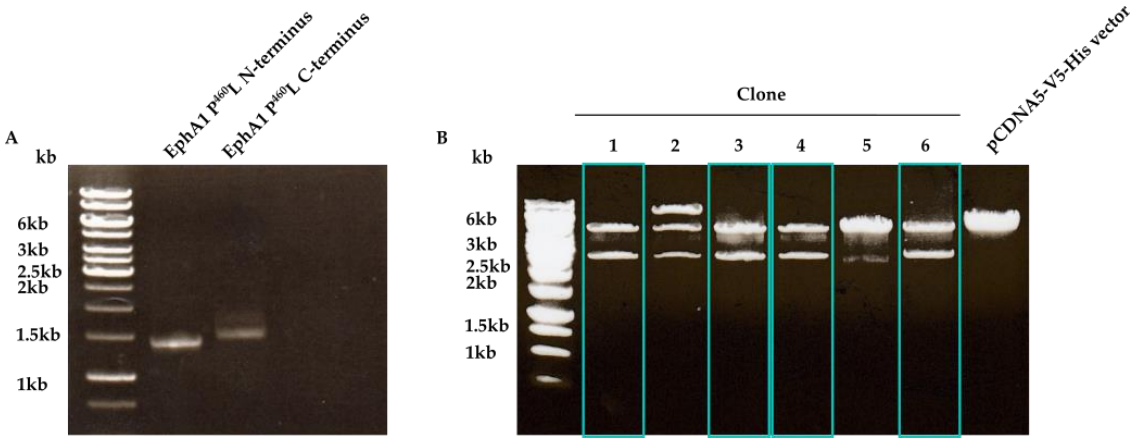

Figure 3.6 Cloning of full-length P460L **A)** Creation of the N-terminus (expected weight 1.3kb) and C-terminus (expected molecular weight 1.7kb) of full-length EphA1 $P^{460}L$ mutation; both regions should contain the mutated sequence. The templates were combined in a second-round of PCR to hybridise the complementary ends and create full-length EphA1 $P^{460}L$. **B)** Restriction analysis of overlap extended clones; cleaved with *NheI* and *NotI*. Clones 4 and 6 were sent for sequence analysis, as they were identified as potentially EphA1-$P^{460}L$ +ve. Weights are shown in kb. Expected insert size 2.6 kb with *NheI* and *NotI* cleavage. Sequencing carried out by Eurofins Genomics confirmed the introduction of the $P^{460}L$ mutation. Clone 6 was used for subsequent transfection.

3.6 Cloning of EphA1 ECD

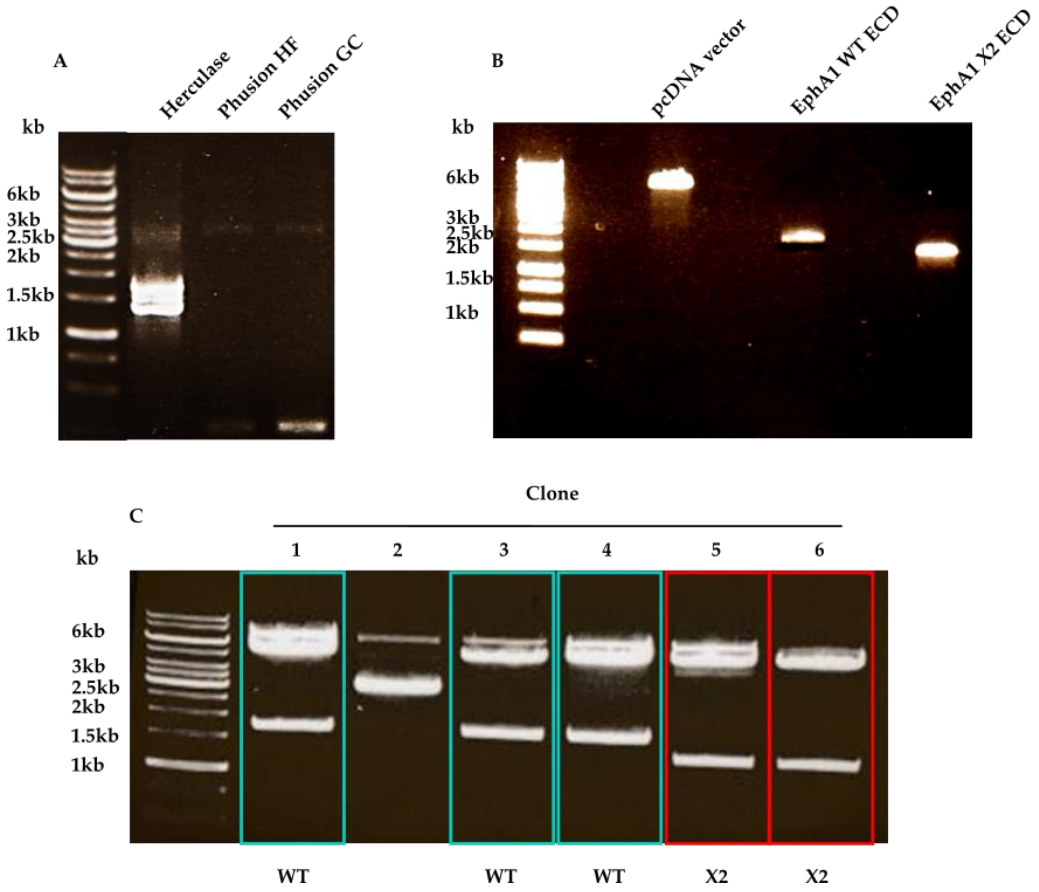

Figure 3.7 Cloning of EphA1 ectodomain. **A)** Optimisation of PCR conditions; H (Herculase) Phusion HF (Phusion High-Fidelity buffer) and Phusion GC (Phusion GC-Rich buffer). **B**) Yield analysis of gel extracted pcDNA/V5/His vector and WT and transcript X2 of EphA1 ectodomain prior to the ligation reaction. **C)** Restriction analysis of clones, identifying clones 1, 3, 4 as probably representing WT and clones 5 and 6 potentially positive for the ectodomain of EphA1 X2. Clone 3 was sent for sequencing by Eurofins Genomics, confirming the amplification of EphA1 ECD

3.7 Cloning of $P^{460}L$ EphA1 ECD fusion protein

To generate EphA1 $P^{460}L$ ECD clone we used OE mutagenesis using mutant PCR primers to introduce the codon changes converting proline to leucine at aa position 460, as described in section 3.2.1.3. Two separate PCR reactions led to the amplification of the coding sequences for N-terminal EphA1 $P^{460}L$ and C-terminal EphA1 $P^{460}L$ respectively (Fig 3.8 A). The purified fragments were overlap extended in a third round of PCR reactions (Fig 3.8 B) and

cloned into pcDNA5-V5-His (Fig 3.8 C). Two positive clones were isolated and sequenced by MWG.

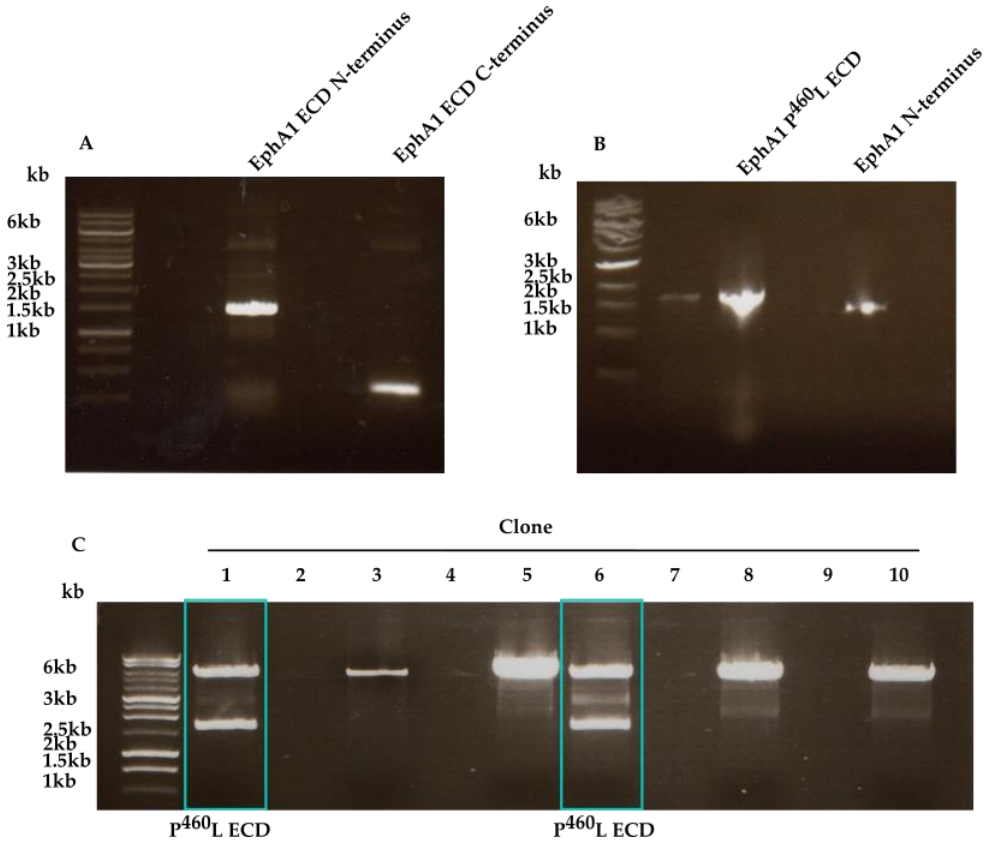

Figure 3.8 Cloning of P460L EphA1 ECD fusion protein **A)** EphA1 WT ECD was used as a template to create the $P^{460}L$ mutation within the ectodomain by creating an N-terminus (expected molecular weight 1.3 kb) and C-terminus (expected weight 300bp) using the inside mutagenic primers. **B)** N-terminus and C-terminus combined in overlap extension (expected weight 1.6kb). The overlap extension PCR product was compared to the N-terminus (1.3 kb) to establish whether an increase in size was observed; which would suggest the complementary ends of the N-terminus and C-terminus had hybridised. **C)** Restriction analysis of clones, identifying clones 1 and 6 potentially positive EphA1-P^{460}L-ECD. Both clones were sent for sequencing by Eurofins Genomics, confirming the amplification of EphA1-P^{460}L-ECD.

3.8 Cell lines expressing EphA1, EphA1 P^{460}L, EphA1 X2, and EphA1 P^{460}L-ECD-Fc

The expression plasmids encoding various EphA1 constructs were co-transfected with POG44, a Flp recombinase, into a HEK293 Flp In cell line followed by culture in Hygromycin B containing selection medium. Cell lysates from EphA1 (Fig 3.9A), EphA1 X2 (Fig 3.9 B) and EphA1 P^{460}L (3.9 C) cell lines were analysed by both western blot and immunocytochemistry (ICC) for anti-V5 signals.

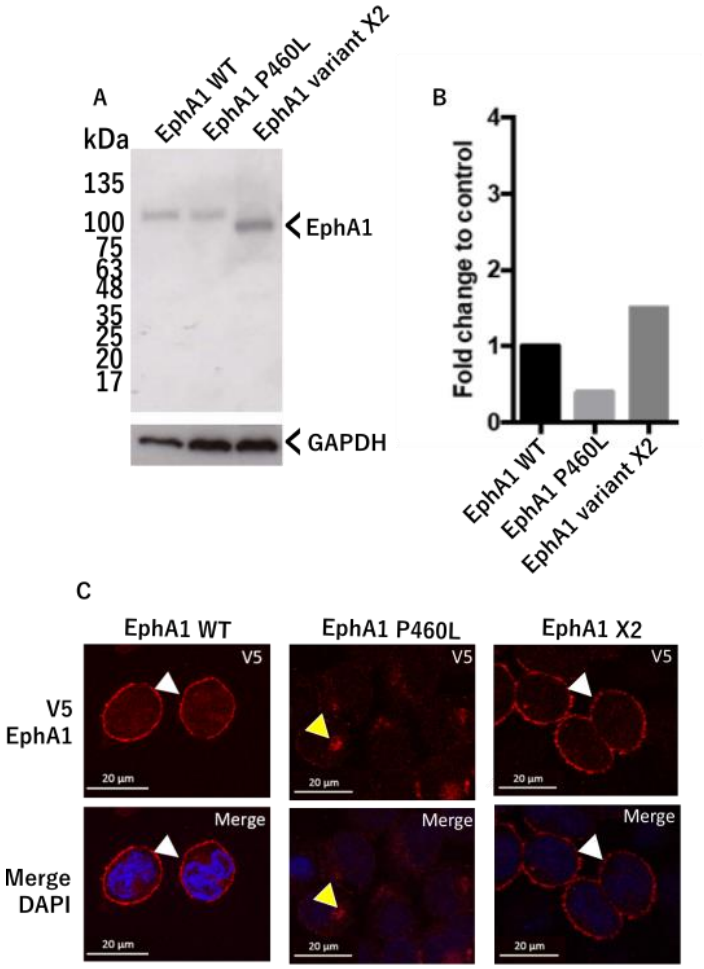

Figure 3.9 Analysis of cell lines expressing EphA1, EphA1 P460L, EphA1 X2, and EphA1 P460L-ECD-Fc **A)** Western blot of full-length EphA1 wild-type, EphA1 P^{460}L and EphA1 X2 lysates using a C-terminal V5 Ab, which detects the V5 tag genetically grafted onto the C-terminus of EphA1 during the cloning process. Expected molecular weight of WT EphA1 ~108kDa **B)** Fold change of expression levels to WT control. **C)** Immunofluorescent stain of EphA1 WT, P^{460}L and X2 using a C-terminal V5 Ab (red). DAPI was used a nuclear counter stain and is shown in blue. White arrows indicate membrane expression, yellow arrows indicate internalisation. Negative controls confirmed the specificity of the V5 Ab (data not shown, n=1.

3.9 Optimisation of P460L ECD expression

Western blotting determined that the optimal growth medium and incubation period for collection of EphA1-P460L-ECD media was SFMII media and that 3 days was likely to give a sufficient yield of EphA1-P460L-ECD once the experiment was scaled up (expected MW of EphA1-P460L-ECD, ~75kDa). This was determined by the heaviest band size on the immunoblot (Fig 3.10).

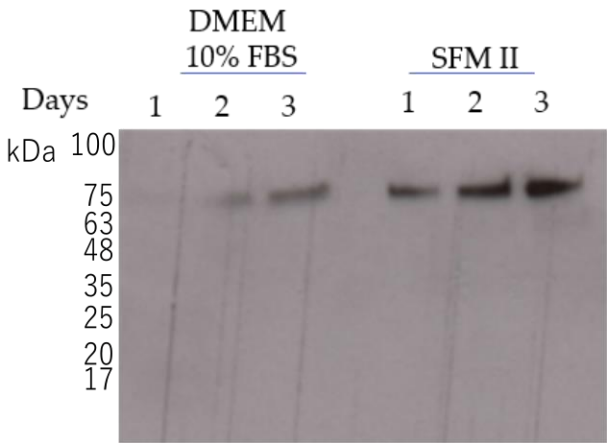

Figure 3.10 Optimisation of EphA1-P460L-ECD expression. The release of the soluble P460L ECD of stably transfected P460L ECD HEK293 cells was assessed over 3 days using DMEM containing 10% FBS or Serum-Free II media (SFM II). The media was immunoblotted using an N-terminal EphA1 Ab. SFM II was deemed optimal as expression is increased using this media.

3.9.1 P460L-EphA1 ECD protein purification

Following P460L-EphA1-ECD protein purification a number of elutions were performed to determine the success of the purification procedure, besides both the starting material (cell conditioned media) and unbound material (supernatant left over after G-protein bead application). This showed that there was still a high proportion of P460L-EphA1-ECD left after protein purification likely due to overloading of the column material, however, elution 1 contained the highest amount of EphA1-ECD. A PBS buffer exchange was subsequently performed on the elution with highest P460L-EphA1-ECD-Fc concentration using PD SpinTrap G-25 columns. 5 elutions were performed to ensure all EphA1 P460L-ECD protein was captured during the buffer exchange procedure, this showed that elution 1 contained

the highest proportion of P460L-EphA1-ECD-Fc (Fig 3.11B), corresponding to 90 μg/μL, as assessed by Nanodrop (Fig 3.11C).

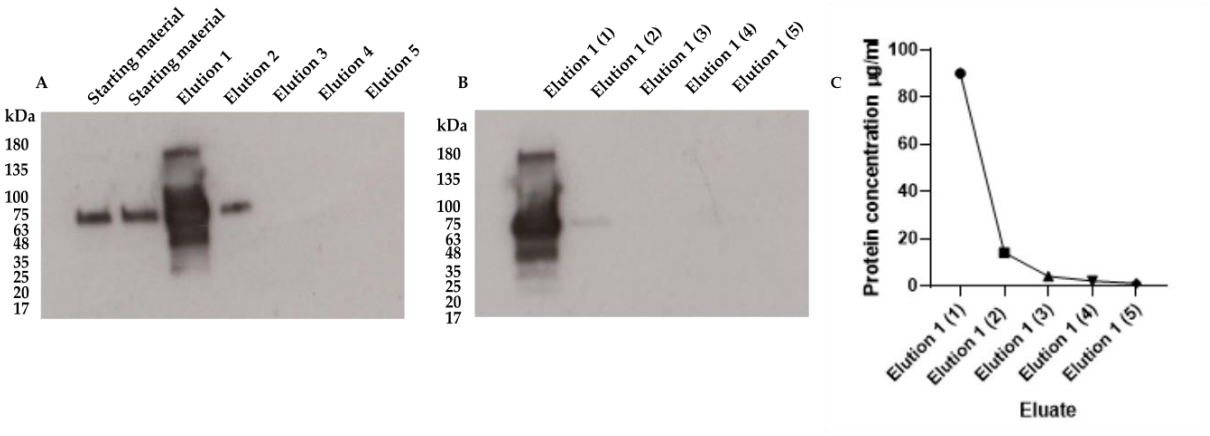

Figure 3.11 Immunoblots showing the purification of P460L-EphA1 ECD. **A)** Immunoblot of the starting material and the elution yield after purification using G protein beads using an N-terminal EphA1 Ab. Elution 1 from the beads contained the highest amount of purified P460L-EphA1 ECD and was used in the subsequent buffer exchange into PBS. **B)** Immunoblot showing the subsequent elutions of elution 1 (Fig 3.9a) following a buffer exchange to PBS. Elution 1(1) contained the highest yield of EphA1-P460L-ECD. **C)** Graph showing the protein concentrations of the eluted buffer exchanged EphA1-P460L-ECD. Elution 1 (1) contains ~90 μg/μL.

3.10 Discussion

Cloning of the desired EphA1 coding sequences was delayed due to the isolation of an EphA1 transcript variant. X2 from the original pDNOR223-EphA1 cDNA clone (Addgene) which was not immediately obvious. The expected size of EphA1 with *BamHI* cleavage would be approximately 2.6kb; the primers used to amplify full length EphA1 (EphA1 (For) EphA1 (Rev); Table 3.1) on the unintended transcript variant X2 would create a product of approximately 2.5kb – indicating that amplification was specific and indicates why this was not identified until sequencing had been conducted. Transcript variant X2 is missing the first FNIII repeat; (amino acid sequence 332-447, see Figure 3.4c, appendix I). Similarly, the double bands seen during the cloning of the ectodomain of EphA1 correspond to the canonical sequence and transcript variant X2; with the predicted PCR products generated using the primers EphA1 (For) and EphA1 ectodomain (Rev)/(Table 3.1 & 3.3) with the use of these templates being 1.6kb and 1.3kb in length, respectively.

3.10.1 Cell line validation

In order to validate that the genetic material was successfully introduced into the HEK-293 Flp-In cells and that the encoded protein was expressed and localised as expected, we performed both western blotting (WB) and immunocytochemistry (ICC), targeting the V5 epitope tag at the C-terminus of the molecule. As described, WT EphA1 is a single-pass type I transmembrane protein containing 976 amino acids, corresponding to a molecular mass of ~108kDa (https://www.uniprot.org/uniprot/P21709). The Western blot analysis indicated that EphA1 was of the predicted molecular mass (see Fig. 3.9a). This has been validated in a previous study investigating EphA1 function, where immunoblotted cell lysates from WT EphA1-green fluorescent protein (GFP) tagged HEK-293 cells show a single band at approximately 108kDa with preserved biological functions (Yamazaki et al., 2009). To determine whether EphA1 was membrane localized, as for other Eph family members such as EphA2 (Wang et al., 2018), immunolabelling of the V5 tag was performed using a monoclonal anti-V5 Ab and a fluorescently tagged secondary Ab (AlexFluor 594). These data indicate that WT EphA1 is predominantly membrane localised with little intracellular staining evident. There have been various other studies confirming the membrane

localisation of the WT protein (Ieguchi et al., 2014; Yamazaki et al., 2009) and thus confident that WT EphA1-V5 is appropriately expressed.

The X2 variant contains 861 aa with a predicted MW of ~96kDa; as Fig 3.9a shows, this is what was found. There is no data on the expression or localisation of the X2 variant. However, it is known that this variant is missing the first FNIII repeat (Fig 3.4 B and C). FNIII are the most common and the largest of the fibronectin subdomain and is evolutionary conserved. They are believed to perform as structural spacers, to arrange further domains. Interestingly, the EphA2 molecule is known to be cleaved within the first FNIII domain by MT1-MPP (Sugiyama et al., 2013). Initial data here has indicated that the overall expression level of the X2 variant is increased in comparison to WT (Fig 3.9 A). This may indicate that EphA1 is cleaved in this region and that the deletion of this region is capable of producing a cleavage resistant molecule. If this is the case, it may indicate that the WT EphA1 molecule undergoes some constitutive proteolysis as has been described for other Eph receptors. However, more work is needed to determine whether this could indeed be the case. The immunofluorescence data of the X2 variant indicates that it is expressed at the cell surface, similarly to that of the WT molecule. Qualitative analysis indicates that there may be lower levels of internalised X2, again indicating that deletion of the first FNIII domain may confer resistance to proteolytic processes, again however, more work is required to asses this hypothesis.

As there is no data available on the outcome of the expression or membrane localisation of EphA1 as a result of the $P^{460}L$ mutation, initial assessment only allowed the formulation of additional hypotheses. It was observed that EphA1-$P^{460}L$ was predominantly localised intracellularly (Fig 3.9 C) with the V5 Ab recognising the C-terminus of EphA1. Moreover, it appears overall expression levels of EphA1 may be reduced as a consequence of the $P^{460}L$ mutation. As previously described, the $P^{460}L$ is located within the second FNIII repeat of the EphA1 molecule. Taken together with the X2 data, it may suggest that the FNIII domains of the EphA1 molecule are important in the regulation of the receptor. The data suggest the mutation may make the molecule more prone to proteolysis and subsequent C-terminal internalisation. It is with this in mind that future chapters will aim to determine the mechanisms by which the mutation confers this effect.

Data indicated that EphA1 can be detected using antibodies to both the N-terminus (EphA1 aa24-547) and C-terminus (V5) of the molecule. These validated antibodies can now be taken forward to subsequent chapters for further analysis of the EphA1 receptor responses to ligand treatment.

3.10.2 Protein purification

The ECD of EphA1 contains 522 aa (26-547) which corresponds to ~75kDa. By immunoblotting the cell free supernatant of EphA1-P^{460}L-ECD-Fc cells using an N-terminal EphA1 Ab it was established that EphA1-ECD was present in the media as a band was identified at the predicting MW of 75 kDa. It was established that SFMII media was optimal over the normal culture media of DMEM and 10% FBS. This is most likely due to a reduction of interfering immunoglobulins in serum-free media. It was confirmed that the EphA1-P^{460}L-ECD-Fc was purified from the media and thus can be used for subsequent experimentation.

Chapter Four

Characterisation of EphA1

4.1 Overview

EphA1 remains one of the least characterised Eph molecules, despite it being the first identified (Hirai et al., 1987). Most of what is known about EphA1 has been established through studies of oncogenesis, with its overexpression identified in several malignancies (Herath et al., 2006; Wang et al., 2015b). To understand the pathological potential of EphA1 AD SNPs, it is first necessary to determine the function of the WT molecule and its regulatory mechanisms. As the EphA1 $P^{460}L$ mutation was successfully cloned and transfected into the HEK-293 Flp-In cell line, direct comparison to the WT molecule will allow appreciation of the pathological potential of the mutant.

4.1.2 EphA1 Ligands

Eph receptors, generally speaking, will interact with ephrin ligands belonging to their respective subclasses, although promiscuity exists within classes. There are some exceptions to interclass interactions however; for instance EphA4 will bind ephrinB ligands (Gale et al., 1996) and EphB2 binds ephrinA5 (Himanen et al., 2004); see Fig 4.1 for a depiction of interclass and across class binding of Eph receptors and their ligands. Binding interactions of immobilized hEphA1 in an enzyme-linked immunosorbent assay (ELISA) was assessed using a mouse ephrinA1-Fc fusion protein, which determined that mEphrinA4 binds with the highest affinity to hEphA1, followed by mEphrinA1 (Noberini et al., 2012). Coulthard and colleagues (2001) demonstrated that murine EphA1 (which was confirmed to occur on the same chromosome of hEphA1), preferentially binds to ephrinA1, but also identified binding to other ephrinA ligands. Other studies, however, have indicated that human ephrinA1 binds with highest affinity to EphA1 and thus likely represents it functional/cognate ligand (Herath et al., 2012). This discrepancy is likely owing to the complexity of the Eph/ephrin system. Nevertheless, as ephrinA1 has been consistently identified as an EphA1 ligand, a recombinant human ephrinA1 fusion protein linked to the Fc region of human IgG_1 (R & D systems) will be used in this chapter to determine the outcome of EphA1-ligand binding. EphrinA1-Fc fusion proteins have been used extensively in studies of Eph-ephrin interactions (Brantley-Sieders et al., 2006; Miao et al., 2009) and whilst these fusion proteins do not confer complete physiological functioning and topology, as ephrinA1 is naturally expressed as a GPI-anchored membrane protein, it is known that

ephrinA1 is capable of being released into the extracellular space as signalling competent monomeric fragments and they are similar to artificially clustered ephrinA1-Fc homodimer (Beauchamp et al., 2012; Wykosky et al., 2008).

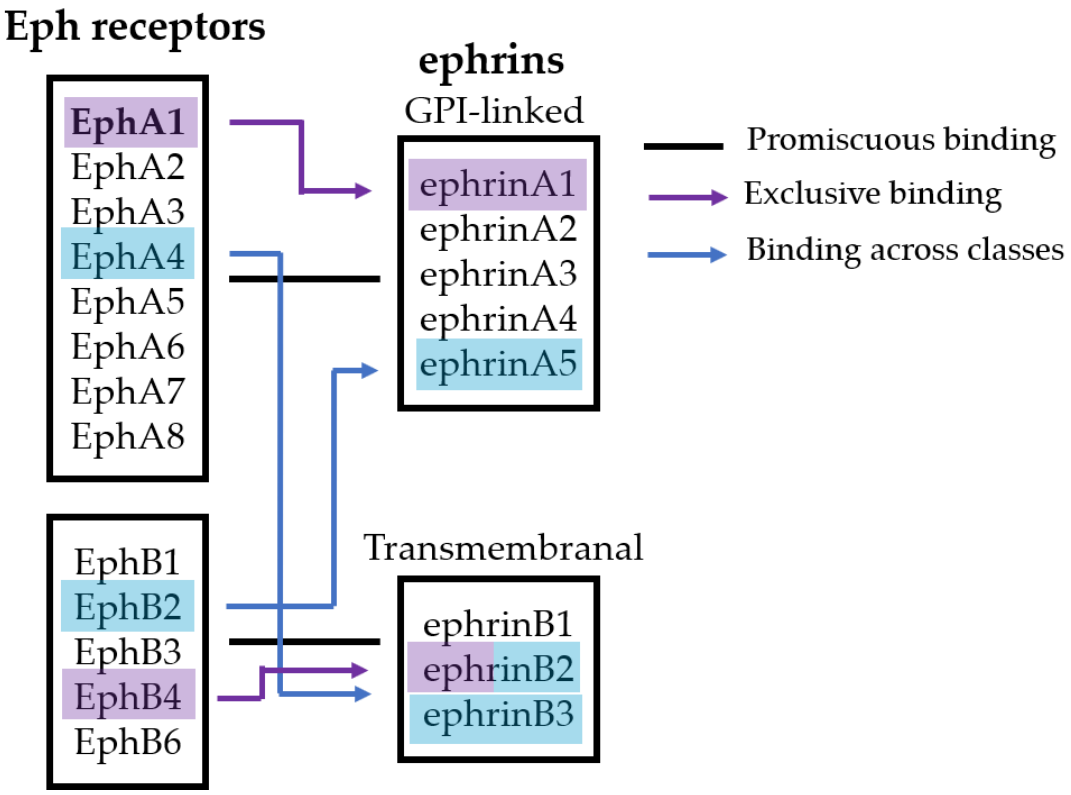

Figure 4.1 Schematic showing binding affinities of Eph receptors and their respective ephrin ligands. EphrinA ligands will bring promiscuously to all EphA receptors and EphB receptors to the ephrinB ligands. However, there are instances of binding across classes (blue arrows) and exclusive binding interactions (purple arrows). EphrinB2 (highlighted in both purple and blue) is characterised by both binding across classes (with EphA4) and is the sole ligand of EphB4.

4.1.3 Potential EphA1 regulatory mechanisms following ephrinA1-Fc engagement

Briefly, when two opposing cells come into close contact, the N-terminal domain of two Eph receptors will recognize two cognate ephrin ligands expressed on the opposite cell resulting in a heterotetrameric Eph-ephrin signalling complex. Studies have shown that EphA2 can also form ligand independent clusters (Himanen et al., 2010; Seiradake et al., 2010) with mutations in the complex interface between EphA2 LBD and the ephrinA5 receptor binding domain (RBD) shown to alter cell-cell contact localization and proteolytic cleavage of the

molecule (Seiradake et al., 2010). Ligand-initiated signal transduction of most RTKs brings about receptor dimerization and subsequent autophosphorylation of their cytoplasmic domains or flexible rotation of monomers in preformed dimers (Fleishman et al., 2002; Moriki et al., 2001; Schlessinger, 2000). Eph receptors, however, require the formation of higher order signalling clusters (Vearing and Lackmann, 2005), where Ephs form arrays interpolated with ephrins (Himanen et al., 2010). The overall size of these signalling clusters correlates with signal strength (Egea et al., 2005) which might go some way in clarifying the variations in cellular responses initiated by Eph signalling. Ephrin-mediated signal transduction is also restricted to specialized membrane microdomains referred to as "lipid rafts" imparting further specificity to the signalling (Gauthier and Robbins, 2003).

As described in section 1.4.6, ligand binding of RTKs generally results in the internalisation of the receptor through endocytosis (Goh and Sorkin, 2013b). The method of internalisation of Eph-ephrin macromolecular complexes, termed trans-endocytosis and can occur in either the Eph or ephrin bearing cell (Marston et al., 2003; Zimmer et al., 2003). There is also a growing body of evidence detailing the role of proteases in the signal termination of Eph-ephrin signalling, followed by regulated intramembrane proteolysis and C-terminal internalisation of Eph/ephrin molecules. For instance, ephrinA1-Fc binding to EphA2 leads to the autophosphorylation of the receptor leading to its eventual internalisation and degradation over time (Walker-Daniels et al., 2002a; Wykosky et al., 2005, 2008). EphrinA1 in complex with EphA2 was reported to be released by proteolysis which was sensitive to the inhibition of MMPs, particularly MMP-1, -2, -9 and -13 (Beauchamp et al., 2012). Importantly, aa positions 175-181 of ephrinA1 are vital for the proteolysis of the complex, with the ephrinA1 fusion protein used in this chapter containing this region (Met1-Ser182). Members of the Eph/ephrin system has been shown to maintain their cleavage potential when expressed as fusion proteins (Lin et al., 2008a). Moreover, EphA2, the EphA1 homologue, is cleaved at the FNIII domain by MT1-MMP, in the region where the $P^{460}L$ mutation is located. Consequently, it would be interesting to determine whether the mutation affects proteolysis of the EphA1 molecule. Following primary processing by MMPs in response to ligand engagement, Ephs can then be further processed by iCliPs such as γ-secretase. As γ-secretase is a complex which is widely studied in are of AD research, we aim to determine whether this complex could impact EphA1 processing. Studies have also

found that ECD shedding can also occur in the absence of ligand through ADAM/MMP activity (modulated by NMDA signalling/Ca^{2+} influx). The membrane bound CTF can then undergo γ-secretase intramembrane cleavage. It is with this in mind that we aim to determine whether EphA1 is regulated similarly to other Eph family members by assessing its overall expression levels and localisation following ligand engagement, and how this is altered in response to inhibition of γ-secretase and MMPs (see Fig 4.2 for the potential regulatory mechanism of EphA1 following ligand engagement). This will also allow determination of whether EphA1 $P^{460}L$ alters the regulatory mechanisms of EphA1.

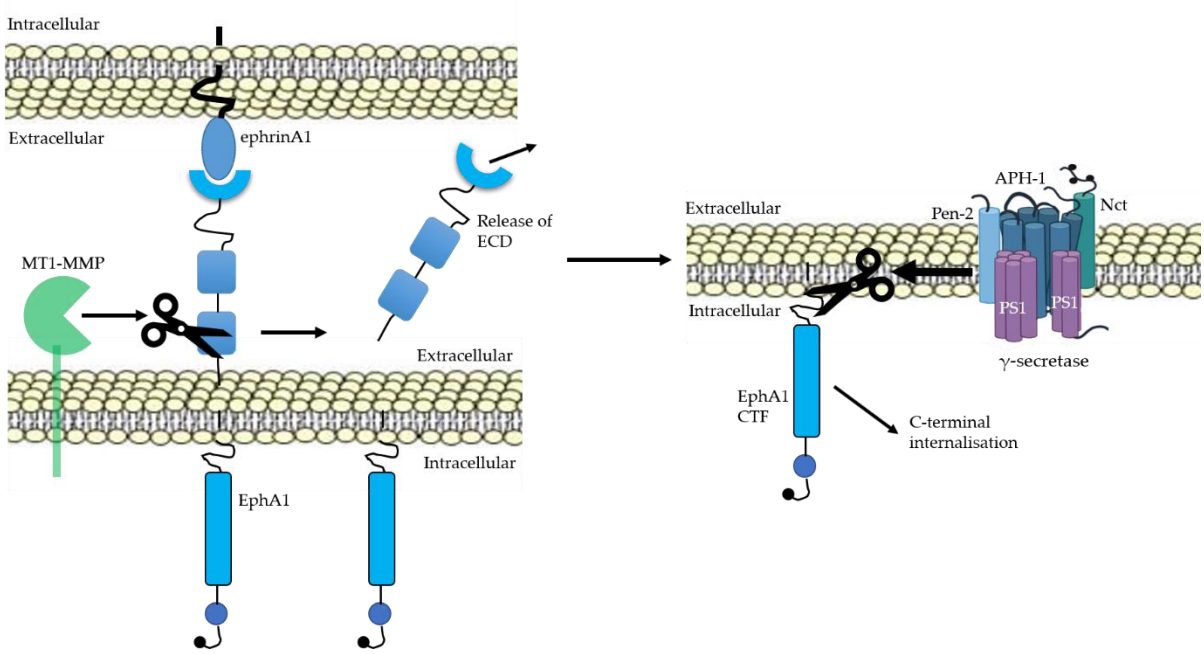

Figure 4.2 Potential regulatory mechanisms of EphA1 following ligand engagement .. EphA1/ephrinA1 interaction could result in sequential ectodomain proteolysis by MMPs e.g. MT1-MMP (left) resulting in the release of the ECD into the extracellular speace and γ-secretase-mediated intramembrane proteolysis resulting in the internalisation of the C-terminal fragment of EphA1 (right).

4.1.4 Possible pathomechanisms of the $P^{460}L$ mutation

The $P^{460}L$ mutation is located in the second fibronectin type-III repeat of the EphA1 molecule. A clear biological function has not been elucidated for this region, making the pathological potential for this mutation unclear. Crystal structures of EphA members have identified a ~90○ kink at the FN1-FN2 linkage region (Himanen et al., 2010) with $P^{460}L$ located close to this junction. Mutations in this region could affect receptor rigidity and

orientation at the membrane, ultimately altering receptor-ligand interactions, as this region is essential for the formation of multimeric Eph signalling clusters. Studies have shown that EphA2 can be cleaved within this region by MT1-MPP (Sugiyama et al., 2013, see section 1.4.3) and thus this mutation could offer a new binding epitope for proteases, ultimately altering the turnover of the molecule. Moreover, it has been shown that the ectodomain of Eph receptors are an important determinant in the biological and functional outcome of ligand-binding through the use of ectodomain-switched chimeric EphA2 and EphA4 (Seiradake et al., 2013) and thus mutations in the region may alter binding responses (e.g. adhesive to repulsive).

Given the evidence that EphA1 dimerises (Vearing & Lackmann, 2005), the $P^{460}L$ mutation may influence the ability of EphA1 to fold properly. The side chain of proline attaches to the protein backbone twice which gives it conformational rigidity and consequently functions to introduce kinks into secondary structure alpha helices and is thus normally found on the surface of proteins. Leucine, conversely, is preferentially buried in hydrophobic cores. It is known that proline does not substitute well with other amino acids. This chapter will aim to determine whether EphA1 $P^{460}L$ alters regulatory mechanisms of EphA1 WT.

4.1.5 Aims

The aim of this chapter is to establish how the EphA1 protein is regulated and the consequences of EphA1-ligand interactions. This will be determined by investigating the membrane stability and cellular localisation of EphA1 WT following ligand engagement with soluble ephrinA1-Fc. We also aim to establish what proteases are responsible for EphA1 turnover should it be cleaved. This will be achieved by using various inhibitors. In particular, we will use GM6001 a broad-spectrum MMP inhibitor and N-[N-(3, 5-difluorophenacetyl-L-alanyl)]-S-phenylglycine t-butyl ester (DAPT) an inhibitor of γ-secretase.

- Determine the effect of ephrinA1-Fc on the membrane stability and cellular localisation of full-length wild-type EphA1.
- Establish what proteases are predicted to cleave EphA1 using the protease specificity prediction server (PROSPER) tool, a webserver for *in silico* prediction of cleavage sites and protease substrates for a given protein sequence.
- Establish what proteases are responsible for EphA1 regulation.
- Determine whether the $P^{460}L$ mutation alters EphA1 regulatory processes.

4.2 Methods

4.2.1 Treatment procedure

Cells were treated with 2 μg/ml of ephrinA1-Fc (R&D systems), a control human IgG at 2 μg/ml, 25μM of DAPT or 25 μM of GM6001 (Millipore) over 0-3h time-points in serum-free DMEM as indicated. The treatment media was collected and centrifuged for 10 mins at 4°C at 250x g to pellet cellular debris and concentrated ~10-fold using Amicon Ultra-4 centrifugal filter units (Millipore) with a nominal molecular weight (MW) limit of 3kDa. For subsequent immunoblotting, the remaining cells were washed in PBS and lysed as described in section 2.2. To determine the cellular localisation of EphA1 WT and $P^{460}L$ following treatment with ephrinA1-Fc, GM6001 or DAPT, cells were prepared as described in section 2.3.

4.2.2 Analysis of membrane and cytosolic staining using Image J

Region-of-interest (ROI) analyses was conducted using ImageJ to determine the membrane or cytosolic membrane intensity of EphA1 cells. Using the *Freehand Tool,* an ROI was selected (i.e. the membrane or cytosol component) followed by *Analyze* > *Plot Profile* with the overall pixel intensity returned. The background immediately adjacent to the ROI was selected using the same freehand drawn shape. This intensity was then subtracted from the given ROI intensity to correct for any differences in background staining between slides and experiments. At least 5 cells were analysed per slide.

4.3 Results

4.3.1 EphrinA1-Fc induced turnover of membrane EphA1

To determine whether ligand engagement alters the overall expression levels of WT EphA1, HEK-293 stably expressing WT EphA1 were incubated with 2 μg/ml of ephrinA1-Fc, or a control IgG for 0-2h and cell lysates were immunoblotted using an anti-V5 Ab, which detects the C-terminus of EphA1. The cellular supernatant was also immunoblotted with an N-terminal EphA1 Ab.

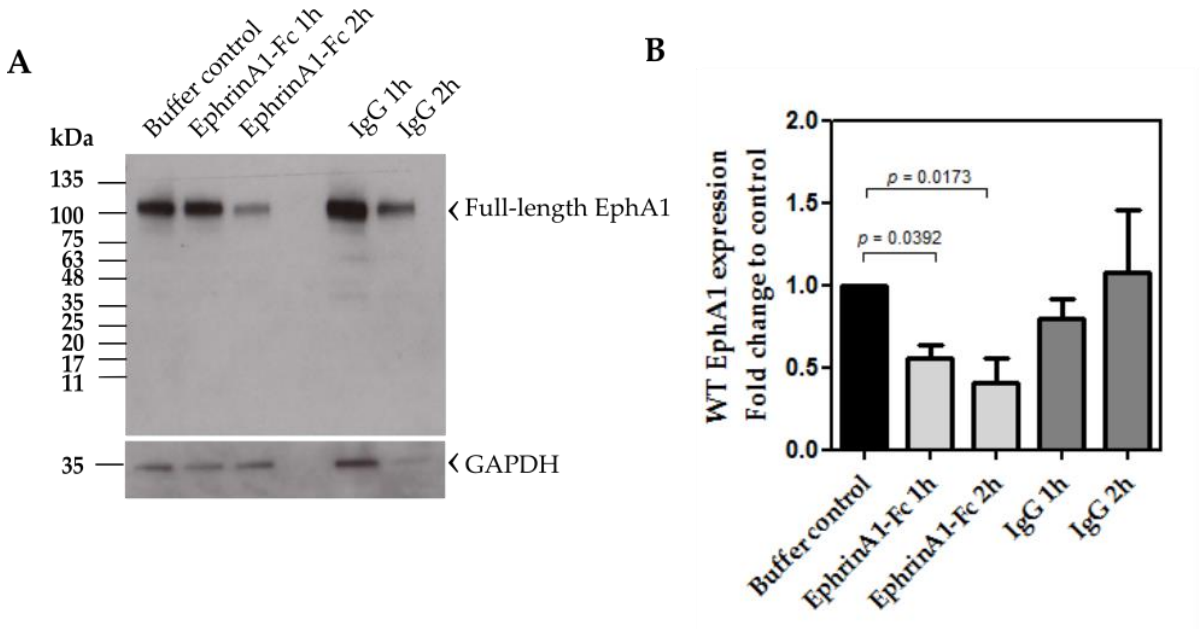

Figure 4.3 The effect of ephrinA1-Fc on the overall expression levels of WT EphA1 **A)** Representative immunoblot indicating full-length WT EphA1 response to ligand engagement (2 μg/ml ephrinA1-Fc) over a 2h time-course. Blots were probed with an anti-V5 Ab which detects the C-terminus of EphA1. Human-IgG was used as a control at the same concentration (i.e. 2 μg/ml) as ephrinA1-Fc which ensures any effects are not due to the Fc portion of the fusion protein. The buffer control contains media only. Molecular weights are indicated in kDa **B)** Histogram shows fold increase compared to the buffer control based on the mean values of three independent experiments. Bands were normalised to the loading control GAPDH. Error bars indicate standard error of the mean (SEM). Analyses were conducted using a one-way analysis of variance (ANOVA).

EphrinA1-Fc (2 μg/ml) incubation with full-length WT EphA1 cells over 2h indicated that ligand engagement caused a decrease in full-length EphA1 expression as assessed by immunoblot analysis of lysates using a V5 C-terminus Ab (Fig 4.3 A, control v 1h $p = 0.0392$; control v 2h $p = 0.0173$). Experimental control cells were treated with a human-IgG to ensure

the effects seen were not due to the Fc-portion of the ephrinA1 fusion protein. Full-length EphA1 expression remains unchanged after IgG treatment at 1h (p = 0.1660) and 2h (p = 0.8530, Fig 4.3 A & B). These results indicate that ephrinA1-Fc is acting upon EphA1. Collected media were immunoblotted, with the same anti-V5 Ab, with no staining evident, suggesting the C-terminal portion of EphA1 remains intracellular upon ligand engagement (data not shown). The experimental supernatant was also immunoblotted prior to and following concentration using Amicon centrifugal filter units, using an EphA1 N-terminal Ab with no staining evident, perhaps suggesting N-terminal EphA1 is below the detection limit for western blot analysis, or that the N-terminus is not released following ligand engagement.

4.3.2 The effect of ephrinA1-Fc on the cellular localisation of WT EphA1

To determine the localisation/expression of WT EphA1 following ephrinA1-Fc (2 μg/ml) ligand engagement over 3h, cells were assessed by indirect immunofluorescence using a V5 C-terminal primary Ab and an AlexaFluor 594 conjugated secondary antibody.

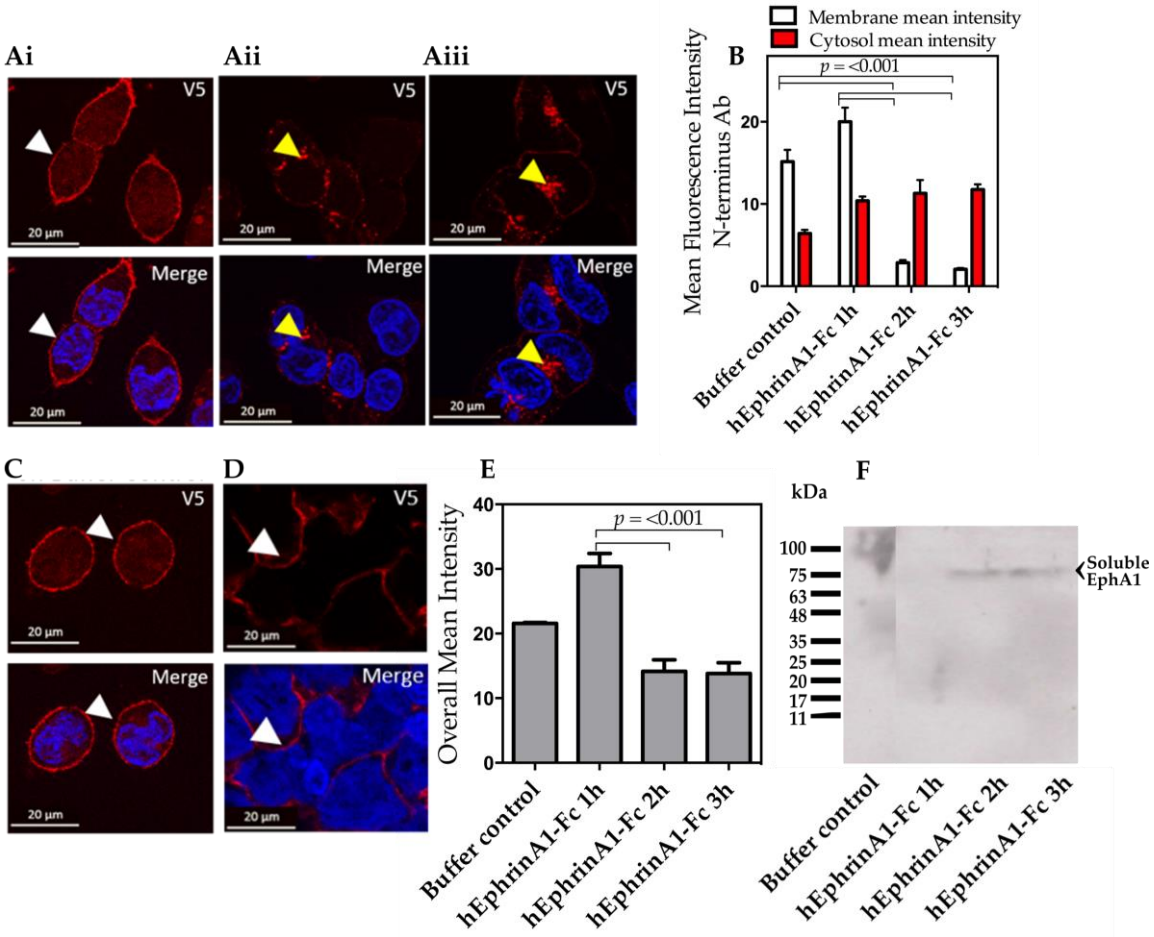

Figure 4.4 The effect of ephrinA1-Fc on the cellular localisation of WT EphA1. Representative immunofluorescence staining of EphA1 (red) using a V5-Ab (C-terminus) treated with ephrinA1-Fc (2 μg/ml) over a 3h time-course (n=3; images taken from at least 3 different fields). DAPI (blue), was used as a nuclear fluorescent counter stain. White arrows indicate membrane localisation, yellow arrows indicate internalisation of EphA1. **Ai)** EphrinA1-Fc treatment for 1h, membrane staining is evident **Aii)** hEphrinA1 treatment for 2h, staining appears punctate, with apparent internalisation of the C-terminus. **Aiii)** EphrinA1 treatment for 3h, EphA1 appears internalised. **B)** Mean fluorescence intensities were determined for the membrane and cytosol using ImageJ. **C)** Buffer control indicating membrane expression of EphA1. **D)** Control hIgG confirms results are not due to the Fc portion of the fusion protein as EphA1 remains at the membrane at 3h **E)** Mean overall fluorescence levels were assessed using ImageJ **F)** Supernatants (i.e. treatment media) from the experiment described herein, were immunoblotted for soluble EphA1 using an N-terminal EphA1 Ab. A cleavage product of ~75 kDa was identified at a 2 and 3h time-point in one experiment. Error bars indicate SEM. Analyses were conducted using a two-way ANOVA.

Following buffer control and ephrinA1-Fc treatment for 1h, EphA1 expression appears membranous as indicated by the white arrows (Fig. 4.4 C & Ai respectively); at a 2h and 3h ephrinA1-Fc treatment timepoint, there appears to be an internalisation of the receptor with V5-staining closer to the nuclei of the EphA1 expressing cells, suggesting that EphA1 may undergo retrograde transport through vesicular compartments for degradation (as indicated by the yellow arrows Fig 4.4 Aii, Aiii). The EphA1-ve and no primary Ab control confirmed the specificity of the V5 Ab (Appendix VI). ROI analysis using ImageJ established mean EphA1 fluorescence intensities in the membrane and the cytosol (whilst subtracting the adjacent background staining for each ROI) as described in section 4.2.2. This confirmed qualitative immunofluorescent analysis of the ephrinA1-Fc treated cells. There is a reduction in membrane staining at 2 and 3h time-point ($p = <0.0001$, Fig. 4.4 B). There is an increase in cytosolic fluorescence levels with increasing treatment time-points (although non-significant) and a reduction in overall fluorescence at a 2 and 3h timepoint, suggesting that the receptor is degraded upon ligand engagement ($p = <0.0001$). A soluble fragment of EphA1, roughly corresponding to the expected MW of the ECD of EphA1 (i.e.~75kDa) was released at a 2 and 3h time-point in one experiment using an N-terminal EphA1 Ab, suggesting EphA1 may be proteolyzed following ligand engagement at the ectodomain (Fig 4.4 F). As this result was not consistently reproducible, this could again highlight the possible lack of sensitivity of immunoblotting to cellular supernatants, due to low protein levels. The manner in which this experiment differed from the analyses of cellular supernatants in the previous experiment (Fig 4.3) is that cells were plated on glass coverslips during their treatment procedure, which could suggest plastic absorption of proteins.

4.3.3 Internalised EphA1: a full-length or cleaved species?

As a potential cleavage product of EphA1 (~75kDa) was identified in the media following ephrinA1-Fc treatment at 2 and 3 h via immunoblotting proved to be inconsistently reproducible, the internalised product identified by fluorescence staining of the C-terminus (Fig 4.4 Aii, Aiii) was assessed further. To determine whether this product corresponded to a full-length or cleaved species may give insight into whether the ECD is released into the extracellular space. This was achieved by dual staining of the N-terminus with a monoclonal EphA1 Ab and the C-terminus with a V5 Ab (Rb) on EphA1 WT cells following ephrinA1-Fc treatment. Should the ECD be cleaved into the extracellular space, one would not expect to see N-terminal staining within the cytosol of the cells. Ligand binding should not prevent N-terminal Ab binding as this Ab detects the whole region of the EphA1 ECD.

4.3.3.1 Optimisation of N-terminal and C-terminal antibodies

Prior to testing this hypothesis, it was necessary to optimise previously unused antibodies. The N-terminal EphA1 (Ms) antibody was previously used to detect the N-terminus of EphA1 via western blotting, but not validated for use in immunofluorescence studies. An alternative V5 Ab (Rb) was sourced as the previously validated V5 antibody was derived from the same species as our N-terminal Ab (i.e Ms). These antibodies were validated independently.

4.3.3.2 Optimisation of the EphA1 N-terminal Ms Ab

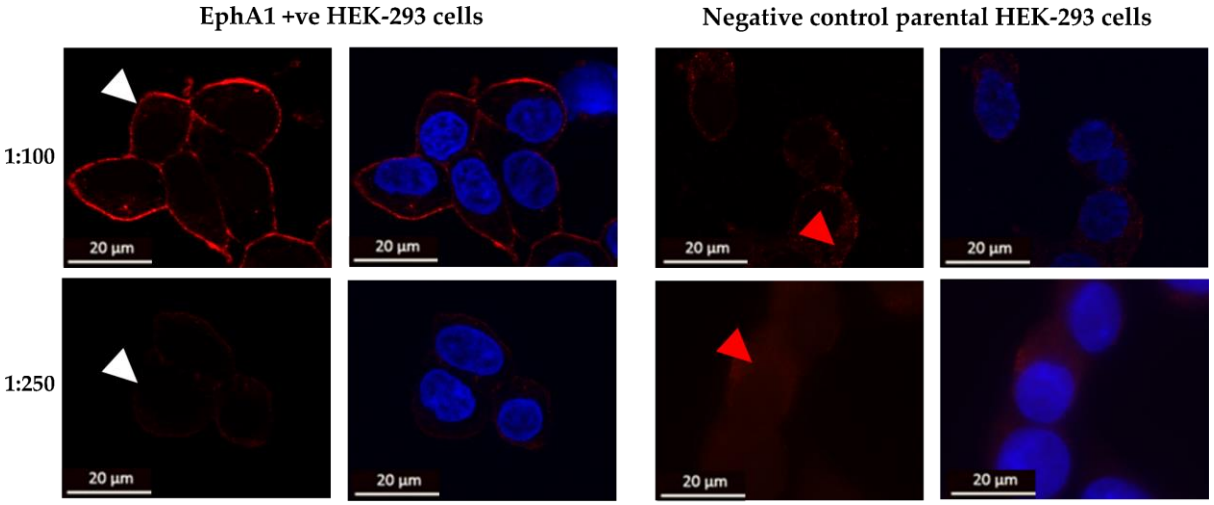

Figure 4.5 Optimisation of EphA1 N-terminal Ms Ab Representative immunofluorescence staining using an EphA1 N-terminal Ab (EphA1: Arg24-Glu547; red) on EphA1 WT HEK-293 cells (left panel) or parental HEK-293 cells (right panel) as a negative control. Cells were tested with 1:100 and 1:250 dilutions. Images were taken from at least 3 different fields. DAPI (blue), was used as a nuclear fluorescent counter stain. White arrows indicate membrane localisation; red arrows indicate background staining.

Data suggested that 1:100 was an optimal dilution, as this dilution showed strong membrane staining with minimal background staining evident in the EphA1 negative control cells.

4.3.3.3 Optimisation of the C-terminal anti-V5 Rb Ab

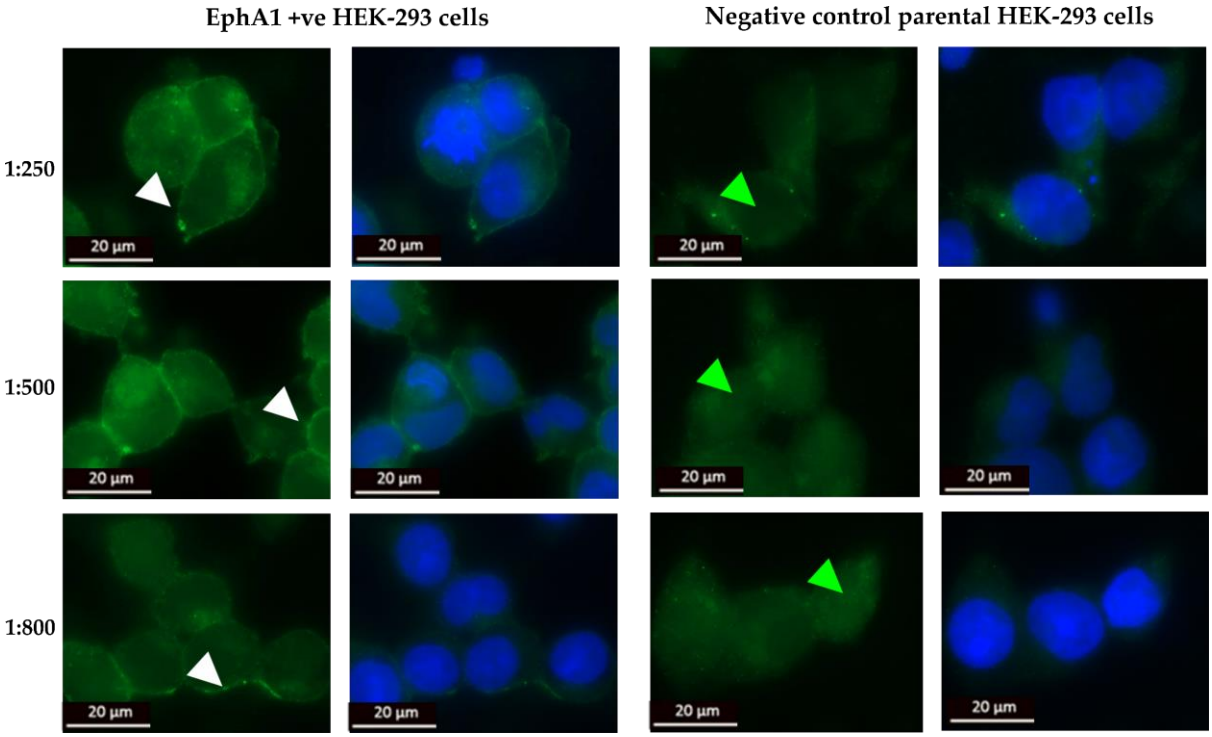

Figure 4.6 Optimisation of C-terminal anti-V5 Rb Ab Representative immunofluorescence staining using an anti-V5 Ab on EphA1-WT HEK-293 cells (left) or parental HEK-293 cells as a negative control (right). Cells were tested with 1:250-1:800 Ab dilutions. Images were taken from at least 3 different fields. DAPI (blue), was used as a nuclear fluorescent counter stain. White arrows indicate membrane localisation; green arrows indicate background staining.

Whilst there seems to be some background staining at all dilutions (as indicated by the green arrows in the right-hand panel), both 1:250 and 1:500 dilutions show membrane staining for EphA1 that is clearly distinguishable from background staining. As a result, future studies employed a dilution of 1:250 for the rabbit anti-V5 Ab.

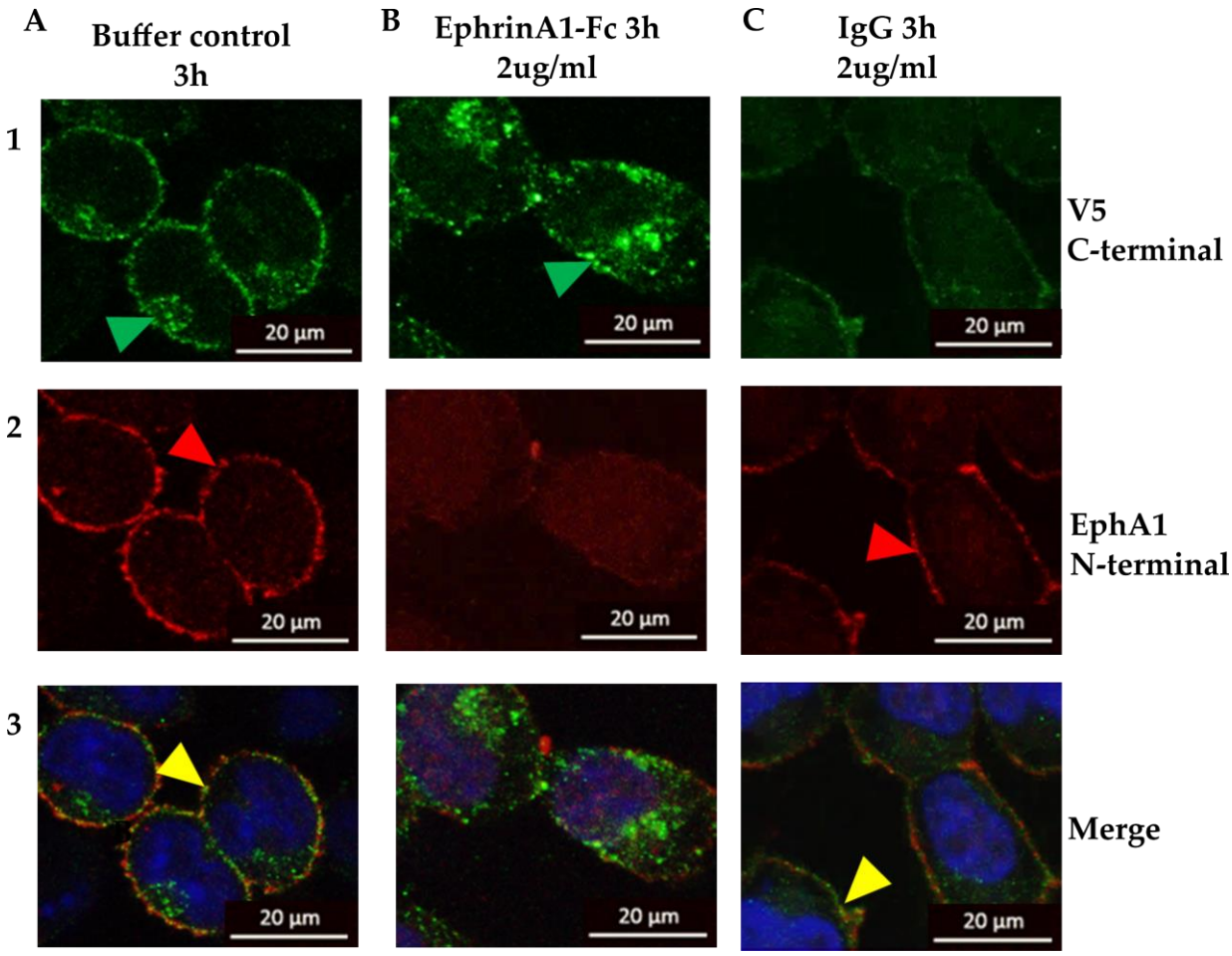

Figure 4.7 Dual staining of EphA1 WT **A)** Representative immunofluorescent staining of EphA1 N-terminus (EphA1: Arg24-Glu547; red) and EphA1 C-terminus (V5; green) treated with ephrinA1-Fc (2 µg/ml) or control IgG ((2 µg/ml) for 3h (n=3; images taken from at least 3 different fields). DAPI (blue), was used as a nuclear fluorescent counter stain. Red arrows indicate membrane localisation; green arrows indicate C-terminal EphA1. Qualitative analysis suggests N-terminal expression of EphA1 decreases at 3 hours following ephrinA1-Fc treatment (B2) i.e. membrane expression is lost or reduced Moreover, there appears to be an increase in the amount of C-terminal staining at 3 h compared to both the buffer control and IgG (top row). Importantly, minimal or no red staining has been identified within the cytosol of the cells following ephrinA1-fc treatment, suggesting that ephrinA1-mediated internalisation of EphA1 is a cleaved species. hIgG control shows similar membrane expression as the buffer control after 3h. Yellow arrows indicate co-localisation of N-terminal and C-terminal EphA1 (bottom row), indicating very little co-localisation following ephrinA1-Fc treatment of WT EphA1 cells, again indicating that the internalised product is a cleaved species.

Qualitatively, it appears membrane expression of EphA1 is reduced by ephrinA1-Fc at 3h as indicated by a reduction in red membrane staining at this time-point (Fig 4.7, B2). There appears to be some co-localisation of N-terminal EphA1 and C-terminal EphA1 as shown by yellow staining (overlap of red and green staining) in both buffer control and IgG treated cells (Fig 4.7 A3, and C3 respectively). This indicates that EphA1 remains full length at the membrane in these conditions as the predominant co-localisation is at the membrane. There appears to be some C-terminal internalisation of EphA1 following treatment with the buffer control indicating that EphA1 may undergo constitutive proteolysis in the absence of ligand or that this corresponds to newly synthesized EphA1 in the Golgi apparatus (Fig 4.7 A1). Following ephrinA1-Fc treatment, there is an increase in C-terminal staining (Fig 4.7 B1, green arrow) with very little or no co-localisation with the N-terminal staining (Fig 4.7 B3). This suggests the internalised product is a cleaved species and does not correspond to full-length EphA1, providing further evidence that ligand engagement causes ectodomain shedding and C-terminal internalisation at 3h. The collected media was immunoblotted with an N-terminal Ab showing no evidence of cleaved ectodomain, but as previously described this could be due to the lack of sensitivity of western blotting to proteolyzed proteins in media. As these data suggest that EphA1 may be proteolyzed at the ECD, the next step was to determine whether the loss of membrane staining, and C-terminal internalisation could be prevented using blocking antibodies to determine mechanisms of EphA1 turnover following ligand engagement.

4.3.4 Is the turnover of WT EphA1, MMP/γ-secretase dependant?

4.3.4.1 *In Silico* analysis using the PROSPER tool predicts EphA1 cleavage sites

As data thus far has indicated that WT EphA1 may be cleaved following ephrinA1-Fc engagement (due to the identification of a potential cleavage product in the media at 75kDa and lack of N-terminal staining within EphA1 WT expressing cells following ephrinA1-Fc treatment), we used the PROSPER webserver tool to predict potential proteases responsible for the cleavage of EphA1 which would give a N-terminal cleavage product of approximately 75 kDa. Also provided are references to other Eph molecules which are cleaved by the identified proteases.

Table 4.1 Prediction of proteases responsible for the cleavage of EphA1 using the Protease specificity prediction server (PROSPER). Proteases giving an N-terminal fragment of ~75kDa are included.

Protease	Position	Segment	N-terminal Fragment (kDa)	C-terminal Fragment (kDa)	Score	Reference
MMP-2	623	DPAW▮LMVD	75.29	43.06	1.02	(Beauchamp et al., 2012; Lin et al., 2008b)
MMP-9	600	KPYV▮DLQA	72.57	45.78	1.11	*As above*
MMP-9	618	FTRE▮LDPA	74.71	43.65	1.05	*As above*
MMP-9	623	DPAW▮LMVD	75.29	43.06	1.19	*As above*

In silico analysis suggested that MMP-2 and MMP-9 are predicted to proteolyze EphA1 to give an N-terminal fragment of ~75kDa. Given that EphA2 has been shown to be cleaved by MT1-MMP at the FNIII domain (the location of the $P^{460}L$ mutation in EphA1), the appropriate next step was to determine whether EphA1 proteolysis is MMP dependant. WT EphA1 HEK-293 cells were treated with the broad-spectrum MMP inhibitor, GM6001/Ilomastat, in both the presence and absence of ephrinA1-Fc ligand. As WT EphA1 undergoes C-terminal internalisation upon ligand engagement, we also aim to determine how this occurs. The γ-secretase complex is responsible for the regulated intramembrane proteolysis of other Eph/ephrin family members and is extensively studied in the area of AD research due to its processing of APP. Appropriately, the γ-secretase inhibitor, DAPT was tested in combination with ephrinA1-Fc to assess WT EphA1 C-terminal internalisation in the first instance.

4.3.4.1 The effect of GM6001/Ilomastat on the localisation of N-terminal WT EphA1

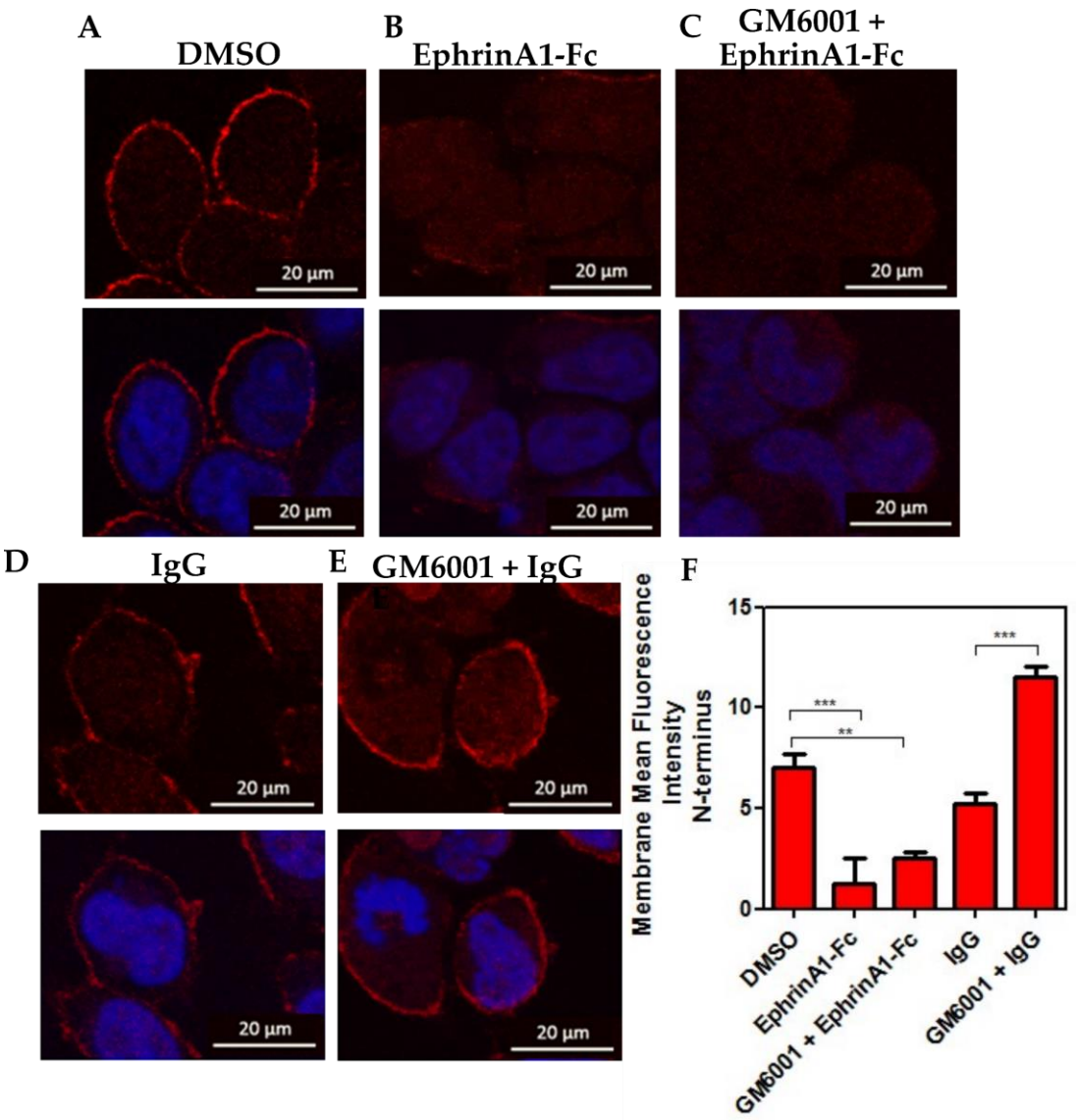

Figure 4.8 The effect of GM6001/Ilomastat on the localisation of N-terminal WT EphA1 Representative immunofluorescence staining of WT EphA1 N-terminus (EphA1: Arg24-Glu547; red). Images taken from at least 3 different fields of view. DAPI (blue), was used as a nuclear fluorescent counter stain. **A)** WT EphA1 cells were treated with DMSO for 3 h. **B)** Treatment with ephrinA1-Fc (2 µg/ml) for 3 h. **C)** Cells were treated with ephrinA1-Fc (2 µg/ml) in combination with the broad spectrum MMP inhibitor, GM6001/Ilomastat (25 µM for 3h. **D)** Cells were treated with an IgG control at the same concentration as ephrinA1-Fc (i.e. 2 µg/ml) for 3h. **E)** Cells were treated with an IgG control at the same concentration as ephrinA1-Fc (i.e. 2 µg/ml) in combination with the broad spectrum MMP inhibitor, GM6001/Ilomastat (25 µM) for 3h. **F)** The mean fluorescent intensity of the membrane staining was determined by identifying a ROI using ImageJ and subtracting the immediate background intensity adjacent to the membrane ROI. Analyses were conducted with a one-way ANOVA with Bonferroni correction, *** $p < 0.01$, ** $p < 0.05$

EphrinA1-Fc treatment of WT EphA1 cells significantly reduced the membrane expression of N-terminal EphA1 as indicated by a drop in mean fluorescence intensity at the membrane compared to the DMSO control (p = <0.01, Fig 4.8 F). Following ephrinA1-Fc treatment in combination with the MMP inhibitor GM6001, N-terminal EphA1 membrane expression was not rescued (Fig 4.8 F). Whilst the control IgG did not significantly alter the membrane expression of EphA1, it does appear that IgG and GM6001 treatment in combination, significantly increases membrane expression, compared to control IgG alone, (p =<0.01, Fig 4 F) again suggesting that EphA1 may undergo some constitutive proteolysis in the absence of ligand and that MMP inhibition may prevent ligand independent proteolysis. Next, it was determined whether γ-secretase inhibition could prevent the C-terminal internalisation of WT EphA1 by assessing membrane and cytosolic fluorescence intensities.

4.3.4.2 The effect of DAPT on the localisation of C-terminal WT EphA1

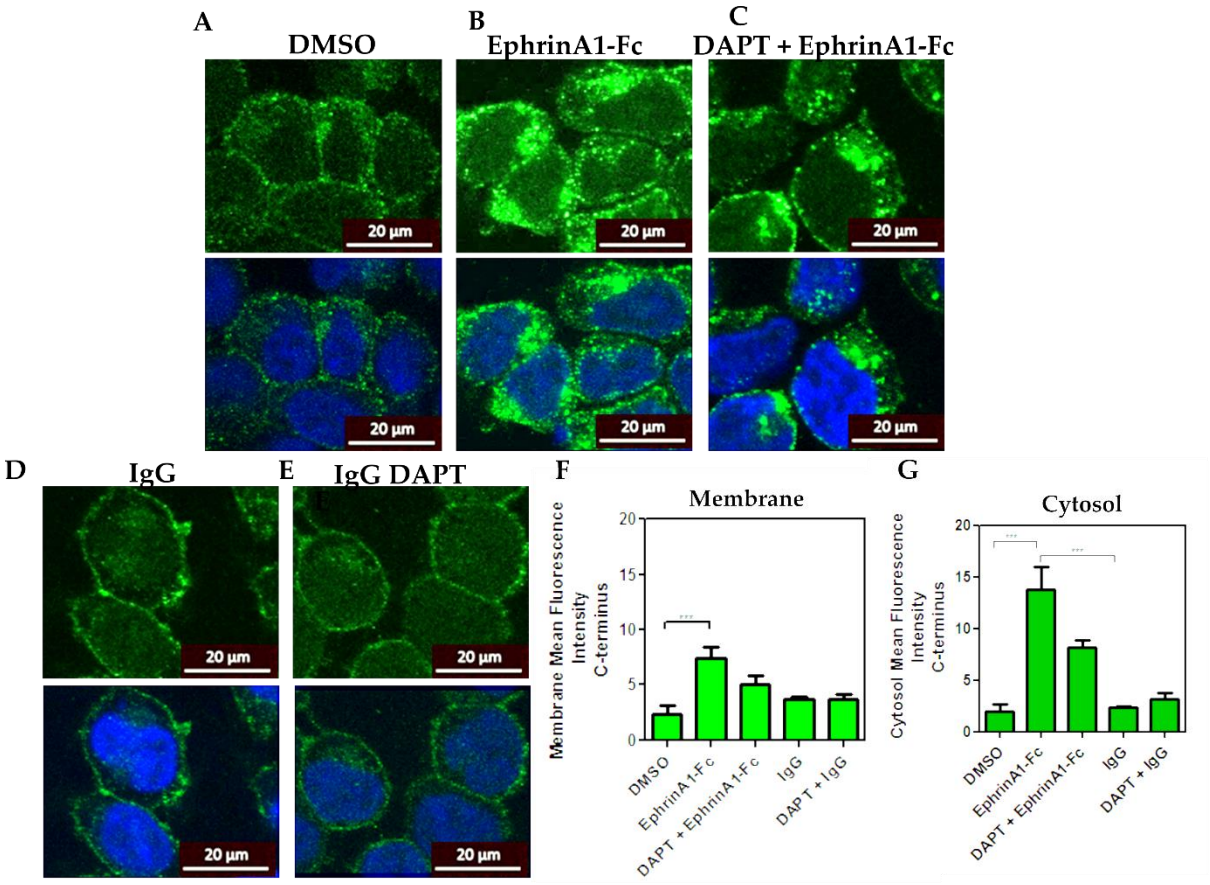

Figure 4.9 The effect of DAPT on the localisation of C-terminal WT EphA1 Representative immunofluorescence staining of WT EphA1 C-terminus (green); images taken from at least 3 different fields. DAPI (blue), was used as a nuclear fluorescent counter stain. **A)** WT EphA1 cells were treated with DMSO for 3 h. **B)** Treatment with ephrinA1-Fc (2 µg/ml) for 3 h. **C)** Cells were treated with ephrinA1-Fc (2 µg/ml) in combination with γ-secretase inhibitor DAPT (5 µM) for 3 h. **D)** Cells were treated with an IgG control at the same concentration as ephrinA1-Fc (i.e. 2 µg/ml) for 3h. **E)** Cells were treated with an IgG control at the same concentration as ephrinA1-Fc (i.e. 2 µg/ml) in combination with γ-secretase inhibitor DAPT (5 µM) for 3 h. F) The mean fluorescence intensity of C-terminal membrane staining was determined by identifying a membrane ROI using using ImageJ **G)** The mean fluorescence intensity of the cytosolic staining was determined by identifying a cytosolic ROI using ImageJ. Analyses were conducted with a one-way ANOVA with Bonferroni correction, *** $p < 0.01$, ** $p < 0.05$

EphrinA1-Fc treatment of WT EphA1 cells significantly increased the internalisation of the C-terminus of WT EphA1 compared to both the DMSO control (p = < 0.01) and the IgG control (p = <0.01) as show in previous experiments (Fig 4.4), established by determining levels of fluorescence within the cytosol. DAPT does not prevent C-terminal internalisation of EphA1 (i.e. the C-terminal fluorescence staining within the cytosol is not blocked by DAPT) but it does appear to reduce internal fluorescence intensities in combination with ephrinA1-Fc treatment (Fig 4.9 F). This suggests that γ-secretase may play a role in the secondary processing of WT EphA1 but that there are alternative methods of C-terminal internalisation following proteolysis of the N-terminus. Neither treatment with the control IgG nor the control IgG along with DAPT alters the localisation of C-terminal EphA1, compared to the DMSO control, showing that these are appropriate controls.

These data indicate that membrane staining of the C-terminus is retained upon ephrinA1-Fc treatment (Fig 4.9 B & F) which is contradictory to previous findings. This may indicate that there is maintenance of full-length EphA1, that there is a membrane bound C-terminal fragment or that the membrane is not easily discernible for manual identification using ImageJ. During these series of experiments, both the N-terminus and C-terminus of EphA1 were stained for and thus to investigate the above possibility, assessment of the N-terminal and C-terminal staining was undertaken.

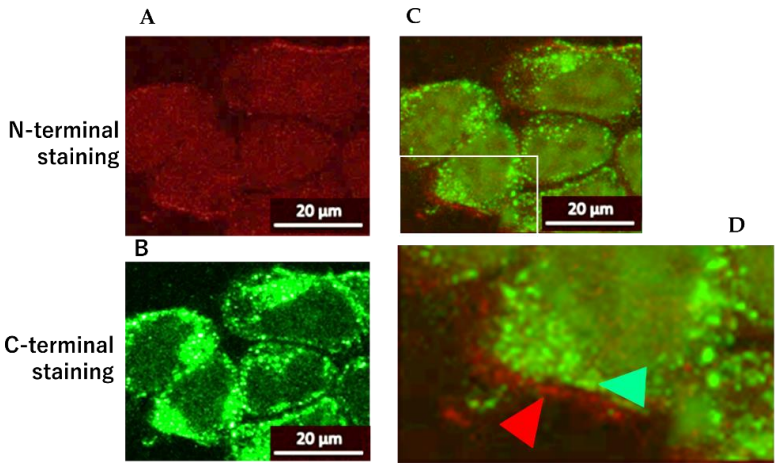

Figure 4.10 Assessement of N-terminal and C-terminal staining following ephrinA1-Fc treatment . A) N-terminal staining of WT EphA1 following ephrinA1-Fc treeatment. B) C-terminal staining of WT EphA1 suggesting there may be some retention of membrane staining. C) Merged image of N-terminal and C-terminal staining. D) Magnification of N-

terminal and C-terminal staining indicating that C-terminal staning is not at the membrane as there is little overlap with N-terminal staining.

These data indicate that ephrinA1-Fc treatment results in a loss of N-terminal EphA1 staining as previously described, (Fig 4.10 A). There is internalization of EphA1 C-terminus upon ligand engagement (Fig 4.10 B). However, there appears to be a retention of membrane staining as described for Fig 4.9. This would be contradictory to previously obtained results. As a result, the merged N-terminal and C-terminal images were magnified to determine whether C-terminal staining was at the membrane or cytosol (Fig 4.10 D). This showed little co-localisation of the N-terminus and C-terminus, suggesting that the C-terminal staining is cytosolic. This suggests that the data indicating membrane staining of the C-terminus in Fig 4.9 B & F following ephrinA1 Fc treatment is likely due to the inability to demarcate between membrane staining and cytosolic staining using the method employed. However, this does suggest that there is not a maintenance of full length EphA1 or membrane-bound C-terminal fragments following eprhnA1-Fc which is line with the previous findings. Future work would require a more precise method to distinguish membrane and cytosolic staining.

As there is now a degree of understanding of the WT EphA1 molecule, it was necessary to analyse the $P^{460}L$ in the same manner described to determine whether its expression or localisation differs when compared to the WT molecule.

4.4 Comparison of overall expression levels of WT, P460L and X2 EphA1

To determine whether the P460L and X2 variant differ in their response to ligand treatment, they were assessed in combination with WT via WB in the first instance to determine whether there would be any potential differences in their overall expression levels. The X2 variant may give additional insight into the WT molecule as it is missing the FNIII domain, which was hypothesized to be an area in which EphA1 is cleaved, as EphA2 is cleaved by MT1-MMP in this region (Sugiyama et al., 2013).

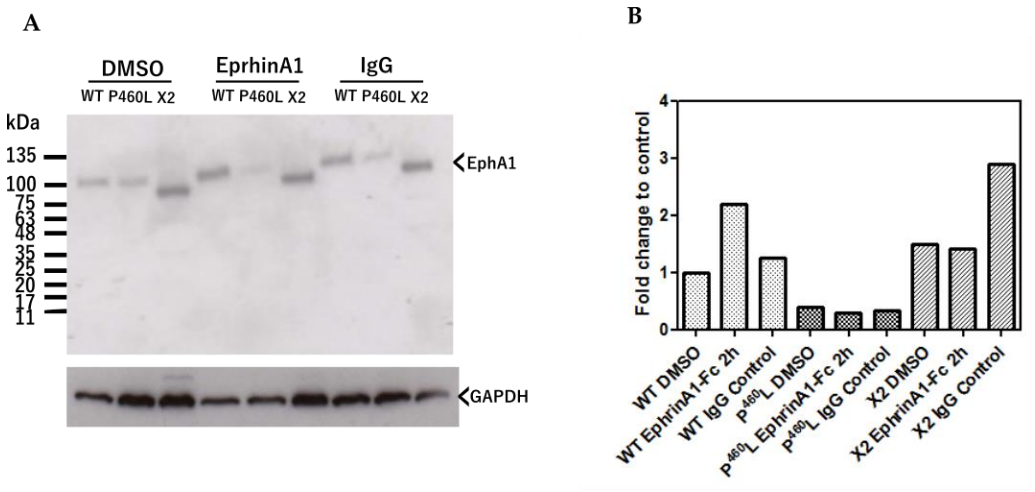

Figure 4.11 Immunoblot of EphA1 WT, P460L and X2 lysates following ephrinA1-Fc treatment. A) EphA1 WT, P460L and X2 were treated with 2 μg/ml of ephrinA1-Fc or control IgG for 2 h. Lysates were probed with an anti-V5 antibody (n=1) Bands were normalised to GAPDH. B) For ease of analysis, fold change to control was plotted in their variant groups

Preliminary data indicated that the P460L mutation reduced the overall expression of EphA1, regardless of treatment procedure, suggesting that the mutation differs from the WT molecule. The X2 variant conversely, appears to be resistant to ephrinA1-Fc mediated regulatory mechanisms. This is only one repeat but indicates that further analysis is warranted.

4.4.1 Does the P460L mutant alter the turnover of EphA1 compared to WT?

Initial data suggested that the $P^{460}L$ mutation results in a reduction of overall expression levels, compared to WT (Fig 4.11). It has been hypothesised that the $P^{460}L$ mutation increases the proteolysis of EphA1 by offering a new binding epitope to proteases, particularly MT1-MMP. This possibility was investigated by assessing EphA1 turnover in EphA1-$P^{460}L$-HEK-293 cells in the same manner as conducted in section 4.3.1 and 4.3.2 on WT EphA1 cells.

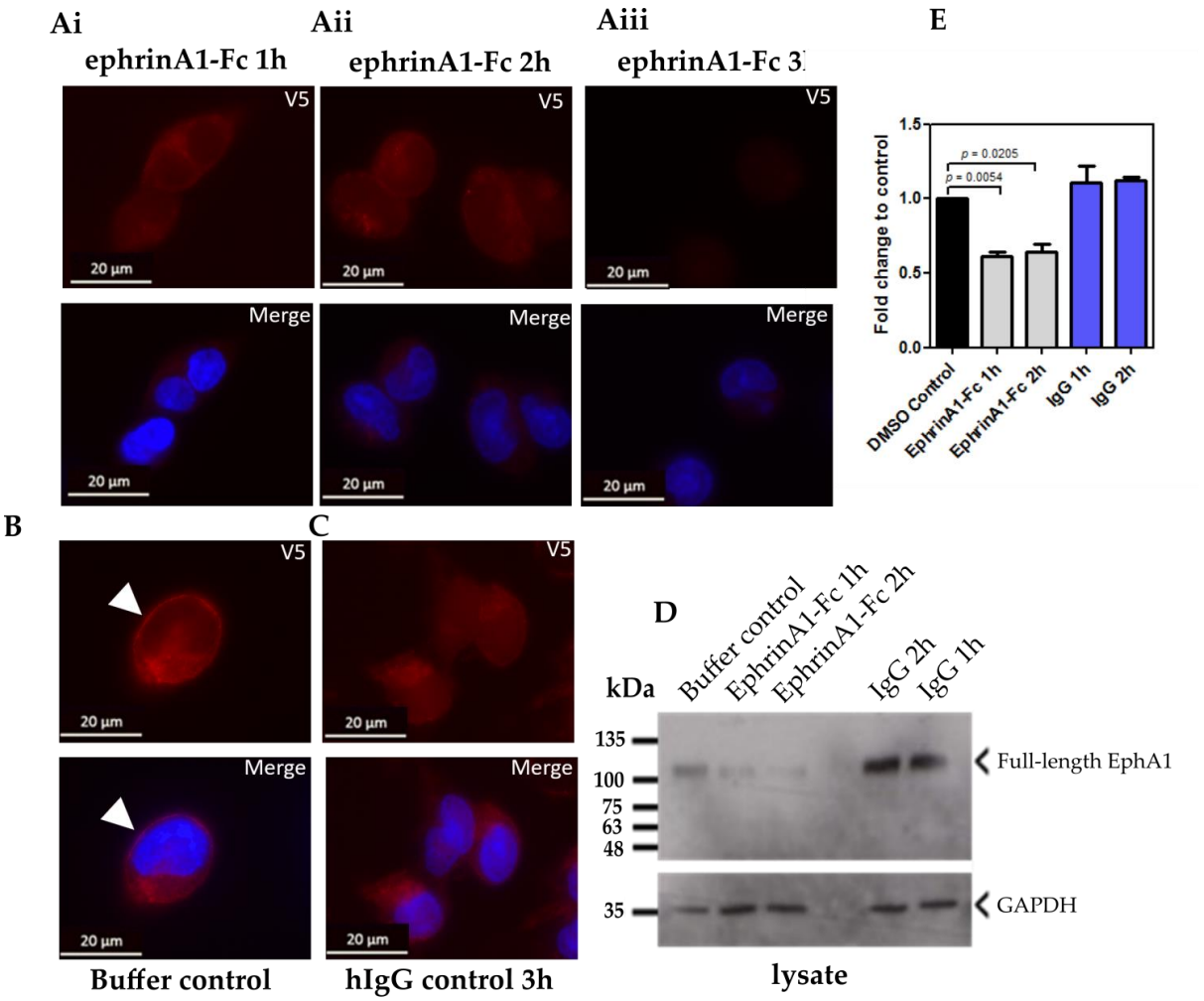

Figure 4.12 The effect of ephrinA1-Fc on the cellular localisation and expression of $P^{460}L$ EphA1 **A)** Representative immunofluorescence staining of EphA1 (red) using a V5-Ab (C-terminus 1:500) treated with ephrinA1-Fc (2 µg/ml) over a 0, 1, 2 and 3h time-course indicating a loss of membrane staining of the receptor at a 1, 2 and 3 h timepoint (n=3; images taken from at least 3 different fields). DAPI (blue), was used as a nuclear fluorescent counter stain. Importantly, qualitative analysis indicates no apparent internalisation of C-terminal EphA1 after ephrinA1-Fc treatment over the 3h time-course; this is in contrast to WT EphA1 where EphA1 was internalised at 2 and 3h, indicating that the receptor may be shed but not internalised due to the $P^{460}L$ mutation. **B)** Cells were treated with buffer control for 3h **C)** Control cells were treated with a control IgG at the same final concentration of ephrinA1-Fc. **D)** Representative immunoblot showing full-length $P^{460}L$ EphA1 response to ligand engagement (2 µg/ml ephrinA1-Fc) over a 2h time-course (n=3). Blots were probed with an anti-V5 Ab which detects the C-terminus of EphA1 (1:2000). **E)** Results were normalised to GAPDH and plotted. Error bars indicate SEM. Analyses were conducted using a student T test.

Immunoblot analyses indicated that EphA1-P^{460}L full length expression is reduced with the addition of ephrinA1-Fc compared to buffer control (buffer control v 1 h, $p = 0.0054$, buffer control v 2h $p = 0.0205$). Moreover, it appears the mechanisms by which the WT molecule and P^{460}L EphA1 are regulated, is markedly different. The WT molecule undergoes C-terminal internalisation following ligand engagement, whereas these data P^{460}L EphA1 does not. Alternatively, it could suggest that the P^{460}L mutation causes rapid degradation of the C-terminus. There does, however, appear to be a degree of C-terminal internalisation in the absence of ligand (Fig 4.12 B) or this could represent newly synthesized protein, comparable to the WT molecule. Next, we wanted to determine whether GM6001 or DAPT were capable of altering the localisation or expression levels of P^{460}L EphA1.

4.4.2 The effect of GM6001/Ilomastat on the expression and localisation of N-terminal P^{460}L EphA1

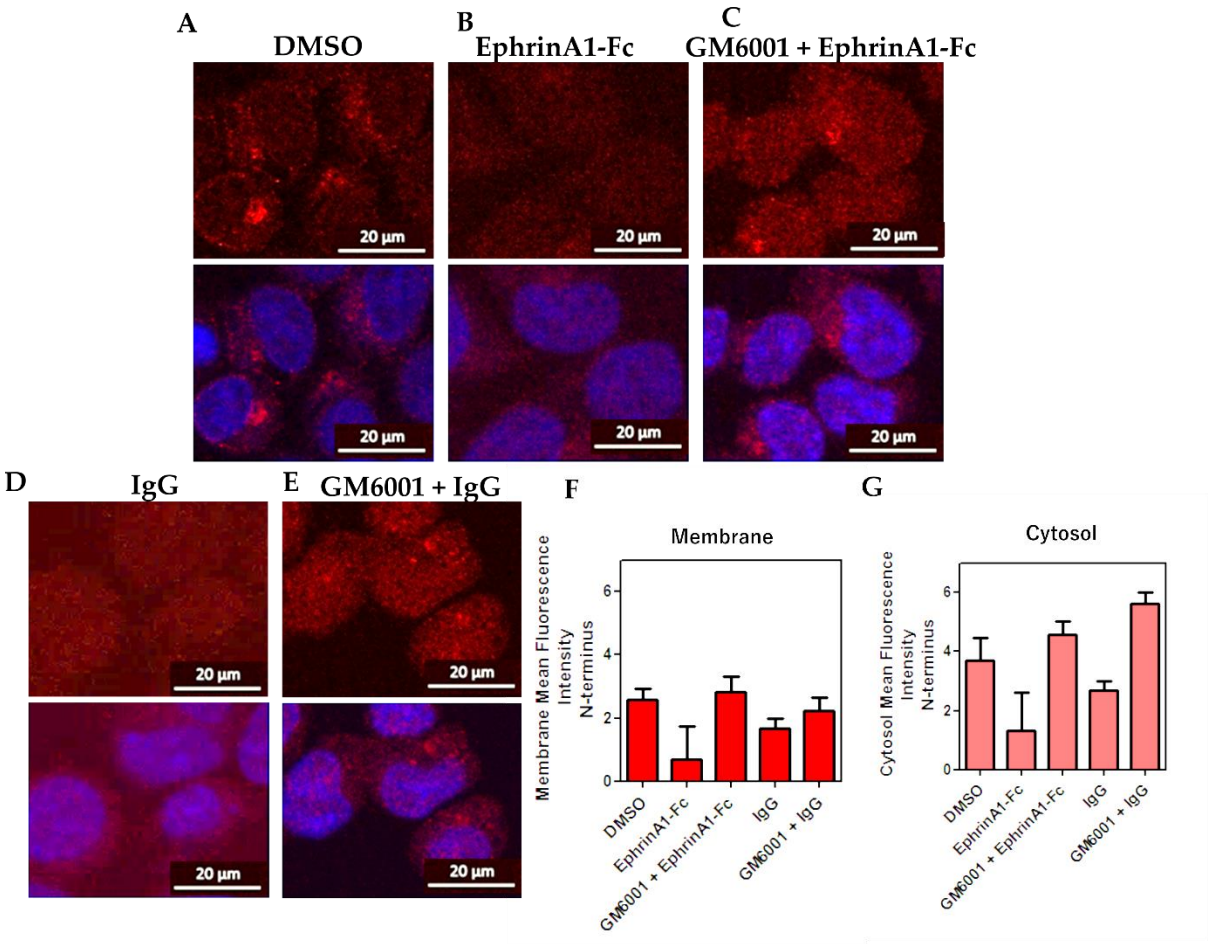

Figure 4.13 The effect of GM6001/Ilomastat on the expression and localisation of N-terminal P^{460}L EphA1 Representative immunofluorescence staining of P^{460}L EphA1 N-terminus (EphA1: Arg24-Glu547; red) n=3; images taken from at least 3 different fields. DAPI (blue), was used as a nuclear fluorescent counter stain. **A)** P^{460}L EphA1 cells were treated with DMSO for 3 h. **B)** Treatment with ephrinA1-Fc (2 µg/ml) for 3 h. **C)** Cells were treated with ephrinA1-Fc (2 µg/ml) in combination with the broad spectrum MMP inhibitor, GM6001/Ilomastat (25 µM for 3h). **D)** Cells were treated with an IgG control at the same concentration as ephrinA1-Fc (i.e. 2 µg/ml) for 3h. **E)** Cells were treated with an IgG control at the same concentration as ephrinA1-Fc (i.e. 2 µg/ml) in combination with the broad spectrum MMP inhibitor, GM6001/Ilomastat (25 µM for 3h). **F)** The mean fluorescence intensity of the membrane staining was determined by identifying a ROI using ImageJ and subtracting the immediate background intensity adjacent to the ROI. **G)** The mean fluorescent intensity of N-terminal cytosolic staining was determined by identifying a cytosolic ROI using ImageJ and subtracting the immediate background intensity adjacent to the ROI. Analyses were conducted with a one-way ANOVA with Bonferroni correction.

These data indicated that there is little N-terminal membrane expression of $P^{460}L$ EphA1 in the control or treatment conditions (Fig 4.13 F), suggesting that the turnover of $P^{460}L$ EphA1 alters from WT EphA1. GM6001 does not rescue N-terminal membrane staining of $P^{460}L$ following ephrinA1-Fc or IgG treatment (Fig 4.13 B & D, respectively), suggesting that if the mutation does offer a new binding epitope for proteases, this is not MMP-mediated. Whilst there was little or no N-terminal membrane staining, N-terminal staining was evident within the cytosol, particularly following GM6001 treatment. Consequently, the cytosolic fluorescence of N-terminal EphA1 was assessed (Fig 4.13 G). Whilst non-significant, GM6001 treatment of $P^{460}L$ EphA1 cells brought cytosolic N-terminal fluorescence levels in line with those in the DMSO control. This could suggest that GM6001 blocks the rapid degradation of $P^{460}L$ following ephrinA1-Fc and IgG treatment. The reason behind IgG mediated alterations in N-terminal staining of $P^{460}L$ EphA1 within the cytosol is unclear. To determine whether γ-secretase inhibition has an impact on the localisation of C-terminal $P^{460}L$ EphA1, $P^{460}L$ cells were treated with DAPT.

4.4.3 The effect of DAPT on the expression and localisation of C-terminal P460L EphA1

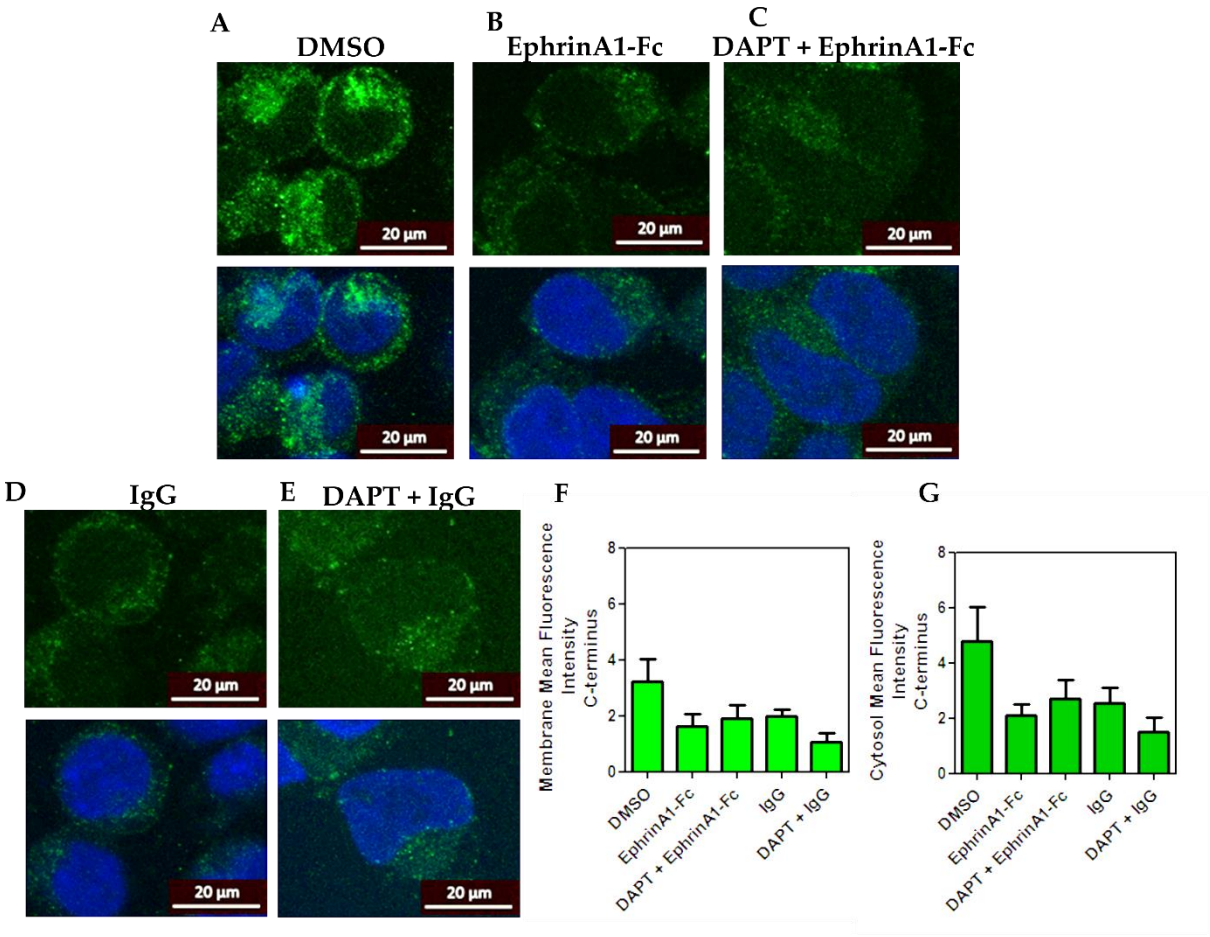

Figure 4.14 The effect of DAPT on the expression and localisation of C-terminal P460L EphA1 Representative immunofluorescence staining of P460L EphA1 C-terminus (green) n=3; images taken from at least 3 different fields. DAPI (blue), was used as a nuclear fluorescent counter stain. **A)** P460L EphA1 cells were treated with DMSO for 3 h. **B)** Treatment with ephrinA1-Fc (2 µg/ml) for 3 h. **C)** Cells were treated with ephrinA1-Fc (2 µg/ml) in combination with γ-secretase inhibitor DAPT (5 µM for 3h). **D)** Cells were treated with an IgG control at the same concentration as ephrinA1-Fc (i.e. 2 µg/ml) for 3h. **E)** Cells were treated with an IgG control at the same concentration as ephrinA1-Fc (i.e. 2 µg/ml) in combination with γ-secretase inhibitor DAPT (5 µM for 3h). **F)** The mean fluorescent intensity of the membrane staining was determined by identifying a ROI using ImageJ and subtracting the immediate background intensity adjacent to the ROI. **G)** The mean fluorescent intensity of the cytosol staining was determined by identifying a ROI using ImageJ Analyses were conducted with a two-way ANOVA.

Previous analysis indicated that the $P^{460}L$ mutation in EphA1 resulted in a degree of C-terminal internalisation in the absence of ligand (Fig 4.12 B), which was confirmed in these series of experiments (Fig 4.14 A). Upon ephrinA1-Fc treatment there is a reduction in C-terminal internalisation, perhaps suggesting that ligand engagement results in rapid degradation of the C-terminus of EphA1 $P^{460}L$ (Fig 4.14 B). Upon γ-secretase inhibition, there is no rescue of C-terminal EphA1 membrane expression following ephrinA1-Fc treatment (Fig 4.14 C & F) indicating that the loss of membrane C-terminal fragments upon ligand engagement is not γ-secretase dependent. Moreover, little or no internalisation of the C-terminus was apparent following ephrinA1-Fc treatment (Fig 4.14 B & G), similarly to what was previously described (Fig 4.12, Ai, Aii, Aiii). This could suggest rapid degradation of the C-terminus of EphA1 upon ligand engagement which cannot be prevented by γ-secretase inhibition (Fig 4.14 C & G). Following IgG treatment and IgG in combination with DAPT there is also a loss of C-terminal internalisation compared to DMSO control, but this was found to be non-significant.

4.5 Discussion

4.5.1 The regulatory mechanisms of EphA1 WT

Immunoblot analysis of ephrinA1-Fc treated EphA1-WT cells indicate that ligand engagement causes a reduction in overall EphA1 expression (Fig. 4.3) as indicated by a consistent time-dependent reduction in band intensity at increasing time-points. Whether this effect is due to receptor degradation or proteolysis of the molecule was initially unclear, as soluble EphA1 was not identified within the media following immunoblot analysis of the supernatants of treatment media. Fc fusion proteins, such as ephrinA1-Fc, compose the Fc domain of IgG which is genetically linked to a protein of interest. The binding of the Fc domain to Fc receptors expressed on the tested cell line could cause alterations in the cell surface expression of other molecules. Consequently, it is vital to ensure that the Fc region of ephrinA1-Fc is not responsible for the alterations observed in EphA1 turnover. The control-IgG did not significantly alter the expression of EphA1 confirming that ephrinA1-Fc is interacting via EphA1. However, the control IgG data tended to provide inconsistent data, especially at the 2h incubation point as indicated by the error bars in figure 4.3 B. This may suggest that EphA1 undergoes constitutive, ligand-independent proteolysis. This would be consistent with data on other Eph family members which also show some level of constitutive proteolysis (e.g. Sugiyama et al., 2013).

Analyses of the localisation of WT EphA1 following ephrinA1-Fc engagement indicated that C-terminal internalisation of WT EphA1 occurs over a 3h time-course (Fig 4.4 Ai, Aii, Aiii). There is also a significant loss of membrane staining (Fig 4.4 B) at 2 and 3 hours, compared to both the buffer control and 1h ephrinA1-Fc treatment. The IgG control did not cause C-terminal internalisation of WT EphA1, with EphA1 remaining at the membrane (Fig 4.4 D). Whilst there was an overall increase in the mean fluorescence intensity within the cytosol, this effect was not significant (Fig 4.4 B), which suggested that the molecule may be degraded following ephrinA1-Fc treatment. As a result, the overall mean intensity was determined which indicated a significant drop in fluorescence at 2h (p = <0.001) and 3h (p = <0.001 Fig 4.4 E) suggesting degradation of the receptor. This is consistent with data on EphA2, where ligand engagement with ephrinA1-Fc has been shown mediate its internalisation and degradation over time (Walker-Daniels et al., 2002b). Generally, upon

ligand-induced activation, RTKs will autophosphorylate, creating sites for signalling or adaptor proteins to dock (Carpenter, 2000). Walker-Daniels and colleagues (2002b) found that the c-Cbl adaptor protein facilitated the degradation of EphA2. c-Cbl is a ubiquitin ligase, which partly targets proteins for degradation through the proteasomal pathway. To determine whether EphA1 degradation is dependent on the c-Cbl adaptor protein, it is necessary to establish, firstly, whether these proteins co-localise and associate upon ephrinA1-Fc stimulation using immunofluorescence and pull-down methods respectively. Should this be the case, inhibition of c-Cbl would determine whether this adaptor protein mediates EphA1 degradation if EphA1 degradation is prevented.

During analysis, a soluble fragment of EphA1 was identified in the media (Fig 4.4 F) at a 2 and 3 h timepoint in one experiment, corresponding to the predicted MW of the ECD of WT EphA1 (i.e. ~75kDa). This suggests that ephrinA1-Fc stimulation induced proteolysis of WT EphA1 resulting in ectodomain release. This indicated that the C-terminal fragment identified using a C-terminal Ab following ephrinA1-Fc treatment (Fig 4.4 Aiii) most likely corresponds to a cleaved species and was likely mediated by regulated intramembrane proteolysis following primary processing by ADAMs/MMPs. However, as the N-terminal fragment was not consistently identified in the media through immunoblotting, even following concentration via ultracentrifugation, dual staining was conducted on ephrinA1-Fc treated EphA1 WT cells such that the N-terminus and C-terminus could be assessed by immunofluorescence. Following both buffer control and IgG treatment, both the N-terminal and C-terminal staining remains predominantly at the membrane (Fig 4.7), with overlap identified in the merged images suggesting that EphA1 is full-length at the membrane. Following ephrinA1-Fc treatment, both N-terminal staining and C-terminal staining is lost at the membrane. C-terminal internalisation is seen within the cell, but importantly no N-terminal staining was evident here. This supports the notion that ephrinA1-Fc activation results in N-terminal proteolysis followed by C-terminal internalisation. Whilst this N-terminal Ab detects the whole region of the EphA1 ECD and thus ephrinA1-Fc engagement should not block antibody binding, future work is needed to clarify this point. There appears to be some C-terminal internalisation following 3h buffer control treatment which may indicate that there are ligand-independent regulatory mechanisms controlling this

internalisation. Studies have shown that EphB2 can be processed by γ-secretase in a ligand dependent and independent manner, for instance (Georgakopoulos et al., 2006)

As mentioned, the N-terminus of WT EphA1 was identified only once in the media through immunoblotting of cell-free supernatant following ephrinA1-Fc treatment and only when EphA1 expressing cells were plated onto glass coverslips. The initial summation was that the amphiphatic nature of the protein was causing plastic absorption and that the glass coverslip caused less absorption of the amphiphilic macromolecules than the plastic. Whilst this might hold true to some respect, we repeated the experiment again on both glass coverslips and plastic and again found no N-terminal EphA1 in the media (data not shown). This was true even after ultracentrifugation of the supernatant. It may also be the case that western blotting is not sensitive enough to detect our protein of interest in the media – it is known that film detection using ECL reagents is inferior over digital camera-based system, for instance. Alternatively, it could mean that the released ECD of EphA1 is rapidly degraded. Analysis of ligand treated EphB2 showed a time-dependent decrease in full-length expression with an accumulation of a membrane bound C-terminal fragment, suggesting proteolytic cleavage at the ECD, however analysis of the conditioned media failed to identify an N-terminal fragment (Litterst et al., 2007a) with the authors suggesting that it may be due to rapid degradation of the cleaved ECD.

Alternative means to analyse N-terminal release into the media would be to add an alkaline phosphatase (AP) tag to the N-terminus EphA1 and subsequently assaying the media for AP-activity. Carl Blobel (Zheng et al., 2002) developed this method to assess the cleavage of EGFR ligands by ADAMs and this method works by quantifying AP levels in the cellular supernatant as measured by the increase of rate of absorption at 405nm, based on the catalysis of a colourless substrate into a yellow product. However, as the necessary supernatants have been collected, it was determined that assessment of EphA1 proteolysis could be undertaken with a recently manufactured ELISA kit which detects the N-terminus of EphA1 (aa27-aa547). Initial analysis has shown that the ELISA detects EphA1 in the media even when bound to ephrinA1-Fc (Appendix VII) and thus, detection of proteolysis products in the media should be possible and is due to be undertaken.

As a means to focus the assessment of potential proteases responsible for N-terminal cleavage, *in silico* analysis was conducted using the PROSPER tool. This tool predicts potential cleavage sites in a given protein sequence. It has the benefit of also offering a list of resulting peptides from the suggested protease cleavage and the subsequent molecular weight in kDa. This allowed further refinement of the model, where only those proteases offering an N-terminal fragment of 75kDa were displayed. The predominant proteases offered by the tool were MMP-2 and MMP-9 (Table 4.1), with these proteases also responsible for the cleavage of other Eph molecules in complex with their respective ligands (Beauchamp et al., 2012; Lin et al., 2008b). Moreover, as MT1-MMP has been shown to cleave in the region of the $P^{460}L$ mutation, it was decided to use a broad-spectrum MMP inhibitor, namely GM6001/Ilomastat to block potential cleavage. Cells were treated with GM6001 in combination with ephrinA1-Fc or control IgG and assessed via ICC. Using an N-terminal Ab, a loss of membrane staining was evident following ephrinA1-Fc treatment (Fig 4.8, $p = <0.01$) as previously described. Following GM6001 treatment in combination with ephrinA1-Fc treatment there appeared to be no recovery of N-terminal staining (Fig 4.8 C & F), potentially suggesting that the N-terminal Ab does bind to its target in the presence of ephrinA1-Fc. Alternatively, it could also suggest that WT EphA1 is preferentially cleaved by alternative proteases and the prevention of MMP cleavage alone will not prevent the processing of EphA1 by other proteases, such as ADAMs. Both the IgG control and IgG + GM6001 showed strong membrane staining of EphA1 (Fig 4.8 D & E, respectively). Interestingly however, the treatment with both IgG and GM6001, resulted in an increased mean fluorescence intensity at the membrane, compared to the IgG control (Fig 4.8 E & F, $p = <0.01$). This could indicate that EphA1 undergoes constitutive proteolysis in the absence of ligand which is MMP-mediated. Indeed, it has been shown that other RTKs, such as ErbB-4, are constitutively shed in the absence of ligand which is metalloprotease-dependent (Vecchi and Carpenter, 1997). An alternative means to assess MMP regulation of EphA1 could be conducted using the calcium ionophore ionomycin, which will directly activate MMP (MMP is activated with Ca^{2+} influx (Litterst et al., 2007b)). If this results in the accumulation of an EphA1 C-terminal fragment it may suggest EphA1 is regulated by MMP in the absence of ligand. Indeed, some initial immunoblotting experiments indicated a 40kDa product which may correspond to the C-terminal fragment of EphA1 (Appendix VIII). This, however, does

not elucidate what molecules are responsible for this effect. Should GM6001 prevent any ionomycin-mediated accumulation of EphA1 CTF then we can confirm EphA1 is constitutively cleaved by MMP. Moreover, studies have shown, for instance, whilst ephrinA3-Fc treated EphA4 expressing hippocampal neurons, stimulated phosphorylation of EphA4, it did not alter its regulation (2h up to 16h). Thus, it would be interesting to look at the phosphorylation status of EphA1 following ephrinA1-Fc treatment. To look at proteolytic processing in the absence of ligand and direct initiation of MMPs might prove more fruitful for future experimentations. Moreover, assessment of alternative proteases responsible for the loss N-terminal staining is warranted.

Upon γ-secretase assessment of WT EphA1 regulation, ephrinA1-Fc treatment resulted in significant C-terminal internalisation (Fig 4.9 B) compared to both DMSO (p = <0.01) and IgG control (p = <0.01) as determined by increased fluorescence intensities within the cell. Cells treated with DAPT in combination with ephrinA1-Fc indicated a drop in mean fluorescence intensity within the cells suggesting γ-secretase is involved in in the C-terminal internalisation of EphA1 (Fig 4.9 C & F), however, DAPT does not rescue membrane expression of C-terminal EphA1. It has been suggested that Eph receptors and their ligands may undergo regulated intramembrane proteolysis which is generally atypical for the RTK family of receptors (Atapattu et al., 2014b). For instance, EphA4 was shown to be a γ-secretase substrate, however, primary processing by metalloprotease activity was found to be ligand independent (Inoue et al., 2009). Another study showed that ligand engagement of EphB2 results in proteolysis of the ECD, endocytosis of the C-terminus and subsequent γ-secretase cleavage within the endosomes resulting in receptor degradation (Litterst et al., 2007a). The staining of the C-terminus of WT EphA1 following both ephrinA1-Fc and ephrinA1-Fc and DAPT treatment (Fig 4.9 B & C, respectively) appears punctate and may indicate that the C-terminus of EphA1 is localised to endosomes. With this in mind, an alternative means to assess whether γ-secretase cleaves EphA1 C-terminus within endosomes would be to subject cells to subcellular fractionation to isolate endosomes following ephrinA1-fc treatment in either the presence or absence of a γ-secretase inhibitor. Alternatively, inhibition of the endocytic processes would determine whether the C-terminus internalisation is within endosomes. IgG did not induce the internalisation of

EphA1 in neither the absence nor presence of DAPT (Fig 4.9 D & E, respectively) indicating that the IgG control is an appropriate control.

4.5.2 The regulatory mechanisms of EphA1 $P^{460}L$

To determine whether the $P^{460}L$ mutation altered the membrane expression of EphA1 as hypothesised, $P^{460}L$ HEK-293 cells were treated in the same manner as WT EphA1 expressing cells. It appears that there is a reduction in the overall expression of EphA1 $P^{460}L$ with a rapid and robust loss (see Figure 4.11 D). This reduction does not appear to be time-dependant as with the WT molecule, suggesting expedited loss of full-length expression. This could indicate the mutation confers expedited proteolysis of the molecule, for instance, the altered amino acid sequence could destabilise the three-dimensional EphA1 protein structure causing a sensitivity to cleavage. Immunoblot analysis of WT and $P^{460}L$ cells treated in parallel indicated that $P^{460}L$ full-length expression is reduced compared to WT in both the presence of absence of ligand (Fig. 4.10 A & B). C-terminal staining of the $P^{460}L$ mutation following ephrinA1-Fc treatment showed rapid loss of C-terminal staining at the membrane, even at a 1h time-point (Fig 4.11 Ai). This contrasts with the WT molecule which remains membranous at this time-point. Moreover, there seems to be little or no C-terminal internalisation of $P^{460}L$ EphA1 over the 3h time-course, with an almost complete loss of fluorescence intensity at 3h (Fig 4.11 Aiii). This is an important finding as C-terminal Eph fragments can be signalling competent and could provide a potential disease related mechanism. For instance, in cultured rat primary neurons, γ-secretase induced C-terminal internalisation of EphB2 was shown to phosphorylate and stimulate cell surface expression of *N*-methyl-D-aspartate receptor (NMDAR) independently of Src kinases, which are usually associated with this function (Xu et al., 2009b). NMDAR receptors play a pivotal role in synaptic plasticity and thus in memory and learning. Mutations in the PS1 component of γ-secretase inhibit the production of the C-terminal EphB2 (Litterst et al., 2007c) promoting deficits in NMDAR functioning. Thus, promoting the production of EphB2 C-terminal fragments may ultimately lead to improved NMDAR function.

It was originally hypothesised that the $P^{460}L$ mutation might increase cleavage by MT1-MPP as EphA2 is cleaved within the FNIII repeat by this protease (Sugiyama et al., 2013). This study predicted that this cleavage was likely to occur *in cis*, since they detected some

constitutive shedding in the absence of ligand (Sugiyama et al., 2013). They found that this cleavage was increased with the addition of soluble ephrinA1. Our data is consistent with the hypothesis that $P^{460}L$ may offer the MT1-MMP protease an additional binding epitope, as we identified constitutive loss of N-terminal membrane staining of the molecule in the absence of ligand (compared to WT) which was increased with the addition of ephrinA1-Fc (Fig 4.11), similarly to what Sugiyama and colleagues discovered (2013). Importantly, throughout the analysis, it was found that $P^{460}L$ EphA1 C-terminal staining is evident at the membrane in the absence of ligand (Fig 4.11 B & 4.13 A) suggesting that the loss of membrane staining is likely the result of proteolysis at the ECD with maintenance of an $P^{460}L$ C-terminal fragment at the membrane Moreover, since there was no juxtaposed cell, this proteolysis must occur *in cis*. HEK-293 cells are known to express MT1-MMP (Liu and Wu, 2006) However, following broad-spectrum MMP inhibition of EphA1 $P^{460}L$, there appears to be no rescue of membrane N-terminal fluorescence intensity levels compared to ephrinA1-Fc treatment alone (Fig 4.12 C & F); this was also true for GM6001 IgG treated cells compared to IgG alone (Fig 4.12 E & F). However, the N-terminal staining is not typical of membrane staining seen in the EphA1 WT cells (e.g. Fig 4.4 Ai). The N-terminal staining following GM6001 treatment appeared diffuse within the cell, with small regions of increased fluorescence intensity (Fig 4.12 C & E). Consequently, the cytosolic membrane intensity of N-terminal staining was also assessed, which indicated that GM6001 generally rescued cytosolic membrane staining intensities to that seen in the DMSO control (Fig 4.12 G) but this effect was not significant. As described Eph internalisation can occur via trans-endocytosis (Klein, 2012), which is believed to remove whole cell Eph-ephrin complexes , resulting in full length proteins within intracellular vesicles. It is possible that the EphA1 $P^{460}L$ promotes trans-endocytosis with the staining indicating its expression within intracellular vesicles. How MMP inhibition may rescue the N-terminal expression of $P^{460}L$ within intracellular vesicles is unclear. One plausible suggestion is that GM6001 prevents the degradation of $P^{460}L$ EphA1. Generally speaking, however, it appears that GM6001 treated of EphA1 $P^{460}L$ does not prevent the loss of N-terminal membrane staining suggesting the mechanism of membrane loss differs from those of the WT molecule but similarly is not MMP dependent.

Previous data indicated that ephrinA1-Fc treatment of $P^{460}L$ EphA1 does not result in C-terminal internalisation of the molecule (Fig 4.11 A) or that the molecule is rapidly degraded once internalised. This question was assessed using DAPT to determine whether C-terminal staining can be rescued at the membrane. Previous data indicated that $P^{460}L$ EphA1 undergoes a degree of C-terminal internalisation in the absence of ligand, but that membrane expression is also evident, suggesting that a proportion of the molecules are full-length at the membrane (Fig 4.11 B). These data support this finding (4.13 A). Upon ephrinA1-Fc treatment this C-terminal staining is lost from the both the membrane and within the cell (Fig 4.13 B), suggesting the molecule is rapidly degraded following ligand treatment. Upon combined treatment with ephrinA1 and DAPT, there is no change in the expression levels or localisation of EphA1 compared to ephrinA1 treatment alone (Fig 4.13 C & B respectively), suggesting that ephrinA1-Fc treatment does not result in γ-secretase mediated internalisation and subsequent degradation. As the N-terminal staining indicated that $P^{460}L$ EphA1 may be confined to intracellular vesicles, this data may support the supposition that $P^{460}L$ undergoes trans-endocytosis rather than proteolytic processing as neither GM6001 or DAPT are capable of preventing the loss of N-terminal or C-terminal staining followin(Miao et al., 2001)g ephrinA1-Fc treatment. Regardless of the mechanism of expedited loss of EphA1 $P^{460}L$ expression, this could have a disease-relevant process. To determine the precise localisation of EphA1 $P^{460}L$, lysates could be fractionated, which would also allow determination of whether the expression levels differ within the certain cellular compartments. Ultimately, more work is needed to fully appreciate the nuances of EphA1 cleavage mechanisms.

4.7.2 Considerations and Future Work

v As described, the use of Fc-tagged ligands have become important reagents within the laboratory with applications ranging from immunotherapy, pharmokinetics, as well a range of *in vitro* assays such as those to assess receptor-ligand interactions (Flanagan et al., 2007). Future work should also aim to test clustering and activation of EphA1 following treatment with both pre-clustered and unclustered ephrinA1-Fc with a subsequent readout of receptor activity. It is known that pre-clustered ephrinA5-Fc results in the assembly of high-order Eph-ephrin complexes with subsequent internalisation of these complexes, whereas

unclustered ephrinA5-Fc results in negligible internalisation and clustering. Receptor activity can be determined by assessing EphA1 phosphorylation status flowing ligand interaction via immunoblotting and this is an important next step to understand receptor activity.

Moreover, the method used in this chapter to assess membrane and cytosolic expression of EphA1 may be improved in the future with the use of membrane marker, such as N-cadherin. This will allow more precise demarcation of membrane and cytosolic expression of EphA1 and will overcome the issues discussed in section 4.3.4.2 (see Fig 4.10).

As described, cells can express a range of various Eph receptors, along with a number of ephrin ligands. This coupled with the inherent promiscuity of the Eph-ephrin system makes analysis of a single Eph molecule complicated due to potential redundancy within the system. HEK-293 cells are known to endogenously express EphA2 (Miao et al., 2001), for instance, and importantly, both EphA1 and EphA2 share the same high affinity ligand, ephrinA1. This possibility must be considered when interpreting the data from any molecules of the Eph family members.

It is clear from the data that the $P^{460}L$ mutation causes a reduction of membrane expression of the EphA1 molecule, compared to the WT molecule, this is particularly clear in Figure 4.13 A and 4.14 A, where there appears to be little or no membrane expression using both an N-terminal and C-terminal Ab. It is possible that this mutation has impacted the ability of the molecule to traffic to the membrane which would render this method of analysis, inappropriate. There are a number of ways this supposition could be tested, for instance, the biotinylation of cell surface proteins is a means to specifically isolate and quantify proteins at the cell membrane (Huang, 2012). This method involves labelling membrane markers with a biotin reagent, lysing the cells and isolating the tagged proteins via pull-down. Lysates can then be immunoblotted as normal and probed with specific antibodies. Alternatively, pulse chase assays use labelled compounds to follow the dynamics of processes and pathways within a cell, and thus provides a means to study the synthesis and transport of EphA1 $P^{460}L$ to determine whether the mutation effects the ability of the molecule to effectively transport to the membrane (Bostrom et al., 1986).

Chapter Five

Investigation of soluble EphA1 on activation of endothelial cells and leucocyte recruitment

5.1 Introduction

Results so far have demonstrated that WT EphA1 undergoes ectodomain shedding and intramembrane cleavage following ephrinA1-Fc engagement, causing the release of EphA1 ECD and C-terminal internalisation. We have also demonstrated a fundamental difference in the processing of WT EphA1 and the Alzheimer's associated $P^{460}L$ mutant; $P^{460}L$ EphA1 undergoes aberrant proteolysis as indicated by a rapid loss of full-length expression of the mutant protein in both the absence and presence of ephrinA1 ligand. Initial work has indicated that commercially obtained EphA1-Fc, corresponding to the ECD, is capable of priming human umbilical vein endothelial cells (HUVECs) for Molt 3 T cell recruitment as assessed by Molt 3 T cell firm adhesion in a static adhesion assay (Ager, unpublished). These data, taken together, suggest that an increase in circulating EphA1 ECD, as a direct consequence of the $P^{460}L$ mutation, may result in a pathological increase in the recruitment of peripheral immune cells to the brain endothelium. To investigate this possibility, an assay which more closely recapitulates the *in vivo* environment of blood flow through the vasculature will be used. Using a microfluidic assay, Molt 3 T cell recruitment to both EphA1-Fc primed HUVECs and the disease relevant human cerebral microvascular endothelial (hCMEC/D3) cell line, which represents a model of the BBB.

5.1.1 The Eph/ephrin system in vascular biology

As described briefly in section 1.4, the Eph/ephrin system has been implicated in numerous aspects of vascular biology. Seminal work on the Eph/ephrin system in vascular biology concluded that *ephrinA1* expression is upregulated in response to TNFα (Dixit et al., 1990). Subsequent investigations found that the expression patterns of both Ephs and ephrins can be significantly altered during inflammation, inducing immune responses, regulating immune cell trafficking and modulating vascular permeability (Larson et al., 2008). Altered regulation of Eph/ephrin proteins has been shown *in vivo* in Wystar Kyoto rats exhibiting lipopolysaccharide (LPS) induced fever where EphA2 was significantly upregulated (in the liver, lung and hypothalamus). LPS is an endotoxin derived from the outer membrane of Gram-negative bacteria and has been shown to cause a polyphasic febrile response in rats

and mice (Oka et al., 2003; Romanovsky et al., 1998) and has subsequently been used to investigate inflammatory responses in these animals. Interestingly, EphA2 upregulation was not limited to LPS-processing organs such as liver and lung, but was also seen in the brain (Ivanov et al., 2005). *In vitro*, it has been purported that EphA2 expression is initiated and sustained through endothelial cell activation by proinflammatory cytokines, whereas EphA2 activation of ECs by soluble ephrinA1-Fc induces the expression of pro-inflammatory dependant genes such as ICAM-1, VCAM-1 and E-selectin that bind leucocyte expressed integrins (Funk et al., 2012b) facilitating the adhesion of immune cells to vessel walls and contributing to inflammatory cell recruitment. Eph receptors have also been implicated in vascular leak; for instance, in Madin-Darby canine kidney (MDCK) cells, ephrinA1-Fc mediated EphA2 activation causes claudin-4 phosphorylation in tight junctions, thus diminishing the association between claudin-4 and ZO-1, causing an increase in paracellular permeability (Tanaka et al., 2005). Studies have also shown that reverse signalling to immune cells influences aspects of the adhesion cascade. EphA2 cross-linking of ephrinA1 on T cells promotes immune cell adhesion to both ICAM-1 and VCAM-1 (Sharfe et al., 2008b). Evidence of EphA2/ephrinA1 modulation of immune cell trafficking seems to point towards the NF-κB pathway (Carpenter et al., 2012). However, more work is needed to uncover the precise mechanisms (see Fig. 5.1 for the proposed EphA2 signalling pathway promoting immune cell trafficking through NF-κB). This could have some relevance to this study as EphA1-Fc could be capable of activating ECs as well as leucocytes, and thus might work via a similar mechanism of EphA2. Whilst much work has been conducted on the closest EphA1 homolog, EphA2, evidence indicates that EphA1 is also implicated in T-cell chemotaxis, *in vitro*. EphA1 is expressed by subpopulations of T cells, and it has been shown that ephrinA1 stimulation of CD4+ and CD8+ T cells promotes chemotaxis in response to the chemokine, stromal cell-derived factor 1α (SDF-1α)/CXCL12. EphA1 stimulation by ephrinA1 on these T cell subsets mediates immune cell trafficking via the recruitment of the Src kinase Lck, FAK-like kinase Pyk2, Rho-GEG, Vav-1 and PI3K (Aasheim et al., 2005; Hjorthaug and Aasheim, 2007). However, T cells also express EphA4, and thus it was not possible to separate downstream signalling of ephrinA1 between EphA1 and EphA4 expressed on these T cells. However, these findings allow us to reason that *EphA1* AD SNPs may assert their influence by causing deleterious alterations in the inflammatory cell

adhesion cascade of the BBB. However, the complete expression patterns of EphA1 on human brain endothelial cells and peripheral immune cells is unknown to date. We aim to determine whether the potential expedited proteolysis of EphA1-P^{460}L-ECD into the blood stream of AD patients could alter leucocyte:endothelium interactions at the BBB using a model system.

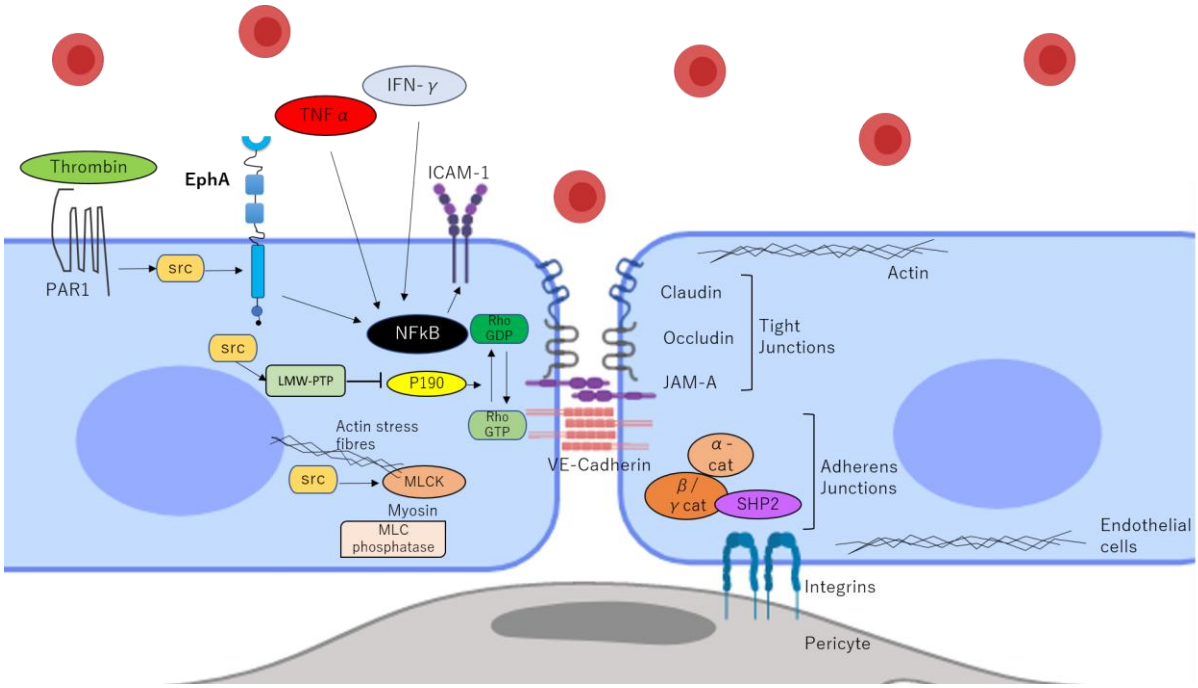

Figure 5.1 Proposed EphA2 signalling mechanisms in the endothelium. Immune cell extravasation is regulated by the shape of the EC and endothelial cell gap junction permeability. Cell shape is controlled by actinomysin contractile elements and are regulated by pathways working via myosin light chain kinase (MLCK). Proteinase-activates receptor-1 (PAR1) activation by thrombin activate the kinase activity of Src, influencing cell shape through MLCK. Signalling through EphA2 recruits Src kinase and low-molecular-weight phosphotyrosine phosphatase (LMW-PTP). This increase in LMW-PTP destabilises adherens junctions by dephosphorylating p190, inhibiting Rho-GAP activity and upregulating Rho-GTP. Leucocyte transmigration and adhesion is facilitated by upregulation of NF-kB by TNFα, for instance, resulting in increased ICAM-1 expression. Cell shape is further mediated by NF-kB by increasing MLCK activity. As EphrinA1 is increased in response to TNFα, and EphA2 upregulated NF-kB, indicating EphA2 may have a role in the permeability of the endothelium and subsequent inflammation. Figure adapted from (Coulthard et al., 2012).

5.1.2 Microfluidic assays in vascular biology

Microfluidic flow assays have been used extensively in the area of vascular biology and as a tool to understand endothelial-leucocyte interactions. These assays attempt to recapitulate the *in vivo* microenvironment by introducing shear stress levels as seen at the vascular bed and allows real-time visualisation of all stages of the leucocyte adhesion cascade using labelled immune cells or phase contrast microscopy. Shear stress, the product of shear rate and viscosity, is expressed in a unit of dyne/cm^2. Shear stress is a critical prerequisite for cell

adhesion as it mediates the activation of β-integrin via E-selectin signalling (Cinamon et al., 2001). The Bioflux 200 system (Fluxion) has been used in various studies analysing leucocyte-endothelium interactions (e.g. French et al., 2018). The chambers within the Bioflux plates are much smaller than conventional flow chambers and thus, the flow remains laminar over a longer distance (i.e. the flow through the chambers are subject to less turbulence than conventional flow chambers). The Bioflux 200 system will be used in this chapter to assess the impact of EphA1-Fc, corresponding to the ECD of EphA1, on the recruitment of leucocytes. The Molt 3 T cells will be chosen as the immune cell line in this chapter (see section 5.2.1.3 for an overview of the Molt 3 T cell line). The Molt 3 T cells will be labelled with CFSE and fluorescently tracked through the viewing window of the Bioflux plates. Fluorescent labelling of immune cells to assess their interactions with endothelial cells has some disadvantages over conventional methods. For instance, non-interacting cells will be visible to the viewer. Moreover, there is no previous research indicating the rolling velocity of Molt-3 T cells over HUVECs or hCMEC/D3 cells. This means it is not possible to definitively characterise a rolling cell, but it is possible to infer whether a cell is rolling or not interacting based on their behaviour. For instance, non-interacting cells will generally have a straight forward motion in the direction of the shear flow whereas slow rolling cells will have a slower velocity than non-interacting cells and their movement will deviate moderately from a linear motion as they overcome obstacles and/or peruse the endothelium for preferential sites of transmigration independent of the direction of flow. Thus, Molt 3 T cells will be categorized in terms of their behaviour to distinguish between slow rolling and fast-rolling/non-interacting cells (i.e. behaviour 1 and behaviour 2, respectively, see section 5.2.3 for a detailed description of how both behaviours were delineated).

Molt 3 T cell interactions with ECs will be measured in a number of ways (see Fig 5.2 for a schematic detailing the adhesion cascade steps which will be assessed).

Molt 3 T cell:EC interactions are to be analysed as follows:

1. Rolling cells
    a. Total number
    b. Rolling velocity (μm/s) with a view to determine the difference in velocities between rolling and non-interacting cells

c. Total contact time between Molt 3 T cells and ECs

d. Duration of interaction as a read-out for stable interactions upon determination of rolling velocity of rolling cells

2. Arrest/firm adhesion

    a. Total number

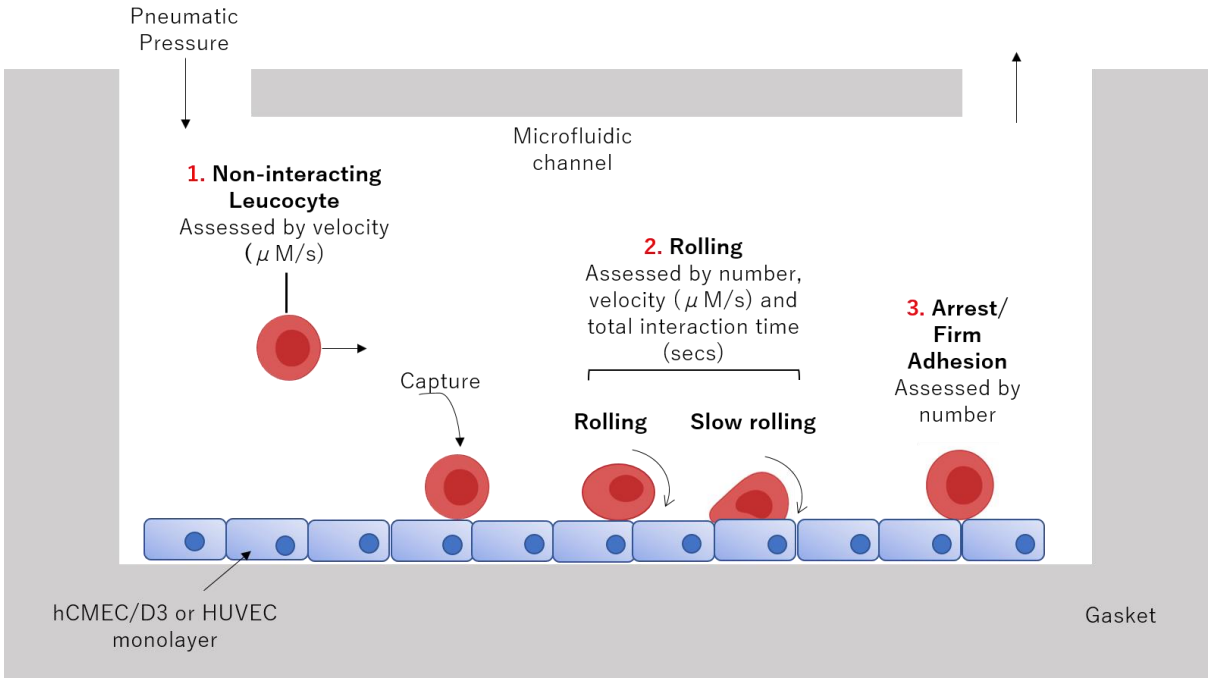

Figure 5.2 Vertical cross-section of a Bioflux 200 microfluidic channel and the leucocyte adhesion steps to be assessed. User defined conditions such as shear stress (0.25-0.5 dynes/cm^2) and temperature (37^{o}C) are controlled by an external control unit. Pneumatic pressure pushes immune cells through the inlet well, across the endothelial cells attached to the bottom of the chamber. We will assess the immune cells in 3 stages of the adhesion cascade; 1. Non-interacting leucocytes (μm/s); 2. Rolling cells by number, velocity (μm/s) and total interaction time of all rolling cells (seconds); 3. Arrest/firm adhesion.

5.1.3 The HUVEC and hCMEC/D3 cell lines as dynamic models of EC-leucocytes under shear stress

5.1.3.1 hCMEC/D3 cell line

Ultimately, *in vivo*, the adhesion cascade at the BBB involves shear stress due to the flow of blood through the vasculature. It has been shown that this shear stress can modulate EC-leucocyte interactions, (Tarbell, 2010) highlighting the need to develop dynamic *in vitro* flow-based assays using cell lines both physiologically relevant and resistant to the stresses of shear flow as would be found *in situ*. The immortalised hCMEC/D3 cell line (Weksler et al., 2005) represents an extensively characterised human brain endothelial cell line which overcomes the impractically of using primary cell lines, of which there is a paucity of available material. As described in section 1.2.2.3, an optimal BBB model will possess mature AJ and TJ function with a strong permeability function. Junction associated proteins, such as PECAM-1 and JAM-A, structural proteins, such as VE-cadherin, occludin and claudin-3 and 5 and scaffold proteins, β-catenin and ZO-1 and ZO-2 are present in the hCMEC/D3 cell line (Afonso et al., 2008; Weksler et al., 2005). Exhibited transendothelial electrical resistance (TEER) levels in hCMEC/D3 monolayers are in the low to medium range at 30-50 Ω cm^2 under static conditions, but can be increased in the presence of hydrocortisone, (~300 Ω cm^2) probably by modulating the expression of claudin-5 and occludin (Förster et al., 2008) and after co-culture with astrocytes (Hatherell et al., 2011).

From an immunological perspective, the adhesion molecules ICAM-1*, ICAM-2*, VCAM1*, CD40*, CD44 and MHC-II* are present on the hCMEC/D3 cell line (*denoting molecules that can be induced or increased by TNFα/IFNγ) along with the CCR3-6 and CXCR1-5. Under basal conditions, the hCMEC/D3 cell line secretes the CCL2 and CXCL8 chemokines and CCL5, CXCL10, CX3CL1 and fractalkine are released following stimulation by proinflammatory cytokines (Hurst et al., 2009; Subileau et al., 2009); see Table 5.1 for the immunological characteristics and BBB/endothelial phenotype of the hCMEC/D3 cell line. Numerous studies have demonstrated the ability of hCMEC/D3 cells to respond to inflammatory stimuli and subsequently support both the adhesion and migration of immune cells (Weksler et al., 2005). It has been shown that monocytes will firmly adhere to

and migrate across a hCMEC/D3 monolayer, resulting in reactive oxygen species (ROS) generation, tissue-type plasminogen activator (tPA) mediated activation of ERK1/2 and subsequent breakdown of the TJ protein, occludin (Reijerkerk et al., 2008). Moreover, peripheral blood mononuclear cell (PBMCs) migration requires the PBMC expressed LFA-1 and PSGL-1. T cells will use these ligands to adhere to the hCMEC/D3 expressed P-selectin and VLA-4, respectively (Bahbouhi et al., 2009). Monocyte migration can also be blocked using VLA-4 antibodies (Weksler et al., 2013).

Table 5.1 Endothelial and BBB phenotype and immunological characteristics of the hCMEC/D3 cell line,

Endothelial and BBB phenotype	Immunological characteristics
PECAM-1, Von Willebrand factor Adherens Junctions: VE-cadherin, γ- and β-catenins Tight Junctions: ZO-1, claudin-5, JAM-1	Adhesion Molecules: ICAM-1*, ICAM-2, VCAM-1*, CD40*, CD44, MCH-II* Chemokine Receptors: CCR3-6, CXCR1-5 *induced or increased by TNFα/IFNγ treatment

The hCMEC/D3 cell line has also been used to study neurodegenerative disease such as Parkinson's disease (PD) and AD. In the context of AD, the cell line has predominantly been used to study the cytotoxic effects of Aβ and its impact on monolayer permeability (Tai et al., 2009) and efflux transporters (Kania et al., 2011). Therefore the hCMEC/D3s represents a stable, disease relevant cell line which maintains its BBB phenotype (Weksler et al., 2013) and is able to support leucocyte migration. As a result, this represents a comprehensive cell line to support the subsequent research questions.

5.1.3.2 HUVECs

Professor Chris Pepper and Dr Elisabeth Walsby, both formerly of Cardiff University, have routinely used the BioFlux 200 system as described in section 5.1.2 to assess cell-cell interactions within the vasculature, using chronic lymphocytic leukaemia (CLL) cells and an

immortalized HUVEC cell line. As the use of the Bioflux 200 system has been optimised using this cell line, they will be studied in addition to the hCMEC/D3 cell line and may uncover a BBB-specific mechanism of EphA1-mediated immune cell trafficking by direct comparison. HUVECs are widely used to assess pathological situations such as metastasis (Wong and Searson, 2014), thrombosis (Zheng et al., 2012), as well as inflammation (Chrobak et al., 2006) but it is important to remember that vascular heterogeneity exists amongst the hierarchies of different blood vessels and organs (Aird, 2007a, 2007b). For instance, ECs of the BBB exhibit TJs whereas the vessels of the liver possess sinusoids and large gaps (Aird, 2007b). HUVECs themselves are isolated from the vein of the umbilical cord (Jaffe et al., 1973) and thus extrapolating results to adult vascular beds should be done with care. Nevertheless, HUVECs have been used extensively in shear flow assays and have been invaluable in broadening the understanding of the multistep paradigm of leucocyte recruitment (Schreiber et al., 2007).

5.1.3.3 Further Considerations

Whilst the use of immortalized EC lines overcomes a number of difficulties related to limited life span and culturing challenges, there is some evidence which indicates immortalization impacts the dynamic interactions with immune cells which may result in functional defects in this process (Oostingh et al., 2007). There are numerous immortalized EC lines which aim to assist disease-related functional studies and overcome the difficulties described above (Ades et al., 1992; Schütz et al., 1997; Venetsanakos et al., 2002). Nevertheless, many of these EC lines fail to support selectin-dependant leucocyte rolling (Oostingh et al., 2007) and thus, their worth in broadening our understanding of leucocyte-EC interactions may be limited. For instance, PBMCs do not roll on TNFα activated human brain microvascular endothelial cells (HBMEC), telomerase immortalized human microvascular endothelial (TIME) cells or human placental microvascular endothelial cells (HPEC-A2) (Oostingh et al., 2007). Activation of HUVECs, however, supports attachment and rolling on TNFα-activated HUVECs, which appears to be largely E-selectin-dependent (Oostingh et al., 2007). As the immortalized hCMEC/D3 cell line is a relatively new EC line, there is limited evidence in its ability to support selectin-mediated rolling and this should be taken into consideration when interpreting data. Evidence suggests that the hCMEC/D3 cell

line can support P-selectin-mediated rolling of PBMCs (Bahbouhi et al., 2009) but more work is required to truly appreciate their usefulness in functional studies of dynamic interactions with leucocytes. Nevertheless, as described in section 5.1.3.1, the hCMEC/D3 cell line has been extensively characterised for its EC phenotype and represents a disease- relevant cell line and thus, its use is justified in this instance.

5.1.3.4 Aims

The aim of this chapter is to assess whether the release of EphA1 ECD into the bloodstream is capable of priming endothelial cells for leucocyte recruitment using a microfluidic system. This will be determined using the Bioflux 200 microfluidic system recapitulating blood flow through the vasculature. We will use a commercially obtained EphA1-Fc (R&D systems) corresponding to the ECD of WT EphA1 and analyse the impact this has on both the rolling interactions and on the firm adhesion of leucocytes to ECs.

5.2 Materials and Methods

5.2.1 Cell culture

5.2.1.1 hCMEC/D3 cell line

The hCMEC/D3 cell line was provided by the Pierre-Olivier Couraud lab and were derived from a surgical excision of the temporal lobe of an adult female with epilepsy (Weksler et al., 2005). The cell line was generated through immortalization using a lentiviral hTERT vector. Cells were delivered cryopreserved at passage 25. Cells were maintained in complete reconstituted EBM-2 media was used to maintain cells (reagents described in section 2.1.1) ReagentPack™ Subculture Reagents (Lonza) were used specifically to the hCMEC/D3 cell line and included EDTA, trypsin neutralising solution (TNS) and HEPES-Buffered Saline Solution (BSS). hCMECs/D3s were not subcultured beyond P35 in order to maintain their cell marker expression and functionality. For passaging of hCMEC/D3s, spent media was removed from the culturing vessels and the cells washed in 10 ml of sterile 1 x PBS for 10 minutes (x 2). Cells were subsequently trypsinized at RT in 3-5 mls of Trypsin/EDTA, depending on vessel size. Trypsin/EDTA activity was quenched using 2-4 ml of TNS and harvested cells were collected in tubes prior to centrifugation at 250x g for 5 minutes. Following aspiration of the supernatant, the cell pellet was re-suspended in an appropriate volume of fresh EMB-2 media and dispensed into fresh 50µG -fibronectin coated-culturing vessels

5.2.1.2 HUVECs

HUVECs are cells which are isolated from the vein of the umbilical cord (Jaffe et al., 1973) and are widely used as a tool to study vascular endothelial cell biology. Immortalized HUVECs (Life Technologies) with a lentiviral hTERT construct were maintained in M199 medium (Sigma Aldrich) with 20% FBS and penicillin/streptomycin (P/S).

5.2.1.3 Molt 3 T cell line

The Molt 3 T-lymphoblast cell line (hereby referred to as Molt 3 T cells) was derived from the peripheral blood of a 19-year-old male suffering from acute lymphoblastic leukaemia

(ATCC) and were provided by Dr John Bridgeman (Cardiff University). Two subpopulations of Molt 3 T cells were used in this thesis, including both L-selectin negative and L-selectin positive cells. The cells expressed a HIV based gag TCR. Dr. Andy Newman (Cardiff University) stably transduced the Molt 3 T cells using a pSxW plasmid expressing a C-terminal V5 His tagged L-selectin.

5.2.2 Quantitative leucocyte flow assay methodology

Molt 3 T cell interactions with HUVECs and hCMEC/D3s were assessed using a Bioflux 200 (Fluxion Biosciences Inc., CA, USA). Channels in a 24-well Bioflux 200 plate (0-20 dynes/cm^2) were coated in 20μg/ml of fibronectin for 1h before 2 x 15 min washes in respective endothelial cell media. ECs were pulsed through the channels and allowed to statically adhere for 2h (2 x 10^6 HUVECs; 4 x 10^6 hCMEC/D3s). Respective culture mediums were then pulsed over the cells O/N. The confluency and alignment of the ECs were visually inspected prior to stimulation and rolling assays. ECs were then stimulated with media only, human recombinant TNFα (2 ng/ml), EphA1-Fc (5 μg/ml) or a control hIgG (5 μg/ml) for 16 hours at 1 dyne/cm^2. For experiments where the impact of SDF-1/CXCL12 on Molt 3 T cell-EC interactions was assessed, 100 ng/ml was added to the medium and passed over the cells 15 minutes prior to cell rolling assays. 7.5 x 10^6 Molt 3 T cells per/ml (p/ml) were labelled with 2 μM carboxyfluorescein succinimidyl ester (CFSE) in PBS for 10 min at RT. Excess dye was then removed by washing twice in PBS. The Molt 3 T cells were then flowed over ECs at the SI unit, 0.05 Pascal (Pa) or 0.5 dynes/cm^2 and 0.025 Pa or 0.25 dynes/cm^2 for HUVECs and hCMEC/D3s respectively and imaged using time-lapse fluorescence microscopy. Shear stress will hereafter be reported in dynes/cm^2, as is standard for studies exploiting the Bioflux system (Tremblay et al., 2015). This resulted in 60 separate Tagged Image Format File (TIFF) images assembled into 60 stacked files. These stacks were converted into audio video interleaved (AVI) files, creating a 7.55 sec video file and unstacked using ImageJ for subsequent analysis. Analyses of cells were conducted using the Fluxion BioFlux 200 software using the cell tracking analysis mode.

5.2.3 Analysis of Molt-3 T cells

Molt 3 T cell behaviour was assessed under flow conditions using CFSE labelled Molt 3 T cells and fluorescent microscopy. Ordinarily, immune cell rolling is assessed using phase contrast or brightfield microscopy and consequently, rolling interactions are directly visualised between leucocytes and ECs as non-interacting cells are generally not observable. The consequence of using CFSE labelled cells is that all cells can be visualised (i.e. non-interacting, rolling and firmly adhered cells). As a result, it was necessary to establish a method by which non-interacting and rolling Molt 3 T cells could be distinguished before analysis of their behaviour was undertaken. Generally, rolling occurs at, or below, the velocity of non-interacting immune cells. However, rolling cells also have easily identifiable characteristics whilst interacting with the endothelium. Rolling cells will **1)** upon capture, rapidly decrease their velocity **2)** meander over the endothelium to overcome obstacles (such as firmly adhered cells) or direct their motion towards chemoattractants or preferential sites of adherence/transmigration. Non-interacting cells, conversely, will generally have a straighter forward motion in the direction of the shear flow, see Fig 5.3 for an example of a non-interacting and rolling cell and the difference in their behaviour. Moreover, as the Bioflux chambers are smaller than conventional flow chambers, the turbulence in these chambers is much lower, meaning non-interacting cells will have a straighter trajectory through the chambers due to improved laminar flow.

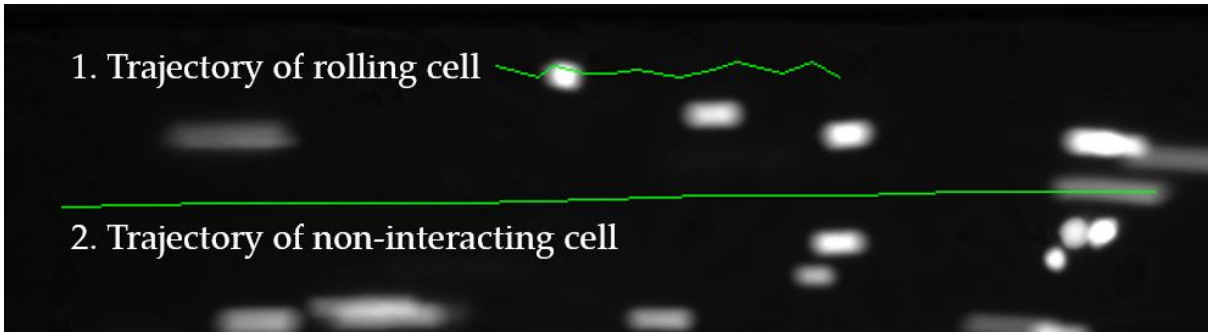

Figure 5.3 Method employed to distinguish between a rolling cell (behaviour 1) and non-interacting cell/fast rolling cell (behaviour 2). **1)** Trajectory of rolling cell taken over 15 frames. Note the zig-zag motion of the cell whilst it surveys the endothelial layer. **2)** Trajectory of a non-interacting cell taken over 5 frames, note the straight path of the cell whilst it flows over the endothelium.

Rolling cells were distinguished from non-interacting cells in the manner described above by a single observer. Rolling analyses was conducted on all rolling cells, with their interaction distance tracked until the cells detached, firmly adhered, or left the field of view. Rolling velocities were calculated by the Bioflux 200 software automatically by using the cell tracking mode. The total contact time of all rolling Molt 3 T cells was established by the number of frames in the time lapse sequence the cells rolled for, multiplied by the time elapsed between each frame (each frame = 0.126 secs). 20 non-interacting Molt 3 T cells were tracked through 5 frames and their global velocity calculated by the Bioflux software. Firmly adhered cells were identified as those which had not made forward motion for at least 40 frames (i.e. 5 seconds). See Fig. 5.4 for a snapshot the channel view of a Bioflux chamber with non-interacting, rolling and firmly adhered Molt 3 T cells highlighted.

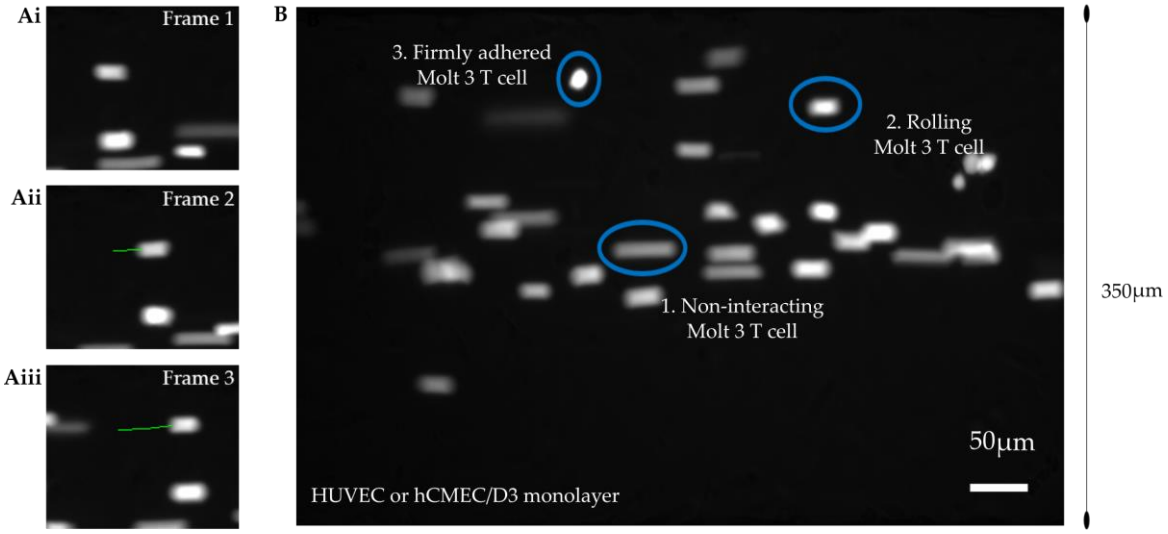

Figure 5.4 Representative snapshot of a Bioflux microfluidic channel. Shown is an adherent monolayer of ECs (in black, not seen) and CFSE labelled Molt 3 T cells (shown in white). Molt 3 T cells were passed through the channel under shear force and their subsequent interactions between the ECs were recorded by time-lapse fluorescent microscopy. **A)** Individual rolling Molt 3 T cells were visually identified and tracked using the Bioflux cell tracking mode across sequential time frames (Fig 5.4 Ai, Aii, Aiii; track shown in green). This allowed quantification of Molt 3 T cell rolling, the total contact time between rolling Molt 3 T cells and ECs, as well as the distance and velocity of each interacting Molt 3 T cells. **B)** Indicated here is **1.** A non-interacting Molt 3 T cells, these were also tracked for their global velocity using the Bioflux cell tracking software. **2.** Rolling Molt 3 T cell as in **A)**, indicated by a slower travelling velocity than the non-interacting Molt 3 T cell and a meandering motion. **3.** The number of firmly adhered Molt 3 T cells was also quantified and were identified as cells which had not made forward motion for at least 40 frames (i.e. 5 seconds). Each channel is 350 µm wide and 70 µm tall.

5.2.4 Flow cytometric analysis of EphA1 and chemokine receptor expression on Molt 3 T cells

Disassociation of adherent cells (i.e. HEK-293 Flp-In/HEK-293 WT EphA1) from the flask was conducted using 5 mM ethylenediaminetetraacetic acid (EDTA) to preserve membrane expression of proteins. The following steps were carried out at 4◦C or on ice. All incubation periods were for 30 mins. Cell suspensions were pelleted by centrifugation at 250x g for 5 mins and resuspended in ice-cold fluorescence-activated cell sorting (FACS) buffer following removal of the supernatant. Cells were centrifuged at 250x g for 3 mins between subsequent staining and washing steps, with the supernatant removed following centrifugation. Cells were plated at 2 x 10^5 in a 96 well plate (100µl per well). Cells were then incubated in live/dead aqua stain (Molecular probes); blocked to control for FcR dependant binding of antibodies (with IgG blocking buffer) and incubated in primary antibody, followed by a fluorophore conjugated secondary antibody (see Table 5.2 for antibodies used for flow cytometry analysis). Cells were either immediately assessed or preserved in 4 % formalin in FACS buffer until subsequent FACS analysis.

Table 5.2 Antibodies used for flow cytometric analyses

Antibody/Probe	**Fluorochrome**	**Vendor/Cat Number**	**Stock Concentration**	**Working Concentration**
N-terminal EphA1 MAb	Unconjugated	R&D systems #MAB638	500 µg/ml	1:400
Goat anti-mouse IgG	Phycoerythrin (PE)	BioLegend #40307	100 µg/ml	1:400
LIVE/DEAD fixable dead cell stain	AmCyan	Molecular Probes #L34959	N/A	1:1000 In FACS buffer

5.3 Results

Flow cytometric analysis has indicated that subpopulations of PBMCs express EphA1 (Ager, unpublished, data not shown). Thus, any future experimentation using patient PBMCs, it would be necessary to sort EphA1 +/- T cells from blood to reduce inter-donor variation. With this in mind, and as a means to simplify the model, it was decided to employ a leucocyte cell line lacking endogenous expression of EphA1. We assessed the Molt 3 T cell line routinely used in the Ager lab via flow cytometry for EphA1 expression. Two subpopulations were assessed. Molt 3 T cells which do not express L-selectin (WT) and Molt 3 T cells transduced to express L-selectin. The previously described WT EphA1-HEK-293 cells and parental Flp-In HEK-293 cells were used as a positive and negative control, respectively.

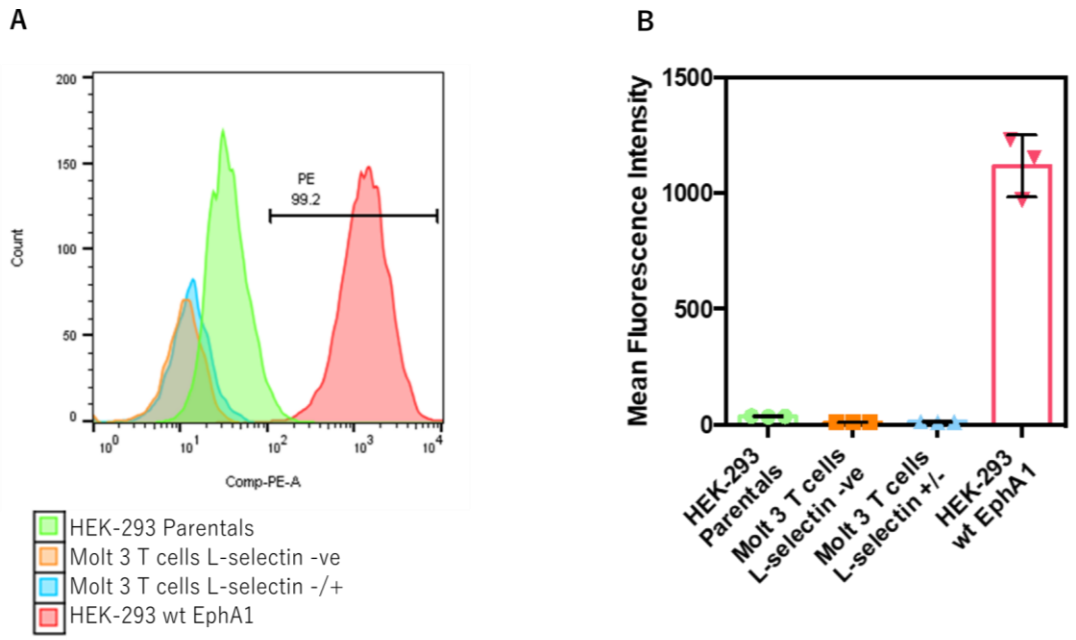

Figure 5.5 Flow cytometric analysis of EphA1 expression by Molt 3 T cell lines. **A**) EphA1 expression in Molt 3 T cells, -ve for L-selectin (orange histogram) and +ve for L-selectin expression (blue histogram) was then analysed against the EphA1 negative HEK-293 parentals (green histogram) and EphA1 +ve HEK-293 cells (red histogram). Both Molt 3 T cell lines overlap partially with the HEK-293 Flp-In parental cells, indicating neither cell lines express EphA1. **B)** Bar chart indicating the mean fluorescence intensity of all cell lines over 3 repeats, confirming the lack of EphA1 expression in both Molt 3 T cell lines (n=3). Work conducted by Lauren Thorburn, Ager Lab.

5.3.1 Expression profiles of HUVEC and hCMEC/D3 cell lines

Section 5.3.1 includes work conducted by the Ager lab as indicated.

As described, the hCMEC/D3 cell line has been extensively characterized for endothelial phenotype and express VE-Cadherin (CD144), PECAM-1 (CD31) and Endoglin (CD105) whilst being negative for CD36 (Weksler et al., 2013) and has been used extensively in the field of BBB research (e.g. Díaz-Perlas et al., 2018; Piazzini et al., 2018). The endothelial origin of the hCMEC/D3 cell line was further verified by the Ager group using the pan-endothelial markers PECAM-1 (CD31) and VEGFR2 (CD309) and VE-cadherin (CD144) (data not shown) to ensure cells had retained their endothelial characteristics.

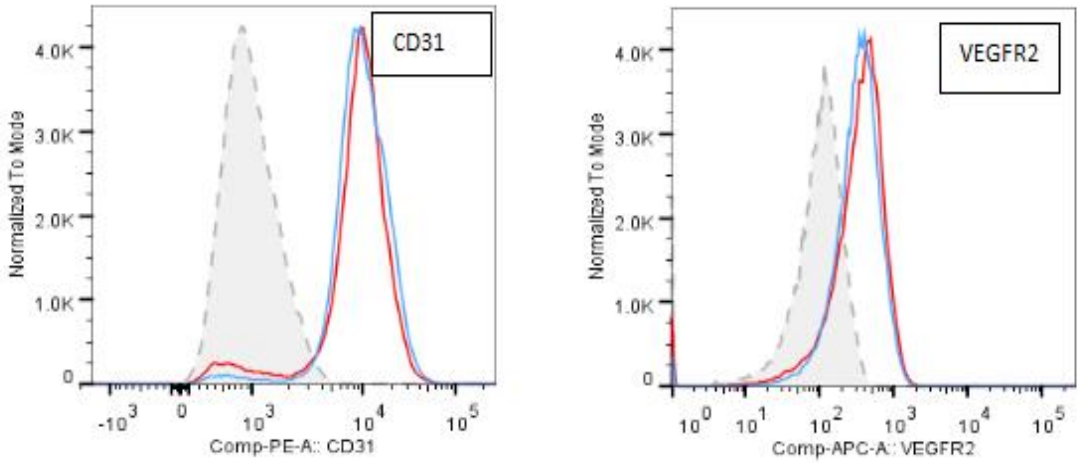

Figure 5.6 Expression of endothelial specific markers by hCMEC/D3 cell line. . The hCMEC/D3 cell line was stained for pan-endothelial markers CD31 and VEGFR2 under basal conditions (blue histogram) and following activation by TNFα for 18 hours (red histogram). Grey filled histograms are cells stained using isotype matched control antibodies. Work conducted by the Ager lab (unpublished).

It was also necessary to determine EphA1 expression on the EC lines to determine the overall potential mechanistic interactions between T cells and the ECs, given the complexities between the Eph receptors and ligands. Both HUVECs (data not shown) and hCMEC/D3s are negative for EphA1 expression and this is not inducible by the inflammatory cytokine, TNFα (Fig 5.7).

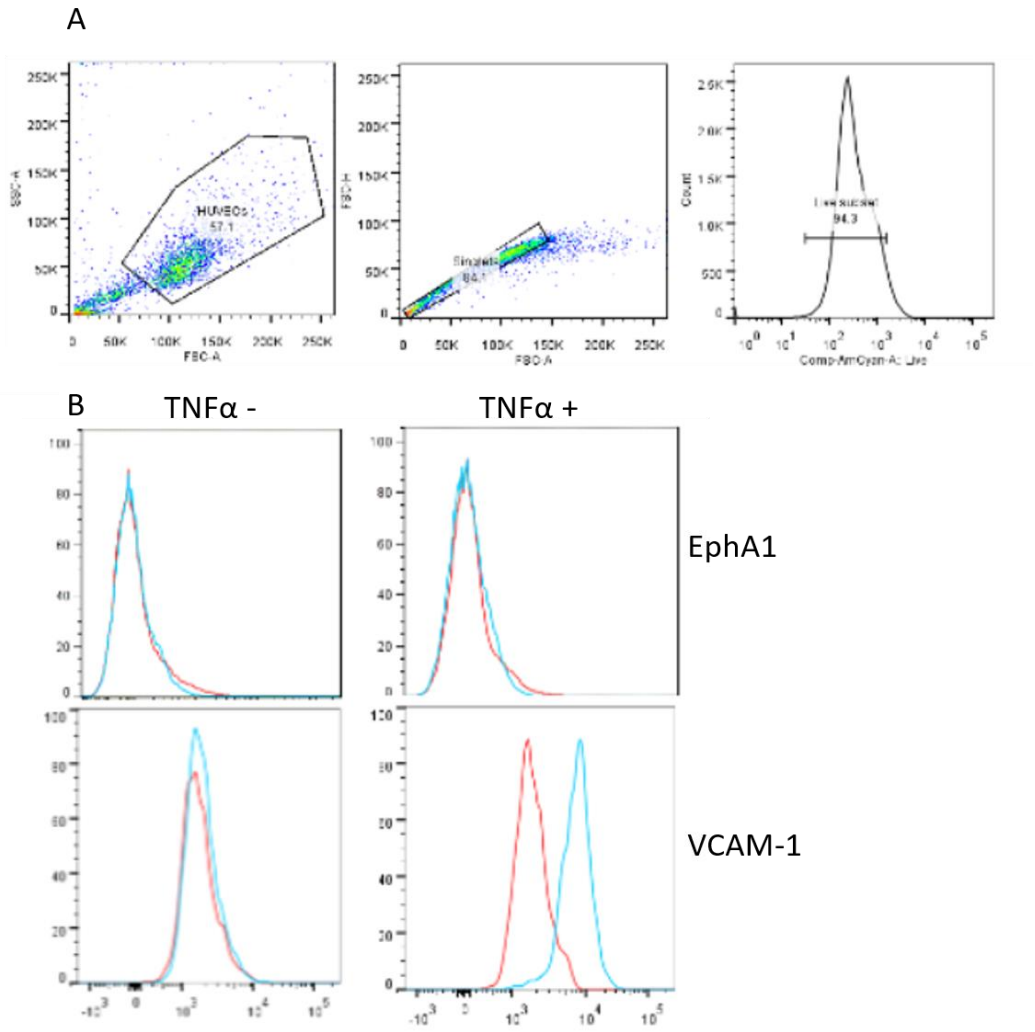

Figure 5.7 Expression of EphA1 on hCMEC/D3 cell line. hCMEC/D3s were stained for EphA1 by flow cytometry. **A)** Gating strategy on forward vs side scatter (left hand panel), single cells (middle panel) and live cells (right hand panel). **B)** Expression of EphA1 or VCAM-1 (blue histogram) and isotype control (red histogram) in absence (left) and presence (right) of TNFα. Expression of VCAM-1 acts as a positive control for TNFα activation of hCMEC/D3s. Work conducted by the Ager lab.

Data from HUVECs and hCMEC/D3 cells also showed that both, ICAM-1 and VCAM-1 were upregulated in response to TNFα, membrane expression of VE-Cadherin (CD144) and PECAM-1 (CD31) remained unaltered and VEGFR2 (CD309) was downregulated. Importantly, both HUVECs and hCMEC/D3s express ephrinA1 under basal conditions which is increased in response to TNFα (Fig 5.8).

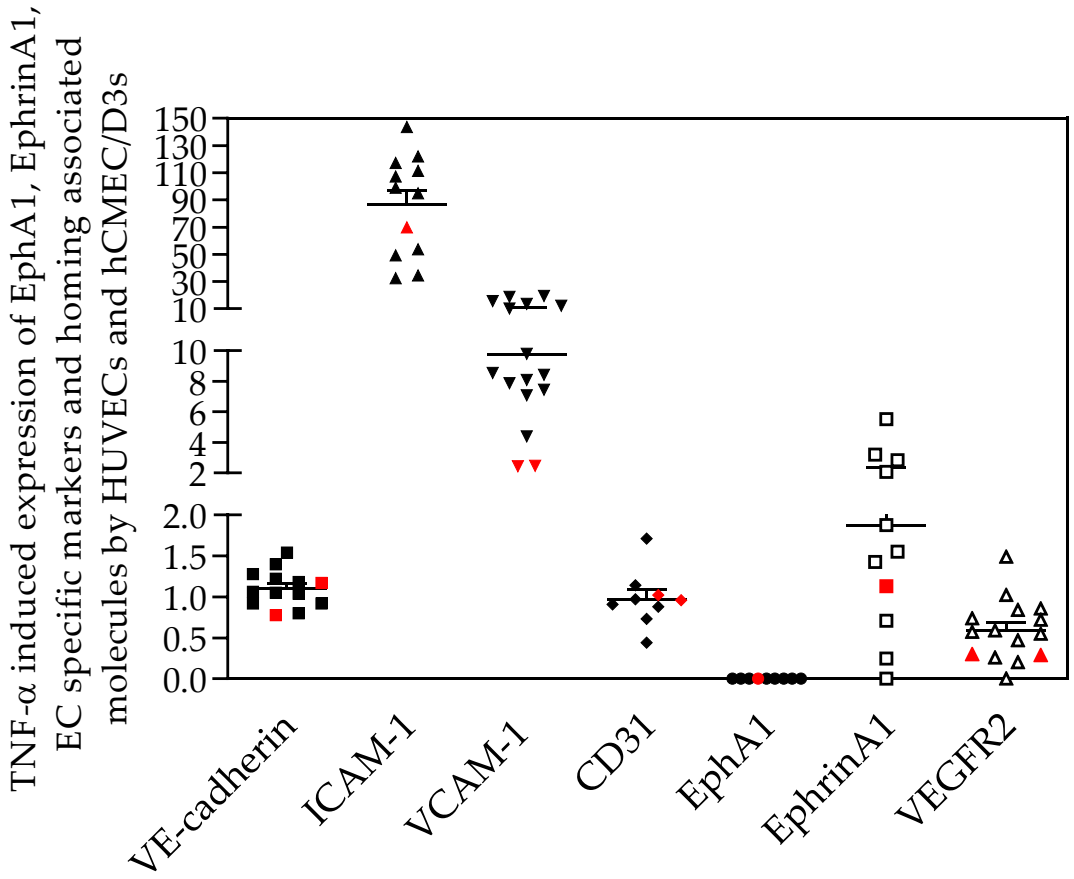

Figure 5.8 Effect of TNFα on expression of EphA1, EphrinA1, endothelial specific markers and homing associated molecules by HUVECs and hCMEC/D3s. HUVECs (black) and hCMEC/D3s (red) were stained for EphA1, EphrinA1, the pan-endothelial markers VE-cadherin, CD31 and VEGFR2, homing associated molecules ICAM-1 and VCAM-1 under basal conditions and following activation by TNFα for 18 h. Median fluorescent intensity of TNFα treated cells was expressed as fold change over unstimulated cells. Scatter plots show pooled data from and HUVEC and hCMEC/D3 cells and bars represent SEM. Work conducted by the Ager lab.

Since hCMEC/D3 cells do not endogenously express EphA1 but constitutively express the ephrinA1 ligand, one might hypothesise that binding of EphA1 expressed on leucocytes with ephrinA1 on brain ECs might regulate BBB function. However, after incubation of hCMECs with EphA1-fc chimera to mimic ligand engagement (in the absence of co-engagement by additional leucocyte expressed receptors), EphA1-Fc had no impact on basal expression of junctional adhesion molecules (JAM's), VE-Cadherin (CD144) or PECAM-1 (CD31), (data not shown). Nevertheless, this assay is incapable of discerning subtle changes in membrane localisation which could control the permeability of the endothelial layer.

In sum, work shows that both HUVECs and the hCMEC/D3 cell lines express pan-endothelial markers, confirming their endothelial origin and suitability for subsequent experimentation. Both the L-selectin -ve, L-selectin +ve Molt 3 T and both EC cell lines are negative for EphA1 expression meaning endogenous expression of EphA1 will not impede assessment of the effect of EphA1-Fc in our microfluidic assay. EphrinA1 is expressed by both HUVECs and hCMEC/D3s and EphA1-Fc may induce reverse signalling in these cells.

5.3.2. TNFα as a positive control for EphA1-Fc mediated Molt 3 T cell-EC interactions

Prior to assessing Molt 3 T cell interactions with EphA1-Fc activated ECs, control experiments were performed using TNFα or media only activated ECs followed by Molt 3 T cell microfluidic analysis. This will allow validation of the Bioflux 200 system and assessment of the characterisation methods as detailed in section 5.2.3. This analysis will also allow us to determine an approximate velocity of cells which roll (behaviour 1) and those which are non-interacting or fast rolling (behaviour 2). Based on the vast amounts of literature on TNFα activated ECs, it is expected that TNFα would lead to the upregulation of adhesion molecules such as VCAM-1 and ICAM-1 which deal with stable adhesion.

5.3.2.1 The effect of TNFα on Molt 3 T cell-HUVEC interactions

5.3.2.1.1 Characterisation of the velocity of non-interacting/fast rolling cells

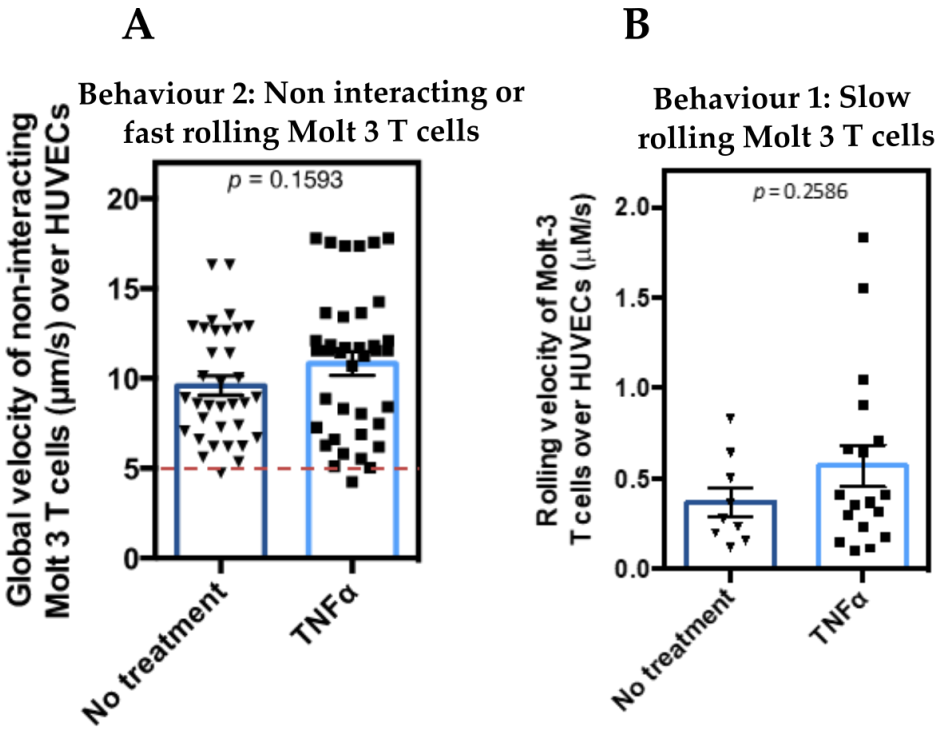

Figure 5.9 Characterisation and analysis of the velocity of interacting (behaviour 1) and non-interacting/fast rolling cells (behaviour 1) **A)** HUVECs were treated with TNFα (2 ng/ml) or media only (no treatment) for 16h at 1 dyne/cm^2. 7.5 x 10^5 CFSE labelled Molt 3 T cells were passed over HUVECs at 0.5 dynes/cm^2. The velocity (µm/s) of Molt 3 T cells exhibiting behaviour 2 was calculated by the Bioflux 200 software following manual identification of cells exhibiting behaviour 2 using the cell tracking analysis mode. Red line indicates Molt 3 T cells did not regularly travel at velocities below 5 µm/s. **B)** HUVECs were treated with TNFα (2 ng/ml) or media only (no treatment) for 16h at 1 dyne/cm^2. 7.5 x 10^5 CFSE labelled Molt 3 T cells were passed over HUVECs at 0.5 dynes/cm^2. The velocity (µm/s) of Molt 3 T cells exhibiting behaviour 1 was calculated by the Bioflux 200 software following manual identification of thse Molt 3 T cells using the cell tracking analysis mode. The average velocity of each rolling interaction or series of transient interactions was calculated automatically by the Bioflux software (n = 3, p = 0.2586), Error bars indicate SEM, analyses were conducted using a student T test.

This analysis indicated that slow-rolling Molt 3 T cells, characterised based on their behavioural attributes (i.e. behaviour 1) did not exceed an average velocity of 2 μm/s. Whereas those Molt 3 T cells which are non-interacting/slow rolling did not travel at velocities below 5 μm/s. As a consequence, cells travelling above an average velocity of 5μm/s were excluded from subsequent analysis of rolling interactions. To determine whether the slow-rolling interactions (i.e cell exhibiting behaviour 1) differ between TNFα and non-treated HUVECs we assessed the average number of rolling cells, distance of interactions, changes in velocity to determine stable interactions and the number of firmly adhered cells. TNFα had no effect on the rolling velocity of Molt 3 T cells (Fig 5.9 B, p = 0.2586) or on the velocity of non-interacting Molt 3 T cells.

5.3.2.1.2 The effect of TNFα on rolling interactions between Molt-3 T cells and HUVECs

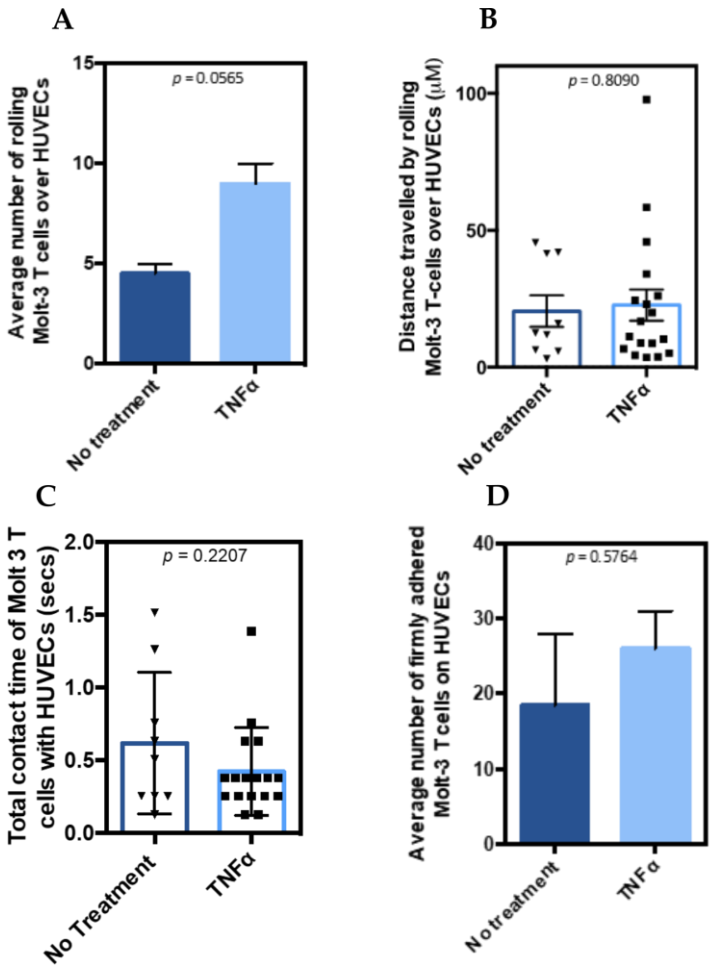

Figure 5.10 The effect of TNFα activation of HUVECs on Molt 3 T cell interactions (cells exhibiting behaviour 1 i.e slow rolling). HUVECs were treated with TNFα (2 ng/ml) or media only (no treatment) for 16h at 1 dyne/cm^2. 7.5 x 10^5 CFSE labelled Molt 3 T cells were subsequently passed over HUVECs at 0.5 dynes/cm^2. Rolling velocity (μm/s) and distance travelled (μm) was calculated by the Bioflux 200 software following manual identification of rolling cells using the cell tracking analysis mode **A)** The effect of TNFα on the average number of rolling Molt 3 T cells (n=3 p = 0.0565 **B)** The total distance (μm) travelled by each individual Molt 3 T cell (data points) (n = 3, p = 0.8090) and the average distance (bar). **C)** The duration of rolling interactions (i.e. the total contact time) between Molt 3 T cells and HUVECs was established by the number of frames in the time lapse sequence rolled for and an average taken (each frame = 0.126 secs) (n = 3, p = 0.2207). **D)** Firmly adhered cells were identified as Molt 3 T cells which has not made forward motion for at least 40 frames (i.e. 5 seconds). (n=3, p = 0.5764).

It was expected that the addition of TNFα would increase the firm adhesion of Molt 3 T cells as TNFα is a powerful inducer of both VCAM-1 and ICAM-1, adhesion molecules involved in this aspect of the adhesion cascade. Whilst TNFα tended to increase the number of firmly adhered Molt 3 T cells (Fig 5.10 D), this effect was non-significant ($p = 0.5764$). Whilst there was a more consistent number of adhered Molt 3 T cells over the 3 repeats, the media only control tended to have a variable number of adhered cells (as indicated by the error bars) ultimately leading to a non-significant result. TNFα also tended to increase the number of rolling Molt 3 T cells on HUVECs when compared to no treatment control (Fig 5.10 A), but this trend was non-significant ($p = 0.0565$). TNFα had no effect on the total distance travelled by the Molt 3 T cells (Fig 5.10 C, $p = 0.8090$), the contact time between the two cell lines (Fig 5.10 B, $p = 0.2207$) This experiment was also conducted using the hCMEC/D3 cell line to determine whether TNFα would have a different mechanism of action. Supplementary video files A1 and A2 show representative AVIs of both no treatment and TNFα activated HUVECs.

5.3.2.2 The effect of TNFα on Molt 3 T cell-hCMEC/D3 interactions

5.3.2.2.1 Characterisation of the velocity of rolling and non-interacting/fast rolling cells

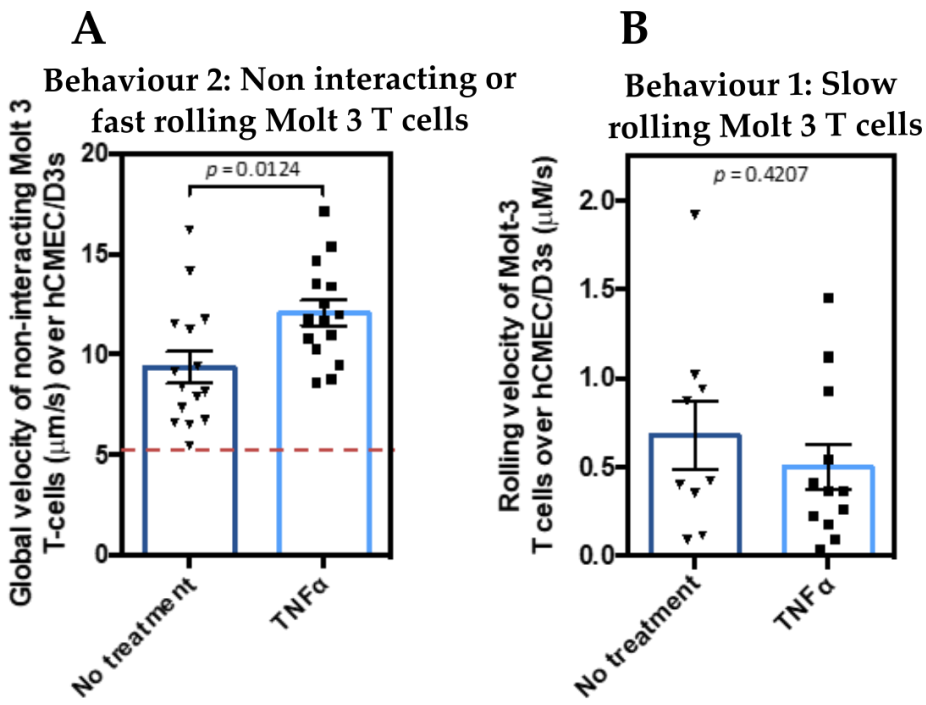

Figure 5.11 Characterisation and analysis of the velocity of interacting (behaviour 1) and non-interacting/fast rolling cells (behaviour 2). **A)** hCMEC/D3s were treated with TNFα (2 ng/ml) or media only (no treatment) for 16h at 1 dyne/cm^2. 7.5 x 10^5 CFSE labelled Molt 3 T cells were passed over hCMEC/D3s at 0.25 dynes/cm^2. The velocity (μm/s) of Molt 3 T cells exhibiting behaviour 2 was calculated by the Bioflux 200 software following manual identification of these Molt 3 T cells using the cell tracking analysis mode. Red line indicates Molt 3 T cells did not travel below 5 μm/s (p = 0.0124). **B)** hCMEC/D3s were treated with TNFα (2 ng/ml) or media only (no treatment) for 16h at 1 dyne/cm^2. 7.5 x 10^5 CFSE labelled Molt 3 T cells were passed over hCMEC/D3s at 0.25 dynes/cm^2. The velocity (μm/s) of Molt 3 T cells exhibiting behaviour 1 (i..e slow rolling) was calculated by the Bioflux 200 software following manual identification of cells showing behaviour 1 using the cell tracking analysis mode. The average velocity of each rolling interaction or series of transient interactions was calculated automatically by the Bioflux software (n = 3, p = 0.4207), Error bars indicate SEM, analyses were conducted using a student T test.

Similarly to TNFα activated HUVECs, slow-rolling Molt 3 T cells, (i.e. behaviour 1) did not exceed a velocity of 2 μm/s, whereas those Molt 3 T cells which exhibited behaviour 2 (i.e. non-interacting/fast rolling) did not travel at velocities below 5 μm/s. As a consequence, cells travelling above an average velocity of 5μm/s were excluded from subsequent analysis of rolling interactions. TNFα had no effect on the rolling velocity of Molt 3 T cells (Fig 5.11 B, p = 0.4207) but did increased the travelling velocity of non-interacting/fast rolling Molt 3 T cells (Fig 5.11 A, p = 0.0124) which may suggest that TNFα is promoting the initial capture of Molt 3 T cells (and thus cells may enter the capture and subsequent fast rolling phase, but TNFα does not support the subsequent slow rolling phase of the adhesion cascade). To determine whether the slow-rolling interactions (i.e. cell exhibiting behaviour 1) differ between TNFα and untreated HUVECs the average number of rolling cells, distance of interactions, total average contact time and the number of firmly adhered cells was assessed

5.3.2.2.2 The effect of TNFα on rolling interactions between Molt-3 T cells and hCMEC/D3s

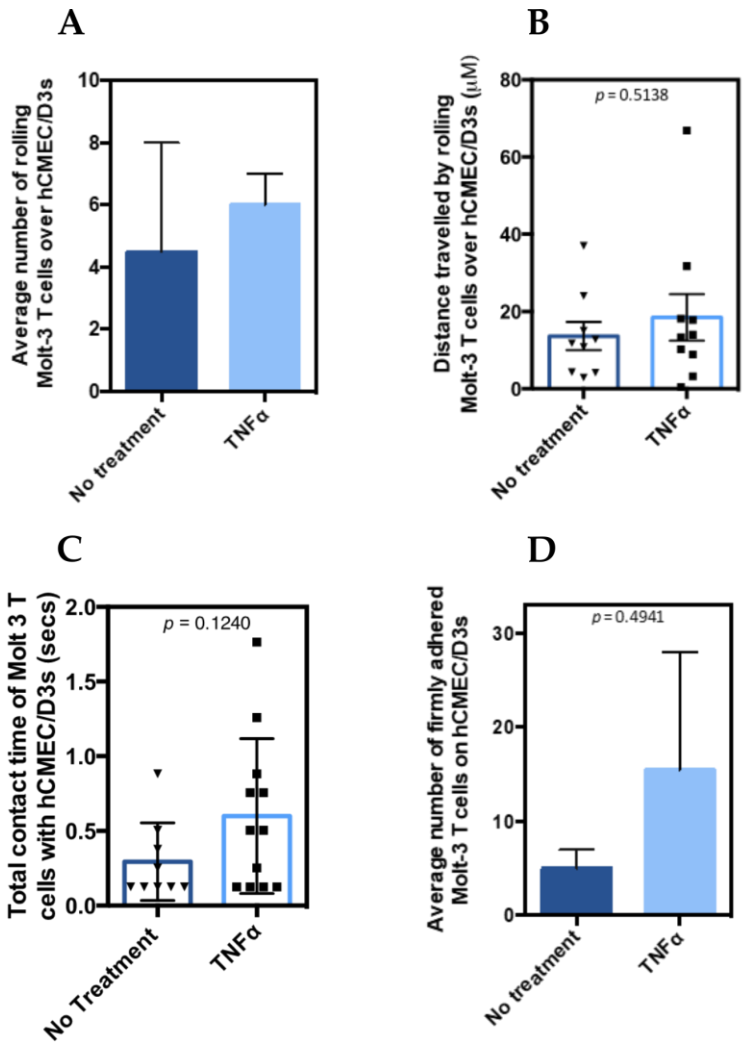

Figure 5.12. The effect of TNFα activation of hCMEC/D3s on Molt 3 T cell interactions. hCMEC/D3s were treated with TNFα (2 ng/ml) or media only (no treatment) for 16h at 1 dyne/cm^2. 7.5 x 10^5 CFSE labelled Molt 3 T cells were passed over hCMEC/D3s at 0.25 dynes/cm^2. Rolling velocity (μm/s) and distance travelled (μm) was calculated by the Bioflux 200 software following manual identification of rolling cells using the cell tracking analysis. **A)** The effect of TNFα on the average number of rolling Molt 3 T cells (n=3) **B)** The total distance (μm) travelled by each individual Molt 3 T cell (data points) and average distance (bar) (n = 3, p = 0.5138). **C)** The duration of rolling interactions (i.e. the total contact time) between Molt 3 T cells and hCMEC/D3s was established by the number of frames in the time lapse sequence rolled for and an average taken (each frame = 0.126 secs) (n = 3, p = <0.1206). **D)** Firmly adhered cells were identified as Molt 3 T cells which had not made forward motion for at least 40 frames (i.e. 5 seconds). (n = 3, p = 0.4941). Error bars indicate SEM. Analyses were conducted using a student T test.

Interestingly, there were no statistical differences between TNFα and no treatment conditions on the interactions between Molt 3 T cells and hCMEC/D3 cells in any assessment. TNFα did not alter the average number of rolling cells (Figure 5.12 A, $p = 0.4207$) when compared to the no treatment control. Moreover, TNFα did not alter the distance travelled by individual Molt 3 T cells over hCMEC/D3s (Figure 5.12 B, $p = 0.5138$) or the total contact time between the cells (Figure 5.12 C, $p = 0.1206$). Whilst there was a general trend towards an increased number of firmly adhered cells, there was variability between experiments and thus non-significant (Figure 5.12 D, $p = 0.4941$). Supplementary video files A3 and A4 show representative AVIs of both no treatment and TNFα activated hCMEC/D3s.

5.3.3 The effect of EphA1-Fc on Molt 3 T cell-EC interactions.

Whilst TNFα did not have a significant effect on any of the areas tested, there was a general trend towards increased adhesion of Molt 3 T cells in both HUVECs (Fig 5.10, D) and hCMEC/D3s (Fig 5.12, D), with TNFα expected to upregulate molecules which deal with firm adhesion. Moreover, it allowed validation of the Bioflux system. As a result, the effect of EphA1-Fc activated ECs was tested.

5.3.3.1 The effect of EphA1-Fc on HUVEC-Molt 3 T cell interactions.

5.3.3.2.1 Characterisation of the velocity of rolling and non-interacting/fast rolling cells

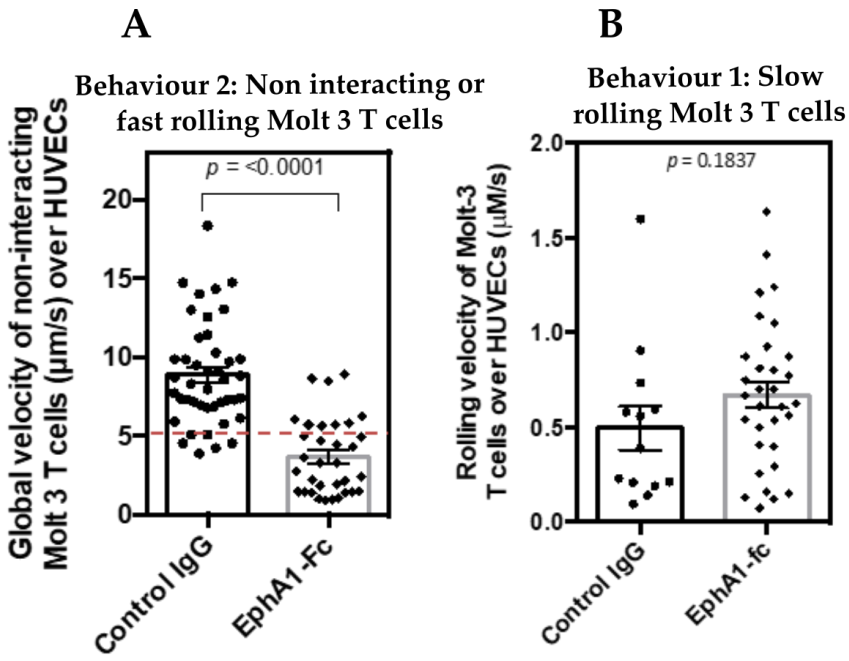

Figure 5.13. Characterisation and analysis of the velocity of interacting (behaviour 1) and non-interacting/fast rolling cells (behaviour 2) . **A)** HUVECs were treated with control IgG (5 μg/ml) or EphA1-Fc (5 μg/ml) for 16h at 1 dyne/cm^2. 7.5 x 10^5 CFSE labelled Molt 3 T cells were passed over HUVECs at 0.5 dynes/cm^2. The velocity (μm/s) of Molt 3 T cells exhibiting behaviour 2 was calculated by the Bioflux 200 software following manual identification of these Molt 3 T cells using the cell tracking analysis mode. Red line indicates Molt 3 T cells following EphA1-Fc treatment of HUVECs decreased the velocity of non-interacting/fast rolling cells as seen in previous conditions (5 μm/s, p = <0.0001). **B)** HUVECs were treated with control IgG (5 μg/ml) or EphA1-Fc (5 μg/ml) for 16h at 1 dyne/cm^2. 7.5 x 10^5 CFSE labelled Molt 3 T cells were passed over HUVECs at 0.5 dynes/cm^2. The velocity (μm/s) of Molt 3 T cells exhibiting behaviour 1 was calculated by the Bioflux 200 software following manual identification of these Molt 3 T cells using the cell tracking analysis mode. The average velocity of each rolling interaction or series of transient interactions was calculated automatically by the Bioflux software (n = 3, p = 0.1837). Error bars indicate SEM, analyses were conducted using a student T test.

Interestingly, and in stark contrast to previous findings, EphA1-Fc significantly reduced the velocity of Molt 3 T cells exhibiting behaviour 2 (i.e. cells undergoing fast rolling/not interacting with the EC layer), (Fig 5.13 A, $p = < 0.0001$). Upon visual inspection of the rolling videos of EphA1-Fc treated HUVECs. it is clear that there is a marked reduction in the velocity at which all Molt 3 T cells travel, compared to all other analysed conditions and thus likely represents a real phenomenon. As a result, for the subsequent analysis of rolling behaviours, we continued to assess these cells based on the explained method of discerning rolling cells. One must be aware however, that these results could indicate that the method of discerning rolling and non-interacting cells is less not an entirely effective method.

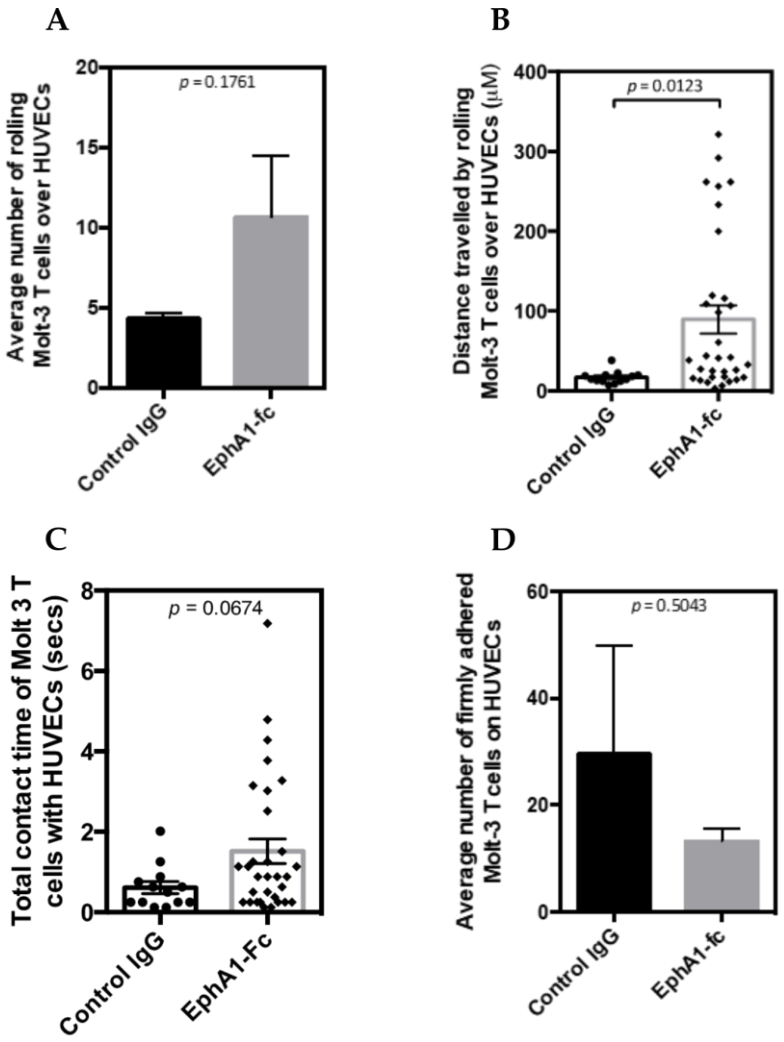

Figure 5.14 The effect of EphA1-Fc activation of HUVECs on Molt 3 T cell interactions. HUVECs were treated with EphA1-Fc (5 μg/ml) or control hIgG (5 μg/ml) for 16 h at 1 dyne/cm^2. 7.5 x 10^5 CFSE labelled Molt 3 T cells were passed over HUVECs at 0.5 dynes/cm^2. Rolling velocity (μm/s) and distance travelled (μm) was calculated by the Bioflux 200 software following manual identification of rolling cells using the cell tracking analysis mode **A)** The effect of EphA1-Fc on the average number of rolling Molt 3 T cells (n=3 p = 0.1761) **B)** The total distance (μm) travelled by each individual Molt 3 T cell (data points) (p = 0.0123) and the average distance (bar). **C)** The duration of rolling interactions (i.e. the total contact time) between Molt 3 T cells and HUVECs was established by the number of frames in the time lapse sequence rolled for and an average taken (each frame = 0.126 secs) (n = 3, p = 0.0674). **D)** Firmly adhered cells were identified as Molt 3 T cells which has lacked forward motion for at least 40 frames (i.e.5 seconds). (n=3, p = 0.5043). Error bars indicate SEM. Analyses were conducted using a student T test.

Whilst EphA1-Fc treatment of HUVECs did not significantly increase the average number of adhered (Fig 5.14 D, p = 0.5043) or rolling (Fig 5.14 A, p = 0.1767) Molt 3 T cells compared to control IgG, it did significantly alter the distance each of the Molt 3 T cells travelled (Fig 5.14

B, $p = 0.0123$). The total contact time remained unaltered between conditions (Fig 5.14 C, $p = 0.0674$) Whilst non-significant, there was a general trend for EphA1-Fc to increase the number of rolling Molt 3 T cells and decrease the number of firmly adhered cells. It is known that not all rolling cells will adhere and not all adhered cells will transmigrate, but cell adherence is a prerequisite for eventual TEM. These results possibly indicate that EphA1 would not cause a pathological alteration in numbers of transmigrating immune cells as it does not alter the number of adhered cells. However, in the context of the BBB, an increase in the number of rolling cells may cause alterations in TJ permeability and any EphA1-mediated leucocyte:hCMEC/D3 interactions may be different to those observed here for HUVECs. As a result, an additional series of experiments were conducted using the disease relevant cell line, hCMEC/D3s. Supplementary video files A5 and A6 show representative AVIs of both control IgG and EphA1-Fc activated HUVECs.

5.3.2.2 The effect of EphA1-Fc on hCMEC/D3-Molt 3 T cell interactions

5.3.3.2.1 Characterisation of the velocity of rolling and non-interacting/fast rolling cells

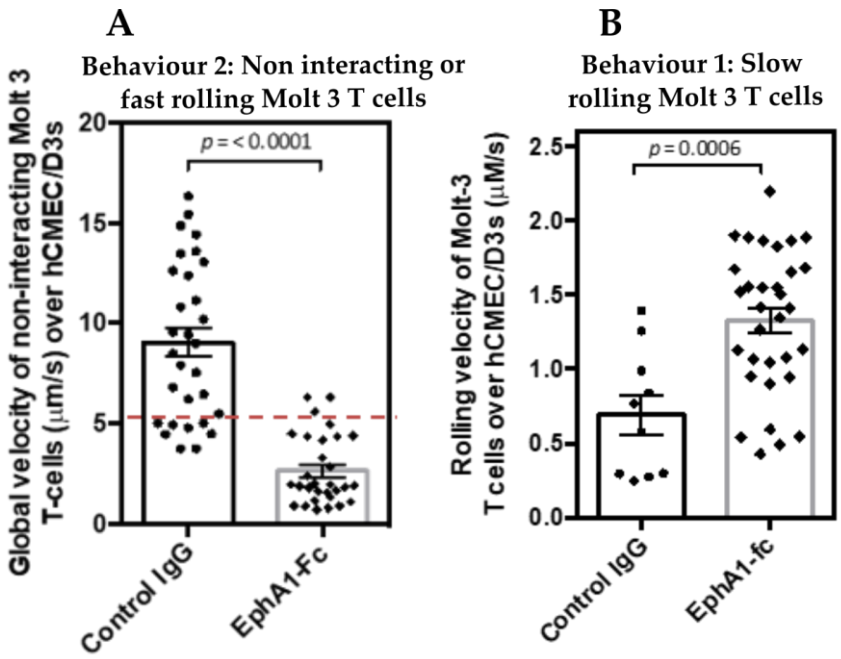

Figure 5.15. Characterisation and analysis of the velocity of interacting (behaviour 1) and non-interacting/fast rolling cells (behaviour 2). **A)** hCMEC/D3s were treated with TNFα (2 ng/ml) or media only (no treatment) for 16h at 1 dyne/cm^2. 7.5 x 10^5 CFSE labelled Molt 3 T cells were passed over hCMEC/D3s at 0.25 dynes/cm^2. The velocity (μm/s) of Molt 3 T cells exhibiting behaviour 2 was calculated by the Bioflux 200 software following manual identification of these Molt 3 T cells using the cell tracking analysis mode. Red line indicates Molt 3 T cells did not travel below 5 μm/s (p = 0.0124). **B)** hCMEC/D3s were treated with TNFα (2 ng/ml) or media only (no treatment) for 16h at 1 dyne/cm^2. 7.5 x 10^5 CFSE labelled Molt 3 T cells were passed over hCMEC/D3s at 0.25 dynes/cm^2. The velocity (μm/s) of Molt 3 T cells exhibiting behaviour 1 was calculated by the Bioflux 200 software following manual identification of these Molt 3 T cells using the cell tracking analysis mode. The average velocity of each rolling interaction or series of transient interactions was calculated automatically by the Bioflux software (n = 3, p = 0.4207). Error bars indicate SEM, analyses were conducted using a student T test.

Similarly to HUVECs, EphA1-Fc significantly reduced the velocity of Molt 3 T cells exhibiting behaviour 2 (i.e. cells undergoing fast rolling/not interacting with the EC layer), (Fig 5.15 A, $p = < 0.0001$) and again upon visual inspection of the rolling videos of EphA1-Fc treated hCMEC/D3s,, it is clear that there is a marked reduction in the velocity at which all Molt 3 T cells travel, compared to all other analysed conditions and thus likely represents a real phenomenon. As a result, for the subsequent analysis of rolling behaviours, we continued to assess these cells based on the explained method of discerning rolling cells.

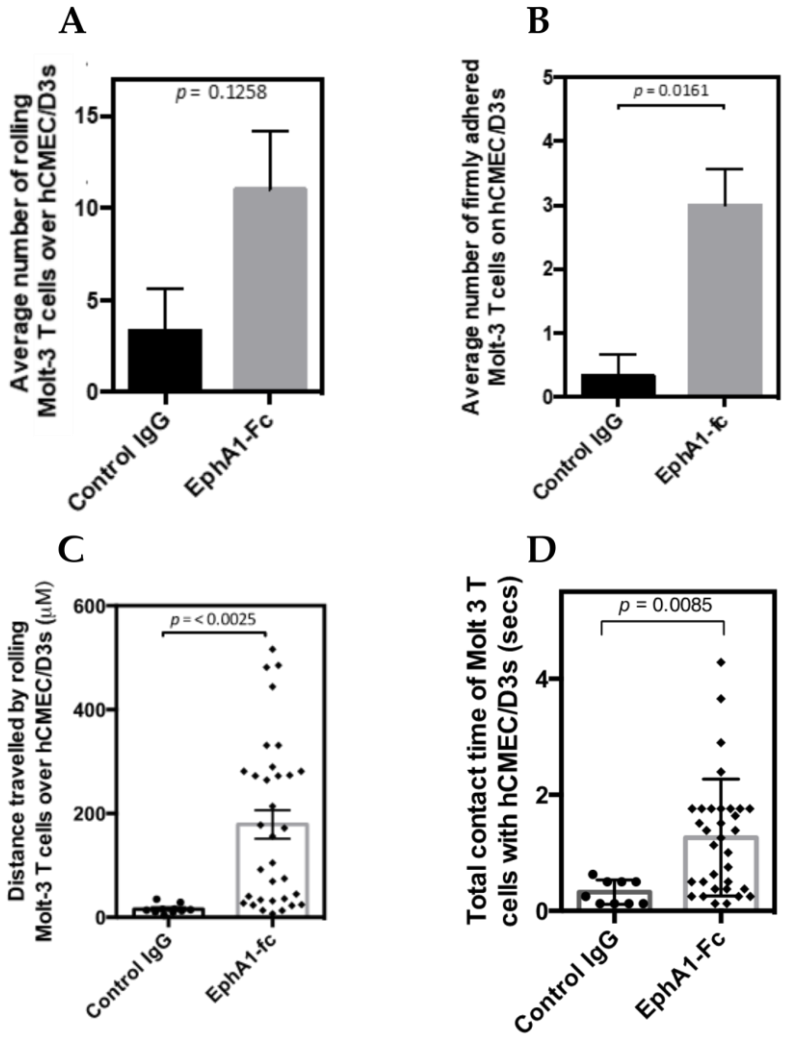

Figure 5.16. The effect of EphA1-Fc on activation of hCMEC/D3s on Molt 3 T cell interactions hCMEC/D3s were treated with EphA1-Fc (5 μg/ml) or control hIgG (5 μg/ml) for 16h at 1 dyne/cm^2. 7.5 x 10^5 CFSE labelled Molt 3 T cells were passed over hCMEC/D3s at 0.25 dynes/cm^2. Rolling velocity (μm/s) and distance travelled (μm) was calculated by the Bioflux 200 software following manual identification of rolling cells using the cell tracking analysis mode **A)** The effect of EphA1-Fc on the average number of rolling Molt 3 T cells (n=3 p = 0.1258). **B)** Firmly adhered cells were identified as Molt 3 T cells which had not made forward motion for at least 40 frames (i.e. 5 seconds). (n = 3, p = 0.0161). **C)** The total distance (μm) travelled by each individual Molt 3 T cell (data points) and average distance (bar) (n = 3, p = <0.0025). **D)** The duration of rolling interactions (i.e. the total contact time) between Molt 3 T cells and hCMEC/D3s was established by the number of frames in the time lapse sequence rolled for and an average taken (each frame = 0.126 secs) (n = 3, p = <0.0085). Error bars indicate SEM. Analysis was conducted using a student T test.

Similarly, to the HUVEC cell line, EphA1-Fc (5 μg/ml) treatment of hCMEC/D3s did not significantly increase the number of rolling Molt 3 T cells (Figure 5.16 A, $p = 0.1258$), however there was a general trend towards increased cell rolling numbers (Fig 5.16 A). EphA1-Fc treatment significantly altered all other measured outcomes. i.e. significantly increasing the number of firmly adhered cells (Fig 5.16 B, $p = 0.0161$), the distance travelled of individual Molt 3 T cells (Fig 5.16 C, $p = <0.0025$ and total contact time (Fig 5.16 D $p = <0.0085$). In contrast to the HUVEC analysis, EphA1-Fc treated hCMEC/D3s showed significantly different interactions with Molt 3 T cells indicating that EphA1 signalling responses were profoundly different, justifying the choice of using hCMEC/D3 cells as a model of the BBB. This suggests that EphA1-mediated alterations in leucocyte:EC interactions is cell type specific and appears to preferentially increase leucocyte interactions with brain ECs. Supplementary video files A7 and A8 show representative AVIs of both control IgG and EphA1-Fc activated hCMEC/D3s.

5.4 The effect of EphA1-Fc on the number stable interactions between rolling Molt-3 T cells and HUVECs and hCMEC/D3s

During the described analysis, it appeared that the addition of EphA1-Fc caused a marked increase in the distance that slow Molt 3 T cells travelled over both EphA1-Fc treated HUVECs and hCMEC/D3 cells and a marked reduction in the velocity that not interacting cells travelled. To investigate this further we wanted to determine whether the increase in the distance travelled actually represents a series of transient interactions between Molt 3 T cells and ECs and as such would represent a different mechanism of action. Moreover, a reduction in the velocity of non-interacting Molt 3 T cells could also represent a series of transient "touch-and-go" interactions which may lower the average velocity of a non-interacting Molt 3 T cell. As described, identification of rolling cells was conducted visually by assessing various factors such as their trajectory and movement along the endothelium (see section 5.2.3). The previous data indicates that an identified non-interacting cell did not typically travel below an average velocity of 5 μm/s in the control IgG, TNFα or untreated conditions (Fig 5.9 B, Fig 5.10 B, Fig 5.11 B, Fig 5.12 B) allowing one to reason that cells traveling at or below this velocity will most likely be a rolling cell. In this section, we aimed to determine whether the average velocity of non-interacting/slow rolling Molt 3 T cells may be altered by assessing number of transient interactions between the immune cells and ECs (i.e. cells moving from slow-rolling to non-interacting during their travel across the EC layer, and thus reducing their average velocity) in each condition. A transient interaction is defined as a cell alternating their velocity <5 μm/s to >5 μm/s with this change described as one transient interaction. A subset of Molt 3 T cells were also analysed and plotted over a number of frame as a means to visualise their changes in velocity.

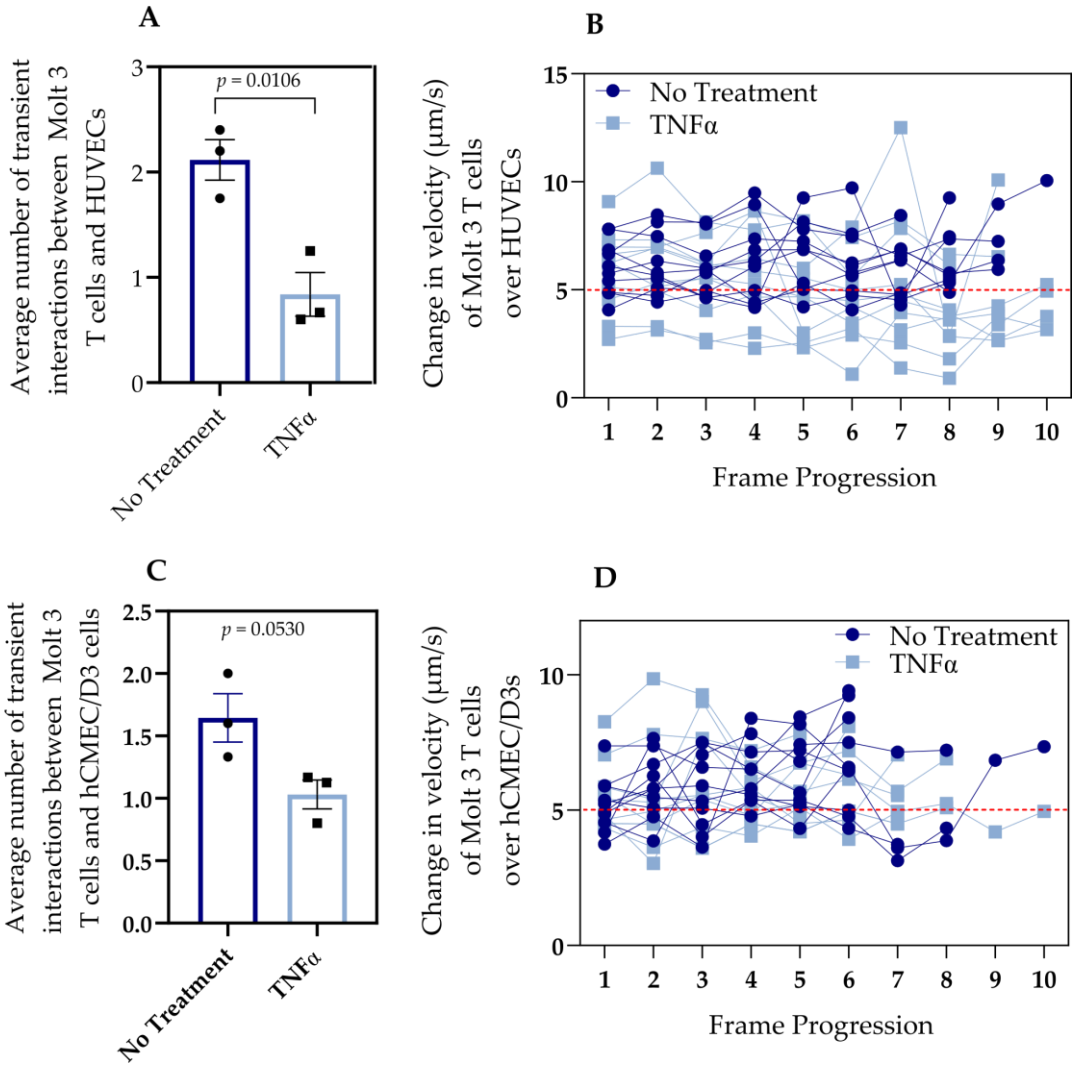

Figure 5.17 The number of transient rolling interactions of Molt 3 T cells following TNFα treatment over HUVECs and hCMEC/D3 cells.. HUVEC or hCMEC/D3 cells were treated with TNFα (2 ng/ml) or media only (no treatment) for 16h at 1 dyne/cm^2. 7.5 x 10^5 CFSE labelled Molt 3 T cells were subsequently passed over ECs at 0.5 dynes/cm^2 or 0.25 dynes/cm^2 for HUVECs and hCMEC/D3 cells, respectively. The average number of transient interactions were established (n=3) for each Molt 3 T cell with an average velocity below 5μm/s with a transient interaction defined as a cell which alternates between rolling (<5μm/s) and no-interaction (>5μm/s), with this change classed as 1 transient interaction. Changes in rolling velocity (μm/s) was calculated by the Bioflux 200 software following manual identification of rolling cells using the cell tracking analysis mode. **A)** Molt 3 T cells underwent fewer transient interactions following TNFα treatment of HUVECs (n = 3, p = 0.0106) indicating that TNFα increased the stable rolling of Molt 3 T cells over HUVECs. **B)** A graphical representation of the velocity changes of a subset of Molt 3 T cells with an average velocity below 5 μm/s (red line) indicating that TNFα treatment of HUVECs promotes more stable rolling of the Molt 3 T cells **C)** Molt 3 T cells did not differ in their transients interactions with hCMEC/D3 cells following TNFα treatment of hCMEC/D3s (n = 3, p = 0.0530). **D)** A graphical representation of the velocity changes of a subset of Molt 3 T cells with an average velocity below 5 μm/s (red line) indicating that TNFα treatment of hCMEC/D3s does not promote an increase in the stable

rolling of Molt 3 T cells. Each dot in B and D represents the change in velocity of an individual cell from one frame to the next.

These results indicated that TNFα reduced the number of transient interactions between Molt 3 T cells and HUVECs ($p = 0.0106$) and there was a general trend of reduced transient interactions between Molt 3 T cells and hCMEC/D3s ($p = 0.0530$). This suggests that TNFα may promote the stable rolling of Molt 3 T cells, despite previous data indicating that TNFα did not significantly increase the number of rolling cells. This finding suggests that those cells which do roll can be classified as stably rolling cells.

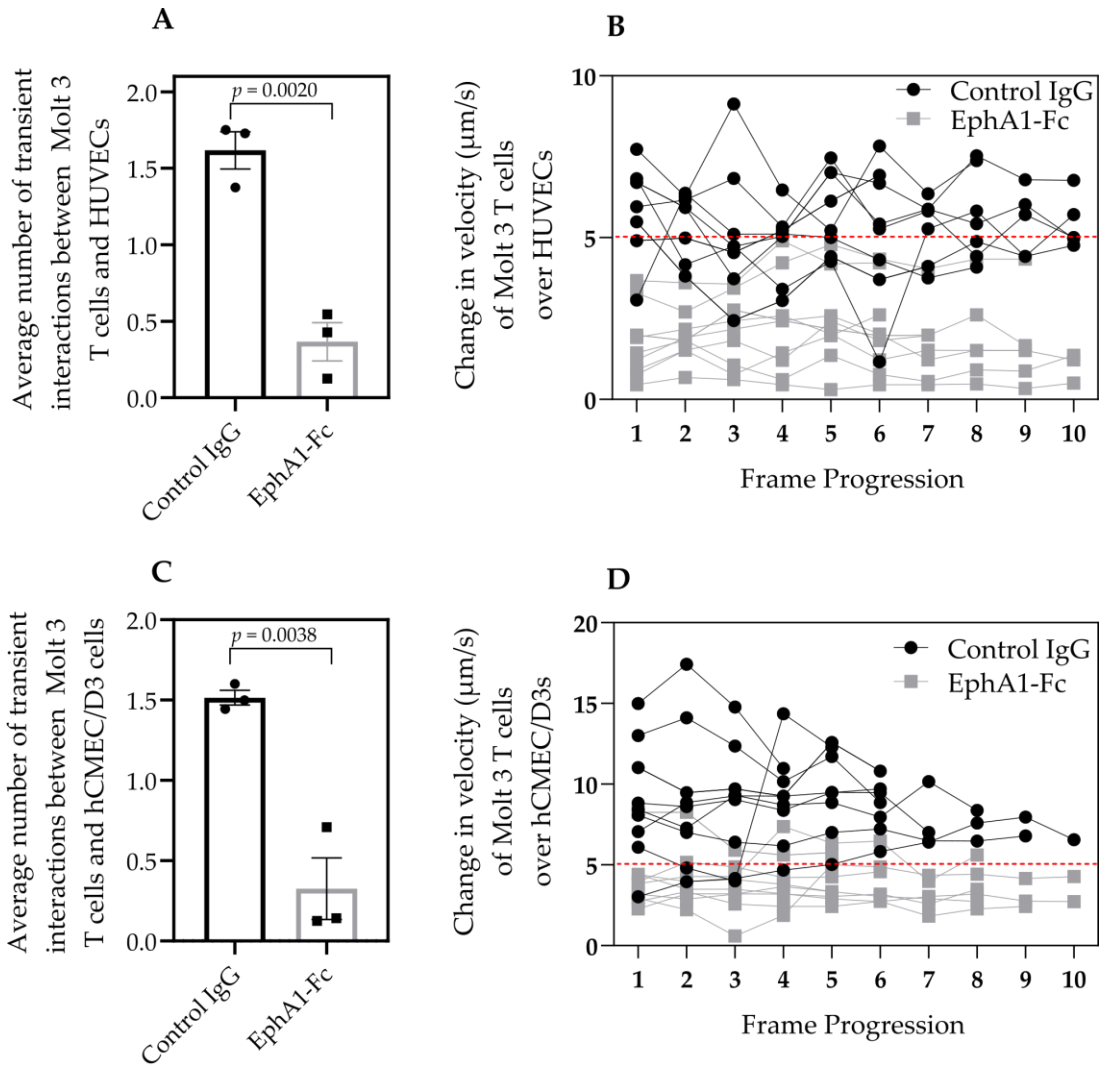

Figure 5.18 The number of transient rolling interactions of Molt 3 T cells following EphA1-Fc treatment over HUVECs and hCMEC/D3 . HUVEC or hCMEC/D3 cells were treated with control IgG (5 µg/ml) or media EphA1-Fc ((5 µg/ml)) for 16h at 1 dyne/cm^2. 7.5 x 10^5 CFSE labelled Molt 3 T cells were subsequently passed over ECs at 0.5 dynes/cm^2 or 0.25 dynes/cm^2 for HUVECs and hCMEC/D3 cells, respectively. The average number of transient interactions were established (n=3) for each Molt 3 T cell with an average velocity below 5µm/s with a transient interaction defined as a cell which alternates between rolling (<5µm/s) and no-interaction (>5µm/s), with this change classed as 1 transient interaction. Changes in rolling velocity (µm/s) was calculated by the Bioflux 200 software following manual identification of rolling cells using the cell tracking analysis mode. **A)** Molt 3 T cells underwent fewer transient interactions following EphA1-Fc treatment of HUVECs (n = 3, p = 0.0020) indicating that EphA1-Fc increased the stable rolling of Molt 3 T cells over HUVECs. **B)** A graphical representation of the velocity changes of a subset of Molt 3 T cells with an average velocity below 5 µm/s (red line) indicating that EphA1-Fc treatment of HUVECs promotes more stable rolling of the Molt 3 T cells **C)** Molt 3 T cells underwent fewer transient interactions following EphA1-Fc treatment of hCMEC/D3s (n = 3, p = 0.0038) meaning EphA1-Fc increased the stable rolling of Molt 3 T cells over HUVECs **D)** A graphical representation of the velocity changes of a subset of Molt 3 T cells with an average velocity below 5 µm/s (red line) indicating that EphA1-Fc treatment of hCMEC/D3s promotes more stable rolling of the Molt 3 T cells. Each

dot in B and D represents the change in velocity of an individual cell from one frame to the next.

These results indicate that EphA1-Fc significantly reduced the number of transient interactions between Molt 3 T cells and HUVECs (p = 0.0020) and Molt 3 T cells and hCMEC/D3s (p = 0.0530). This suggests that EphA1-Fc promotes the stable rolling of Molt 3 T cells. This is nicely represented in Figures 5.18 B & D, where EphA1-Fc treatment results in a more linear velocity below the pre-specified velocity of 5 μm/s. This has consequences on the previously reported data which showed that there was an overall reduction in the velocity at which non-interacting Molt 3 T cells travelled. One could argue that a cells average velocity could be greatly reduced by a series of transient, "touch-and-go" interactions. This data however shows that there are few transient interactions between Molt 3 T cells and EphA1-Fc treated ECs. Moreover, it shows that Molt 3 T cells will travel stably for long distances, as previous data indicated that EphA1-Fc treatment of ECs will greatly increase the distance travelled by Molt 3 T cells; this data suggests that this increase in distance travelled is not characterised by a series of transient interactions.

5.5 The impact of SDF-1/CXCL12 on Molt 3 T cell interactions with EphA1-Fc activated hCMEC/D3s

SDF-1 or alternatively, C-X-C motif chemokine 12 (CXCL12) is a pleiotropic chemokine expressed in multiple tissues, including human brain microvessel endothelial cells (HBMEC). The seven-span transmembrane GPCR, CXCR4, represents its cognate receptor (Horuk, 2001). SDF-1 is considered an important regulator of immune cell trafficking (Kucia et al., 2003; Ratajczak et al., 2003) and thus its biological effects relates to the induction of motility, chemotaxis and adhesion. Moreover, SDF-1 is capable of increasing the adhesion of immune cells through the modulation of several leucocyte expressed integrins. SDF-1 has been shown to be expressed in the brain, particularly the SDF-1β isoform is expressed on ECs of cerebral microvessels. In the penumbra, increased SDF-1β expression results in an increased TEM of CXCR4 expressing peripheral immune cells (Stumm et al., 2002). Importantly, EphA1 has been shown to increase the concentration of SDF-1 in a tumour microenvironment thus activating the SDF-1/CXCR4 axis and leading to an increase the recruitment of endothelial progenitor cells (EPCs) to hepatocellular carcinoma (HCC) cells (Wang et al., 2016). Furthermore, SDF-1 has been shown to modulate transmigration of $CD4^+$ and $CD8^+$ T cells, $CD19^+$ B cells and $CD14^+$ monocytes across a BBB model under shear flow (Man et al., 2012). As this axis is mediated by EphA1 activation, it would be interesting to examine the effect of the addition of SDF-1 could have on EphA1 activated ECs. As EphA1-Fc had a more robust effect on hCMEC/D3 cells, it was decided to use this cell line for the following analyses.

5.5.1 Expression of chemokine receptors in Molt 3 T cells

To investigate the potential for SDF-1 to influence Molt 3 T cell interactions with hCMECs, it was first necessary to determine the chemokine receptor expression of Molt 3 T cells. Molt 3 T cells were assessed for their expression of CCR2, CCR7, CXCR3 and the SDF-1 receptor, CXCR4.

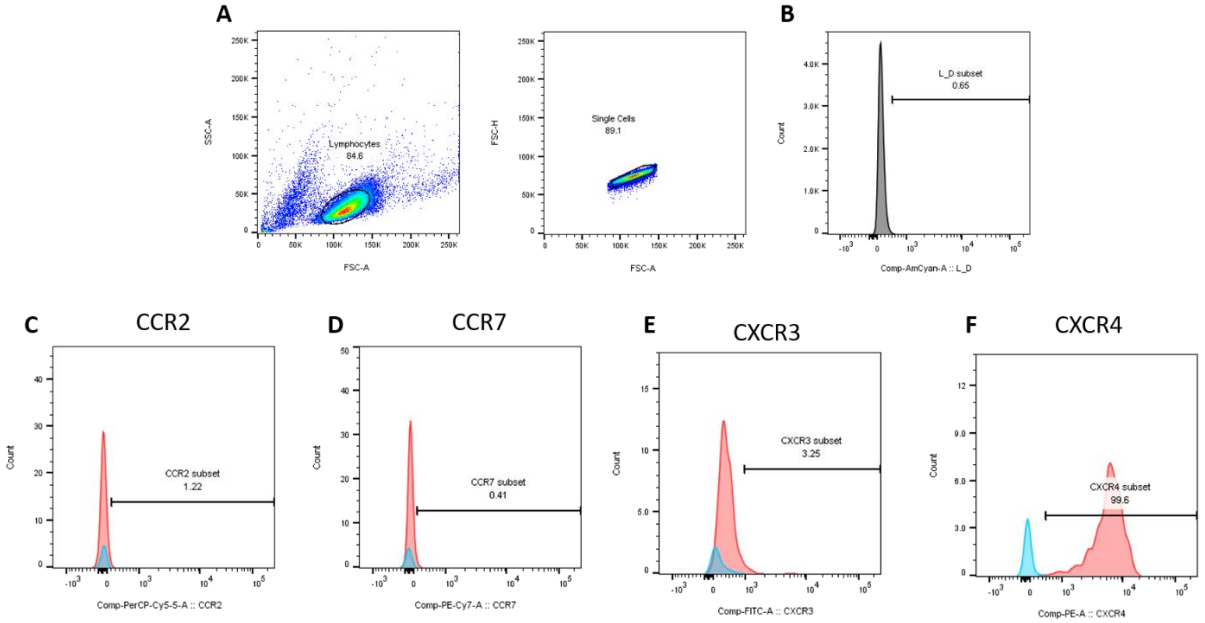

Figure 5.19 Flow cytometric analysis indicating chemokine receptor expression on Molt 3 T cells.**A)** Gating strategy of Molt 3 T cells**. B)** Chart indicating the live/dead subset in the AmCyan channel **C)** CCR2 expression (pink histogram) compared to isotype control (blue histogram) indicating MOLT-3 T cells do not express the chemokine receptor, CCR2 **D)** CCR7 expression (pink histogram) compared to isotype control (blue histogram) indicating Molt 3 T cells do not express the chemokine receptor, CCR7 **E)** CCR3 expression (pink histogram) compared to isotype control (blue histogram) indicating Molt 3 T cells have low expression levels of the chemokine receptor, CCR3 **F)** CXCR4 expression (pink histogram) compared to isotype control (blue histogram) indicating Molt 3 T cells express the chemokine receptor, CXCR4. Work conducted by Markella Alatsatianos.

As flow cytometric analysis indicated that Molt 3 T cells express the SDF-1 receptor, CXCR4, this chemokine can be included in further Bioflux experiments to determine the impact of SDF-1 on the recruitment of leucocytes on EphA1-Fc activated hCMEC/D3s.

5.5.2 The effect of SDF-1 on TNFα activated hCMEC/D3s

As before, TNFα activated hCMEC/D3s were also assessed in the absence and presence of SDF-1. As the TNFα data described earlier in the chapter does not significantly support the notion that TNFα is supporting the upregulation of adhesion molecules such as VCAM-1 and ICAM-1 as there was not a significant increase in the number of firmly adhered Molt 3 T cells, these series of experiments may enhance the ability of Molt 3 T cells to adhere. In some circumstances, it has been shown that TNFα alone has little effect on firm adherence. For instance TNFα treatment of vascular ECs does not promote the adherence of CD117/c-kit+ cells, however following a combined treatment of these ECs with TNFα and SDF-1, the adherence of these cells were significantly increased in an ICAM-1 and CXCR4-dependant manner (Kaminski et al., 2008). Thus, Molt 3 T cell specific mechanisms of interactions with hCMEC/D3s may require additional signals to support their adherence.

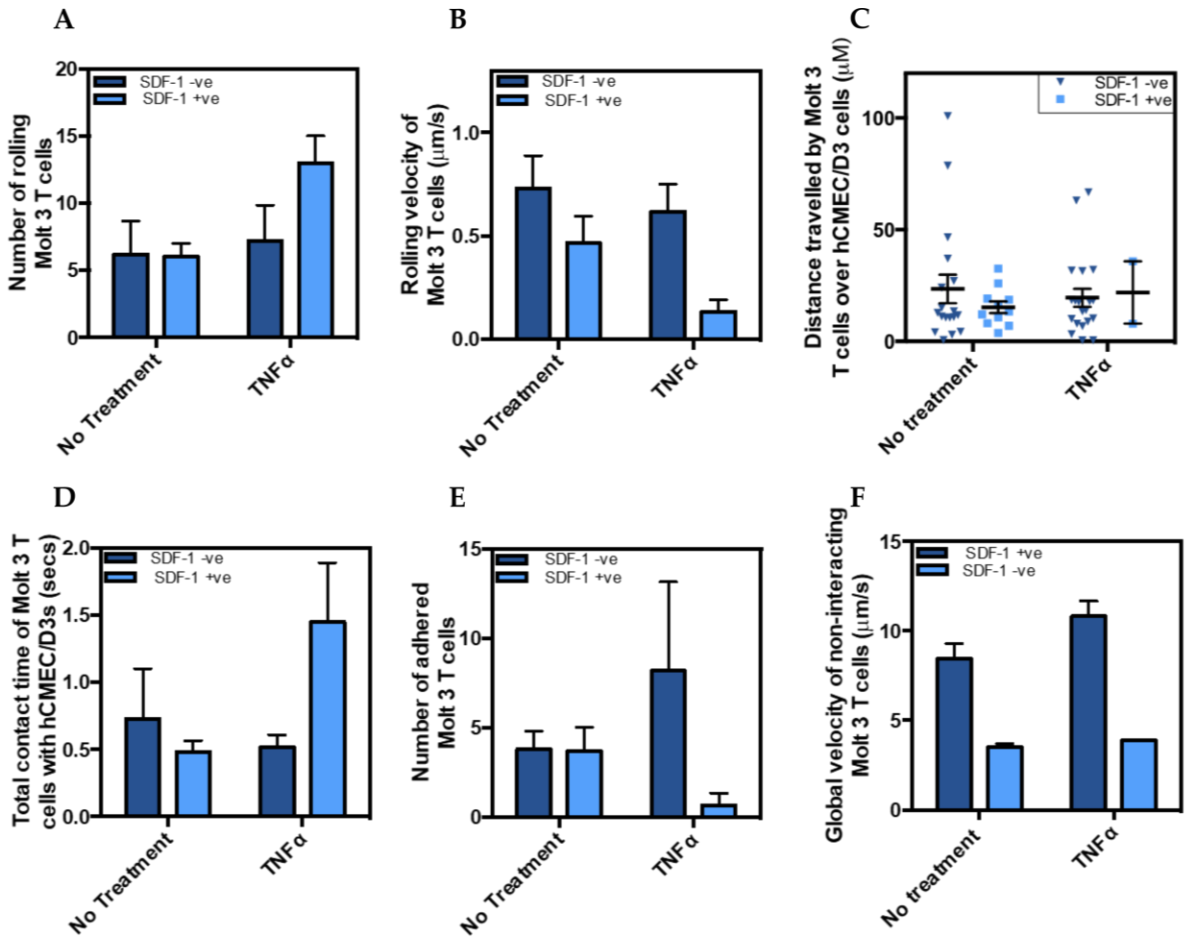

Figure 5.20 The effect of SDF-1 on TNFα activated hCMEC/D3s. hCMEC/D3s were treated with TNFα (2 ng/ml) or media only (no treatment) for 16h at 1 dyne/cm^2. 100ng/ml of SDF-1 was added to EC media and passed over hCMEC/D3s 15 mins prior to cell rolling assays. 7.5 x 10^5 CFSE labelled Molt 3 T cells were passed over ECs at 0.25 dynes/cm^2. Rolling velocity (μm/s) and distance travelled (μm) was calculated by the Bioflux 200 software after manual identification of rolling cells using cell tracking analysis mode. **A)** The effect of 100ng/ml SDF-1 on the number of rolling cells. **B)** The effect of SDF-1 on the velocity (μm/s) of rolling cells. **C)** The effect of SDF-1 on the distance travelled of individual Molt 3 T cells **D)** The duration of rolling interactions (i.e. the total contact time) between Molt 3 T cells and hCMEC/D3s was established by the number of frames in the time lapse sequence rolled for and an average taken (each frame = 0.126 secs). **E)** The impact of SDF-1 on number of firmly adhered Molt 3 T cells. **F)** The impact of the addition of SDF-1 on the global velocity of non-interacting Molt 3 T cells. Error bars indicate SEM, n = 3, analyses were conducted using a two-way ANOVA.

SDF-1 has no significant effect on any of the measured outcomes in with the no treatment or TNFα activated hCMEC/D3s. There were, however, some general trends. For instance, SDF-1 appears to reduce the number of firmly adhered Molt 3 T cells following TNFα activation of ECs (Fig 5.20 E). There was also a general trend for SDF-1 to reduce the global velocity of non-interacting Molt 3 T cells, regardless of prior treatment (Fig 5.20 F). For TNFα activated

hCMECs, SDF-1 mostly increased the number of rolling cells (Fig 5.20 A) and the total contact time between Molt 3 T cells and ECs (Fig 5.20 D) whilst decreasing the rolling velocity of Molt 3 T cells (Fig 5.20 B). To determine whether EphA1-Fc could have a different effect with the addition of SDF-1, these experiments were repeated with EphA1-Fc and IgG activated hCMEC/D3s.

5.5.3 The impact of SDF-1/CXCL12 on EphA1-mediated T cell-EC interactions

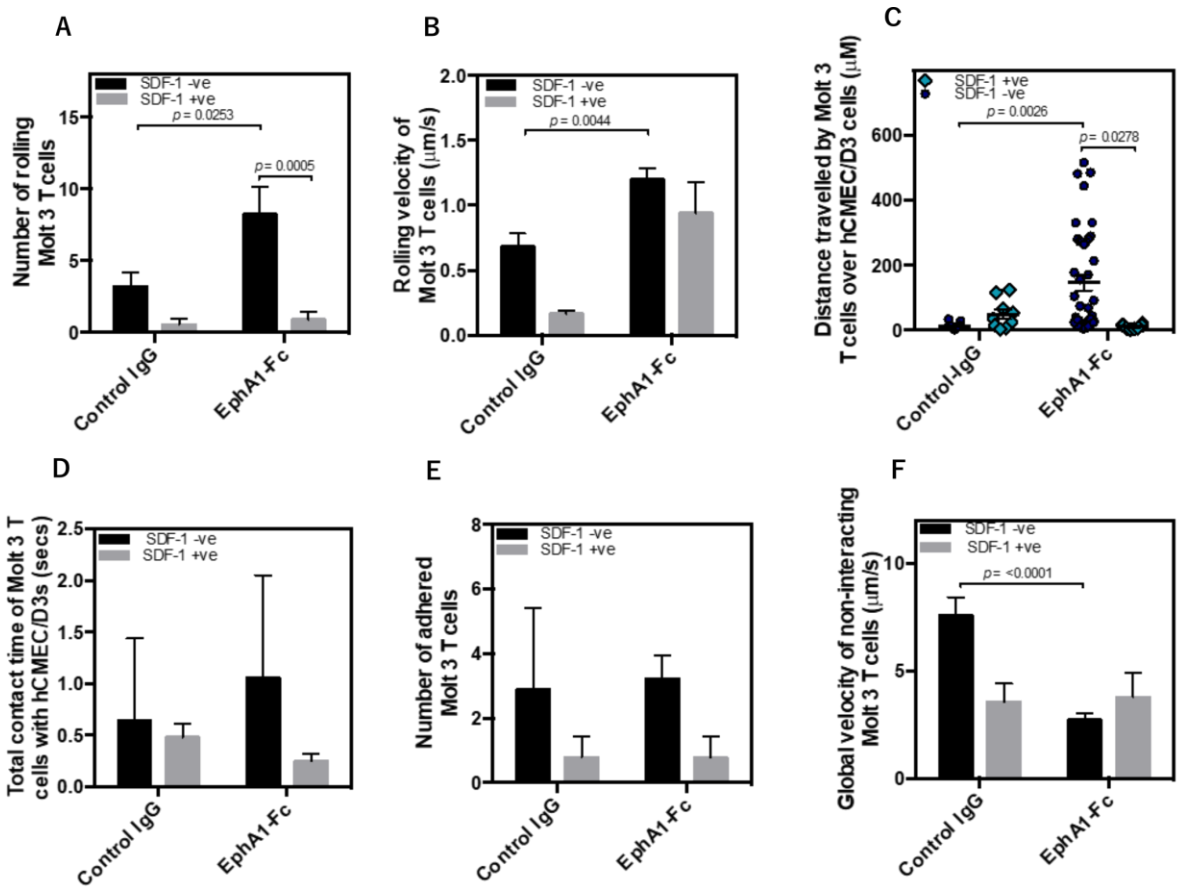

Figure 5.21 The effect of SDF-1 on Molt 3 T cells and hCMEC/D3 interactions. hCMEC/D3s were treated with EphA1-fc (5μg/ml) or control hIgG (5μg/ml) for 16h at 1 dyne/cm^2. 7.5 x 10^5 CFSE labelled Molt 3 T cells were passed over ECs at 0.25 dynes/cm^2. 100ng/ml of SDF-1 was added to EC media and passed over ECs 15 mins prior to cell rolling assays. Rolling velocity (μm/s) and distance travelled (μm) was calculated by the Bioflux 200 software after manual identification of rolling cells using cell tracking analysis mode. **A)** The effect of 100ng/ml SDF-1 on the number of rolling cells. Comparison of SDF-1(-ve) EphA1 and control IgG indicates EphA1-fc increases number of cells rolling (n = 6, p = 0.0253). SDF-1 abrogates EphA1-fc mediated increases in cell rolling (p=0.0005). **B)** The effect of SDF-1 on the velocity (μm/s) of rolling cells. Without SDF-1, rolling velocity is significantly increased in EphA1-fc treatment group compared to control IgG (n = 6, p = 0.0044) as previously described. SDF-1 does not alter the rolling velocity of Molt 3 T cells in the EphA1-fc treatment group. **C)** Distance travelled without SFD-1 is significantly increased with EphA1-fc (n = 6, p = 0.0026). Addition of SDF-1 to EphA1-fc treated hCMEC/D3s abrogates this effect, significantly reducing distance travelled (n = 3, p = 0.0278). **D)** The duration of rolling interactions (i.e. the total contact time) between Molt 3 T cells and hCMEC/D3s was established by the number of frames in the time lapse sequence rolled for and an average taken (each frame = 0.126 secs) (n = 3. Addition of SDF-1 has no effect on total contact time, and there are no significant differences between EphA1-fc treated and control IgG treated cells. **E)** Addition of SDF-1 has no effect on number

of firmly adhered Molt 3 T cells, and there are no significant differences between EphA1-fc treated and control IgG treated cells. **F)** Global velocity significantly reduced with the addition of EphA1-fc compared to control IgG in the SDF-1 -ve treatment group. (p=0.0001). Error bars indicate SEM, n = 3, analyses were conducted using a two-way ANOVA.

Interestingly, it appears that the addition of SDF-1 generally abrogated the effect of EphA1-Fc on Molt 3 T cell:EC interactions identified in previous experiments. These data also mostly corroborate the findings of EphA1-Fc mediated alterations in Molt 3 T cell:hCMEC/D3 interactions in the absence of SDF-1. Whilst previous experiments suggested a trend towards increased numbers of rolling cells, these experiments showed a significant increase following treatment with EphA1-Fc (Fig 5.21 A, $p = 0.0253$). The combination of EphA1 and SDF-1 significantly reduced cell rolling numbers compared to the EphA1-Fc treatment in the absence of SDF-1 ($p = 0.0005$), almost to the levels seen in the control IgG group (Fig 5.21 A). Similarly, the rolling velocity of Molt 3 T cells is significantly increased in the EphA1-Fc treatment group compared to control IgG, in the absence of SDF-1 ($p = 0.0044$) as seen in previous experiments. The addition of SDF-1 does not significantly alter the rolling velocity of Molt 3 T cells in the EphA1-Fc treatment groups; however, there is a general trend that EphA1-fc increases rolling velocity compared to control IgG in both the presence and absence of SDF-1.

Perhaps the most potent abrogating effect of SDF-1 can be seen in its effects on distance travelled by individual Molt 3 T cells. As seen in previous experiments, treatment with EphA1-Fc alone significantly increases the distance travelled of individual Molt 3 T cells, compared to control IgG (p=0.0026). The addition of SDF-1 to EphA1-Fc treated hCMEC/D3s completely abrogates this effect ($p = 0.0278$), reducing the distance travelled to levels seen in control IgG groups. SDF-1 seems to reduce the total contact time in both the EphA1 and control IgG Fig 5.21 D (although this is not significant).The number of firmly adhered Molt 3 T cells also appears to be reduced following SDF-1 treatment in both the control IgG and EphA1-fc treatment, although this was, again, non-significant (Fig 5.21 E). Global velocity of non-interacting Molt 3 T cells is significantly reduced with the addition of EphA1-Fc compared to control IgG in the absence of SDF-1 (p=0.0001), as seen in previous experiments. Interestingly however, there are no differences in the global velocity between EphA1 and control IgG with the addition of SDF-1 and it appears that SDF-1 is also capable

of reducing global velocity, regardless of prior treatment (Fig 5.21 F) as was seen for untreated or TNFα activated hCMEC/D3s in the presence of SDF-1 (Fig 5.21 F).

5.6 Discussion

This chapter assessed EphA1-Fc priming of both HUVECs and the hCMEC/D3 BBB model. Our findings suggest that there is a fundamental difference in the way HUVECs and hCMEC/D3s respond to treatment and that the mechanisms by which EphA1-Fc alters leucocyte-endothelium interactions differs from those of TNFα.

5.6.1 TNFα and EphA1-Fc mediated Molt 3 T cell interactions with hCMEC/D3 cells

Data suggest that TNFα has no effect on rolling velocity, (p = 0.4207) number of rolling cells, (p = 0.7202), on distance travelled by individual Molt 3 T cells (p = 0.5138) or on the total contact time between Molt 3 T cells and hCMEC/D3s (p = 0.1206); see Figure 5.12. Whilst murine CAMs, such a P-selectin, are readily expressed in response to this cytokine (Sanders et al., 1992; Weller et al., 1992) there appears to be some debate as to whether human ECs are transcriptionally regulated by TNFα (Luscinskas et al., 1996; Pan et al., 1998). Our data suggests that TNFα does not or is ineffectively upregulating E- and P-selectin in the studied human ECs. This conclusion is reached based on analyses indicating that whilst TNFα does not significantly increase the number of rolling cells, there is a general trend towards increase rolling. Moreover, upon analysis of the transient interactions of rolling Molt 3 T cells, data suggest that upon TNFα activation of ECs, those cells which do roll, do so in a stable manner. TNFα is a powerful inducer of both VCAM-1 and ICAM-1 which deal with stable adhesion and transmigration; these data supports this notion as there was approximately a 5-fold increase in the number of adhered Molt 3 T cells in TNFα activated hCMEC/D3 cells compared to untreated ECs despite this effect being non-significant. There is also an approximate 3-fold increase in the number of adhered Molt 3 T cells in comparison to rolling cells in the TNFα treated cells, again suggesting TNFα is upregulating molecules responsible for stable adhesion.

The reason why TNFα was incapable of inducing a statistically significant effect on Molt 3 T cell adherence to hCMEC/D3s is unclear. It is possible that the concentration of TNFα (2

ng/ml) used in these series of experiments is not sufficient to upregulate VCAM-1 and ICAM-1. Whilst some experiments have shown that 2 ng/ml of TNFα increases ICAM-1 expression (Nie et al., 2012), other studies have shown that an excess of 40 ng/ml is necessary to upregulate both ICAM-1 and VCAM-1 (Zhu et al., 2013). This could mean 2 ng/ml of TNFα preferentially upregulates ICAM-1 which is binding the Molt 3 T cell expressed LFA-1 integrin to support adhesion, but that upregulation of both ICAM-1 and VCAM-1 is required for a significant effect on Molt 3 T cell adhesion. Future work is required to determine the optimal concentration of TNFα to induce a robust upregulation of both ICAM-1 and VCAM-1.

There may be an additional mechanism supporting the general trend towards increased Molt 3 T cell adherence, however. Initial rolling events during the inflammatory cascade involves the assistance of chemoattractants at the surface of the EC which is capable of inducing various secondary adhesion receptors (e.g. β1 and β2 leucocyte expressed integrins, Chandrasekharan et al., 2007). These integrins will interact with counter receptors expressed by endothelial cells to induce firm adhesion of leucocytes (Davis et al., 2003). Thus, it is possible that hCMEC/D3 cells express a chemokine which is increased at the EC surface by TNFα, triggering adhesion events. Under basal conditions, the hCMEC/D3 cell line secretes the CCL2 and CXCL8 chemokines and CCL5, CXCL10, CX3CL1 and fractalkine are released following stimulation by proinflammatory cytokines (Hurst et al., 2009; Subileau et al., 2009). Importantly, Subileau and colleagues (2009) demonstrated that CXCL10 is secreted following the addition of TNFα. As we have shown that the Molt 3 T cell line express the CXCR3 chemokine receptor for CXCL10 in low levels (Fig 5.21 E) it is possible that TNFα is causing the secretion of this chemokine and it is the CXCR3/CXCL10 axis which is supporting the adherence of Molt 3 T cells. It is possible that a significant effect was not induced due to the low expression levels of CXCR3 expressed on Molt 3 T cells. Indeed, it was recently demonstrated that CXCL10 secreted by ECs, induce firm adhesion of T cells and the preservation of their attachment to the brain vasculature, *in vivo* (Sorensen et al., 2018) which may go some way in explaining these data.

Data demonstrated that EphA1-Fc increased the distance travelled of Molt 3 T cells over hCMECs/D3s (p = <0.0025) compared to the IgG control. To ensure that the control IgG was an appropriate control for EphA1-Fc mediated Molt 3 T cell:EC interactions, it was necessary to ensure that the control IgG was inactive. This was assessed by comparing the measured outcomes of unstimulated (no treatment) and control IgG treated hCMEC/D3s. This indicated that there were no significant differences between unstimulated and control IgG treated hCMEC/D3s (data not shown) confirming that the control IgG is inactive, an appropriate control and that the effect of EphA1-Fc on leucocyte rolling is robust. Whilst the overall number of rolling Molt 3 T cells is not significantly increased by EphA1-Fc (p = 0.125), there is a general trend towards an increase in rolling numbers in EphA1-Fc treated hCMEC/D3s. This finding, taken together with the significant increase in the distance travelled by Molt 3 T cells (p = <0.0025) and the total contact time between Molt 3 T cells and hCMEC/D3s (p = 0.0085) indicates that there is a mechanism controlling the avidity of leucocytes to roll. Moreover, as we established that this increase in the average distance rolled by a Molt 3 T cells is not characterised by a series of transient interactions (Fig 5.18 C & D), this gives further support to the supposition that EphA1-Fc upregulates a rolling ligand on hCMEC/D3s potentially stimulating signalling in the Molt 3 T cells in turn activating leucocyte specific integrins. GlyCAM-1, a high endothelial venule (HEV) specific proteoglycan, for instance, is capable of engaging the β2 integrin, LFA-1 on $CD45RA^+$ lymphocytes enhancing avidity of LFA-1 (Hwang et al., 1996). Indeed, LFA-1 has been shown to be important in the rolling of leucocytes along the endothelium, for instance when E-selectin and ICAM-1 is immobilized (Chestnutt et al., 2006). Ultimately, the conformation of LFA-1 can alter it from a tethering to a rolling ligand dependant on activation state (Salas et al., 2004). It may well be that EphA1 acts via a similar mechanism Should EphA1 upregulate a rolling ligand on the hCMEC/D3 cells line, it is possible this rolling ligand is capable of effecting the avidity (i.e. conformational state) of its counter integrin altering it into a rolling interaction (see Fig 5.22 for a proposed EphA1-Fc mediated increase in Molt 3 T cell rolling). This could be tested by using blocking antibodies to various integrins on the Molt 3 T cells to see whether this abrogates the EphA1-Fc-mediated increases on rolling distances. The mRNA of rolling ligands on ECs can also be tested following EphA1-Fc activated hCMEC/D3s.

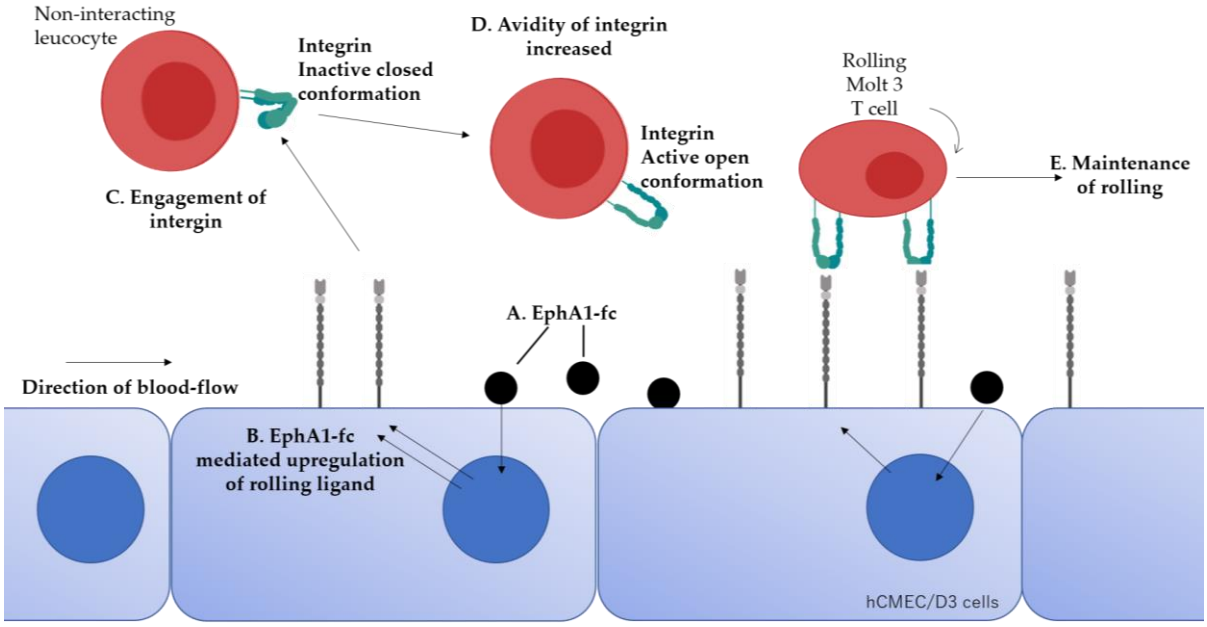

Figure 5.22 Proposed EphA1-Fc mediated mechanism of increased rolling distances. **A & B)** The addition of EphA1-Fc upregulates a rolling ligand on hCMEC/D3s. **C)** This rolling ligand will engage a leucocyte expressed integrin **D)** The avidity of the integrin is increased **E)** The conformational state of the integrin maintains the rolling of Molt 3 T cells over hCMEC/D3 cells.

EphA1-Fc also increased the velocity of rolling of Molt 3 T cells ($p = 0.0006$, Fig 5.12 B) whilst decreasing the velocity of non-interacting Molt-3 T cells using the method employed to distinguish cells in these stages of the adhesion cascade. Firstly, it may suggest that EphA1-Fc causes a reduction in the number of rolling cells entering the integrin-mediated "slow rolling" stage and there is a maintenance of leucocytes in the selectin-mediated capture and fast rolling phase (see Figure 1.3). This could suggest that the method used to distinguish cells in the slow rolling (behaviour 1) and fast rolling/non-interacting (behaviour 2) is an ineffective method. Whilst it is clear that there are limitations in the approach, upon visual inspection of the rolling videos, the effect EphA1-Fc on the velocity of *all* Molt 3 T cells is clear and likely reflects some real phenomena. The increase in the slow rolling velocity however, could reflect mis-characterisation of cells into the slow rolling category, when they are in fact fast rolling (this is plausible as cells were travelling at similar velocities despite exhibiting distinct behaviours). The possibility of EphA1-Fc is maintaining cells in the fast-rolling phase is plausible if EphA1 preferentially upregulating a selectin on the hCMEC/D3

cell line responsible for the initial rolling event of the adhesion cascade. Future work would require the use of selectin blocking antibodies to assess whether this is a possibility.

Alternatively, there is a small possibility that the increase in velocity of rolling Molt 3 T cells could be a direct consequence of the EphA1-Fc mediated reduction in the global velocity of non-interacting Molt 3 T cells (described in the results section 5.4 and later in this chapter, section 5.9.3). It is known that cell rolling is a phenomenon supported by quick association and disassociation of bonds at the center and rear of a rolling cell. The catch bond hypothesis supposes that at increasing levels of shear flow, the rolling cell will flatten, causing an increase in the footprint of the cell, reducing the hydrodynamic drag. The strength of the bond is increased with increased tensile force, and thus at increasing levels of shear flow, catch bonds between, for instance P-selectin-PSGL-1, is strengthened, causing a *reduction* in the rolling velocity (Sundd et al., 2013). A consequence of EphA1-mediated reduction in the global velocity may be a reduction in the shear flow applied to the rolling Molt 3 T cells and thus, the catch bond hypothesis could explain the increase in the velocity of rolling cells. This possibility could be assessed by measuring the relative strength of these adhesive interactions which is described as the mean velocity of rolling cells compared to the velocity of flowing Molt 3 T cells. However, this possibility is unlikely considering the relatively low levels of shear stress applied to the leucocytes.

5.6.3 TNFα and EphA1-Fc mediated Molt 3 T cell interactions with HUVECs

Similarly to the hCMEC/D3 cell line, TNFα tended to increase both the number of rolling (p = 0.0565) and firmly adhered (p = 0.5764) Molt 3 T cells but had no effect in any other measured outcome. As described in section 5.6.1, this may be because the concentration of TNFα used here is not sufficient to cause upregulation of both VCAM-1 and ICAM-1. Upregulation of VCAM-1 and ICAM-1 on HUVECs have been shown at TNFα concentrations in excess of 10 ng/ml (Sawa et al., 2007) and thus future work would require increased concentrations of this cytokine.

The mechanisms of TNFα and EphA1-Fc activation of HUVECs appear distinct, similarly to the hCMEC/D3 cell line; whilst EphA1-Fc causes a general increase in the number of rolling

cells (p = 0.1761), it appears that EphA1-Fc causes a reduction on the number of firmly adhered Molt 3 T cells (p = 0.5043) although non-significant. This again suggests that EphA1-Fc supports the avidity of Molt 3 T cells to roll, but not to eventually adhere. This is further supported by the increase in the distance travelled by rolling Molt 3 T cells (p = 0.0123) which again, is not characterised by a series of transient interactions. These data, however, suggest that mechanisms of activation differ between HUVECs and hCMEC/D3s. For instance, the rolling velocity of Molt 3 T cells remains unaltered following EphA1-Fc treatment (p = 0.1837) with the rolling velocity in line with those seen in all other experimental conditions. Moreover, EphA1-Fc does not significantly alter the total contact time between Molt 3 T cells and HUVECs (p = 0.0674) suggesting that Molt 3 T cells have more transient interactions with HUVECs than with hCMEC/D3s. However, this was shown to not been the case. Ultimately, future work is needed to clarify the precise rolling velocity through these chambers using fluorescently labelled latex beads to unpick the non-interacting velocity of particles through these chambers (to clearly discern what the rolling velocity of Molt 3 T cells would be) such that this data can be understood more precisely.

5.6.4 EphA1-Fc impact on the global velocity of fast rolling/non-interacting Molt 3 T cells

As alluded to, the global velocity of non-interacting cells Molt 3 T cells is significantly reduced following EphA1-Fc stimulation of both HUVECs (p = <0.0001, Fig 5.14 A) and hCMEC/D3s (p = <0.0001, Fig 5.14 B). These Molt 3 T cells were defined as those which are not actively interacting with the endothelial layer and thus would be considered circulating leucocytes, *in vivo* or fast rolling. A recent study investigating mechanisms behind reduced cerebral blood flow (CBF) in LOAD patients using APP/PS1 and 5xFAD mice showed that cortical capillaries exhibited stalled blood flow primarily due to neutrophils which had adhered to capillary segments (Cruz Hernández et al., 2019). Our data indicates that the number of adhered Molt 3 T cells increased with EphA1-Fc stimulation of hCMEC/D3 cells compared to IgG (p = 0.0161) and whilst the number of rolling cells was not significantly increased; there was a trend towards increased rolling (p = 0.1258). Thus, it is plausible that EphA1-Fc mediated increases in adhered and rolling cells is sufficient to cause resistance to the shear force applied to the non-interacting Molt 3 T cells, essentially mimicking the

reduction in CBF identified in APP/PS1 and 5xFAD mice. *In vivo*, it is known that inflammatory responses triggered by soluble factors results in activated endothelium, leucocyte recruitment, thrombus formation, pertinently causing locally reduced blood flow (Cines et al., 1998; Johnson-Leger and Imhof, 2003), presumably decreasing the speed at which non-interacting leucocytes travel. However, in this *in vitro* assay, our soluble factor, TNFα, did not cause a reduction in the global velocity of non-interacting leucocytes. However, as stated, microfluidic assays are performed using brightfield or confocal microscopy, meaning that non-interacting leucocytes is not observable and thus not measured. It may well be that soluble factors are capable of decreasing global velocity, *in vitro*, and that this phenomenon has not be measured.

Another potential explanation is that in fact, *all* Molt 3 T cells in the EphA1-Fc treated conditions are rolling (i.e. fast rolling). If this was the case, it would mean that the velocity of rolling interactions is diverse, possibly due to different mechanistic processes. Should this be true, it would be incorrect to decipher between an interacting and non-interacting cell in this instance. Interestingly, work conducted to determine what the centreline velocity of non-interacting Molt 3 T cells would be through the chambers determined that, at 0.25 dynes/cm^2, the global velocity would be approximately 4μM/s. However, our data throughout the studies suggested that the velocity of the flowing Molt 3 T cells over both HUVECs and hCMEC/D3 cell, in the untreated, control IgG and TNFa groups was approximately 10μM/s (data not shown). This work will need to be investigated further using a whole Bioflux plate uncoated +/- EphA1-Fc and control, along with the use of fluorescently labelled beads to check every well for equivalent global velocities.

5.6.5 The impact of SDF-1 on the leucocyte recruitment.

As previously described, SDF-1 is a CXC chemokine which is abundantly expressed by endothelial cells and interacts with its leucocyte expressed CXCR4 receptor. Importantly, SDF-1 promotes integrin-mediated adhesion of leucocytes to the endothelium and aids in their subsequent extravasation (Peled et al., 1999, 2000). In stark contrast, it appears SDF-1 treatment of hCMEC/D3 cells does not alter the number of adhered Molt 3 T cells in either the control IgG or EphA1-Fc treatment groups - in fact, the general trend was a reduction the

number of adhered leucocytes. This is an unexpected finding as SDF-1 has been consistently shown to promote the adhesion of leucocytes. A possible explanation for a reduction in cell adherence in the EphA1-Fc treated groups in the presence of SDF-1 may lie in the effect soluble EphA1-Fc + SDF-1 has on the signaling downstream of ephrinA1 expressed on the hCMEC/D3 cell line. It is well established that the Eph-ephrin system is characterized by bi-directional signaling which in which the biological outcome (i.e. cellular adhesion or repulsion) is based on an intricate balance of various factors (e.g. temporal and spatial distribution of the receptors and their ligands). Moreover, should EphA1-Fc cause upregulation of a rolling ligand on hCMEC/D3s cells, subsequently altering the conformation of integrins (such as LFA-1 and VLA-4) expressed on the Molt 3 T cells, as hypothesized earlier (Fig 5.22), SDF-1 could subsequently compete with these integrins through CXCR4, altering EphA1-mediated Molt 3 T cell:EC interactions.

The addition of SDF-1 in the EphA1-Fc treated hCMEC/D3s also abrogated the increase in the number rolling Molt 3 T cells ($p = 0.0005$). Similarly, whilst non-significant, the addition of SDF-1 seems to reduce the total contact time between Molt 3 T cells and hCMEC/D3s in both the control IgG and EphA1-Fc treatment groups and abolished the EphA1-Fc mediated significant increase in the distance travelled by rolling Molt 3 T cells ($p = 0.0278$) whilst maintaining results seen in previous experiments, where EphA1-fc dramatically increases the distance travelled by Molt 3 T cells in the absence of the chemokine ($p = 0.0026$). The addition of SDF-1 in the control IgG group brings the global velocity of non-interacting Molt 3 T cells in the IgG condition in line with that seen in EphA1-fc (SDF-1+ve and –ve conditions), however, the only significant difference in the global velocity was in the control IgG v EphA1-Fc SDF-1-ve condition ($p=<0.0001$) as seen in previous experiment. The rolling velocity of SDF-1+/- treated control IgG cells, whilst non-significant, is slightly reduced by SDF-1, which supports much of the literature on SDF-1. However, the velocity of rolling Molt 3 T cells in both the SDF-1+ve and SDF-1-ve EphA1-Fc conditions is increased compared to respective control IgG experiments (as seen in our previous studies) but only significantly when EphA1-Fc was not in the presence of SDF-1 ($p = 0.0044$); again suggesting SDF-1 has a negating effect on EphA1-mediated leucocyte/endothelium interactions. It is important to highlight the fact that there is only exogenous EphA1 in this system, ephrinA1 expressed by hCMEC/D3s should respond to exogenous EphA1, and CXCR4 expressed by

the Molt 3 T cells should react to exogenous addition of SDF-1. However, from the literature, it is unclear whether hCMEC/D3s express CXCR4 and thus, these ECs could respond to SDF-1, ultimately altering EphA1-mediated alterations in Molt 3 T cell-EC interactions. *In vivo*, it has been shown that EphrinA1-Fc stimulated EphA1 is capable of activating SDF-1/CXCR4 signaling in hepatocellular carcinoma (HCC) cells, promoting the homing of endothelial progenitor cells (EPCs), one might expect to see a synergistic effect with the addition of EphA1-fc and SDF-1. However, neither our Molt 3 T cells nor hCMEC/D3s express EphA1, so the addition of EphA1-Fc will most likely initiate reverse signaling into the EphrinA1 bearing hCMECs. Studies have shown that reverse signaling into EphrinB bearing cerebellar granule cells inhibited SDF-1 induced chemotaxis demonstrating the potential for an antagonistic association between Eph/Ephrin and SDF-1/CXCR4 signaling (Lu et al., 2001). However, this inhibition was, in part, controlled by PDZ-RGS3, a protein which binds to the cytoplasmic tail of EphrinBs, subsequently inactivating G-protein signaling. As EphrinAs lack a cytoplasmic domain, how this inhibition would occur is unclear. It is indeed possible that EphA1-Fc is initiating signaling in a range of Ephrins in the hCMEC/D3 cells (such as EphrinBs). It is well known that Ephs are promiscuous - EphA4, for example, is capable of interacting ephrinB2 and ephrinB3 and the ligands of EphA1 may be incompletely described. Other studies have demonstrated antagonistic relationships between the Eph/SDF-1/CXCR4 axis. Sharfe et al., (2002) showed that activation of EphA receptors inhibited SDF-1 chemotaxis by affecting the activity of GTPases in T cells.

Furthermore, it is known that interactions of SDF-1 and CXCR4 mediates cell secretion events by activating the NF-κB pathway. Thus, stimulation of cells with SDF-1 allows the secretion of MMPs (such as MMP-2 and -9); consequently, it may be the case that SDF-1 has promoted the MMP-mediated cleavage of the rolling ligand which has supported EphA1-Fc mediated increases in Molt 3 T cell rolling. If hCMEC/D3s express CXCR4, it is plausible that SDF-1 could also cleave a receptor from the ECs that are vital for EphA1-Fc mediated alterations in Molt 3 T cell:EC interactions. Based on the literature, it appears that Eph/SDF-1 interactions can be agonistic or antagonistic and future work is required to disseminate the precise mechanisms responsible for negating EphA1-mediated effects.

5.6.6 Future work

Future work is required to understand the precise molecules and pathways responsible for the effects described in this chapter. As a means to assess this, blocking antibodies can be used to molecules responsible for capture, rolling and adhesion (e.g. LFA-1/VLA-4). Should these blocking antibodies abolish the EphA1-Fc induced effect, it would suggest pathway involvement and would focus attention for subsequent experimentation. Deciphering these mechanisms would also provide a potential therapeutic target for future treatments in EphA1-induced AD pathogenesis. This would also allow identification of potential pathways involved in the described data. Non-bias RNA analysis of non-activated and EphA1-activated hCMEC/D3 cells would also allow identification of the pathways responsible for the effects seen.

Determining how the $P^{460}L$ mutation would impact the rolling and adherence of Molt 3 T cells is also required; due to time constraints, THIS was not possible. However, the soluble version of $P^{460}L$ mutant has been purified and is ready for subsequent analysis. Should this mutation further alter leucocyte endothelium interactions, future work could be conducted on patient-derived leucocytes; in patients expressing previously described non-coding *EphA1* AD SNPs. Now that the microfluidic assay has been tested using commercially obtained EphA1-Fc and reagents and parameters have been established, using invaluable patient material is hopefully justified. Analyses of post-mortem brains of AD patients with *EphA1* AD SNPs could also allow elucidation of whether these SNPs result in an increased number of peripheral immune cells within the brain parenchyma after controlling for various other factors (e.g. *ApoE* status).

5.6.7 Limitations

At this stage, we can only hypothesise that an increase in the amount of circulating soluble $P^{460}L$ EphA1- ECD resulting from expedited proteolysis of the receptor would lead to an increase in leucocyte/BBB interactions as we have not tested the mutant protein in this system. Moreover, it is possible that the mutation may prevent priming of endothelial cells.

It is clear that the structural composition of the ECD of Eph molecules are a vital determinant in the functional and biological outcome; using ECD-switched chimeric EphA2 and EphA4 (Seiradake et al., 2013) indicates that the ECD may be a more important player in cellular outcome than kinase activity. As a result, any mutations in this region may alter signalling capabilities of the proteolyzed EphA1-ECD molecule. However, the soluble mutant protein is ready for future testing of this hypothesis and would provide a greater understanding potential pathomechanisms of the $P^{460}L$ mutation.

Further limitations include some aspects of the Bioflux 200 system. For instance, in practice, a firmly adhered leucocyte should be defined as those which remain stationary for at least 30 seconds as cells which remain stationary for this period of time then go on to extravasate (Zuidema and Korthuis, 2015). Unfortunately, the setup of the Bioflux system allows the sequential analysis of 60 frames, corresponding to a 7.55 second AVI file. This does not allow one to determine for certain that a cell will not become detached after this period and re-circulate, or even that that particular cell will go on to saltate before becoming firmly adhered. As a result, cell adherence data from this chapter should be viewed with caution. Future work may need to utilise a system whereby extended viewing of the leucocytes is possible. Moreover, the vast majority of shear flow assays use phase contrast video microscopy and very rarely use fluorescent microscopy with CFSE labelled cells. Phase contrast microscopy has one major advantage over fluorescent microscopy, only the rolling and adhered immune cells are visible. This means that non-interacting cells do not interfere with the analysis. The ability to view the non-interacting cells in this instance did uncover EphA1-mediated reduction in the global velocity of non-interacting cells, but this added a layer of complexity as cells were reduced in their velocity to such an extent that it made it difficult to distinguish rolling and non-interacting cells. As a means to overcome this difficulty, the use of fluorescently labelled beads within the system would indicate the true centreline velocity of non-interacting particles, with any cells subsequently travelling below this velocity to be deemed interacting. Moreover, one needs to be cautious when interpreting EphA1-Fc data in the future, it will be necessary to ensure that this fusion protein is working as an agonist by employing a functional readout of EphA1-Fc mediated activity.

Another potential limitation of the described data could be heterogeneity of Molt 3 T size, as this could skew the results when assessing the distance travelled of the immune cells. However preliminary data from the Ager lab suggests that Molt 3 T cells tend to consistent in their diameter (Moon, Ager lab, unpublished) however this needs to be confirmed in future experiments.

Chapter Six

General Discussion

6.1 General discussion and future experiments

6.2 Summary of the results

This thesis successfully cloned the WT EphA1 and AD-associated $P^{460}L$ EphA1 into the HEK-293 Flp-In system. Moreover, soluble $P^{460}L$ was successfully purified to take forward for future experimentation. The data showed that full-length WT EphA1 expression is reduced and undergoes C-terminus internalisation following ephrinA1-Fc engagement. GM6001 did not prevent the loss of EphA1 N-terminus in the presence of ligand but it does appear to block constitutive proteolysis of the molecule, suggesting alternative proteases regulate EphA1 following ligand engagement. γ secretase inhibition does not rescue membrane expression of WT EphA1 C-terminus however, it does result in a drop in fluorescence of C-terminal staining. This appears contradictory and the precise mechanism is unclear. The staining pattern of C-terminal fragments appear punctate and may suggest the C-terminus is confined to endosomes. N-terminal membrane staining of the $P^{460}L$ EphA1 molecule is low in the absence of ligand which is decreased further in the presence of ephrinA1-Fc. This suggests that the molecule either undergoes aberrant proteolysis of the N-terminus or that it is internalised and undergoes rapid degradation. Alternatively, this might represent a trafficking issue, with the P460L mutation abolishing the ability of the molecule to travel to the membrane. Interestingly, GM6001 seemed to prevent N-terminal degradation within the cytosol of $P^{460}L$ EphA1 treated with ephrinA1-Fc which may suggest the N-terminus is internalised and that GM6001 prevents its degradation. However, future work is needed to clarify this point. The $P^{460}L$ mutation resides with the second FNIII repeat with one other study identifying the FNIII domain as an important region in the proteolysis of EphA2. (Sugiyama et al., 2013). They showed that EphA2 is cleaved within the first FNIII domain by MT1-MMP and preliminary data has indicated that the X2 variant (which is missing the first FNIII repeat) appears to be resistant to ligand induced proteolysis. This data, along with the finding that N-terminal staining of $P^{460}L$ molecule can be partially rescued by MMP inhibition suggest that the mutation offers a new binding epitope for an MMP, which might correspond to MT1-MPP.

The potential for expedited proteolysis of the ECD of $P^{460}L$ to offer a pathomechanism in AD was determined using a microfluidic assay. It was shown that incubation of HUVECs and

hCMEC/D3 cell with soluble EphA1, corresponding to the ECD, increased Molt 3 T cell and EC interactions in a number of ways. EphA1-Fc increased the distance travelled of rolling Molt 3 T cells ($p = 0.0123$) and the total contact time with HUVECs ($p = 0.0138$). The BBB model cell line hCMEC/D3, appeared more sensitive to EphA1-Fc activation, increasing the number of firmly adhered cells ($p = 0.0006$), the distance travelled by rolling cells ($p = < 0.0025$) and the total contact time of between Molt 3 T cells and hCMEC/D3s ($p = <0.0001$). SDF-1/CXCL12 appeared to abrogate these EphA1-mediated alterations in Molt 3 T cell-hCMEC/D3 interactions potentially through SDF-1-mediated CXCR4 internalisation reversing the EphA1-Fc mediated effects (Signoret et al., 1998).

6.3 Conclusions

Since the discovery that *EphA1* was a susceptibility locus for AD, there have been very few studies attempting to decipher the mechanism by which the gene confers its risk. This may partly be because very little is known about the EphA1 protein and its precise biological role, especially in the developed human body. The identified SNPs which confer the greatest AD risk includes the rs11771145, rs11767557 and rs10808026, which are intronic and located in the EphA1 Antisense RNA 1 gene. The A allele of rs11771145 has been shown to prevent hippocampal atrophy in MCI patients whilst preventing atrophy and increasing the cerebral metabolic rate for glucose in both the right lateral occipitotemporal gyrus and inferior temporal gyrus in AD patients (Wang et al., 2015a). The rs11767557 variant is in high LD with rs11771145 with the minor C allele believed to be associated with lower levels of Aβ deposition (Hughes et al., 2014). $P^{460}L$, conversely, has not been investigated to date. As a means to appreciate any $P^{460}L$ mediated alterations in the encoded protein, the WT molecule was first assessed through immunoblotting and immunolocalization following ephrinA1-Fc engagement. This thesis provides the first laboratory-based observation that an identified LOAD EphA1 SNP may confer risk, rather than non-risk or protective factor.

As described, neuroinflammation is a well-documented deleterious insult within the CNS of AD patients. Much of the early work supposed that neuroinflammation was a direct consequence of Aβ (Hardy and Higgins, 1992) and tau (Maccioni et al., 2010) related pathology . However, AD is now considered a multifactorial disorder in which a range of factors appear to trigger neurodegeneration Recent work, however, has suggested that neuroinflammation is, in itself, capable of causing disease-associated symptoms (Kinney et al., 2018).. This work was driven on the supposition that AD is a systemic disease, with neuroinflammation a primary factor in disease trajectory. Based on the data presented in chapter 4, where -$P^{460}L$ EphA1 undergoes aberrant proteolysis in both the absence and presence of ligand; one can suppose that there would be an increase in the circulating levels of soluble EphA1. The results presented in this chapter indicate that soluble EphA1 is capable of causing the recruitment of immune cells to the hCMEC/D3 cell line. Data shows that the treatment of hCMEC/D3 cells with EphA1-Fc increases the distance travelled of Molt 3 T cells ($p = <0.0025$) and also increases the number of adhered Molt 3 T cells

(p=0.0161). As firm adherence is a prerequisite for leucocyte transmigration, one might conclude that increased adherence could cause an increase in the eventual migration of these cells into the brain parenchyma (and subsequently causing the associated neurotoxicity).

Many studies have provided evidence of BBB breakdown in AD patients (Montagne et al., 2015; Sweeney et al., 2018), with this thesis attempting to clarify potential mechanisms of this jeopardized barrier within the framework of an identified genetic risk. Whilst this thesis did not directly assess the effect of EphA1 on the integrity of the BBB, it did provide evidence that EphA1-ECD is proteolyzed, which may be increased as a result of the $P^{460}L$ mutation, with the ECD fragment subsequently capable of priming endothelial cells and altering the recruitment of leucocytes. This finding allows one to hypothesise that EphA1, which is expressed on subpopulations of PBMCs, could be released as a soluble circulating protein in AD patients and thus increase the recruitment of leucocytes to the BBB. This finding implicates peripheral immunity in the context of Alzheimer's disease which challenges the ACH and the traditional view of AD as a brain-specific disease. This work conforms to recent observations indicating that genetic factors are capable of regulating a broad range of cellular and molecular pathways, including those involved with immunity (Efthymiou and Goate, 2017; Lambert et al., 2013; Sims et al., 2017) which has given rise to The Neuroinflammation Hypothesis (Cao and Zheng, 2018). Both experimental and clinical observations provide evidence that systemic immune signals, those derived from beyond the brain, partake in the pathogenesis of AD (Cao and Zheng, 2018), with peripheral immune cell infiltrates found in both AD mouse models (Zenaro et al., 2015), and in the post-mortem brains of patients (Togo et al., 2002). Moreover, studies have shown that infiltrating T cells in APP/PS1 mice produced IFN-γ and interleukin-17 (IL-17) where IFN-γ from Th1 cells, specifically, accelerated disease-related markers and impaired cognitive function in these mice (Browne et al., 2013) positing chronic, unbridled neuroinflammation as a driving force in AD. Others, however have shown infiltrating T cells to adopt an inactivated phenotype with a reduction in IFN-γ production with the authors concluding that this demonstrates an incapability to orchestrate a protective immune response to Aβ deposition (Ferretti et al., 2016). This highlights an ongoing topic of debate within the scientific community: whether the infiltration of immune cells into the brain parenchyma is beneficial or detrimental in the pathogenesis of AD. Nevertheless, many of these studies

attempt primarily attempt to align their findings to the amyloid and tau depositions. There has also been substantial evidence indicating that unbridled activation of microglia, the brain-resident macrophages, can also lead to AD-related pathogenesis. As EphA1 is expressed on peripheral immune cells, it may be possible that it is expressed by microglia. This is an important next step and could indicate that EphA1 P460L exerts its risk from within the brain as well as outside.

Both Eph receptors and their ligands have been implicated in many diseases, primarily and cancer and metastasis along with other immune-related disorders, such as atherosclerosis. As discussed in section 5.1.1, this complex has also been implicated in many aspects of vascular biology, from the induction of immune responses, regulating immune cell trafficking as well as modulating vascular permeability (Larson et al., 2008). This thesis further supports the notion that Eph/ephrin complex dysregulation may cause disease, with their risk effect asserted through alterations in immune processes. Moreover, it highlights their role in mediating immune cell trafficking, as detailed in chapter 5.

Previous studies have indicated that ligand engagement of Eph receptors results in their degradation and internalisation over time. Data presented in this thesis suggests EphA1 responds in a similar manner to its Eph family members, whereby EphA1 full-length expression is reduced following ligand engagement along with C-terminal internalisation. Generally speaking, Eph/ephrin complexes are internalised into either the Eph- or ephrin bearing cells through trans-endocytosis. However, data presented here indicates that WT EphA1 may be regulated by proteolysis following ligand engagement, as a soluble fragment corresponding to the predicted MW of the ECD was identified in the media in one experiment, and dual staining concluded that the internalised product corresponded to the C-terminus of EphA1, with N-terminal staining lost at the membrane and not identified within the cells. However, this result must be viewed with caution as we were unable to reproducibly confirm EphA1 N-terminal fragments in the media. This novel finding that EphA1 undergoes ectodomain shedding followed by C-terminal internalisation represents a somewhat rare method of ligand-induced processing for the Eph family members as eph/eprhin complexes are usually cleaved in trans from an opposing cell. However, this conclusion can only be reached if it future work proves that internalised EphA1 $P^{460}L$ is not a

consequence of a trafficking issue at to the plasma membrane. It was hypothesized that MMPs may be responsible for the proteolysis of WT EphA1 following ligand engagement, as the PROPSER tool predicted MMP-2 and MMP-9 to cleave EphA1 at the ECD, resulting in an N-terminal fragment of 75kDa. However, upon MMP inhibition with GM6001, N-terminal membrane staining was not rescued. Thus, other proteases must be responsible for this effect. ADAMs how been found to cleave other Eph family members and need to be investigated next. During initial experimentation, ephrinA1-Fc treatment occasionally resulted in the accumulation of a 40kDa cleavage product at a 2 and 3h timepoint, which would correspond to the expected molecular weight of the internalised C-terminal fragment, or a membrane-bound intracellular domain of EphA1, following N-terminal cleavage. It could be argued that this 40kDa cleavage product of EphA1 is not reproducibly detected via immunoblot analysis, either because it is rapidly degraded or that it is contained within subcellular compartments, prior to secondary processing, which were not lysed effectively during the lysis protocol. To prevent degradation of this cleavage product, cells could be treated with lysosomal/proteasomal inhibitors and again assessed via immunoblotting.

It is plausible that EphA1 would undergo trans-endocytosis should ephrinA1 stimulation occur via a juxtaposed ligand expressing cell rather than an ephrinA1 fusion protein. As such, it would be interesting to determine EphA1 regulation in a situation which more closely recapitulates the *in vivo* environment. Moreover, the manner in which Eph receptors undergo regulated intramembrane has been shown to be atypical in nature. EphB2, for instance, undergoes primary processing at the ECD, with subsequent C-terminal endocytosis with the C-terminus then undergoing γ-secretase processing within endosomes (Litterst et al., 2007c). This could also be the method by which EphA1 is regulated and future work is necessary to determine whether this is the case. Indeed, the data presented here indicates that the C-terminal staining following ephrinA1-Fc treatment of EphA1 WT cells appears punctate. This could suggest that the C-terminus is confined to endosomes as is the case for EphB2. Treatment of EphA1 WT expressing cells with ephrinA1-Fc in combination with DAPT resulted in reduced C-terminal fluorescence intensity within the cell but no recovery of membrane expression of C-terminal EphA1, suggesting that γ-secretase does not play a role in EphA1 C-terminal internalisation. It would also be interesting to determine whether it differs when its ligand is expressed in its natural GPI-anchored form.

It predicted that the $P^{460}L$ mutation may result in increased proteolysis of the molecule due to the position of the mutation. EphA2 has been found to be cleaved in this region by MT1-MPP. As the X2 variant is missing the first FNIII repeat, some preliminary analysis of the X2 variant was undertaken, which suggested that it may be resistant to ligand induced proteolysis, indicating that this region may well be important for the turnover of the molecule. However, future work is required to assess whether this is the case. The $P^{460}L$ mutation appeared to undergo expedited proteolysis in the presence of ligand, however, there appears to be less internalisation of the C-terminus upon ligand engagement, suggesting that the receptor undergoes rapid degradation following C-terminal internalisation. Moreover, the N-terminal staining differs from the WT molecule which indicated that even in the absence of ligand, there is a loss of strong membrane staining and that upon ephrinA1-Fc treatment is reduced. The staining however does appear to be inside the cell. This could suggest that a proportion of the N-terminal regions of EphA1 molecules have been internalised. However, if this was the case, you might expect to see an overlap of N-terminal and C-terminal staining which was not the case.

As the data indicated that the $P^{460}L$ mutation may confer increased proteolysis to the molecule, potential AD related disease mechanisms were assessed. This was conducted using a commercially obtained soluble EphA1 fusion protein corresponding to the ECD of EphA1 and its ability to prime endothelial cells for the recruitment of leucocytes. These data indicated that EphA1-ECD is capable of increasing the distance travelled of Molt 3 T cells over ECs in both tested EC cell lines. Moreover, in the disease relevant hCMEC/D3 cell line, EphA1-Fc increased the number of firmly adhered Molt 3 T cells, as well as the total contact time and the rolling velocity of the Molt 3 T cells. This indicates that EphA1-Fc activation of ECs differs between cell lines and may preferentially target disease relevant cell lines, resulting in AD risk. It would be interesting to determine the expression pattern of other Eph receptors and ephrins expressed on both hCMEC/D3s and Molt 3 T cells to determine the potential impact EphA1 may have on the expression of these molecules.

Taken together, this thesis has shown, for the first time, that the method of regulation between the WT and $P^{460}L$ molecule differs and that this is likely to be directly related to the risk associated with the mutant.

6.4 Future Work

As mentioned, we were unable to determine whether the ECD of the $P^{460}L$ mutant is capable of priming ECs in the manner in which the commercially obtained WT EphA1 fusion protein did. However, soluble $P^{460}L$ has been purified from EphA1 $P^{460}L$-ECD-Fc expressing cells. As a result, it is vital to determine whether the mutation, is, firstly, capable of priming ECs for leucocyte recruitment and whether it alters the priming of ECs compared to the WT molecule. This can be tested in static adhesion assays in the first instance to determine whether it is capable of altering the number of firmly adhered Molt 3 T cells and subsequently be introduced to the microfluidic assay described here. Moreover, it would be interesting to determine the target genes and pathways responsible for this EphA1-mediated priming of ECs. Pharmacological inhibition of signalling pathways known to be involved in the leucocyte adhesion cascade can be conducted to implicate or eliminate major pathway involvement. Non-biased transcriptome analysis can be conducted by comparing EphA1 stimulated and unstimulated hCMEC/D3 cells and RNA collected and sequenced at a range of timepoints. Moreover, blocking antibodies to molecules responsible for the rolling of leucocytes along ECs could be inhibited to similarly implicate or disregard these molecules or their downstream pathways from future analyses.

The Molt 3 T cell line is negative for endogenous expression of EphA1. However, the impact of EphA1 activation on different leucocyte subpopulations may vary and may be related the overall expression levels on various subsets. It would be interesting to analyse the impact of EphA1 on the activation of hCMEC/D3s of various leucocyte subsets from healthy controls. Moreover, PBMCs from individuals which are homozygous for minor (protective) or major (risk) allele for the non-coding variants rs11771145 and rs10808026 can be tested in microfluidic assays, such as the described Bioflux 200 system to determine their impact on the recruitment of leucocytes to hCMEC/D3s. It is also vital to investigate the effect of EphA1 on the global velocity of non-interacting Molt 3 T cells.

Bibliography

Aasheim, H.-C., Delabie, J., Finne, E.F., Newman, W., Avraham, H., Avraham, S., and Groopman, J.E. (2005). Ephrin-A1 binding to CD4+ T lymphocytes stimulates migration and induces tyrosine phosphorylation of PYK2. Blood *105*, 2869–2876.

Aasheim, H.C., Munthe, E., Funderud, S., Smeland, E.B., Beiske, K., and Logtenberg, T. (2000). A splice variant of human ephrin-A4 encodes a soluble molecule that is secreted by activated human B lymphocytes. Blood *95*, 221–230.

Abbate, C., Arosio, B., Cantatore, A., Viti, N., Giunco, F., Bagarolo, R., Nicolini, P., Gussago, C., Ferri, E., Casati, M., et al. (2016). Familial late-onset Alzheimer's disease: description of an Italian family with four affected siblings and one case of early-onset dementia in the preceding generation. Aging Clin. Exp. Res. *28*, 991–995.

Abbruscato, T.J., and Davis, T.P. (1999). Protein expression of brain endothelial cell E-cadherin after hypoxia/aglycemia: influence of astrocyte contact. Brain Res. *842*, 277–286.

Ades, E.W., Candal, F.J., Swerlick, R.A., George, V.G., Summers, S., Bosse, D.C., and Lawley, T.J. (1992). HMEC-1: Establishment of an immortalized human microvascular endothelial cell line. J. Invest. Dermatol. *99*, 683–690.

Afonso, P. V., Ozden, S., Cumont, M.-C., Seilhean, D., Cartier, L., Rezaie, P., Mason, S., Lambert, S., Huerre, M., Gessain, A., et al. (2008). Alteration of Blood–Brain Barrier Integrity by Retroviral Infection. PLoS Pathog. *4*, e1000205.

Aird, W.C. (2007a). Phenotypic Heterogeneity of the Endothelium. Circ. Res. *100*, 174–190.

Aird, W.C. (2007b). Phenotypic Heterogeneity of the Endothelium. Circ. Res. *100*, 158–173.

Albert, M.S., DeKosky, S.T., Dickson, D., Dubois, B., Feldman, H.H., Fox, N.C., Gamst, A., Holtzman, D.M., Jagust, W.J., Petersen, R.C., et al. (2011). The diagnosis of mild cognitive impairment due to Alzheimer's disease: recommendations from the National Institute on Aging-Alzheimer's Association workgroups on diagnostic guidelines for Alzheimer's disease. Alzheimers. Dement. *7*, 270–279.

Alon, R., Hammer, D.A., and Springer, T.A. (1995). Lifetime of the P-selectin-carbohydrate bond and its response to tensile force in hydrodynamic flow. Nature *374*, 539–542.

Alonso-C, L.M., Trinidad, E.M., de Garcillan, B., Ballesteros, M., Castellanos, M., Cotillo, I., Muñoz, J.J., and Zapata, A.G. (2009). Expression profile of Eph receptors and ephrin ligands in healthy human B lymphocytes and chronic lymphocytic leukemia B-cells. Leuk. Res. *33*, 395–406.

Atapattu, L., Lackmann, M., and Janes, P.W. (2014a). The role of proteases in regulating Eph/ephrin signaling. Cell Adh. Migr. *8*, 294–307.

Atapattu, L., Lackmann, M., and Janes, P.W. (2014b). The role of proteases in regulating Eph/ephrin signaling. Cell Adh. Migr. *8*, 294–307.

Bahbouhi, B., Berthelot, L., Pettré, S., Michel, L., Wiertlewski, S., Weksler, B., Romero, I.-A., Miller, F., Couraud, P.-O., Brouard, S., et al. (2009). Peripheral blood CD4+ T lymphocytes from multiple sclerosis patients are characterized by higher PSGL-1 expression and transmigration capacity across a human blood-brain barrier-derived endothelial cell line. J. Leukoc. Biol. *86*, 1049–1063.

Baker, E., Sims, R., Leonenko, G., Frizzati, A., Harwood, J.C., Grozeva, D., Morgan, K., Passmore, P., Holmes, C., Powell, J., et al. (2019). Gene-based analysis in HRC imputed genome wide association data identifies three novel genes for Alzheimer's disease. PLoS One *14*, e0218111.

Bancher, C., Brunner, C., Lassmann, H., Budka, H., Jellinger, K., Wiche, G., Seitelberger, F., Grundke-Iqbal, I., Iqbal, K., and Wisniewski, H.M. (1989). Accumulation of abnormally phosphorylated τ precedes the formation of neurofibrillary tangles in Alzheimer's disease. Brain Res. *477*, 90–99.

Bazzoni, G., and Dejana, E. (2004). Endothelial Cell-to-Cell Junctions: Molecular Organization and Role in Vascular Homeostasis. Physiol. Rev. *84*, 869–901.

Beauchamp, A., Lively, M.O., Mintz, A., Gibo, D., Wykosky, J., and Debinski, W. (2012). EphrinA1 is released in three forms from cancer cells by matrix metalloproteases. Mol. Cell. Biol. *32*, 3253–3264.

Bélanger, C., Elimam, H., Lefebvre, J., Borgeat, P., and Marleau, S. (2008). Involvement of endogenous leukotriene B4 and platelet-activating factor in polymorphonuclear leucocyte recruitment to dermal inflammatory sites in rats. Immunology *124*, 295–303.

Ben-Ze'ev, A., and Geiger, B. (1998). Differential molecular interactions of beta-catenin and plakoglobin in adhesion, signaling and cancer. Curr. Opin. Cell Biol. *10*, 629–639.

Berlin, C., Bargatze, R.., Campbell, J.., von Andrian, U.., Szabo, M.., Hasslen, S.., Nelson, R.., Berg, E.., Erlandsen, S.., and Butcher, E.. (1995). α4 integrins mediate lymphocyte attachment and rolling under physiologic flow. Cell *80*, 413–422.

Bixel, M.G., Li, H., Petri, B., Khandoga, A.G., Khandoga, A., Zarbock, A., Wolburg-Buchholz, K., Wolburg, H., Sorokin, L., Zeuschner, D., et al. (2010). CD99 and CD99L2 act at the same site as, but independently of, PECAM-1 during leukocyte diapedesis. Blood *116*, 1172–1184.

Bocharov, E. V, Mayzel, M.L., Volynsky, P.E., Goncharuk, M. V, Ermolyuk, Y.S.,

Schulga, A.A., Artemenko, E.O., Efremov, R.G., and Arseniev, A.S. (2008). Spatial structure and pH-dependent conformational diversity of dimeric transmembrane domain of the receptor tyrosine kinase EphA1. J. Biol. Chem. *283*, 29385–29395.

Bogen, S., Pak, J., Garifallou, M., Deng, X., and Muller, W.A. (1994). Monoclonal antibody to murine PECAM-1 (CD31) blocks acute inflammation in vivo. J. Exp. Med. *179*, 1059–1064.

Bondi, M.W., Serody, A.B., Chan, A.S., Eberson-Shumate, S.C., Delis, D.C., Hansen, L.A., and Salmon, D.P. (2002). Cognitive and neuropathologic correlates of Stroop Color-Word Test performance in Alzheimer's disease. Neuropsychology *16*, 335–343.

Bostrom, K., Wettesten, M., Boren, J., Bondjers, G., Wiklund, O., and Olofsson, S.O. (1986). Pulse-chase studies of the synthesis and intracellular transport of apolipoprotein B-100 in Hep G2 cells. J. Biol. Chem. *261*, 13800–13806.

Bradshaw, E.M., Chibnik, L.B., Keenan, B.T., Ottoboni, L., Raj, T., Tang, A., Rosenkrantz, L.L., Imboywa, S., Lee, M., Von Korff, A., et al. (2013). CD33 Alzheimer's disease locus: altered monocyte function and amyloid biology. Nat. Neurosci. *16*, 848–850.

Brantley-Sieders, D.M., Fang, W. Bin, Hwang, Y., Hicks, D., and Chen, J. (2006). Ephrin-A1 Facilitates Mammary Tumor Metastasis through an Angiogenesis-Dependent Mechanism Mediated by EphA Receptor and Vascular Endothelial Growth Factor in Mice. Cancer Res. *66*, 10315–10324.

BRION, J., Passareiro, H., and NUNEZ, J. (1985). MISE EN ÉVIDENCE IMMUNOL OGIQ UE DE LA PROTEINEÏA U, 54 q NI VEA U DES LESIONS DE DEGENERESCENCE NEUR OFIBRILLAIRE DE LA.

Brown, M.S., Ye, J., Rawson, R.B., and Goldstein, J.L. (2000). Regulated Intramembrane Proteolysis: A Control Mechanism Conserved from Bacteria to Humans. Cell *100*, 391–398.

Buccione, R., Orth, J.D., and McNiven, M.A. (2004). Foot and mouth: Podosomes, invadopodia and circular dorsal ruffles. Nat. Rev. Mol. Cell Biol. *5*, 647–657.

Cai, Y., An, S.S.A., and Kim, S. (2015). Mutations in presenilin 2 and its implications in Alzheimer's disease and other dementia-associated disorders. Clin. Interv. Aging *10*, 1163–1172.

Carman, C. V, and Springer, T.A. (2003). Integrin avidity regulation: are changes in affinity and conformation underemphasized? Curr. Opin. Cell Biol. *15*, 547–556.

Carman, C. V, and Springer, T.A. (2004). A transmigratory cup in leukocyte diapedesis both through individual vascular endothelial cells and between them. J. Cell Biol. *167*, 377–388.

Carman, C. V., Sage, P.T., Sciuto, T.E., de la Fuente, M.A., Geha, R.S., Ochs, H.D.D.,

Dvorak, H.F., Dvorak, A.M., and Springer, T.A. (2007). Transcellular Diapedesis Is Initiated by Invasive Podosomes. Immunity *26*, 784–797.

Carpenter, G. (2000). The EGF receptor: a nexus for trafficking and signaling. BioEssays *22*, 697–707.

Carpenter, T.C., Schroeder, W., Stenmark, K.R., and Schmidt, E.P. (2012). Eph-A2 Promotes Permeability and Inflammatory Responses to Bleomycin-Induced Lung Injury. Am. J. Respir. Cell Mol. Biol. *46*, 40–47.

Castellano, J.M., Kim, J., Stewart, F.R., Jiang, H., DeMattos, R.B., Patterson, B.W., Fagan, A.M., Morris, J.C., Mawuenyega, K.G., Cruchaga, C., et al. (2011). Human apoE Isoforms Differentially Regulate Brain Amyloid-β Peptide Clearance. Sci. Transl. Med. *3*, 89ra57-89ra57.

Cereijido, M., Valdés, J., Shoshani, L., and Contreras, R.G. (1998). ROLE OF TIGHT JUNCTIONS IN ESTABLISHING AND MAINTAINING CELL POLARITY. Annu. Rev. Physiol. *60*, 161–177.

Chandrasekharan, U.M., Siemionow, M., Unsal, M., Yang, L., Poptic, E., Bohn, J., Ozer, K., Zhou, Z., Howe, P.H., Penn, M., et al. (2007). Tumor necrosis factor alpha (TNF-alpha) receptor-II is required for TNF-alpha-induced leukocyte-endothelial interaction in vivo. Blood *109*, 1938–1944.

Chavakis, T., Keiper, T., Matz-Westphal, R., Hersemeyer, K., Sachs, U.J., Nawroth, P.P., Preissner, K.T., and Santoso, S. (2004). The junctional adhesion molecule-C promotes neutrophil transendothelial migration in vitro and in vivo. J. Biol. Chem. *279*, 55602–55608.

Chertoff, M., Shrivastava, K., Gonzalez, B., Acarin, L., and Giménez-Llort, L. (2013). Differential modulation of TREM2 protein during postnatal brain development in mice. PLoS One *8*.

CHESNUTT, B.C., SMITH, D.F., RAFFLER, N.A., SMITH, M.L., WHITE, E.J., and LEY, K. (2006). Induction of LFA-1-Dependent Neutrophil Rolling on ICAM-1 by Engagement of E-Selectin. Microcirculation *13*, 99–109.

Chrobak, K.M., Potter, D.R., and Tien, J. (2006). Formation of perfused, functional microvascular tubes in vitro. Microvasc. Res. *71*, 185–196.

Cinamon, G., Shinder, V., and Alon, R. (2001). Shear forces promote lymphocyte migration across vascular endothelium bearing apical chemokines. Nat. Immunol. *2*, 515–522.

Cines, D.B., Pollak, E.S., Buck, C.A., Loscalzo, J., Zimmerman, G.A., McEver, R.P., Pober, J.S., Wick, T.M., Konkle, B.A., Schwartz, B.S., et al. (1998). Endothelial cells in physiology and in the pathophysiology of vascular disorders. Blood *91*, 3527–3561.

Colombo, E., and Farina, C. (2016). Astrocytes: Key Regulators of

Neuroinflammation. Trends Immunol. *37*, 608–620.

Corder, E., Saunders, A., Strittmatter, W., Schmechel, D., Gaskell, P., Small, G., Roses, A., Haines, J., and Pericak-Vance, M. (1993). Gene dose of apolipoprotein E type 4 allele and the risk of Alzheimer's disease in late onset families. Science (80-.). *261*, 921–923.

da Costa Martins, P., García-Vallejo, J.-J., van Thienen, J. V., Fernandez-Borja, M., van Gils, J.M., Beckers, C., Horrevoets, A.J., Hordijk, P.L., and Zwaginga, J.-J. (2007). P-Selectin Glycoprotein Ligand-1 Is Expressed on Endothelial Cells and Mediates Monocyte Adhesion to Activated Endothelium. Arterioscler. Thromb. Vasc. Biol. *27*, 1023–1029.

Coulthard, M.G., Lickliter, J.D., Subanesan, N., Chen, K., Webb, G.C., Lowry, A.J., Koblar, S., Bottema, C.D., and Boyd, A.W. (2001a). Characterization of the Epha1 receptor tyrosine kinase: expression in epithelial tissues. Growth Factors *18*, 303–317.

Coulthard, M.G., Lickliter, J.D., Subanesan, N., Chen, K., Webb, G.C., Lowry, A.J., Koblar, S., Bottema, C.D., and Boyd, A.W. (2001b). Characterization of the Epha1 receptor tyrosine kinase: expression in epithelial tissues. Growth Factors *18*, 303–317.

Coulthard, M.G., Morgan, M., Woodruff, T.M., Arumugam, T. V., Taylor, S.M., Carpenter, T.C., Lackmann, M., and Boyd, A.W. (2012). Eph/Ephrin Signaling in Injury and Inflammation. Am. J. Pathol. *181*, 1493–1503.

Crone, C., and Christensen, O. (1981). Electrical resistance of a capillary endothelium. J. Gen. Physiol. *77*, 349–371.

Cruts, M., Theuns, J., and Van Broeckhoven, C. (2012). Locus-specific mutation databases for neurodegenerative brain diseases. Hum. Mutat. *33*, 1340–1344.

Cruz Hernández, J.C., Bracko, O., Kersbergen, C.J., Muse, V., Haft-Javaherian, M., Berg, M., Park, L., Vinarcsik, L.K., Ivasyk, I., Rivera, D.A., et al. (2019). Neutrophil adhesion in brain capillaries reduces cortical blood flow and impairs memory function in Alzheimer's disease mouse models. Nat. Neurosci. *22*, 413–420.

Cucullo, L., Marchi, N., Hossain, M., and Janigro, D. (2011). A Dynamic *in vitro* BBB Model for the Study of Immune Cell Trafficking into the Central Nervous System. J. Cereb. Blood Flow Metab. *31*, 767–777.

Cummings, J.L., Tong, G., and Ballard, C. (2019). Treatment Combinations for Alzheimer's Disease: Current and Future Pharmacotherapy Options. J. Alzheimers. Dis. *67*, 779–794.

Dai, M.-H., Zheng, H., Zeng, L.-D., and Zhang, Y. (2018). The genes associated with early-onset Alzheimer's disease. Oncotarget *9*, 15132–15143.

Darling, T.K., and Lamb, T.J. (2019). Emerging Roles for Eph Receptors and Ephrin Ligands in Immunity. Front. Immunol. *10*, 1473.

Das, H.K., McPherson, J., Bruns, G.A., Karathanasis, S.K., and Breslow, J.L. (1985). Isolation, characterization, and mapping to chromosome 19 of the human apolipoprotein E gene. J. Biol. Chem. *260*, 6240–6247.

Davis, C., Fischer, J., Ley, K., and Sarembock, I.J. (2003). The role of inflammation in vascular injury and repair. J. Thromb. Haemost. *1*, 1699–1709.

DeTure, M.A., and Dickson, D.W. (2019). The neuropathological diagnosis of Alzheimer's disease. Mol. Neurodegener. *14*, 32.

Díaz-Perlas, C., Oller-Salvia, B., Sánchez-Navarro, M., Teixidó, M., and Giralt, E. (2018). Branched BBB-shuttle peptides: chemoselective modification of proteins to enhance blood-brain barrier transport. Chem. Sci. *9*, 8409–8415.

Dixit, V.M., Green, S., Sarma, V., Holzman, L.B., Wolf, F.W., O'Rourke, K., Ward, P.A., Prochownik, E. V, and Marks, R.M. (1990). Tumor necrosis factor-alpha induction of novel gene products in human endothelial cells including a macrophage-specific chemotaxin. J. Biol. Chem. *265*, 2973–2978.

Duering, M., Grimm, M.O.W., Grimm, H.S., Schröder, J., and Hartmann, T. (2005). Mean age of onset in familial Alzheimer's disease is determined by amyloid beta 42. Neurobiol. Aging *26*, 785–788.

Dunne, J.L., Ballantyne, C.M., Beaudet, A.L., and Ley, K. (2002). Control of leukocyte rolling velocity in TNF-alpha-induced inflammation by LFA-1 and Mac-1. Blood *99*, 336–341.

Egea, J., Nissen, U.V., Dufour, A., Sahin, M., Greer, P., Kullander, K., Mrsic-Flogel, T.D., Greenberg, M.E., Kiehn, O., Vanderhaeghen, P., et al. (2005). Regulation of EphA4 Kinase Activity Is Required for a Subset of Axon Guidance Decisions Suggesting a Key Role for Receptor Clustering in Eph Function. Neuron *47*, 515–528.

Engelhardt, B., and Ransohoff, R.M. (2012). Capture, crawl, cross: the T cell code to breach the blood–brain barriers. Trends Immunol. *33*, 579–589.

Erickson, M.A., and Banks, W.A. (2013). Blood-brain barrier dysfunction as a cause and consequence of Alzheimer's disease. J. Cereb. Blood Flow Metab. *33*, 1500–1513.

Escott-Price, V., Bellenguez, C., Wang, L.-S., Choi, S.-H., Harold, D., Jones, L., Holmans, P., Gerrish, A., Vedernikov, A., Richards, A., et al. (2014). Gene-Wide Analysis Detects Two New Susceptibility Genes for Alzheimer's Disease. PLoS One *9*, e94661.

Fahrenhold, M., Rakic, S., Classey, J., Brayne, C., Ince, P.G., Nicoll, J.A.R., and Boche, D. (2018). TREM2 expression in the human brain: a marker of monocyte recruitment? Brain Pathol. *28*, 595–602.

Farrer, L.A., Adrienne Cupples, L., Van Duijn, C.M., Kurz, A., Zimmer, R., Müller, U., Green, R.C., Clarke, V., Shoffner, J., Wallace, D.C., et al. (1995). Apolipoprotein E

genotype in patients with alzheimer's disease: Implications for the risk of dementia among relatives. Ann. Neurol. *38*, 797–808.

Fasen, K., Cerretti, D.P., and Huynh-Do, U. (2008). Ligand Binding Induces Cbl-Dependent EphB1 Receptor Degradation Through the Lysosomal Pathway. Traffic *9*, 251–266.

Feldman, G.J., Mullin, J.M., and Ryan, M.P. (2005). Occludin: Structure, function and regulation. Adv. Drug Deliv. Rev. *57*, 883–917.

Fiala, M., Zhang, L., Gan, X., Sherry, B., Taub, D., Graves, M.C., Hama, S., Way, D., Weinand, M., Witte, M., et al. (1998). Amyloid-beta induces chemokine secretion and monocyte migration across a human blood--brain barrier model. Mol. Med. *4*, 480–489.

Flanagan, J.G., and Vanderhaeghen, P. (1998). The ephrins and Eph receptors in neural development. Annu. Rev. Neurosci. *21*, 309–345.

Flanagan, M.L., Arias, R.S., Hu, P., Khawli, L.A., and Epstein, A.L. (2007). Soluble Fc fusion proteins for biomedical research. Methods Mol. Biol. *378*, 33–52.

Fleishman, S.J., Schlessinger, J., and Ben-Tal, N. (2002). A putative molecular-activation switch in the transmembrane domain of erbB2. Proc. Natl. Acad. Sci. *99*, 15937–15940.

Forabosco, P., Ramasamy, A., Trabzuni, D., Walker, R., Smith, C., Bras, J., Levine, A.P., Hardy, J., Pocock, J.M., Guerreiro, R., et al. (2013). Insights into TREM2 biology by network analysis of human brain gene expression data. Neurobiol. Aging *34*, 2699–2714.

Förster, C., Burek, M., Romero, I.A., Weksler, B., Couraud, P.-O., and Drenckhahn, D. (2008). Differential effects of hydrocortisone and TNFα on tight junction proteins in an *in vitro* model of the human blood-brain barrier. J. Physiol. *586*, 1937–1949.

Förstl, H., and Kurz, A. (1999). Clinical features of Alzheimer's disease. Eur. Arch. Psychiatry Clin. Neurosci. *249*, 288–290.

French, B.M., Sendil, S., Sepuru, K.M., Ranek, J., Burdorf, L., Harris, D., Redding, E., Cheng, X., Laird, C.T., Zhao, Y., et al. (2018). Interleukin-8 mediates neutrophil-endothelial interactions in pig-to-human xenogeneic models. Xenotransplantation *25*, e12385.

Funk, S.D., and Orr, A.W. (2013). Ephs and ephrins resurface in inflammation, immunity, and atherosclerosis. Pharmacol. Res. *67*, 42–52.

Funk, S.D., Yurdagul, A., Jr., Albert, P., Traylor, J.G., Jr., Jin, L., Chen, J., and Orr, A.W. (2012a). EphA2 Activation Promotes the Endothelial Cell Inflammatory Response: a potential role in atherosclerosis. Arterioscler. Thromb. Vasc. Biol. *32*, 686.

Funk, S.D., Yurdagul, A., Albert, P., Traylor, J.G., Jin, L., Chen, J., and Orr, A.W. (2012b). EphA2 activation promotes the endothelial cell inflammatory response: a potential role in atherosclerosis. Arterioscler. Thromb. Vasc. Biol. *32*, 686–695.

Gale, N.W., Holland, S.J., Valenzuela, D.M., Flenniken, A., Pan, L., Ryan, T.E., Henkemeyer, M., Strebhardt, K., Hirai, H., Wilkinson, D.G., et al. (1996). Eph receptors and ligands comprise two major specificity subclasses and are reciprocally compartmentalized during embryogenesis. Neuron *17*, 9–19.

Gauthier, L.R., and Robbins, S.M. (2003). Ephrin signaling: One raft to rule them all? One raft to sort them? One raft to spread their call and in signaling bind them? Life Sci. *74*, 207–216.

GBD 2016 Dementia Collaborators, E., Szoeke, C.E.I., Vollset, S.E., Abbasi, N., Abd-Allah, F., Abdela, J., Aichour, M.T.E., Akinyemi, R.O., Alahdab, F., Asgedom, S.W., et al. (2019). Global, regional, and national burden of Alzheimer's disease and other dementias, 1990-2016: a systematic analysis for the Global Burden of Disease Study 2016. Lancet. Neurol. *18*, 88–106.

Geng, J.-G., Bevilacquat, M.P., Moore, K.L., Mclntyre, T.M., Prescott, S.M., Kim, J.M., Bliss, G.A., Zimmerman, G.A., and McEver, R.P. (1990). Rapid neutrophil adhesion to activated endothelium mediated by GMP-140. Nature *343*, 757–760.

Georgakopoulos, A., Litterst, C., Ghersi, E., Baki, L., Xu, C., Serban, G., and Robakis, N.K. (2006). Metalloproteinase/Presenilin1 processing of ephrinB regulates EphB-induced Src phosphorylation and signaling. EMBO J. *25*, 1242–1252.

Giri, R., Shen, Y., Stins, M., Du Yan, S., Schmidt, A.M., Stern, D., Kim, K.-S., Zlokovic, B., and Kalra, V.K. (2000). β-Amyloid-induced migration of monocytes across human brain endothelial cells involves RAGE and PECAM-1. Am. J. Physiol. Physiol. *279*, C1772–C1781.

Goh, L.K., and Sorkin, A. (2013a). Endocytosis of receptor tyrosine kinases. Cold Spring Harb. Perspect. Biol. *5*, a017459.

Goh, L.K., and Sorkin, A. (2013b). Endocytosis of receptor tyrosine kinases. Cold Spring Harb. Perspect. Biol. *5*, a017459.

Gratuze, M., Leyns, C.E.G., and Holtzman, D.M. (2018). New insights into the role of TREM2 in Alzheimer's disease. Mol. Neurodegener. *13*.

Griciuc, A., Serrano-Pozo, A., Parrado, A.R., Lesinski, A.N., Asselin, C.N., Mullin, K., Hooli, B., Choi, S.H., Hyman, B.T., and Tanzi, R.E. (2013). Alzheimer's Disease Risk Gene CD33 Inhibits Microglial Uptake of Amyloid Beta. Neuron *78*, 631–643.

Grozeva, D., Saad, S., Menzies, G.E., and Sims, R. (2019). Benefits and Challenges of Rare Genetic Variation in Alzheimer's Disease. Curr. Genet. Med. Rep. *7*, 53–62.

Guarino, A., Favieri, F., Boncompagni, I., Agostini, F., Cantone, M., and Casagrande,

M. (2018). Executive Functions in Alzheimer Disease: A Systematic Review. Front. Aging Neurosci. *10*, 437.

Guerreiro, R., Wojtas, A., Bras, J., Carrasquillo, M., Rogaeva, E., Majounie, E., Cruchaga, C., Sassi, C., Kauwe, J.S.K., Younkin, S., et al. (2013a). *TREM2* Variants in Alzheimer's Disease. N. Engl. J. Med. *368*, 117–127.

Guerreiro, R., Wojtas, A., Bras, J., Carrasquillo, M., Rogaeva, E., Majounie, E., Cruchaga, C., Sassi, C., Kauwe, J.S.K., Younkin, S., et al. (2013b). *TREM2* Variants in Alzheimer's Disease. N. Engl. J. Med. *368*, 117–127.

Guerreiro, R., Wojtas, A., Bras, J., Carrasquillo, M., Rogaeva, E., Majounie, E., Cruchaga, C., Sassi, C., Kauwe, J.S.K., Younkin, S., et al. (2013c). TREM2 variants in Alzheimer's disease. N. Engl. J. Med. *368*, 117–127.

Gussago, C., Casati, M., Ferri, E., and Arosio, B. (2019). The Triggering Receptor Expressed on Myeloid Cells-2 (TREM-2) as Expression of the Relationship between Microglia and Alzheimer's Disease: A Novel Marker for a Promising Pathway to Explore. J. Frailty Aging *8*, 54–56.

El Haj, M., Antoine, P., Amouyel, P., Lambert, J.-C., Pasquier, F., and Kapogiannis, D. (2016). Apolipoprotein E (APOE) ε4 and episodic memory decline in Alzheimer's disease: A review. Ageing Res. Rev. *27*, 15–22.

Hardy, J., and Higgins, G. (1992a). Alzheimer's disease: the amyloid cascade hypothesis. Science (80-.). *256*, 184–185.

Hardy, J.A., and Higgins, G.A. (1992b). Alzheimer's disease: the amyloid cascade hypothesis. Science *256*, 184–185.

Harold, D., Abraham, R., Hollingworth, P., Sims, R., Gerrish, A., Hamshere, M.L., Pahwa, J.S., Moskvina, V., Dowzell, K., Williams, A., et al. (2009). Genome-wide association study identifies variants at CLU and PICALM associated with Alzheimer's disease. Nat. Genet. *41*, 1088–1093.

Hatherell, K., Couraud, P.-O., Romero, I.A., Weksler, B., and Pilkington, G.J. (2011). Development of a three-dimensional, all-human in vitro model of the blood–brain barrier using mono-, co-, and tri-cultivation Transwell models. J. Neurosci. Methods *199*, 223–229.

Hattori, M., Osterfield, M., and Flanagan, J.G. (2000). Regulated cleavage of a contact-mediated axon repellent. Science *289*, 1360–1365.

Hattori, R., Hamilton, K.K., Fugate, R.D., McEver, R.P., and Sims, P.J. (1989). Stimulated secretion of endothelial von Willebrand factor is accompanied by rapid redistribution to the cell surface of the intracellular granule membrane protein GMP-140. J. Biol. Chem. *264*, 7768–7771.

Heneka, M.T., Kummer, M.P., Stutz, A., Delekate, A., Schwartz, S., Vieira-Saecker,

A., Griep, A., Axt, D., Remus, A., Tzeng, T.-C., et al. (2013). NLRP3 is activated in Alzheimer's disease and contributes to pathology in APP/PS1 mice. Nature *493*, 674–678.

Heneka, M.T., Carson, M.J., Khoury, J. El, Landreth, G.E., Brosseron, F., Feinstein, D.L., Jacobs, A.H., Wyss-Coray, T., Vitorica, J., Ransohoff, R.M., et al. (2015). Neuroinflammation in Alzheimer's disease. Lancet Neurol. *14*, 388–405.

Herath, N.I., Spanevello, M.D., Sabesan, S., Newton, T., Cummings, M., Duffy, S., Lincoln, D., Boyle, G., Parsons, P.G., and Boyd, A.W. (2006). Over-expression of Eph and ephrin genes in advanced ovarian cancer: ephrin gene expression correlates with shortened survival. BMC Cancer *6*, 144.

Herath, N.I., Spanevello, M.D., Doecke, J.D., Smith, F.M., Pouponnot, C., and Boyd, A.W. (2012). Complex expression patterns of Eph receptor tyrosine kinases and their ephrin ligands in colorectal carcinogenesis. Eur. J. Cancer *48*, 753–762.

Hidalgo, A., Peired, A.J., Wild, M.K., Vestweber, D., and Frenette, P.S. (2007). Complete Identification of E-Selectin Ligands on Neutrophils Reveals Distinct Functions of PSGL-1, ESL-1, and CD44. Immunity *26*, 477–489.

Himanen, J.-P., Henkemeyer, M., and Nikolov, D.B. (1998). Crystal structure of the ligand-binding domain of the receptor tyrosine kinase EphB2. Nature *396*, 486–491.

Himanen, J.-P., Chumley, M.J., Lackmann, M., Li, C., Barton, W.A., Jeffrey, P.D., Vearing, C., Geleick, D., Feldheim, D.A., Boyd, A.W., et al. (2004). Repelling class discrimination: ephrin-A5 binds to and activates EphB2 receptor signaling. Nat. Neurosci. *7*, 501–509.

Himanen, J.P., Yermekbayeva, L., Janes, P.W., Walker, J.R., Xu, K., Atapattu, L., Rajashankar, K.R., Mensinga, A., Lackmann, M., Nikolov, D.B., et al. (2010). Architecture of Eph receptor clusters. Proc. Natl. Acad. Sci. U. S. A. *107*, 10860–10865.

Hirai, H., Maru, Y., Hagiwara, K., Nishida, J., and Takaku, F. (1987). A novel putative tyrosine kinase receptor encoded by the eph gene. Science *238*, 1717–1720.

Hjorthaug, H.S., and Aasheim, H.-C. (2007). Ephrin-A1 stimulates migration of CD8+CCR7+ T lymphocytes. Eur. J. Immunol. *37*, 2326–2336.

Hodges, J.R., Erzinçlioğlu, S., and Patterson, K. (2006). Evolution of Cognitive Deficits and Conversion to Dementia in Patients with Mild Cognitive Impairment: A Very-Long-Term Follow-Up Study. Dement. Geriatr. Cogn. Disord. *21*, 380–391.

Hogg, N., Patzak, I., and Willenbrock, F. (2011). The insider's guide to leukocyte integrin signalling and function. Nat. Rev. Immunol. *11*, 416–426.

Hollingworth, P., Harold, D., Sims, R., Gerrish, A., Lambert, J.-C., Carrasquillo, M.M., Abraham, R., Hamshere, M.L., Pahwa, J.S., Moskvina, V., et al. (2011).

Common variants at ABCA7, MS4A6A/MS4A4E, EPHA1, CD33 and CD2AP are associated with Alzheimer's disease. Nat. Genet. *43*, 429–435.

Hooli, B. V., Mohapatra, G., Mattheisen, M., Parrado, A.R., Roehr, J.T., Shen, Y., Gusella, J.F., Moir, R., Saunders, A.J., Lange, C., et al. (2012). Role of common and rare APP DNA sequence variants in Alzheimer disease. Neurology *78*, 1250–1257.

Horuk, R. (2001). Chemokine receptors. Cytokine Growth Factor Rev. *12*, 313–335.

Huang, G. (2012). Biotinylation of Cell Surface Proteins. BIO-PROTOCOL *2*.

Hughes, T.M., Lopez, O.L., Evans, R.W., Kamboh, M.I., Williamson, J.D., Klunk, W.E., Mathis, C.A., Price, J.C., Cohen, A.D., Snitz, B.E., et al. (2014). Markers of cholesterol transport are associated with amyloid deposition in the brain. Neurobiol. Aging *35*, 802–807.

Hultman, K., Strickland, S., and Norris, E.H. (2013). The *APOE* ε4/ε4 Genotype Potentiates Vascular Fibrin(Ogen) Deposition in Amyloid-Laden Vessels in the Brains of Alzheimer's Disease Patients. J. Cereb. Blood Flow Metab. *33*, 1251–1258.

von Hundelshausen, P., Weber, K.S.C., Huo, Y., Proudfoot, A.E.I., Nelson, P.J., Ley, K., and Weber, C. (2001). RANTES Deposition by Platelets Triggers Monocyte Arrest on Inflamed and Atherosclerotic Endothelium. Circulation *103*, 1772–1777.

Huo, Y., Schober, A., Forlow, S.B., Smith, D.F., Hyman, M.C., Jung, S., Littman, D.R., Weber, C., and Ley, K. (2003). Circulating activated platelets exacerbate atherosclerosis in mice deficient in apolipoprotein E. Nat. Med. *9*, 61–67.

Hurst, L.A., Bunning, R.A.D., Couraud, P.-O., Romero, I.A., Weksler, B.B., Sharrack, B., and Woodroofe, M.N. (2009). Expression of ADAM-17, TIMP-3 and fractalkine in the human adult brain endothelial cell line, hCMEC/D3, following pro-inflammatory cytokine treatment. J. Neuroimmunol. *210*, 108–112.

Hwang, S.T., Singer, M.S., Giblin, P.A., Yednock, T.A., Bacon, K.B., Simon, S.I., and Rosen, S.D. (1996). GlyCAM-1, a physiologic ligand for L-selectin, activates beta 2 integrins on naive peripheral lymphocytes. J. Exp. Med. *184*, 1343–1348.

Hyun, Y.-M., Sumagin, R., Sarangi, P.P., Lomakina, E., Overstreet, M.G., Baker, C.M., Fowell, D.J., Waugh, R.E., Sarelius, I.H., and Kim, M. (2012). Uropod elongation is a common final step in leukocyte extravasation through inflamed vessels. J. Exp. Med. *209*, 1349–1362.

Ieguchi, K., Tomita, T., Omori, T., Komatsu, A., Deguchi, A., Masuda, J., Duffy, S.L., Coulthard, M.G., Boyd, A., and Maru, Y. (2014). ADAM12-cleaved ephrin-A1 contributes to lung metastasis. Oncogene *33*, 2179–2190.

Inoue, E., Deguchi-Tawarada, M., Togawa, A., Matsui, C., Arita, K., Katahira-Tayama, S., Sato, T., Yamauchi, E., Oda, Y., and Takai, Y. (2009). Synaptic activity prompts gamma-secretase-mediated cleavage of EphA4 and dendritic spine

formation. J. Cell Biol. *185*, 551–564.

Ionta, M., Ferreira, R., Pfister, S., and Machado-Santelli, G. (2009). Exogenous Cx43 expression decrease cell proliferation rate in rat hepatocarcinoma cells independently of functional gap junction. Cancer Cell Int. *9*, 22.

Iqbal, K., Liu, F., Gong, C.-X., and Grundke-Iqbal, I. (2010). Tau in Alzheimer disease and related tauopathies. Curr. Alzheimer Res. *7*, 656–664.

Van Itallie, C.M., and Anderson, J.M. (2006). CLAUDINS AND EPITHELIAL PARACELLULAR TRANSPORT. Annu. Rev. Physiol. *68*, 403–429.

Ivanov, A.I., Steiner, A.A., Scheck, A.C., and Romanovsky, A.A. (2005). Expression of Eph receptors and their ligands, ephrins, during lipopolysaccharide fever in rats. Physiol. Genomics *21*, 152–160.

Ivetic, A., Green, H.L.H., and Hart, S.J. (2019). L-selectin: A major regulator of leukocyte adhesion, migration and signaling. Front. Immunol. *10*.

Iwasaki, A., and Medzhitov, R. (2010). Regulation of Adaptive Immunity by the Innate Immune System. Science (80-.). *327*, 291–295.

Jaffe, E.A., Nachman, R.L., Becker, C.G., and Minick, C.R. (1973). Culture of human endothelial cells derived from umbilical veins. Identification by morphologic and immunologic criteria. J. Clin. Invest. *52*, 2745–2756.

Janes, P.W., Saha, N., Barton, W.A., Kolev, M. V, Wimmer-Kleikamp, S.H., Nievergall, E., Blobel, C.P., Himanen, J.-P., Lackmann, M., and Nikolov, D.B. (2005). Adam meets Eph: an ADAM substrate recognition module acts as a molecular switch for ephrin cleavage in trans. Cell *123*, 291–304.

Janssen, J.C., Beck, J.A., Campbell, T.A., Dickinson, A., Fox, N.C., Harvey, R.J., Houlden, H., Rossor, M.N., and Collinge, J. (2003). Early onset familial Alzheimer's disease: Mutation frequency in 31 families. Neurology *60*, 235–239.

Jarmolowicz, A.I., Chen, H.-Y., and Panegyres, P.K. (2015). The Patterns of Inheritance in Early-Onset Dementia. Am. J. Alzheimer's Dis. Other Dementiasr *30*, 299–306.

Jellinghaus, S., Poitz, D.M., Ende, G., Augstein, A., Weinert, S., Stütz, B., Braun-Dullaeus, R.C., Pasquale, E.B., and Strasser, R.H. (2013). Ephrin-A1/EphA4-mediated adhesion of monocytes to endothelial cells. Biochim. Biophys. Acta - Mol. Cell Res. *1833*, 2201–2211.

Johnson-Leger, C., and Imhof, B.A. (2003). Forging the endothelium during inflammation: pushing at a half-open door? Cell Tissue Res. *314*, 93–105.

Johnson-Léger, C.A., Aurrand-Lions, M., Beltraminelli, N., Fasel, N., and Imhof, B.A. (2002). Junctional adhesion molecule-2 (JAM-2) promotes lymphocyte

transendothelial migration. Blood *100*, 2479–2486.

Jonsson, T., Atwal, J.K., Steinberg, S., Snaedal, J., Jonsson, P. V., Bjornsson, S., Stefansson, H., Sulem, P., Gudbjartsson, D., Maloney, J., et al. (2012). A mutation in APP protects against Alzheimer's disease and age-related cognitive decline. Nature *488*, 96–99.

Jonsson, T., Stefansson, H., Steinberg, S., Jonsdottir, I., Jonsson, P. V., Snaedal, J., Bjornsson, S., Huttenlocher, J., Levey, A.I., Lah, J.J., et al. (2013). Variant of *TREM2* Associated with the Risk of Alzheimer's Disease. N. Engl. J. Med. *368*, 107–116.

Jun, G.R., Chung, J., Mez, J., Barber, R., Beecham, G.W., Bennett, D.A., Buxbaum, J.D., Byrd, G.S., Carrasquillo, M.M., Crane, P.K., et al. (2017). Transethnic genome-wide scan identifies novel Alzheimer's disease loci. Alzheimer's Dement. *13*, 727–738.

Kahle, P.J., and De Strooper, B. (2003). Attack on amyloid. EMBO Rep. *4*, 747–751.

Kalaria, R.N. (2010). Vascular basis for brain degeneration: faltering controls and risk factors for dementia. Nutr. Rev. *68*, S74–S87.

Kameritsch, P., Pogoda, K., and Pohl, U. (2012). Channel-independent influence of connexin 43 on cell migration. Biochim. Biophys. Acta - Biomembr. *1818*, 1993–2001.

Kaminski, A., Ma, N., Donndorf, P., Lindenblatt, N., Feldmeier, G., Ong, L.-L., Furlani, D., A Skrabal, C., Liebold, A., Vollmar, B., et al. (2008). Endothelial NOS is required for SDF-1α/CXCR4-mediated peripheral endothelial adhesion of c-kit+ bone marrow stem cells. Lab. Investig. *88*, 58–69.

Kania, K.D., Wijesuriya, H.C., Hladky, S.B., and Barrand, M.A. (2011). Beta amyloid effects on expression of multidrug efflux transporters in brain endothelial cells. Brain Res. *1418*, 1–11.

Kelleher, R.J., Shen, J., and Shen, J. (2017). Presenilin-1 mutations and Alzheimer's disease. Proc. Natl. Acad. Sci. U. S. A. *114*, 629–631.

Kerfoot, S.M., and Kubes, P. (2002). Overlapping roles of P-selectin and alpha 4 integrin to recruit leukocytes to the central nervous system in experimental autoimmune encephalomyelitis. J. Immunol. *169*, 1000–1006.

KIDD, M. (1963). Paired Helical Filaments in Electron Microscopy of Alzheimer's Disease. Nature *197*, 192–193.

Kim, J., Onstead, L., Randle, S., Price, R., Smithson, L., Zwizinski, C., Dickson, D.W., Golde, T., and McGowan, E. (2007). A 40 Inhibits Amyloid Deposition In Vivo. J. Neurosci. *27*, 627–633.

Kim, J., Yoon, H., Basak, J., and Kim, J. (2014). Apolipoprotein E in Synaptic Plasticity and Alzheimer's Disease: Potential Cellular and Molecular Mechanisms.

Mol. Cells *37*, 767–776.

Kinney, J.W., Bemiller, S.M., Murtishaw, A.S., Leisgang, A.M., Salazar, A.M., and Lamb, B.T. (2018). Inflammation as a central mechanism in Alzheimer's disease. Alzheimer's Dement. Transl. Res. Clin. Interv. *4*, 575–590.

Kipps, C.M., Mioshi, E., and Hodges, J.R. (2009). Emotion, social functioning and activities of daily living in frontotemporal dementia. Neurocase *15*, 182–189.

Klein, R. (2012). Eph/ephrin signalling during development. Development *139*, 4105–4109.

Kober, D.L., and Brett, T.J. (2017). TREM2-Ligand Interactions in Health and Disease. J. Mol. Biol. *429*, 1607–1629.

Koistinaho, M., Lin, S., Wu, X., Esterman, M., Koger, D., Hanson, J., Higgs, R., Liu, F., Malkani, S., Bales, K.R., et al. (2004). Apolipoprotein E promotes astrocyte colocalization and degradation of deposited amyloid-β peptides. Nat. Med. *10*, 719–726.

Krause, G., Winkler, L., Mueller, S.L., Haseloff, R.F., Piontek, J., and Blasig, I.E. (2008). Structure and function of claudins. Biochim. Biophys. Acta - Biomembr. *1778*, 631–645.

Kucia, M., Jankowski, K., Reca, R., Wysoczynski, M., Bandura, L., Allendorf, D.J., Zhang, J., Ratajczak, J., and Ratajczak, M.Z. (2003). CXCR4–SDF-1 Signalling, Locomotion, Chemotaxis and Adhesion. J. Mol. Histol. *35*, 233–245.

Kumar-Singh, S., Theuns, J., Van Broeck, B., Pirici, D., Vennekens, K., Corsmit, E., Cruts, M., Dermaut, B., Wang, R., and Van Broeckhoven, C. (2006). Mean age-of-onset of familial alzheimer disease caused by presenilin mutations correlates with both increased Abeta42 and decreased Abeta40. Hum. Mutat. *27*, 686–695.

Kunkel, E.J., and Ley, K. (1996). Distinct phenotype of E-selectin-deficient mice. E-selectin is required for slow leukocyte rolling in vivo. Circ. Res. *79*, 1196–1204.

Kunkle, B.W., Grenier-Boley, B., Sims, R., Bis, J.C., Damotte, V., Naj, A.C., Boland, A., Vronskaya, M., van der Lee, S.J., Amlie-Wolf, A., et al. (2019). Genetic meta-analysis of diagnosed Alzheimer's disease identifies new risk loci and implicates Aβ, tau, immunity and lipid processing. Nat. Genet. *51*, 414–430.

Lambert, J.-C., Heath, S., Even, G., Campion, D., Sleegers, K., Hiltunen, M., Combarros, O., Zelenika, D., Bullido, M.J., Tavernier, B., et al. (2009). Genome-wide association study identifies variants at CLU and CR1 associated with Alzheimer's disease. Nat. Genet. *41*, 1094–1099.

Lambert, J.-C., Ibrahim-Verbaas, C.A., Harold, D., Naj, A.C., Sims, R., Bellenguez, C., Jun, G., Destefano, A.L., Bis, J.C., Beecham, G.W., et al. (2013). Meta-analysis of 74,046 individuals identifies 11 new susceptibility loci for Alzheimer's disease. Nat.

Genet. *45*, 1452–1458.

Larson, J., Schomberg, S., Schroeder, W., and Carpenter, T.C. (2008). Endothelial EphA receptor stimulation increases lung vascular permeability. Am. J. Physiol. Cell. Mol. Physiol. *295*, L431–L439.

Leibson, C.L., Rocca, W.A., Hanson, V.A., Cha, R., Kokmen, E., O'Brien, P.C., and Palumbo, P.J. (1997). Risk of Dementia among Persons with Diabetes Mellitus: A Population-based Cohort Study. Am. J. Epidemiol. *145*, 301–308.

Ley, K., Laudanna, C., Cybulsky, M.I., and Nourshargh, S. (2007). Getting to the site of inflammation: the leukocyte adhesion cascade updated. Nat. Rev. Immunol. *7*, 678–689.

Lin, K.-T., Sloniowski, S., Ethell, D.W., and Ethell, I.M. (2008a). Ephrin-B2-induced cleavage of EphB2 receptor is mediated by matrix metalloproteinases to trigger cell repulsion. J. Biol. Chem. *283*, 28969–28979.

Lin, K.-T., Sloniowski, S., Ethell, D.W., and Ethell, I.M. (2008b). Ephrin-B2-induced Cleavage of EphB2 Receptor Is Mediated by Matrix Metalloproteinases to Trigger Cell Repulsion. J. Biol. Chem. *283*, 28969–28979.

Linder, S., and Aepfelbacher, M. (2003). Podosomes: adhesion hot-spots of invasive cells. Trends Cell Biol. *13*, 376–385.

Litterst, C., Georgakopoulos, A., Shioi, J., Ghersi, E., Wisniewski, T., Wang, R., Ludwig, A., and Robakis, N.K. (2007a). Ligand binding and calcium influx induce distinct ectodomain/gamma-secretase-processing pathways of EphB2 receptor. J. Biol. Chem. *282*, 16155–16163.

Litterst, C., Georgakopoulos, A., Shioi, J., Ghersi, E., Wisniewski, T., Wang, R., Ludwig, A., and Robakis, N.K. (2007b). Ligand Binding and Calcium Influx Induce Distinct Ectodomain/γ-Secretase-processing Pathways of EphB2 Receptor. J. Biol. Chem. *282*, 16155–16163.

Litterst, C., Georgakopoulos, A., Shioi, J., Ghersi, E., Wisniewski, T., Wang, R., Ludwig, A., and Robakis, N.K. (2007c). Ligand Binding and Calcium Influx Induce Distinct Ectodomain/γ-Secretase-processing Pathways of EphB2 Receptor. J. Biol. Chem. *282*, 16155–16163.

Liu, C.-H., and Wu, P.-S. (2006). Characterization of matrix metalloproteinase expressed by human embryonic kidney cells. Biotechnol. Lett. *28*, 1725–1730.

Liu, Y.-J., Guo, D.-W., Tian, L., Shang, D.-S., Zhao, W.-D., Li, B., Fang, W.-G., Zhu, L., and Chen, Y.-H. (2010a). Peripheral T cells derived from Alzheimer's disease patients overexpress CXCR2 contributing to its transendothelial migration, which is microglial TNF-α-dependent. Neurobiol. Aging *31*, 175–188.

Liu, Y., Nusrat, A., Schnell, F.J., Reaves, T.A., Walsh, S., Pochet, M., and Parkos, C.A.

(2000). Human junction adhesion molecule regulates tight junction resealing in epithelia. J. Cell Sci. *113*.

Liu, Z., Miner, J.J., Yago, T., Yao, L., Lupu, F., Xia, L., and McEver, R.P. (2010b). Differential regulation of human and murine P-selectin expression and function in vivo. J. Exp. Med. *207*, 2975–2987.

López-Otín, C., and Bond, J.S. (2008). Proteases: Multifunctional Enzymes in Life and Disease. J. Biol. Chem. *283*, 30433–30437.

Lu, D.C., Rabizadeh, S., Chandra, S., Shayya, R.F., Ellerby, L.M., Ye, X., Salvesen, G.S., Koo, E.H., and Bredesen, D.E. (2000). A second cytotoxic proteolytic peptide derived from amyloid β-protein precursor. Nat. Med. *6*, 397–404.

Lu, Q., Sun, E.E., Klein, R.S., and Flanagan, J.G. (2001). Ephrin-B Reverse Signaling Is Mediated by a Novel PDZ-RGS Protein and Selectively Inhibits G Protein–Coupled Chemoattraction. Cell *105*, 69–79.

Luissint, A.-C., Artus, C., Glacial, F., Ganeshamoorthy, K., and Couraud, P.-O. (2012). Tight junctions at the blood brain barrier: physiological architecture and disease-associated dysregulation. Fluids Barriers CNS *9*, 23.

Luo, Y., and Radice, G.L. (2005). N-cadherin acts upstream of VE-cadherin in controlling vascular morphogenesis. J. Cell Biol. *169*, 29–34.

Luo, H., Yu, G., Wu, Y., and Wu, J. (2002). EphB6 crosslinking results in costimulation of T cells. J. Clin. Invest. *110*, 1141–1150.

Luscinskas, F.W., Ding, H., Tan, P., Cumming, D., Tedder, T.F., and Gerritsen, M.E. (1996). L- and P-selectins, but not CD49d (VLA-4) integrins, mediate monocyte initial attachment to TNF-alpha-activated vascular endothelium under flow in vitro. J. Immunol. *157*, 326–335.

Luu, N.T., Rainger, G.E., and Nash, G.B. (2000). Differential Ability of Exogenous Chemotactic Agents to Disrupt Transendothelial Migration of Flowing Neutrophils. J. Immunol. *164*, 5961–5969.

Ma, R., Zhang, Y., Hong, X., Zhang, J., Wang, J.-Z., and Liu, G. (2017). Role of microtubule-associated protein tau phosphorylation in Alzheimer's disease. J. Huazhong Univ. Sci. Technol. [Medical Sci. *37*, 307–312.

Maccioni, R.B., Farías, G., Morales, I., and Navarrete, L. (2010). The Revitalized Tau Hypothesis on Alzheimer's Disease. Arch. Med. Res. *41*, 226–231.

Mahley, R.W., and Rall, S.C. (2000). A POLIPOPROTEIN E: Far More Than a Lipid Transport Protein. Annu. Rev. Genomics Hum. Genet. *1*, 507–537.

Mamdouh, Z., Mikhailov, A., and Muller, W.A. (2009). Transcellular migration of leukocytes is mediated by the endothelial lateral border recycling compartment. J.

Exp. Med. *206*, 2795–2808.

Man, S.-M., Ma, Y.-R., Shang, D.-S., Zhao, W.-D., Li, B., Guo, D.-W., Fang, W.-G., Zhu, L., and Chen, Y.-H. (2007). Peripheral T cells overexpress MIP-1α to enhance its transendothelial migration in Alzheimer's disease. Neurobiol. Aging *28*, 485–496.

MARCHESI, V.T. (1961). The site of leucocyte emigration during inflammation. Q. J. Exp. Physiol. Cogn. Med. Sci. *46*, 115–118.

MARCHESI, V.T., and FLOREY, H.W. (1960). Electron micrographic observations on the emigration of leucocytes. Q. J. Exp. Physiol. Cogn. Med. Sci. *45*, 343–348.

Marston, D.J., Dickinson, S., and Nobes, C.D. (2003). Rac-dependent trans-endocytosis of ephrinBs regulates Eph–ephrin contact repulsion. Nat. Cell Biol. *5*, 879–888.

Mass, E., Jacome-Galarza, C.E., Blank, T., Lazarov, T., Durham, B.H., Ozkaya, N., Pastore, A., Schwabenland, M., Chung, Y.R., Rosenblum, M.K., et al. (2017). A somatic mutation in erythro-myeloid progenitors causes neurodegenerative disease. Nature *549*, 389–393.

Matsuoka, Y., Picciano, M., Malester, B., LaFrancois, J., Zehr, C., Daeschner, J.M., Olschowka, J.A., Fonseca, M.I., O'Banion, M.K., Tenner, A.J., et al. (2001). Inflammatory Responses to Amyloidosis in a Transgenic Mouse Model of Alzheimer's Disease. Am. J. Pathol. *158*, 1345–1354.

McEver, R.P. (2015). Selectins: initiators of leucocyte adhesion and signalling at the vascular wall. Cardiovasc. Res. *107*, 331–339.

McKhann, G., Drachman, D., Folstein, M., Katzman, R., Price, D., and Stadlan, E.M. (1984). Clinical diagnosis of Alzheimer's disease: report of the NINCDS-ADRDA Work Group under the auspices of Department of Health and Human Services Task Force on Alzheimer's Disease. Neurology *34*, 939–944.

McKhann, G.M., Knopman, D.S., Chertkow, H., Hyman, B.T., Jack, C.R., Kawas, C.H., Klunk, W.E., Koroshetz, W.J., Manly, J.J., Mayeux, R., et al. (2011a). The diagnosis of dementia due to Alzheimer's disease: recommendations from the National Institute on Aging-Alzheimer's Association workgroups on diagnostic guidelines for Alzheimer's disease. Alzheimers. Dement. *7*, 263–269.

McKhann, G.M., Knopman, D.S., Chertkow, H., Hyman, B.T., Jack, C.R., Kawas, C.H., Klunk, W.E., Koroshetz, W.J., Manly, J.J., Mayeux, R., et al. (2011b). The diagnosis of dementia due to Alzheimer's disease: recommendations from the National Institute on Aging-Alzheimer's Association workgroups on diagnostic guidelines for Alzheimer's disease. Alzheimers. Dement. *7*, 263–269.

Medzhitov, R. (2008). Origin and physiological roles of inflammation. Nature *454*, 428–435.

Miao, H., Wei, B.R., Peehl, D.M., Li, Q., Alexandrou, T., Schelling, J.R., Rhim, J.S., Sedor, J.R., Burnett, E., and Wang, B. (2001). Activation of EphA receptor tyrosine kinase inhibits the Ras/MAPK pathway. Nat. Cell Biol. *3*, 527–530.

Miao, H., Li, D.-Q., Mukherjee, A., Guo, H., Petty, A., Cutter, J., Basilion, J.P., Sedor, J., Wu, J., Danielpour, D., et al. (2009). EphA2 Mediates Ligand-Dependent Inhibition and Ligand-Independent Promotion of Cell Migration and Invasion via a Reciprocal Regulatory Loop with Akt. Cancer Cell *16*, 9–20.

Mildner, A., Schmidt, H., Nitsche, M., Merkler, D., Hanisch, U.-K., Mack, M., Heikenwalder, M., Brück, W., Priller, J., and Prinz, M. (2007). Microglia in the adult brain arise from Ly-6ChiCCR2+ monocytes only under defined host conditions. Nat. Neurosci. *10*, 1544–1553.

Mimche, P.N., Brady, L.M., Keeton, S., Fenne, D.S.J., King, T.P., Quicke, K.M., Hudson, L.E., and Lamb, T.J. (2015). Expression of the Receptor Tyrosine Kinase EphB2 on Dendritic Cells Is Modulated by Toll-Like Receptor Ligation but Is Not Required for T Cell Activation. PLoS One *10*, e0138835.

Mitroulis, I., Alexaki, V.I., Kourtzelis, I., Ziogas, A., Hajishengallis, G., and Chavakis, T. (2015). Leukocyte integrins: role in leukocyte recruitment and as therapeutic targets in inflammatory disease. Pharmacol. Ther. *147*, 123–135.

Montagne, A., Barnes, S.R., Sweeney, M.D., Halliday, M.R., Sagare, A.P., Zhao, Z., Toga, A.W., Jacobs, R.E., Liu, C.Y., Amezcua, L., et al. (2015). Blood-brain barrier breakdown in the aging human hippocampus. Neuron *85*, 296–302.

Moriki, T., Maruyama, H., and Maruyama, I.N. (2001). Activation of preformed EGF receptor dimers by ligand-induced rotation of the transmembrane domain11Edited by B. Holland. J. Mol. Biol. *311*, 1011–1026.

Muller, W.A. (2013). Getting Leukocytes to the Site of Inflammation. Vet. Pathol. *50*, 7–22.

Muller, W.A. (2015). The regulation of transendothelial migration: new knowledge and new questions. Cardiovasc. Res. *107*, 310–320.

Muller, W.A., Weigl, S.A., Deng, X., and Phillips, D.M. (1993). PECAM-1 is required for transendothelial migration of leukocytes. J. Exp. Med. *178*, 449–460.

Müller, T., Meyer, H.E., Egensperger, R., and Marcus, K. (2008). The amyloid precursor protein intracellular domain (AICD) as modulator of gene expression, apoptosis, and cytoskeletal dynamics—Relevance for Alzheimer's disease. Prog. Neurobiol. *85*, 393–406.

Nagele, R.G., D'Andrea, M.R., Lee, H., Venkataraman, V., and Wang, H.-Y. (2003). Astrocytes accumulate A beta 42 and give rise to astrocytic amyloid plaques in Alzheimer disease brains. Brain Res. *971*, 197–209.

Naj, A.C., Jun, G., Beecham, G.W., Wang, L.-S., Vardarajan, B.N., Buros, J., Gallins, P.J., Buxbaum, J.D., Jarvik, G.P., Crane, P.K., et al. (2011). Common variants at MS4A4/MS4A6E, CD2AP, CD33 and EPHA1 are associated with late-onset Alzheimer's disease. Nat. Genet. *43*, 436–441.

Nakanishi, H., Nakamura, T., Canaani, E., and Croce, C.M. (2007). ALL1 fusion proteins induce deregulation of EphA7 and ERK phosphorylation in human acute leukemias. Proc. Natl. Acad. Sci. *104*, 14442–14447.

Newcombe, E.A., Camats-Perna, J., Silva, M.L., Valmas, N., Huat, T.J., and Medeiros, R. (2018). Inflammation: the link between comorbidities, genetics, and Alzheimer's disease. J. Neuroinflammation *15*, 276.

Nie, Z., Fryer, A.D., and Jacoby, D.B. (2012). β2-Agonists inhibit TNF-α-induced ICAM-1 expression in human airway parasympathetic neurons. PLoS One *7*, e44780.

Nishida, N., Xie, C., Shimaoka, M., Cheng, Y., Walz, T., and Springer, T.A. (2006). Activation of leukocyte beta2 integrins by conversion from bent to extended conformations. Immunity *25*, 583–594.

Noberini, R., Rubio de la Torre, E., and Pasquale, E.B. (2012). Profiling Eph receptor expression in cells and tissues. Cell Adh. Migr. *6*, 102–156.

Nourshargh, S., and Alon, R. (2014). Leukocyte Migration into Inflamed Tissues. Immunity *41*, 694–707.

O'Brien, R.J., and Wong, P.C. (2011). Amyloid Precursor Protein Processing and Alzheimer's Disease. Annu. Rev. Neurosci. *34*, 185.

Oka, T., Oka, K., Kobayashi, T., Sugimoto, Y., Ichikawa, A., Ushikubi, F., Narumiya, S., and Saper, C.B. (2003). Characteristics of thermoregulatory and febrile responses in mice deficient in prostaglandin EP1 and EP3 receptors. J. Physiol. *551*, 945–954.

Olsson, F., Schmidt, S., Althoff, V., Munter, L.M., Jin, S., Rosqvist, S., Lendahl, U., Multhaup, G., and Lundkvist, J. (2014). Characterization of Intermediate Steps in Amyloid Beta (Aβ) Production under Near-native Conditions. J. Biol. Chem. *289*, 1540–1550.

Oostingh, G.J., Schlickum, S., Friedl, P., and Schön, M.P. (2007). Impaired induction of adhesion molecule expression in immortalized endothelial cells leads to functional defects in dynamic interactions with lymphocytes. J. Invest. Dermatol. *127*, 2253–2258.

Ostermann, G., Weber, K.S.C., Zernecke, A., Schröder, A., and Weber, C. (2002). JAM-I is a ligand of the β2 integrin LFA-I involved in transendothelial migration of leukocytes. Nat. Immunol. *3*, 151–158.

Page-McCaw, A., Ewald, A.J., and Werb, Z. (2007). Matrix metalloproteinases and the regulation of tissue remodelling. Nat. Rev. Mol. Cell Biol. *8*, 221–233.

Pan, J., Xia, L., and McEver, R.P. (1998). Comparison of Promoters for the Murine and Human P-selectin Genes Suggests Species-specific and Conserved Mechanisms for Transcriptional Regulation in Endothelial Cells. J. Biol. Chem. *273*, 10058–10067.

Pasquale, E.B. (2010). Eph receptors and ephrins in cancer: bidirectional signalling and beyond. Nat. Rev. Cancer *10*, 165–180.

Peled, A., Grabovsky, V., Habler, L., Sandbank, J., Arenzana-Seisdedos, F., Petit, I., Ben-Hur, H., Lapidot, T., and Alon, R. (1999). The chemokine SDF-1 stimulates integrin-mediated arrest of CD34+ cells on vascular endothelium under shear flow. J. Clin. Invest. *104*, 1199–1211.

Peled, A., Kollet, O., Ponomaryov, T., Petit, I., Franitza, S., Grabovsky, V., Slav, M.M., Nagler, A., Lider, O., Alon, R., et al. (2000). The chemokine SDF-1 activates the integrins LFA-1, VLA-4, and VLA-5 on immature human CD34(+) cells: role in transendothelial/stromal migration and engraftment of NOD/SCID mice. Blood *95*, 3289–3296.

Perl, D.P. (2010). Neuropathology of Alzheimer's disease. Mt. Sinai J. Med. *77*, 32–42.

Pfaff, D., Heroult, M., Riedel, M., Reiss, Y., Kirmse, R., Ludwig, T., Korff, T., Hecker, M., and Augustin, H.G. (2008). Involvement of endothelial ephrin-B2 in adhesion and transmigration of EphB-receptor-expressing monocytes. J. Cell Sci. *121*, 3842–3850.

Phillipson, M., Kaur, J., Colarusso, P., Ballantyne, C.M., and Kubes, P. (2008). Endothelial Domes Encapsulate Adherent Neutrophils and Minimize Increases in Vascular Permeability in Paracellular and Transcellular Emigration. PLoS One *3*, e1649.

Piazzini, V., Landucci, E., Graverini, G., Pellegrini-Giampietro, D., Bilia, A., and Bergonzi, M. (2018). Stealth and Cationic Nanoliposomes as Drug Delivery Systems to Increase Andrographolide BBB Permeability. Pharmaceutics *10*, 128.

Pietronigro, E.C., Bianca, V. Della, Zenaro, E., and Constantin, G. (2017). NETosis in Alzheimer's Disease. Front. Immunol. *8*, 211.

Piontek, J., Winkler, L., Wolburg, H., Müller, S.L., Zuleger, N., Piehl, C., Wiesner, B., Krause, G., and Blasig, I.E. (2008). Formation of tight junction: determinants of homophilic interaction between classic claudins. FASEB J. *22*, 146–158.

Pober, J.S., and Sessa, W.C. (2007). Evolving functions of endothelial cells in inflammation. Nat. Rev. Immunol. *7*, 803–815.

Priller, C., Bauer, T., Mitteregger, G., Krebs, B., Kretzschmar, H.A., and Herms, J. (2006). Synapse Formation and Function Is Modulated by the Amyloid Precursor Protein. J. Neurosci. *26*, 7212–7221.

Prince, M., Knapp, M., Guerchet, M., McCrone, P., Prina, M., Comas-Herrera, A.,

Wittenberg, R., Adelaja, B., Hu, B., King, D., et al. (2014). Dementia UK: second edition - overview.

Proebstl, D., Voisin, M.-B., Woodfin, A., Whiteford, J., D'Acquisto, F., Jones, G.E., Rowe, D., and Nourshargh, S. (2012). Pericytes support neutrophil subendothelial cell crawling and breaching of venular walls in vivo. J. Exp. Med. *209*, 1219–1234.

Qiu, C., Kivipelto, M., and von Strauss, E. (2009). Epidemiology of Alzheimer's disease: occurrence, determinants, and strategies toward intervention. Dialogues Clin. Neurosci. *11*, 111–128.

Rademakers, R., Cruts, M., and Van Broeckhoven, C. (2003). Genetics of Early-Onset Alzheimer Dementia. Sci. World J. *3*, 497–519.

Rainger, G.E., Fisher, A.C., and Nash, G.B. (1997). Endothelial-borne platelet-activating factor and interleukin-8 rapidly immobilize rolling neutrophils. Am. J. Physiol. *272*, H114-22.

Ransohoff, R.M., Kivisäkk, P., and Kidd, G. (2003). Three or more routes for leukocyte migration into the central nervous system. Nat. Rev. Immunol. *3*, 569–581.

Ratajczak, M.Z., Majka, M., Kucia, M., Drukala, J., Pietrzkowski, Z., Peiper, S., and Janowska-Wieczorek, A. (2003). Expression of Functional CXCR4 by Muscle Satellite Cells and Secretion of SDF-1 by Muscle-Derived Fibroblasts is Associated with the Presence of Both Muscle Progenitors in Bone Marrow and Hematopoietic Stem/Progenitor Cells in Muscles. Stem Cells *21*, 363–371.

Raux, G., Guyant-Maréchal, L., Martin, C., Bou, J., Penet, C., Brice, A., Hannequin, D., Frebourg, T., and Campion, D. (2005). Molecular diagnosis of autosomal dominant early onset Alzheimer's disease: an update. J. Med. Genet. *42*, 793–795.

Rebeck, G.W., Reiter, J.S., Strickland, D.K., and Hyman, B.T. (1993). Apolipoprotein E in sporadic Alzheimer's disease: allelic variation and receptor interactions. Neuron *11*, 575–580.

Redzic, Z. (2011). Molecular biology of the blood-brain and the blood-cerebrospinal fluid barriers: similarities and differences. Fluids Barriers CNS *8*, 3.

Reijerkerk, A., Kooij, G., van der Pol, S.M.A., Leyen, T., van het Hof, B., Couraud, P.-O., Vivien, D., Dijkstra, C.D., and de Vries, H.E. (2008). Tissue-Type Plasminogen Activator Is a Regulator of Monocyte Diapedesis through the Brain Endothelial Barrier. J. Immunol. *181*, 3567–3574.

Reiman, E.M., Chen, K., Liu, X., Bandy, D., Yu, M., Lee, W., Ayutyanont, N., Keppler, J., Reeder, S.A., Langbaum, J.B.S., et al. (2009). Fibrillar amyloid- burden in cognitively normal people at 3 levels of genetic risk for Alzheimer's disease. Proc. Natl. Acad. Sci. *106*, 6820–6825.

Ridge, P.G., Ebbert, M.T.W., and Kauwe, J.S.K. (2013a). Genetics of Alzheimer's

disease. Biomed Res. Int. *2013*, 254954.

Ridge, P.G., Ebbert, M.T.W., and Kauwe, J.S.K. (2013b). Genetics of Alzheimer's disease. Biomed Res. Int. *2013*, 254954.

Ridley, A.J., Schwartz, M.A., Burridge, K., Firtel, R.A., Ginsberg, M.H., Borisy, G., Parsons, J.T., and Horwitz, A.R. (2003). Cell Migration: Integrating Signals from Front to Back. Science (80-.). *302*, 1704–1709.

Ries, M., and Sastre, M. (2016). Mechanisms of Aβ Clearance and Degradation by Glial Cells. Front. Aging Neurosci. *8*, 160.

Rivera-Nieves, J., Burcin, T.L., Olson, T.S., Morris, M.A., McDuffie, M., Cominelli, F., and Ley, K. (2006). Critical role of endothelial P-selectin glycoprotein ligand 1 in chronic murine ileitis. J. Exp. Med. *203*, 907–917.

Romanovsky, A.A., Kulchitsky, V.A., Simons, C.T., and Sugimoto, N. (1998). Methodology of fever research: why are polyphasic fevers often thought to be biphasic? Am. J. Physiol. Integr. Comp. Physiol. *275*, R332–R338.

Ruiz, A., Heilmann, S., Becker, T., Hernández, I., Wagner, H., Thelen, M., Mauleón, A., Rosende-Roca, M., Bellenguez, C., Bis, J.C., et al. (2014). Follow-up of loci from the International Genomics of Alzheimer's Disease Project identifies TRIP4 as a novel susceptibility gene. Transl. Psychiatry *4*, e358–e358.

Sabbagh, M.N., Lue, L.-F., Fayard, D., and Shi, J. (2017). Increasing Precision of Clinical Diagnosis of Alzheimer's Disease Using a Combined Algorithm Incorporating Clinical and Novel Biomarker Data. Neurol. Ther. *6*, 83–95.

Sajja, V.S.S.S., Hlavac, N., and VandeVord, P.J. (2016). Role of Glia in Memory Deficits Following Traumatic Brain Injury: Biomarkers of Glia Dysfunction. Front. Integr. Neurosci. *10*, 7.

Salas, A., Shimaoka, M., Kogan, A.N., Harwood, C., von Andrian, U.H., and Springer, T.A. (2004). Rolling Adhesion through an Extended Conformation of Integrin αLβ2 and Relation to α I and β I-like Domain Interaction. Immunity *20*, 393–406.

Salat, D.H., Kaye, J.A., and Janowsky, J.S. (2001). Selective Preservation and Degeneration Within the Prefrontal Cortex in Aging and Alzheimer Disease. Arch. Neurol. *58*, 1403.

Sanders, W.E., Wilson, R.W., Ballantyne, C.M., and Beaudet, A.L. (1992). Molecular cloning and analysis of in vivo expression of murine P-selectin. Blood *80*, 795–800.

Sawa, Y., Sugimoto, Y., Ueki, T., Ishikawa, H., Sato, A., Nagato, T., and Yoshida, S. (2007). Effects of TNF-α on Leukocyte Adhesion Molecule Expressions in Cultured Human Lymphatic Endothelium. J. Histochem. Cytochem. *55*, 721–733.

Schenkel, A.R., Mamdouh, Z., Chen, X., Liebman, R.M., and Muller, W.A. (2002). CD99 plays a major role in the migration of monocytes through endothelial junctions. Nat. Immunol. *3*, 143–150.

Schlessinger, J. (2000). Cell signaling by receptor tyrosine kinases. Cell *103*, 211–225.

Schmid, C.D., Sautkulis, L.N., Danielson, P.E., Cooper, J., Hasel, K.W., Hilbush, B.S., Sutcliffe, J.G., and Carson, M.J. (2002). Heterogeneous expression of the triggering receptor expressed on myeloid cells-2 on adult murine microglia. J. Neurochem. *83*, 1309–1320.

Schnoor, M., Lai, F.P.L., Zarbock, A., Kläver, R., Polaschegg, C., Schulte, D., Weich, H.A., Oelkers, J.M., Rottner, K., and Vestweber, D. (2011). Cortactin deficiency is associated with reduced neutrophil recruitment but increased vascular permeability in vivo. J. Exp. Med. *208*, 1721–1735.

Schreiber, T.H., Shinder, V., Cain, D.W., Alon, R., and Sackstein, R. (2007). Shear flow-dependent integration of apical and subendothelial chemokines in T-cell transmigration: implications for locomotion and the multistep paradigm. Blood *109*, 1381–1386.

Schütz, M., Teifel, M., and Friedl, P. (1997). Establishment of a human placental endothelial cell line with extended life span after transfection with SV 40 T-antigens. Eur. J. Cell Biol. *74*, 315–320.

Seiradake, E., Harlos, K., Sutton, G., Aricescu, A.R., and Jones, E.Y. (2010). An extracellular steric seeding mechanism for Eph-ephrin signaling platform assembly. Nat. Struct. Mol. Biol. *17*, 398–402.

Seiradake, E., Schaupp, A., del Toro Ruiz, D., Kaufmann, R., Mitakidis, N., Harlos, K., Aricescu, A.R., Klein, R., and Jones, E.Y. (2013). Structurally encoded intraclass differences in EphA clusters drive distinct cell responses. Nat. Struct. Mol. Biol. *20*, 958–964.

Selkoe, D.J., and Hardy, J. (2016). The amyloid hypothesis of Alzheimer's disease at 25 years. EMBO Mol. Med. *8*, 595–608.

Serlin, Y., Shelef, I., and Knyazer, B. (2015). Anatomy and physiology of the blood–brain barrier. Semin. Cell Dev. Biol. *38*, 2–6.

Seshadri, S., Fitzpatrick, A.L., Ikram, M.A., DeStefano, A.L., Gudnason, V., Boada, M., Bis, J.C., Smith, A. V, Carassquillo, M.M., Lambert, J.C., et al. (2010). Genome-wide Analysis of Genetic Loci Associated With Alzheimer Disease. JAMA *303*, 1832.

Sessa, G., Podini, P., Mariani, M., Meroni, A., Spreafico, R., Sinigaglia, F., Colonna, M., Panina, P., and Meldolesi, J. (2004). Distribution and signaling of TREM2/DAP12, the receptor system mutated in human polycystic lipomembraneous osteodysplasia with sclerosing leukoencephalopathy dementia. Eur. J. Neurosci. *20*, 2617–2628.

Sharfe, N., Freywald, A., Toro, A., Dadi, H., and Roifman, C. (2002). Ephrin stimulation modulates T?cell chemotaxis. Eur. J. Immunol. *32*, 3745–3755.

Sharfe, N., Nikolic, M., Cimpeon, L., Van De Kratts, A., Freywald, A., and Roifman, C.M. (2008a). EphA and ephrin-A proteins regulate integrin-mediated T lymphocyte interactions. Mol. Immunol. *45*, 1208–1220.

Sharfe, N., Nikolic, M., Cimpeon, L., Van De Kratts, A., Freywald, A., and Roifman, C.M. (2008b). EphA and ephrin-A proteins regulate integrin-mediated T lymphocyte interactions. Mol. Immunol. *45*, 1208–1220.

Shi, X., Hapiak, V., Zheng, J., Muller-Greven, J., Bowman, D., Lingerak, R., Buck, M., Wang, B.-C., and Smith, A.W. (2017). A role of the SAM domain in EphA2 receptor activation. Sci. Rep. *7*, 45084.

Signoret, N., Rosenkilde, M.M., Klasse, P.J., Schwartz, T.W., Malim, M.H., Hoxie, J.A., and Marsh, M. (1998). Differential regulation of CXCR4 and CCR5 endocytosis. J. Cell Sci. *111 (Pt 18)*, 2819–2830.

Sims, R., van der Lee, S.J., Naj, A.C., Bellenguez, C., Badarinarayan, N., Jakobsdottir, J., Kunkle, B.W., Boland, A., Raybould, R., Bis, J.C., et al. (2017). Rare coding variants in PLCG2, ABI3, and TREM2 implicate microglial-mediated innate immunity in Alzheimer's disease. Nat. Genet. *49*, 1373–1384.

Singh, D.R., Cao, Q., King, C., Salotto, M., Ahmed, F., Zhou, X.Y., Pasquale, E.B., and Hristova, K. (2015). Unliganded EphA3 dimerization promoted by the SAM domain. Biochem. J. *471*, 101–109.

Sjöbeck, M., Haglund, M., and Englund, E. (2005). Decreasing myelin density reflected increasing white matter pathology in Alzheimer's disease--a neuropathological study. Int. J. Geriatr. Psychiatry *20*, 919–926.

Sleegers, K., Brouwers, N., Gijselinck, I., Theuns, J., Goossens, D., Wauters, J., Del-Favero, J., Cruts, M., Duijn, C.M. v., and Broeckhoven, C. V. (2006). APP duplication is sufficient to cause early onset Alzheimer's dementia with cerebral amyloid angiopathy. Brain *129*, 2977–2983.

Sloane, P.D., Zimmerman, S., Suchindran, C., Reed, P., Wang, L., Boustani, M., and Sudha, S. (2002). The Public Health Impact of Alzheimer's Disease, 2000–2050: Potential Implication of Treatment Advances. Annu. Rev. Public Health *23*, 213–231.

Smith, C.W., Kishimoto, T.K., Abbassi, O., Hughes, B., Rothlein, R., McIntire, L. V, Butcher, E., Anderson, D.C., and Abbass, O. (1991). Chemotactic factors regulate lectin adhesion molecule 1 (LECAM-1)-dependent neutrophil adhesion to cytokine-stimulated endothelial cells in vitro. J. Clin. Invest. *87*, 609–618.

Smits, H.A., Rijsmus, A., van Loon, J.H., Wat, J.W.Y., Verhoef, J., Boven, L.A., and Nottet, H.S.L.M. (2002). Amyloid-beta-induced chemokine production in primary

human macrophages and astrocytes. J. Neuroimmunol. *127*, 160–168.

Sorensen, E.W., Lian, J., Ozga, A.J., Miyabe, Y., Ji, S.W., Bromley, S.K., Mempel, T.R., and Luster, A.D. (2018). CXCL10 stabilizes T cell-brain endothelial cell adhesion leading to the induction of cerebral malaria. JCI Insight *3*.

Spangenberg, E.E., and Green, K.N. (2017). Inflammation in Alzheimer's disease: Lessons learned from microglia-depletion models. Brain. Behav. Immun. *61*, 1–11.

Sperling, R.A., Aisen, P.S., Beckett, L.A., Bennett, D.A., Craft, S., Fagan, A.M., Iwatsubo, T., Jack, C.R., Kaye, J., Montine, T.J., et al. (2011). Toward defining the preclinical stages of Alzheimer's disease: recommendations from the National Institute on Aging-Alzheimer's Association workgroups on diagnostic guidelines for Alzheimer's disease. Alzheimers. Dement. *7*, 280–292.

Stamatovic, S.M., Johnson, A.M., Keep, R.F., and Andjelkovic, A. V (2016). Junctional proteins of the blood-brain barrier: New insights into function and dysfunction. Tissue Barriers *4*, e1154641.

Strober, W. (2001). Trypan blue exclusion test of cell viability. Curr. Protoc. Immunol. *Appendix 3*, Appendix 3B.

Stumm, R.K., Rummel, J., Junker, V., Culmsee, C., Pfeiffer, M., Krieglstein, J., Höllt, V., and Schulz, S. (2002). A dual role for the SDF-1/CXCR4 chemokine receptor system in adult brain: isoform-selective regulation of SDF-1 expression modulates CXCR4-dependent neuronal plasticity and cerebral leukocyte recruitment after focal ischemia. J. Neurosci. *22*, 5865–5878.

Subileau, E.A., Rezaie, P., Davies, H.A., Colyer, F.M., Greenwood, J., Male, D.K., and Romero, I.A. (2009). Expression of Chemokines and Their Receptors by Human Brain Endothelium: Implications for Multiple Sclerosis. J. Neuropathol. Exp. Neurol. *68*, 227–240.

Suenobu, S., Takakura, N., Inada, T., Yamada, Y., Yuasa, H., Zhang, X.-Q., Sakano, S., Oike, Y., and Suda, T. (2002). A role of EphB4 receptor and its ligand, ephrin-B2, in erythropoiesis. Biochem. Biophys. Res. Commun. *293*, 1124–1131.

Sugiyama, N., Gucciardo, E., Tatti, O., Varjosalo, M., Hyytiäinen, M., Gstaiger, M., and Lehti, K. (2013). EphA2 cleavage by MT1-MMP triggers single cancer cell invasion via homotypic cell repulsion. J. Cell Biol. *201*, 467–484.

Sun, L., Zhou, R., Yang, G., and Shi, Y. (2017). Analysis of 138 pathogenic mutations in presenilin-1 on the in vitro production of Aβ42 and Aβ40 peptides by γ-secretase. Proc. Natl. Acad. Sci. *114*, E476–E485.

Sundd, P., Pospieszalska, M.K., and Ley, K. (2013). Neutrophil rolling at high shear: Flattening, catch bond behavior, tethers and slings. Mol. Immunol. *55*, 59–69.

Tai, L.M., Holloway, K.A., Male, D.K., Loughlin, A.J., and Romero, I.A. (2009).

Amyloid-β-induced occludin down-regulation and increased permeability in human brain endothelial cells is mediated by MAPK activation. J. Cell. Mol. Med. *14*, 1101–1112.

Takahashi, K., Rochford, C.D.P., and Neumann, H. (2005). Clearance of apoptotic neurons without inflammation by microglial triggering receptor expressed on myeloid cells-2. J. Exp. Med. *201*, 647–657.

Takami, M., Nagashima, Y., Sano, Y., Ishihara, S., Morishima-Kawashima, M., Funamoto, S., and Ihara, Y. (2009). -Secretase: Successive Tripeptide and Tetrapeptide Release from the Transmembrane Domain of -Carboxyl Terminal Fragment. J. Neurosci. *29*, 13042–13052.

Takeuchi, O., and Akira, S. (2010). Pattern Recognition Receptors and Inflammation. Cell *140*, 805–820.

Tanaka, M., Kamata, R., and Sakai, R. (2005). EphA2 Phosphorylates the Cytoplasmic Tail of Claudin-4 and Mediates Paracellular Permeability. J. Biol. Chem. *280*, 42375–42382.

Tarbell, J.M. (2010). Shear stress and the endothelial transport barrier. Cardiovasc. Res. *87*, 320–330.

Teich, A.F., and Arancio, O. (2012). Is the amyloid hypothesis of Alzheimer's disease therapeutically relevant? Biochem. J. *446*, 165–177.

Terry, R.D. (1963). THE FINE STRUCTURE OF NEUROFIBRILLARY TANGLES IN ALZHEIMER'S DISEASE. J. Neuropathol. Exp. Neurol. *22*, 629–642.

Thinakaran, G., and Koo, E.H. (2008). Amyloid precursor protein trafficking, processing, and function. J. Biol. Chem. *283*, 29615–29619.

Tremblay, Y.D.N., Vogeleer, P., Jacques, M., and Harel, J. (2015). High-throughput microfluidic method to study biofilm formation and host-pathogen interactions in pathogenic Escherichia coli. Appl. Environ. Microbiol. *81*, 2827–2840.

Trinidad, E.M., Zapata, A.G., and Alonso-Colmenar, L.M. (2010). Eph-ephrin bidirectional signaling comes into the context of lymphocyte transendothelial migration. Cell Adh. Migr. *4*, 363–367.

Tsukita, S., Furuse, M., and Itoh, M. (2001). Multifunctional strands in tight junctions. Nat. Rev. Mol. Cell Biol. *2*, 285–293.

Tzioras, M., Davies, C., Newman, A., Jackson, R., and Spires-Jones, T. (2019). Invited Review: APOE at the interface of inflammation, neurodegeneration and pathological protein spread in Alzheimer's disease. Neuropathol. Appl. Neurobiol. *45*, 327–346.

Vajkoczy, P., Laschinger, M., and Engelhardt, B. (2001). Alpha4-integrin-VCAM-1 binding mediates G protein-independent capture of encephalitogenic T cell blasts to

CNS white matter microvessels. J. Clin. Invest. *108*, 557–565.

Vaporciyan, A.A., DeLisser, H.M., Yan, H.C., Mendiguren, I.I., Thom, S.R., Jones, M.L., Ward, P.A., and Albelda, S.M. (1993). Involvement of platelet-endothelial cell adhesion molecule-1 in neutrophil recruitment in vivo. Science (80-.). *262*, 1580–1582.

Vardarajan, B.N., Ghani, M., Kahn, A., Sheikh, S., Sato, C., Barral, S., Lee, J.H., Cheng, R., Reitz, C., Lantigua, R., et al. (2015). Rare coding mutations identified by sequencing of Alzheimer disease genome-wide association studies loci. Ann. Neurol. *78*, 487–498.

Vearing, C.J., and Lackmann, M. (2005). Eph receptor signalling; dimerisation just isn't enough. Growth Factors *23*, 67–76.

Vecchi, M., and Carpenter, G. (1997). Constitutive proteolysis of the ErbB-4 receptor tyrosine kinase by a unique, sequential mechanism. J. Cell Biol. *139*, 995–1003.

Venetsanakos, E., Mirza, A., Fanton, C., Romanov, S.R., Tlsty, T., and McMahon, M. (2002). Induction of tubulogenesis in telomerase-immortalized human microvascular endothelial cells by glioblastoma cells. Exp. Cell Res. *273*, 21–33.

Verga, L., Frangione, B., Tagliavini, F., Giaccone, G., Migheli, A., and Bugiani, O. (1989). Alzheimer patients and Down patients: Cerebral preamyloid deposits differ ultrastructurally and histochemically from the amyloid of senile plaques. Neurosci. Lett. *105*, 294–299.

Verghese, P.B., Castellano, J.M., and Holtzman, D.M. (2011). Apolipoprotein E in Alzheimer's disease and other neurological disorders. Lancet. Neurol. *10*, 241–252.

VESTWEBER, D., and BLANKS, J.E. (1999). Mechanisms That Regulate the Function of the Selectins and Their Ligands. Physiol. Rev. *79*, 181–213.

Vleminckx, K., and Kemler, R. (1999). Cadherins and tissue formation: integrating adhesion and signaling. BioEssays *21*, 211–220.

Walker-Daniels, J., Riese, D.J., and Kinch, M.S. (2002a). c-Cbl-dependent EphA2 protein degradation is induced by ligand binding. Mol. Cancer Res. *1*, 79–87.

Walker-Daniels, J., Riese, D.J., and Kinch, M.S. (2002b). c-Cbl-dependent EphA2 protein degradation is induced by ligand binding. Mol. Cancer Res. *1*, 79–87.

Wallon, D., Rousseau, S., Rovelet-Lecrux, A., Quillard-Muraine, M., Guyant-Maréchal, L., Martinaud, O., Pariente, J., Puel, M., Rollin-Sillaire, A., Pasquier, F., et al. (2012). The French Series of Autosomal Dominant Early Onset Alzheimer's Disease Cases: Mutation Spectrum and Cerebrospinal Fluid Biomarkers. J. Alzheimer's Dis. *30*, 847–856.

Wang, H.-F., Tan, L., Hao, X.-K., Jiang, T., Tan, M.-S., Liu, Y., Zhang, D.-Q., and Yu,

J.-T. (2015a). Effect of EPHA1 genetic variation on cerebrospinal fluid and neuroimaging biomarkers in healthy, mild cognitive impairment and Alzheimer's disease cohorts. J. Alzheimers. Dis. *44*, 115–123.

Wang, X., Liu, Y., Cao, G., Zhang, X., Xu, H., Xu, H., and Wang, J. (2015b). Expression of the EphA1 protein is associated with Fuhrman nuclear grade in clear cell renal cell carcinomas. Int. J. Clin. Exp. Pathol. *8*, 6821–6827.

Wang, Y., Yu, H., Shan, Y., Tao, C., Wu, F., Yu, Z., Guo, P., Huang, J., Li, J., Zhu, Q., et al. (2016). EphA1 activation promotes the homing of endothelial progenitor cells to hepatocellular carcinoma for tumor neovascularization through the SDF-1/CXCR4 signaling pathway. J. Exp. Clin. Cancer Res. *35*, 65.

Wang, Y., Shang, Y., Li, J., Chen, W., Li, G., Wan, J., Liu, W., and Zhang, M. (2018). Specific Eph receptor-cytoplasmic effector signaling mediated by SAM–SAM domain interactions. Elife *7*.

Wang, Z., Miura, N., Bonelli, A., Mole, P., Carlesso, N., Olson, D.P., and Scadden, D.T. (2002). Receptor tyrosine kinase, EphB4 (HTK), accelerates differentiation of select human hematopoietic cells. Blood *99*, 2740–2747.

Wattmo, C., and Wallin, Å.K. (2017). Early- versus late-onset Alzheimer's disease in clinical practice: cognitive and global outcomes over 3 years. Alzheimers. Res. Ther. *9*, 70.

Weksler, B., Romero, I.A., and Couraud, P.-O. (2013). The hCMEC/D3 cell line as a model of the human blood brain barrier. Fluids Barriers CNS *10*, 16.

Weksler, B.B., Subileau, E.A., Perrière, N., Charneau, P., Holloway, K., Leveque, M., Tricoire-Leignel, H., Nicotra, A., Bourdoulous, S., Turowski, P., et al. (2005). Blood-brain barrier-specific properties of a human adult brain endothelial cell line. FASEB J. *19*, 1872–1874.

Weller, A., Isenmann, S., and Vestweber, D. (1992). Cloning of the mouse endothelial selectins. Expression of both E- and P-selectin is inducible by tumor necrosis factor alpha. J. Biol. Chem. *267*, 15176–15183.

Weller, R.O., Hawkes, C.A., Kalaria, R.N., Werring, D.J., and Carare, R.O. (2015). White Matter Changes in Dementia: Role of Impaired Drainage of Interstitial Fluid. Brain Pathol. *25*, 63–78.

West, H.L., Rebeck, G.W., and Hyman, B.T. (1994). Frequency of the apolipoprotein E epsilon 2 allele is diminished in sporadic Alzheimer disease. Neurosci. Lett. *175*, 46–48.

Whitmer, R.A., Sidney, S., Selby, J., Johnston, S.C., and Yaffe, K. (2005). Midlife cardiovascular risk factors and risk of dementia in late life. Neurology *64*, 277–281.

Williams, M.R., Azcutia, V., Newton, G., Alcaide, P., and Luscinskas, F.W. (2011).

Emerging mechanisms of neutrophil recruitment across endothelium. Trends Immunol. *32*, 461–469.

Winger, R.C., Koblinski, J.E., Kanda, T., Ransohoff, R.M., and Muller, W.A. (2014). Rapid Remodeling of Tight Junctions during Paracellular Diapedesis in a Human Model of the Blood–Brain Barrier. J. Immunol. *193*, 2427–2437.

Wolfe, M.S. (2007). When loss is gain: reduced presenilin proteolytic function leads to increased Aβ42/Aβ40. Talking Point on the role of presenilin mutations in Alzheimer disease. EMBO Rep. *8*, 136–140.

Wong, A.D., and Searson, P.C. (2014). Live-Cell Imaging of Invasion and Intravasation in an Artificial Microvessel Platform. Cancer Res. *74*, 4937–4945.

Wykosky, J., Gibo, D.M., Stanton, C., and Debinski, W. (2005). EphA2 as a Novel Molecular Marker and Target in Glioblastoma Multiforme. Mol. Cancer Res. *3*, 541–551.

Wykosky, J., Palma, E., Gibo, D.M., Ringler, S., Turner, C.P., and Debinski, W. (2008). Soluble monomeric EphrinA1 is released from tumor cells and is a functional ligand for the EphA2 receptor. Oncogene *27*, 7260–7273.

Wyss-Coray, T., and Rogers, J. (2012). Inflammation in Alzheimer Disease--A Brief Review of the Basic Science and Clinical Literature. Cold Spring Harb. Perspect. Med. *2*, a006346–a006346.

Wyss-Coray, T., Loike, J.D., Brionne, T.C., Lu, E., Anankov, R., Yan, F., Silverstein, S.C., and Husemann, J. (2003). Adult mouse astrocytes degrade amyloid-beta in vitro and in situ. Nat. Med. *9*, 453–457.

Xia, D., Watanabe, H., Wu, B., Lee, S.H., Li, Y., Tsvetkov, E., Bolshakov, V.Y., Shen, J., and Kelleher, R.J. (2015). Presenilin-1 Knockin Mice Reveal Loss-of-Function Mechanism for Familial Alzheimer's Disease. Neuron *85*, 967–981.

Xu, J., Litterst, C., Georgakopoulos, A., Zaganas, I., and Robakis, N.K. (2009a). Peptide EphB2/CTF2 generated by the gamma-secretase processing of EphB2 receptor promotes tyrosine phosphorylation and cell surface localization of N-methyl-D-aspartate receptors. J. Biol. Chem. *284*, 27220–27228.

Xu, J., Litterst, C., Georgakopoulos, A., Zaganas, I., and Robakis, N.K. (2009b). Peptide EphB2/CTF2 generated by the gamma-secretase processing of EphB2 receptor promotes tyrosine phosphorylation and cell surface localization of N-methyl-D-aspartate receptors. J. Biol. Chem. *284*, 27220–27228.

Xu, L., Nirwane, A., and Yao, Y. (2019). Basement membrane and blood–brain barrier. Stroke Vasc. Neurol. *4*, 78–82.

Yamaguchi, H., Ishiguro, K., Sugihara, S., Nakazato, Y., Kawarabayashi, T., Sun, X., and Hirai, S. (1994). Presence of apolipoprotein E on extracellular neurofibrillary

tangles and on meningeal blood vessels precedes the Alzheimer beta-amyloid deposition. Acta Neuropathol. *88*, 413–419.

Yamaguchi, H., Wyckoff, J., and Condeelis, J. (2005). Cell migration in tumors. Curr. Opin. Cell Biol. *17*, 559–564.

Yamazaki, T., Masuda, J., Omori, T., Usui, R., Akiyama, H., and Maru, Y. (2009). EphA1 interacts with integrin-linked kinase and regulates cell morphology and motility. J. Cell Sci. *122*, 243–255.

Yao, L., Setiadi, H., Xia, L., Laszik, Z., Taylor, F.B., and McEver, R.P. (1999). Divergent inducible expression of P-selectin and E-selectin in mice and primates. Blood *94*, 3820–3828.

Ye, F., and Zhang, M. (2013). Structures and target recognition modes of PDZ domains: recurring themes and emerging pictures. Biochem. J. *455*, 1–14.

Yin, K.-J., Cirrito, J.R., Yan, P., Hu, X., Xiao, Q., Pan, X., Bateman, R., Song, H., Hsu, F.-F., Turk, J., et al. (2006). Matrix Metalloproteinases Expressed by Astrocytes Mediate Extracellular Amyloid-beta Peptide Catabolism. J. Neurosci. *26*, 10939–10948.

Young-Pearse, T.L., Bai, J., Chang, R., Zheng, J.B., LoTurco, J.J., and Selkoe, D.J. (2007). A Critical Function for -Amyloid Precursor Protein in Neuronal Migration Revealed by In Utero RNA Interference. J. Neurosci. *27*, 14459–14469.

Yu, G., Luo, H., Wu, Y., and Wu, J. (2003a). Ephrin B2 Induces T Cell Costimulation. J. Immunol. *171*, 106–114.

Yu, G., Luo, H., Wu, Y., and Wu, J. (2003b). Mouse EphrinB3 Augments T-cell Signaling and Responses to T-cell Receptor Ligation. J. Biol. Chem. *278*, 47209–47216.

Yu, G., Luo, H., Wu, Y., and Wu, J. (2004). EphrinB1 Is Essential in T-cell-T-cell Co-operation during T-cell Activation. J. Biol. Chem. *279*, 55531–55539.

Zenaro, E., Pietronigro, E., Bianca, V. Della, Piacentino, G., Marongiu, L., Budui, S., Turano, E., Rossi, B., Angiari, S., Dusi, S., et al. (2015a). Neutrophils promote Alzheimer's disease–like pathology and cognitive decline via LFA-1 integrin. Nat. Med. *21*, 880–886.

Zenaro, E., Pietronigro, E., Bianca, V. Della, Piacentino, G., Marongiu, L., Budui, S., Turano, E., Rossi, B., Angiari, S., Dusi, S., et al. (2015b). Neutrophils promote Alzheimer's disease–like pathology and cognitive decline via LFA-1 integrin. Nat. Med. *21*, 880–886.

Zenaro, E., Piacentino, G., and Constantin, G. (2017). The blood-brain barrier in Alzheimer's disease. Neurobiol. Dis. *107*, 41–56.

Zhang, B., Gaiteri, C., Bodea, L.-G., Wang, Z., McElwee, J., Podtelezhnikov, A.A.,

Zhang, C., Xie, T., Tran, L., Dobrin, R., et al. (2013). Integrated Systems Approach Identifies Genetic Nodes and Networks in Late-Onset Alzheimer's Disease. Cell *153*, 707–720.

Zhao, J., O'Connor, T., and Vassar, R. (2011). The contribution of activated astrocytes to Aβ production: Implications for Alzheimer's disease pathogenesis. J. Neuroinflammation *8*, 150.

Zheng, Y., Schlöndorff, J., and Blobel, C.P. (2002). Evidence for Regulation of the Tumor Necrosis Factor α-Convertase (TACE) by Protein-tyrosine Phosphatase PTPH1. J. Biol. Chem. *277*, 42463–42470.

Zheng, Y., Chen, J., Craven, M., Choi, N.W., Totorica, S., Diaz-Santana, A., Kermani, P., Hempstead, B., Fischbach-Teschl, C., Lopez, J.A., et al. (2012). In vitro microvessels for the study of angiogenesis and thrombosis. Proc. Natl. Acad. Sci. *109*, 9342–9347.

Zhu, X.-C., Tan, L., Wang, H.-F., Jiang, T., Cao, L., Wang, C., Wang, J., Tan, C.-C., Meng, X.-F., and Yu, J.-T. (2015a). Rate of early onset Alzheimer's disease: a systematic review and meta-analysis. Ann. Transl. Med. *3*, 38.

Zhu, X.-C., Tan, L., Wang, H.-F., Jiang, T., Cao, L., Wang, C., Wang, J., Tan, C.-C., Meng, X.-F., and Yu, J.-T. (2015b). Rate of early onset Alzheimer's disease: a systematic review and meta-analysis. Ann. Transl. Med. *3*, 38.

Zhu, Y., Shen, T., Lin, Y., Chen, B., Ruan, Y., Cao, Y., Qiao, Y., Man, Y., Wang, S., and Li, J. (2013). Astragalus polysaccharides suppress ICAM-1 and VCAM-1 expression in TNF-α-treated human vascular endothelial cells by blocking NF-κB activation. Acta Pharmacol. Sin. *34*, 1036–1042.

Zimmer, M., Palmer, A., Köhler, J., and Klein, R. (2003). EphB–ephrinB bi-directional endocytosis terminates adhesion allowing contact mediated repulsion. Nat. Cell Biol. *5*, 869–878.

Zuidema, M.Y., and Korthuis, R.J. (2015). Intravital Microscopic Methods to Evaluate Anti-inflammatory Effects and Signaling Mechanisms Evoked by Hydrogen Sulfide. Methods Enzymol. *555*, 93.

Appendix I: Solutions and buffers

Buffer	Recipe
50mM NH_4Cl	0.027g NH_4Cl 10mL ddH_2O
ECL solution	1:50 Solution A:Solution B
FACs buffer	Phosphate buffered saline 1 % Fetal Bovine Serum (v/v)
LB Agar	1 Ll of LB Broth 15g agar
Lysis buffer	1% Triton X-100 2% glycerol 1mM ethylenediaminetetraacetic acid 10mM $MgCl_2$ 25mM 4-(2-hydroxyethyl)-1- piperazineethanesulfonic acid pH 7.4 150mM NaCl 0.05% orthophenantroline 1x protease inhibitor cocktail
PBS-T	1 X PBS 0.1% Tween 20
SDS (4X) reducing buffer/Laemmli buffer	660 mM Tris-HCl (pH 6.8) 26 % glycerol (v/v) 4 % SDS (w/v) 0.01 % bromophenol blue (w/v) 5 % β2-meracaptoethanol (v/v).
Western blotting running buffer	10% SDS 2.5mM tris-base 192mM glycine ddH2O
Western blotting transfer buffer	10% 1x SDS

	20% methanol ddH2O

Appendix II: Consumables and Laboratory Equipment

Consumable	Manufacturer
Amicon® Ultra-4 Centrifugal Filter Units	Millipore Ltd, Hertfordshire, UK
Western blotting foam	Bio-Rad Laboratories Ltd, Hertfordshire, UK
Immobilon-PSQ 0.2 μM polyvinylidendifluorid (PVDF) membrane	Millipore Ltd, Hertfordshire, UK
Whatman filter Paper	Fisher Scientific, Loughborough, UK
Cryovials	Greiner Bio-One Ltd. Stonehouse, UK
Pipette tips	

Equipment	Manufacturer
BD FACs Canto II	BD FACs Canto II
Bioflux 200 system	Fluxion Biosciences Inc., CA, USA
Glass coverslips	
Balance MXX-212	Denver Instrument GmbH, Göttingen, Germany
Freezing container	Nalgene Labware, Thermo Fisher Scientific, Basingstoke, UK
Gel electrophoresis tank, Mini-proteanII	Bio-Rad Laboratories Ltd., Hertfordshire, UK
Incubator	Binder GmbH, Tuttlingen, Germany
Labofuge H100 R Heraeus	Thermo Fisher Scientific, Basingstoke, UK
Magnetic stirrer	Falc Instruments, Tremglio, Italy
Microcentrifuge (Centrifuge 5415 R)	Eppendorf UK Limited, Cambridge, UK
Microscope slides	
Neubauer counting chamber	VWR International Inc., Chicago, USA
OMEGA plate reader	VWR International Inc., Chicago, US

Pipettes	Starlab, Milton Keynes, UK and Gilson Scientific Ltd., Bedfordshire, UK
Pipette boy	Integra Biosciences AG, Zizers, Switzerland
Power supply (Power Pac HC)	Bio-Rad Laboratories Ltd., Hertfordshire, UK
pH meter (pH209)	Hanna Instruments
X-ray hypercassettes	Amersham Bioscience, GE Healthcare Ltd., Buckinghamshire, UK

Appendix III: EphA1 variant X2 amino acid sequence

MERRWPLGLGLVLLLCAPLPPGARAKEVTLMDTSKAQGELGWLLDPPKDGWSEQQQILNGTPLY
MYQDCPMQGRRDTDHWLRSNWIYRGEEASRVHVELQFTVRDCKSFPGGAGPLGCKETFNLLYME
SDQDVGIQLRRPLFQKVTTVAADQSFTIRDLVSGSVKLNVERCSLGRLTRRGLYLAFHNPGACVAL
VSVRVFYQRCPETLNGLAQFPDTLPGPAGLVEVAGTCLPHARASPRPSGAPRMHCSPDGEWLVPV
GRCHCEPGYEEGGSGEACVACPSGSYRMDMDTPHCLTCPQQSTAESEGATICTCESGHYRAPGEGP
QVACTESLSGLSLRLVKKEPRQLELTWAGSRPRSPGANLTYELHVLNQDEERYQMVLEPRVLLTEL
QPDTTYIVRVRMLTPLGPGPFSPDHEFRTSPPVSRGLTGGEIVAVIFGLLLGAALLLGILVFRSRRAQR
QRQQRQRDRATDVDREDKLWLKPYVDLQAYEDPAQGALDFTRELDPAWLMVDTVIGEGEFGEVY
RGTLRLPSQDCKTVAIKTLKDTSPGGQWWNFLREATIMGQFSHPHILHLEGVVTKRKPIMIITEFME
NGALDAFLREREDQLVPGQLVAMLQGIASGMNYLSNHNYVHRDLAARNILVNQNLCCKVSDFG
LTRLLDDFDGTYETQGGKIPIRWTAPEAIAHRIFTTASDVWSFGIVMWEVLSFGDKPYGEMSNQEV
MKSIEDGYRLPPPVDCPAPLYELMKNCWAYDRARRPHFQKLQAHLEQLLANPHSLRTIANFDPRM
TLRLPSLSGSDGIPYRTVSEWLESIRMKRYILHFHSAGLDTMECVLELTAEDLTQMGITLPGHQKRIL
CSIQGFKD
861 aa predicted 96431.62

Appendix IV: Expression construct EphA1

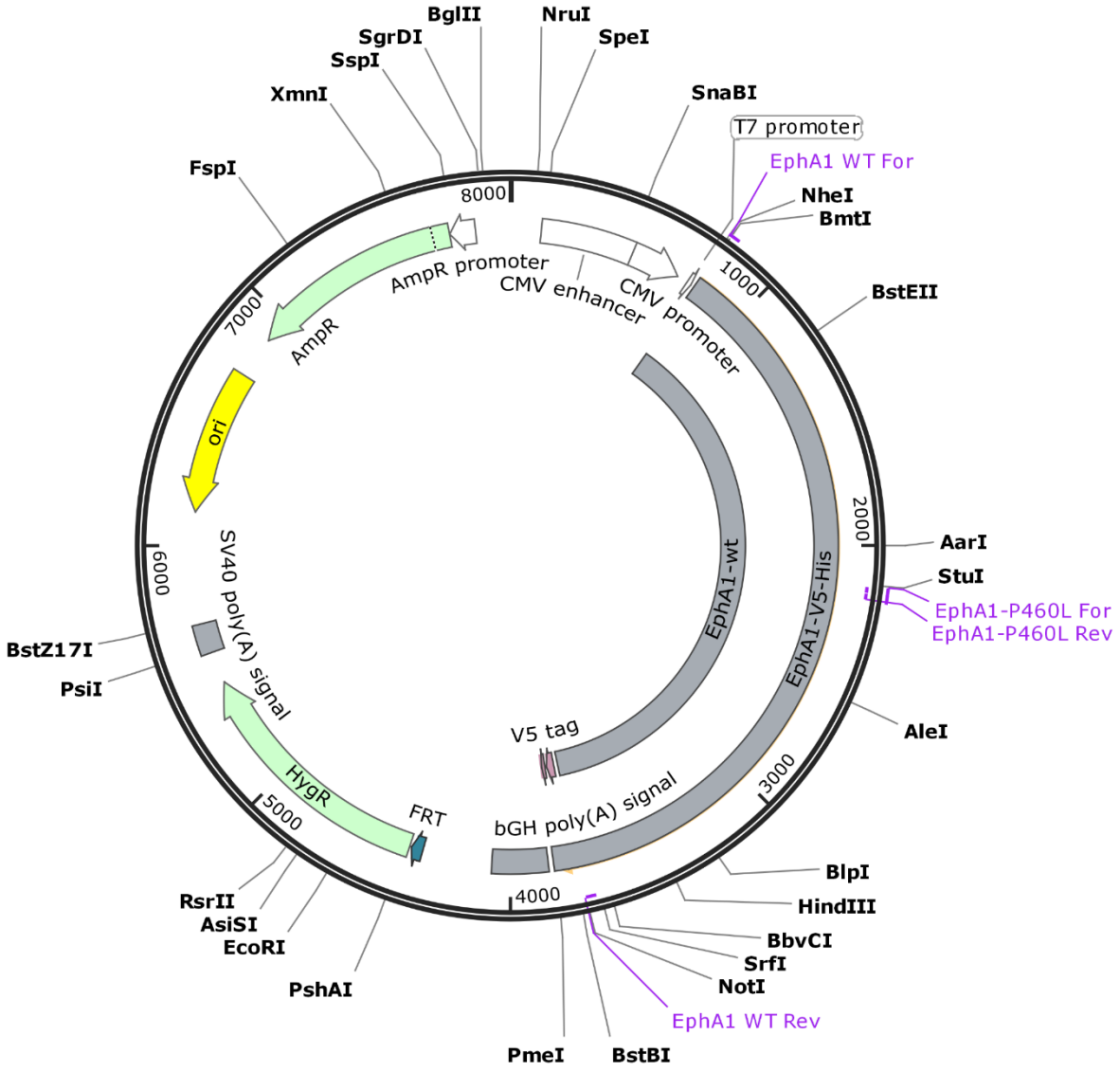

EphA1-pcDNA5-V5-His wild type sequence
8000 bp

Appendix V: MT1-MMP cleavage site in EphA2

>AAH37166.1 EPH receptor A2 [Homo sapiens]
MELQAARACFALLWGCALAAAAAAQGKEVVLLDFAAAGGELGWLTHPYGKGWDLMQNIMNDMPIYMYSVC
NVMSGDQDNWLRTNWVYRGEAERIFIELKFTVRDCNSFPGGASSCKETFNLYYAESDLDYGTNFQKRLFT
KIDTIAPDEITVSSDFEARHVKLNVEERSVGPLTRKGFYLAFQDIGACVALLSVRVYYKKCPELLQGLAH
FPETIAGSDAPSLATVAGTCVDHAVVPPGGEEPRMHCAVDGEWLVPIGQCLCQAGYEKVEDACQACSPGF
FKFEASESPCLECPEHTLPSPEGATSCECEEGFFRAPQDPASMPCTRPPSAPHYLTAVGMGAKVELRWTP
PQDSGGREDIVYSVTCEQCWPESGECGPCEASVRYSEPPHGLTRTSVTVSDLEPHMNYTFTVEARNGVSG
LVTSRSFRTASVSINQTEPPKVRLEGRSTTSLSVSWSIPPPQQSRVWKYEVTYRKKGDSNSYNVRRTEGF
SVTLDDLAPDTTYLVQVQALTQEGQGAGSKVHEFQTLSPEGSGNLAVIGGVAVGVVLLLVLAGVGFFIHR
RRKNQRARQSPEDVYFSKSEQLKPLKTYVDPHTYEDPNQAVLKFTTEIHPSCVTRQKVIGAGEFGEVYKG
MLKTSSGKKEVPVAIKTLKAGYTEKQRVDFLGEAGIMGQFSHHNIIRLEGVISKYKPMMIITEYMENGAL
DKFLREKDGEFSVLQLVGMLRGIAAGMKYLANMNYVHRDLAARNILVNSNLVCKVSDFGLSRVLEDDPEA
TYTTSGGKIPIRWTAPEAISYRKFTSASDVWSFGIVMWEVMTYGERPYWELSNHEVMKAINDGFRLPTPM
DCPSAIYQLMMQCWQQERARRPKFADIVSILDKLIRAPDSLKTLADFDPRVSIRLPSTSGSEGVPFRTVS
EWLESIKMQQYTEHFMAAGYTAIEKVVQMTNDDIKRIGVRLPGHQKRIAYSLLGLKDQVNTVGIPI
Yellow= MT1-MMP cleavage site in EphA2

MT1-MPP cleavage site in EphA2 as indicated by (Sugiyama et al., 2013) which is located in the first FNII repeat.

Appendix VI: V5 negative control

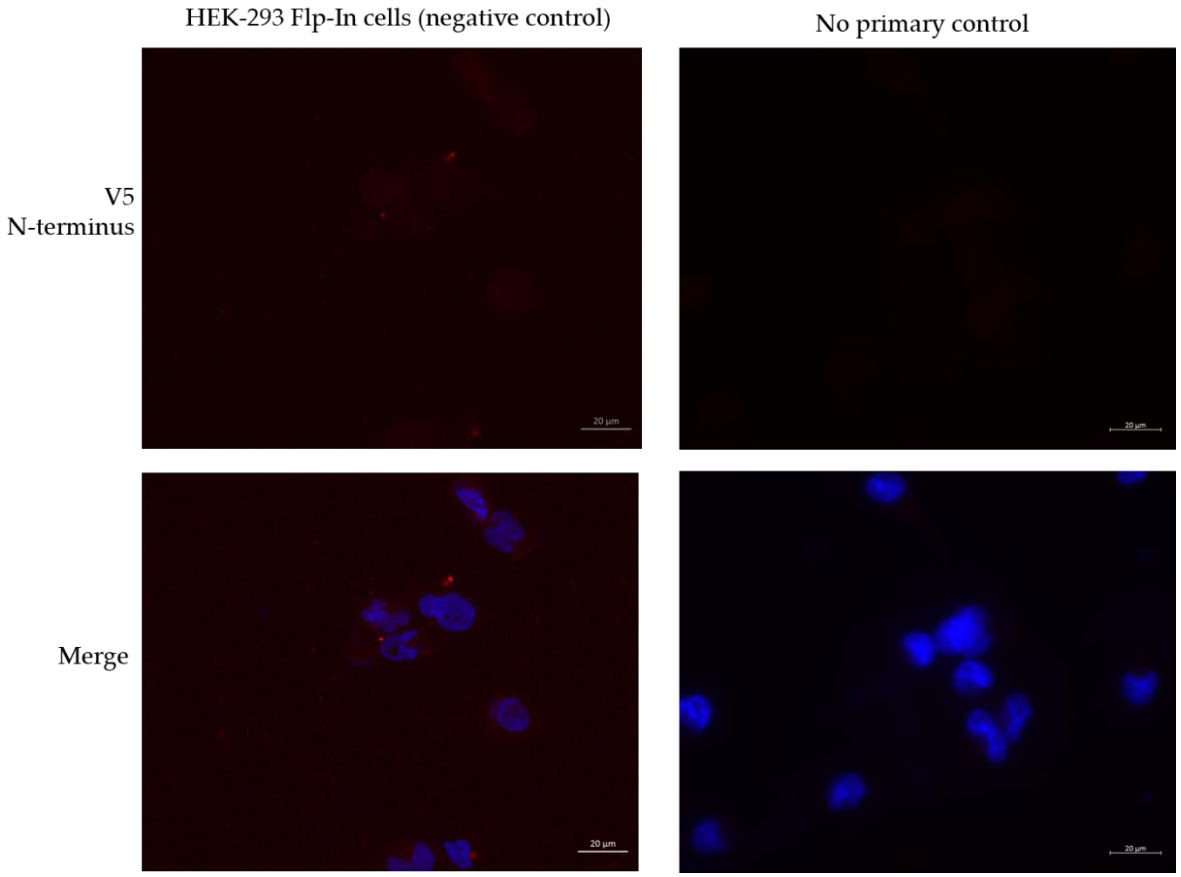

Appendix VII: Standard curve ELISA

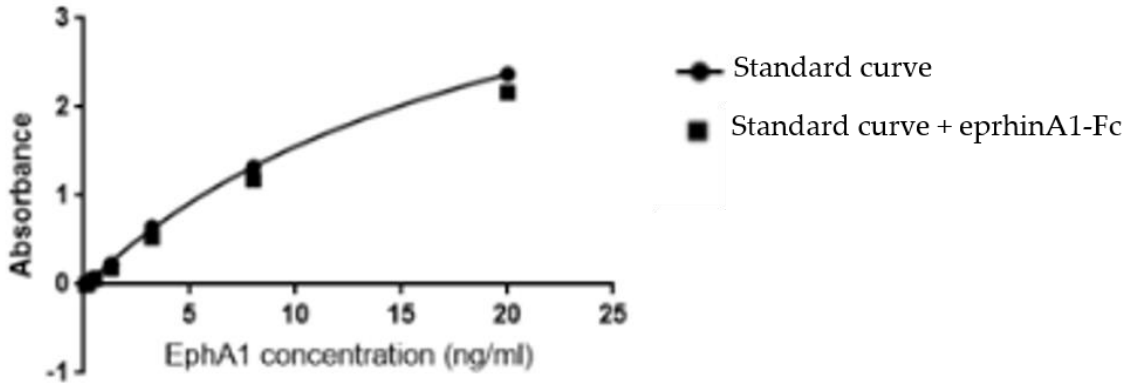

Standard curve indicating EphA1 ELISA can be used on cell free supernatant of ephrinA1-mediated EphA1 proteolysis as ephrinA1-Fc binding does not hinder the detection of EphA1 ECD in the media.

Appendix VIII: Identification of a potential C-terminal fragment in EphA1-WT cells via immunoblotting

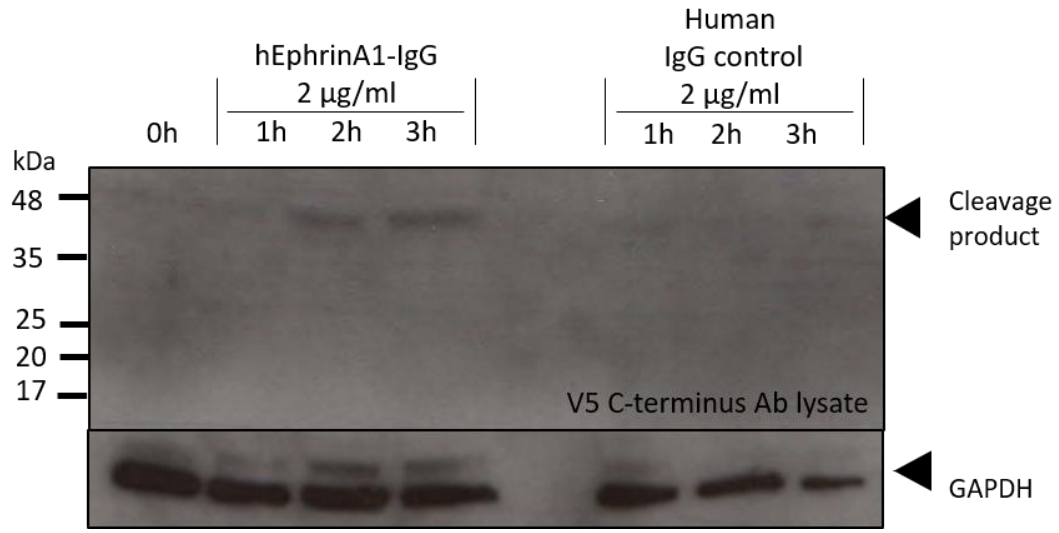

Accumulation of a potential EphA1 CTF (~40kDda) upon ligand engagement in initial experiments which proved difficult to reproduce.

Supplement I: Video files index

A1 – HUVEC No treatment

A2 – HUVEC TNFα

A3 – hCMEC/D3 No treatment

A4 – hCMEC/D3 TNFα

A5 – HUVEC IgG

A6 – HUVEC EphA1-Fc

A7 – hCMEC/D3 IgG

A8 – hCMEC/D3 EphA1 Fc

A9 – HUVEC No treatment + SDF-1

A10 – HUVEC TNFα + SDF-1

A11 – hCMEC/D3 IgG + SDF-1

A12 – hCMEC/D3 EphA1 + SDF-1